Chair of Energy Network Technology
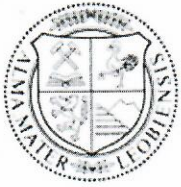
Doctoral Thesis

Advanced Modeling and Analysis of Electrical Grids for Multi-Energy System Approaches

Dipl.-Ing. Anna Maria Traupmann, BSc

November 2022

MONTANUNIVERSITÄT LEOBEN
www.unileoben.ac.at

EIDESSTATTLICHE ERKLÄRUNG

Ich erkläre an Eides statt, dass ich diese Arbeit selbständig verfasst, andere als die angegebenen Quellen und Hilfsmittel nicht benutzt, und mich auch sonst keiner unerlaubten Hilfsmittel bedient habe.

Ich erkläre, dass ich die Richtlinien des Senats der Montanuniversität Leoben zu "Gute wissenschaftliche Praxis" gelesen, verstanden und befolgt habe.

Weiters erkläre ich, dass die elektronische und gedruckte Version der eingereichten wissenschaftlichen Abschlussarbeit formal und inhaltlich identisch sind.

Datum 09.08.2022

Unterschrift Verfasser/in
Anna Maria Traupmann

ABSTRACT

The key driver for fundamental changes in current energy systems is the need to create a sustainable energy future. However, these changes pose major challenges for the energy system. Above all, the electrical grids represent bottlenecks of these developments. They limit the expansion of decentralized, volatile renewable energy sources (RES), as well as modern consumers (electric vehicles (EV), heat pumps (HP), Power-to-Gas (PtG), etc.) due to the required steady balance between generation and consumption to maintain a stable energy supply and to not cause overloads in the electrical equipment. One possibility to make these strict balance requirements in the electrical grid more flexible in the future are multi-energy systems (MES). MES couple currently independently operated energy carrier grids (e.g., electricity, natural gas, and heat) and thus enable intersectoral load shifts to other energy carrier grids.

To explore these MES, suitable models are required with which scenarios and simulations can be calculated in advance. Modeling presents as an additional challenge as the individual energy carrier grids are coupled via a higher-level MES framework and therefore have common connection points where similar characteristics of the grids are necessary. Since the individual grid models have different levels of temporal and spatial detail due to physical constraints, modeling these connection points proves difficult. Therefore, this thesis aims to present a comprehensive modeling approach that not only shows a potential approach to define similar grid characteristics for all energy carrier grids, but also provides a compromise between the temporally and spatially highly resolved electrical grid model to save computation time. This approach includes a network reduction method developed in this thesis, which allows to achieve higher modeling accuracies in the reduced grid models compared to the previous methods and therefore represents the original grid with minimal deviations. For this purpose, the method is validated using customized developed synthetic test grids that represent real grid behavior for all voltage levels.

In addition to electrical grid modeling for MES applications, a suitable analysis must be performed to identify the influence of MES on the electrical grid. Therefore, this paper presents three different use cases in which the developed network reduction method is applied to create equivalent reduced electrical grid models. Via subsequently performed hybrid load flow calculations with the multi-energy carrier simulation framework HyFlow, which was developed at the Chair of Energy Network Technology, the effects of hybrid load shifts in MES on the electrical grid are analyzed. For this purpose, voltage quality and stability analyses as well as analyses of thermal line overloads and self-consumption are performed.

KURZFASSUNG

Der Haupttreiber für tiefgreifende Veränderungen im derzeitigen Energiesystem ist die Notwendigkeit ein nachhaltiges Energiezukunft zu schaffen. Diese Veränderungen stellen aber große Herausforderungen für das Energiesystem dar. Vor allem die elektrischen Netze sind eine Schwachstelle dieser Entwicklungen. Sie begrenzen den Ausbau an dezentralen, volatilen erneuerbaren Energien (RES), sowie moderner Verbraucher (Elektromobilität, Wärmepumpen, Power-to-Gas, etc.) aufgrund des geforderten stetigen Gleichgewichts zwischen Erzeugung und Verbrauch, um eine stabile Energieversorgung aufrechtzuerhalten und die Betriebsmittel nicht zu überlasten. Eine Möglichkeit diese harten Gleichgewichtsanforderungen im elektrischen Netz zukünftig zeitlich zu flexibilisieren, sind Multi-Energie-Systeme (MES). MES koppeln die derzeit individuell betriebenen Netze (z.B. Strom, Gas und Wärme) und ermöglichen intersektorale Lastverschiebungen in andere Energieträgernetze.

Um derartige MES zu erforschen, braucht es auch geeignete Modelle, mit denen Szenarien und Simulationen vorab betrachtet werden können. Auch die Modellierung stellt eine Herausforderung dar, da die einzelnen Energieträgernetze über das übergeordnete MES gekoppelt sind und daher gemeinsame Anknüpfungspunkte haben. Da die einzelnen Netzmodelle unterschiedliche zeitliche und örtliche Detailierungsgrade aufgrund physikalischer Gegebenheiten besitzen, gestalten sich diese Anknüpfungspunkte schwierig. Daher soll in dieser Arbeit ein umfassender Modellierungsansatz vorgestellt werden, der nicht nur eine mögliche Gestaltung dieser Anknüpfungspunkte zeigt, sondern auch einen Kompromiss zwischen dem zeitlich und örtlich hochaufgelösten elektrischen Netzmodell bietet, um Berechnungszeit einzusparen. Dieser Ansatz beinhaltet eine in dieser Arbeit entwickelte Netzreduktionsmethode, die es ermöglicht gegenüber den bisherigen Methoden höhere Abbildungsgenauigkeiten in den reduzierten Netzmodellen zu erreichen. Dazu wird die Methode anhand von eigens entwickelten synthetischen Testnetzen, die reales Netzverhalten auf allen Spannungsebenen abbilden, validiert.

Neben der Modellierung von elektrischen Netzen in MES, muss auch eine geeignete Analyse durchgeführt werden, die es ermöglicht den Einfluss von MES auf das elektrische Netz zu identifizieren. Dazu werden in dieser Arbeit drei verschiedene Use Cases vorgestellt, in denen die entwickelte Netzreduktionsmethode angewendet wurde, um elektrische Netzmodelle zu erstellen. Über anschließend durchgeführte hybride Lastflussberechnungen mit dem am Lehrstuhl für Energieverbundtechnik entwickelten hybriden Lastflussberechnungsprogramm HyFlow werden die Auswirkungen von hybriden Lastverschiebungen auf das elektrische Netz analysiert. Dazu werden Spannungsqualität- und -stabilitätsanalysen, sowie Analysen zu thermischen Leitungsüberlastungen sowie zum Eigenverbrauch durchgeführt.

FOREWORD

It was my great pleasure to be able to continue the research I started in my Master Thesis at the Chair of Energy Network Technology about modeling electrical grids in October 2018 as a PhD student. In these over four years many people have supported me and therefore I would like to kindly thank them for their assistance, contribution, and encouragement.

First, I would like to thank my supervisor and head of the Chair of Energy Network Technology, Thomas. Thank you, Thomas, for your support, scientific input to my research and all the opportunities and new fascinating challenges I was able to work on at the Chair. I really enjoyed our discussions regarding research and projects as well as about other interesting topics. It was a great pleasure to work with you and learn from you. Thank you for all your efforts.

Second, I would like to thank my colleagues at the Chair of Energy Network Technology, who have also become my friends. To begin with, I would like to thank Julia, who supervised my Master Thesis, for your everything you shared with me regarding scientific work and for our work together afterwards at the Chair. Then, I would like to thank Jasmin, generally for all the great work you do at the Chair and your support for all the PhD students. Matthias, Josef and Rebecca thank you for all your valuable input and effort in contributing significantly to my thesis. Kerstin, Lukas, Christoph, Benjamin, Andreas, Johannes, Roberta, Lisa, David, Thomas, Vanessa, Paul, Peter, Christopher, Nouman, Maedeh, and Elisabeth thank you for making working at the Chair so great for me. I will miss working with you.

Most importantly, I would like to thank very best friend and one of the most important people to me, Bernd. Thank you so much for your professional and scientific contribution to my research and for your input that broadened my knowledge in the field of electrical grids substantially. While I have enjoyed working with you a lot, I am even more grateful for your support, company, and friendship outside of work. Everything is better with you.

Finally, I would like to thank my parents, Werner, Sabine, Tanja and Karli for everything they have done and do for me, for their encouragement and patience. Also, I would like to thank my grandparents, Ilse and Fritz for their constant support. Thank you all for making this possible for me.

CONTENTS

Contents

Nomenclature

Abbreviation

CO_2	Carbon Dioxide
RES	Renewable Energy Sources
PV	Photovoltaics
EV	Electric Vehicle
HP	Heat Pump
MES	Multi-Energy-Systems
ETS	Emission Trading System
LP	Linear Programming
MILP	Mixed-Integer Linear Programming
MINLP	Mixed-Integer Non-Linear Programming
DP	Dynamic Programming
DC	Direct Current
AC	Alternating Current
LV	Low-Voltage
MV	Medium-Voltage
HV	High-Voltage
MaxV	Maximum-Voltage
PtG	Power-to-Gas
GtP	Gas-to-Power
CFPP	Coal-Fired Power Plant
p.u.	Per unit
TSO	Transmission System Operator
OpEx	Operational Expenditures
FCR	Frequency Control Reserve

aFRR	Automated Frequency Restoration Reserve
mFRR	Manual Frequency Restoration Reserve
CapEx	Capital Expenditure

Indices

Indices	Explanation [Unit]
R'	Specific Line Resistance [Ω/km]
L'	Specific Line Inductance [mH/km]
C'	Specific Line Capacitance [nF/km]
G'	Specific Line Conductance [S/km]
l	Line Length [km]
$\underline{U}_1$	Complex Voltage at the Beginning of the Line [V]
$\underline{I}_1$	Complex Current at the Beginning of the Line [A]
$\Delta\underline{U}_{12}$	Complex Voltage Drop over the Line [V]
$\underline{I}_{12}$	Complex Line Current [A]
$\underline{U}_2$	Complex Voltage at the End of the Line [V]
$\underline{I}_2$	Complex Current at the End of the Line [A]
ϑ_L	Voltage Phase Angle [°]
φ_1	Phase Angle between $\underline{U}_1$ and $\underline{I}_1$ [°]
φ_2	Phase Angle between $\underline{U}_2$ and $\underline{I}_2$ [°]
ω	Circular Frequency [Hz]
j	Complex Index [-]
$\underline{S}_1$	Complex Apparent Power at the Beginning of the Line [VA]
$\underline{S}_2$	Complex Apparent Power at the End of the Line [VA]
δ	Phase Angle between $\underline{S}_1$ and $\underline{S}_2$ [°]
P_{loss}	Active Power Losses [W]

Q_{loss}	Reactive Power Losses [Var]
Z_W	Characteristic Impedance [Ω]
R_{is}	Specific Isolation Resistance [Ω]
P_{nat}	Natural Power [W]
U_{nN}	Nominal Voltage [V]
Q_L	Inductive Power Demand/ Inductive Charging Power [Var]
Q_C	Capacitive Power Demand/ Capacitive Charging Power [Var]
$\underline{U}$	Complex Nodal Voltage [V]
$\underline{I}$	Complex Nodal Current [A]
$\underline{Y}$	Nodal Admittance Matrix [S]
P	Active Nodal Power [W]
Q	Reactive Nodal Power [Var]
$\underline{S}$	Complex Apparent Nodal Power [VA]
e	Euler´s Number [-]
α	Admittance Phase Angle [°]
U	Voltage Magnitude [V]
J	Jacobian Matrix [-]
P_{spec}, Q_{spec}	Specified Active and Reactive Nodal Powers [W], [Var]
P_{calc}, Q_{calc}	Calculated Active and Reactive Nodal Powers [W], [Var]
ε	Error Limit (Newton Raphson Method) [-]
$\underline{S}_{ij}$	Load Flow over a Line [Var]
$\underline{S}_{loss,ij}$	Load Flow Power Losses over a Line [Var]
B_{ii}	Nodal Susceptance [S]
v	p.u. Voltage [-]
p	p.u. Active Power [-]
q	p.u. Reactive Power [-]

X	Reactance [Ω]
$\underline{S}_{k,N}''$	Short-Circuit Power at Node N [VA]
$\underline{I}_{k,N}''$	Short-Circuit Current at Node N [A]
$\underline{Z}_N$	Short-Circuit Impedance at Node N [Ω]
$\underline{Z}_G$	Generator Impedance [Ω]
$\underline{Z}_O$	Overhead Line Impedance [Ω]
$\underline{Z}_C$	Cable Impedance [Ω]
$\underline{Z}_T$	Transformer Impedance [Ω]
r_t	Transformation Ratio [-]
ε_{ESS}	Degree of Energy Self-Sufficiency [-]
ε_{PSS}	Degree of Power Self-Sufficiency [-]
ε_{SCR}	Self-Consumption Ratio [-]
$P_L(t)$	Load Curve/ Consumption Time-Series [W]
$P_G(t)$	Generation Curve/ Generation Time-Series [W]
E_L	Energy under Load Curve [Wh]
E_G	Energy under Generation Curve [Wh]
E_{SC}	Self-Consumption Energy [Wh]
x	Optimization Variable
$f(x)$	Objective Function
$P_{res}(t)$	Residual Load Time-Series [W]
R_{RLC}	Compensation Module Resistance [Ω]
L_{RLC}	Compensation Module Inductance [mH]
C_{RLC}	Compensation Module Capacitance [nS]
$\underline{U}_{fic}$	Ficitious Voltage Potential [V]
ΔP_{rel}	Relative Deviation [%]

LIST OF FIGURES

LIST OF TABLES

1 INTRODUCTION

The current key driver for changing and advancing the existing energy system is the need for transitioning towards a future sustainable energy generation to mitigate climate change and therefore carbon dioxide (CO_2) emissions [1]. Today's energy supply infrastructures are designed to transport the energy generated in central power generation units via the transmission and distribution system to the respective end users. Therefore, current energy grids, in particular electrical grids, are not yet adapted to the future challenges resulting from energy transition [2]. National and international policies that advance energy transition include changes in current generation and consumption structures and technologies to deal with the challenges arising from this change [2].

In order to enable for such a climate neutral energy system to emerge, the energy generation structure has to be based mainly or even entirely on renewable energy sources (RES) [3]. However, RES are usually volatile, and therefore not always predictable or available, and can thus not ensure a stable energy supply [4, 5]. Globally, there is already a large share of about 30 % including volatile (such as wind and photovoltaic (PV) power) and non-volatile (such as hydropower and geothermal energy) RES [6]. Despite these current efforts to decarbonize energy generation by increasing the share of RES, global CO_2 emissions continue to rise in particular in the energy supply sector (cf. Figure 1), which accounts for 46 % of global CO_2 emission increase to meet the growing electricity demand [7]. Therefore, generation-side measures to mitigate climate change additionally need to focus on substituting existing fossil-fueled power plants with sustainable technologies [8]. For example, coal-fired power generation accounts for over 30 % of global CO_2 emissions, making the coal phase-out necessary to permanently reduce global CO_2 emissions [9].
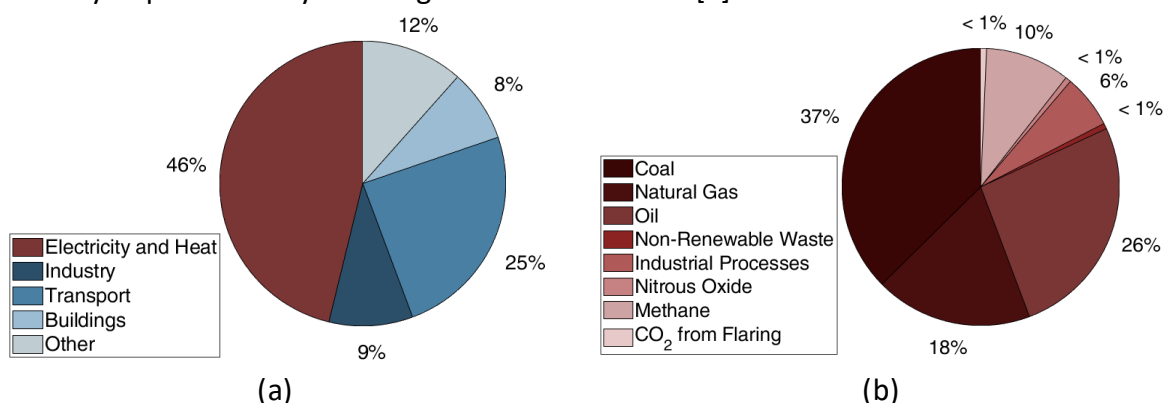
Figure 1: (a) Annual increase in CO_2 emissions by sector for 2021 and (b) CO2 emissions from electricity and heat generation by fuel type for 2021 (data taken from [7])

However, since decarbonization in the electric energy system is already further advanced than in the heat sector, where decarbonization is expected to prove more difficult, electrification will increase [10]. Therefore, to create a decarbonized energy system additionally, consumer-

side efficiency measures and innovative technologies, such as electric vehicles (EV) and heat pumps (HP) must be implemented [11]. However, integrating these technologies will result in an increase of electricity demand by about 17 % in 2050 according to Engel et al. ([12]).

The mainly decentralized RES which introduce high volatility into the grid and the load peaks that occur due to charging processes of EVs as well as reduced inertia in the system put great stress on electrical grids [13]. However, due to increasing decentralization of generation units and local differences for potential RES expansion, electrical transmission and distribution grids become more relevant in the future [14]. Thus, the energy system decarbonization process also entails equipping electrical grids for the upcoming challenges of energy transition [14].

Since generated and consumed power in electrical grids must be balanced at all times, which will be impeded in the future due to these changes, a stable energy supply may be at risk. While grids, however, only enable spatial decoupling of consumption and generation, it will also be necessary to achieve temporal decoupling so that this balance can be maintained. As a result, the need for flexibility options (e.g., Demand-Side-Management, Energy Storage Systems) arises, which enable this temporal shift between generation and consumption. Thus, sustainable technologies can be efficiently integrated, and the grids are relieved to maintain stable energy supply. To provide an even more efficient system, a Multi-Energy-Systems (MES) approach or sector coupling allows for these flexibility options to be used across energy carriers. [15] Figure 2 shows how a future energy system with the above-mentioned changes in energy generation and consumption and the necessary flexibility options may be structured.

Figure 2: Future energy system with necessary components and connections (adapted from [16], icons taken from [17])

Thus, it provides solutions for successfully achieving the transition to a sustainable energy future by effectively integrating RES and efficiently using the available energy in the overall system [10, 15].

However, sector coupling requires adaptions in the structure and operation of current energy grids to be made. Since current grids distribute grid-bound energy to customers and are operated as independent structures, synergies between energy carrier grids are hardly utilized. These synergies, such as energy exchange and intersectoral load shifts between the different energy grids, can reduce or even avoid excessive strain on electrical grids. This enables a more flexible reaction to volatile, decentralized, and unpredictable RES generation as well as load peaks due to EV or HP utilization. Thus, it is easier to preserve the balance between energy generation and consumption within the grid and enable grid-friendly operation [18]. Significant advantages regarding primary energy use due to cascaded energy chains and exergetic potentials can, additionally, be achieved and improve system efficiency as well as provide seasonal energy storages. [10, 19]

To ensure the above-mentioned advantages of MES, efficient design and planning within the entire energy systems is required. Therefore, MES must be further researched, in particular on how cross-energy carrier infrastructures impact the individual grids (e.g., bottlenecks, overloads, etc.). As grids represent bottlenecks within the energy system, grid-based MES tools are essential to conclusively analyze future developments within the energy system [20]. Such tools must enable performing efficient and accurate load flow calculations across energy carriers, in order to obtain reliable results regarding the impact of flexibility options on the grids. [14]

1.1 Structure of the Work

Chapter 2 provides the state-of-research on modeling and analysis approaches for electrical grids in MES as these represent one of the future key challenges in energy transition and are therefore also the focus of this paper. Chapter 2 additionally underlines present research needs on this topic. Chapter 3 presents the research objectives derived from existing literature and models currently available and shows an overview of the correlations between the individual research papers within this work. Then, Chapter 4 provides theoretical background to the considered technical research subjects within this work. This chapter also highlights the importance of accurate energy system models, in particular for electrical grids. Chapter 5 summarizes the results of this thesis and provides a detailed discussion in correspondence with the identified research objectives of this work. Finally, in Chapter 6 there is a conclusion section including a future outlook on what research still has to be done in the future.

2 STATE OF RESEARCH – MODELING AND ANALYSIS APPROACHES FOR MULTI-ENERGY-SYSTEMS

Energy system models represent an approximation of the real energy system due to estimations, past or statistical trends as well as assumptions for future developments [21]. According to the energy system model categorization in van Beeck (1999) [22] and Kriechbaum et al. (2018) [20], energy system models are characterized by 8 aspects. These characteristics also define the requirements for the grid models in the case of grid-based multi-energy-systems (MES) framework models: [22]

1. *Analytical Modelling Approach*

There are two approaches for modeling energy systems according to their intended use: Top-down models and Bottom-up models. When both modeling approaches are applied to model the same system, they produce diverging results due to different adoption of individual components within the system. [22]

Top-down models aim at modeling the entire economy of a region or even nation and provide an aggregated view of the energy sectors and economy which is why they are also referred to as macroeconomic models. Such Top-down models simulate future energy demand and supply based on economic developments in the future. Therefore, they are used for analyzing effects of general energy or climate policies, for example energy taxes or emission trading schemes (ETS) as well as feed-in tariffs for RES. In contrast, Bottom-up models focus on technological detail to estimate future energy demand and supply. Thus, they cannot easily incorporate macroeconomic considerations of energy or climate policies. In Bottom-up models technologies and their impact as well as development are analyzed based on specific objectives such as energy efficiency enhancement, decarbonization or synergy utilization between energy sectors. Then these models evaluate how the technologies affect the energy system and the political and economic policies set to achieve these specific objectives or may even provide recommendations. [21]To illustrate the two modeling approaches, Figure 3 presents an overview. It is also possible to link the two modeling approaches and thus mitigate the limitations of the individual approaches, which are referred to as Hybrid Energy System Models [21]. These models combine at least one set of Bottom-up models (e.g. for final energy demand) with one macroeconomic Top-down model [21].
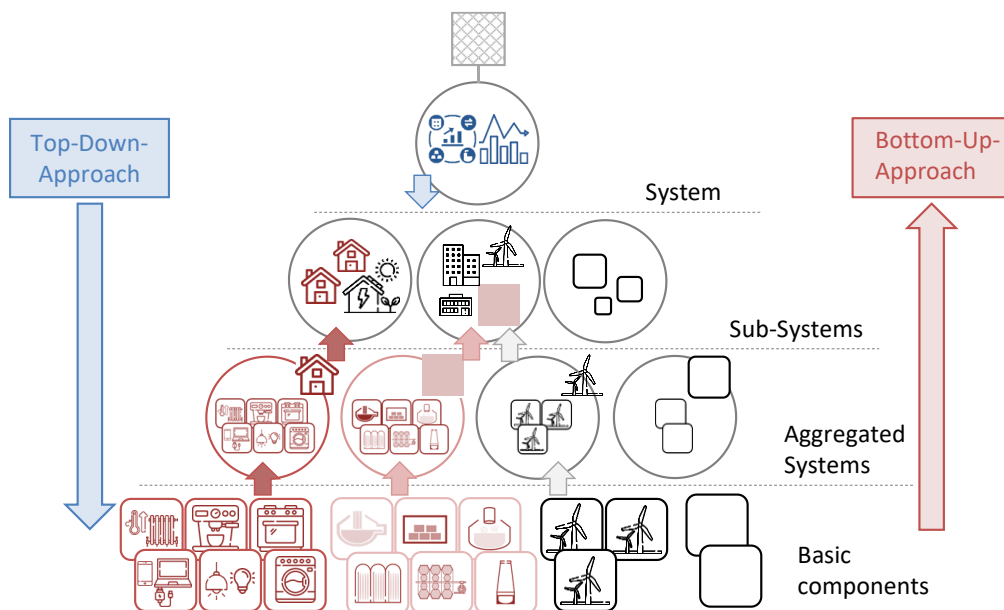
Figure 3: Overview Top-down and Bottom-up modeling approach (adapted from [23], icons taken from [17])

2. Modeling Perspective

The modeling perspective describes the way in which the identification of future developments is addressed in the model. There are three different perspectives which are depicted in Figure 4. First, there is the Forecasting-Method, which performs an extrapolation of historical trends to predict future developments. However, since this method is based on the past, models with this perspective can usually only be applied reasonably for a relatively short time horizon in the future. [22]

Then, there is the scenario planning method which explores the future. To obtain conclusive results with this method, an associated reference scenario (e.g., business-as-usual) is required which serves as a comparison for the formed scenarios. The scenarios are strongly based on assumptions, exemplarily about economic behavior, technological advances, or necessary resources. Therefore, it is often useful to combine this method with sensitivity analyses. [22]

(a)   (b)   (c)
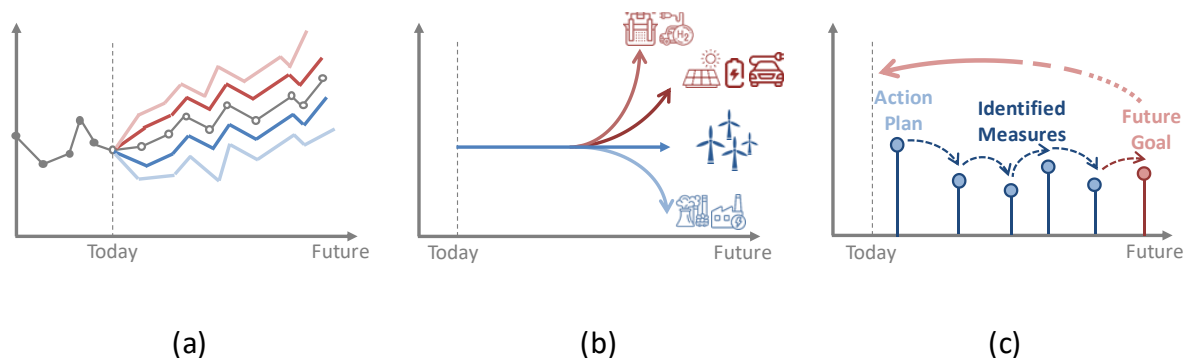
Figure 4: Qualitative illustration of different modeling perspectives (a) Forecasting-Method, (b) Scenario Planning Method and (c) Backcasting-Method (icons taken from [17])

Finally, the Backcasting-Method is based on a vision of the future (e.g., intended expansion of RES or electro mobility, etc.), for which an action plan including concrete measures is identified in order to achieve this vision. [22]

3. Model Structure and Internal Assumptions

The model structure refers to what level of detail is incorporated in the model, there are three different representations [20]. The concepts of the three model structures, White-box models, Grey-box models and Black-box models are simplistically illustrated in Figure 5.
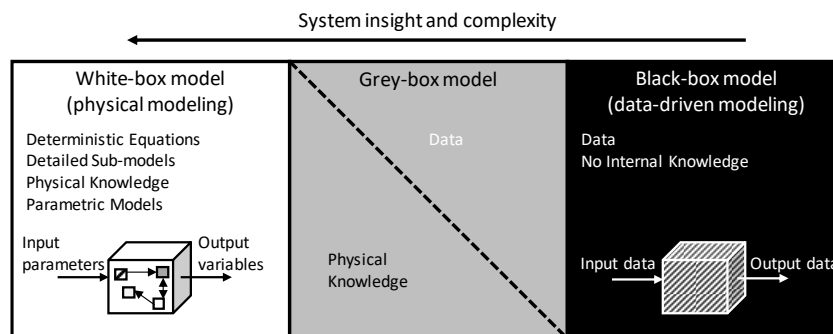
Figure 5: Simplistic concept illustration of White-, Grey- and Black-box-models (adapted from [24, 25])

White-box models represent mathematical models that describe real systems using physical equations. In the Black-box model a complex real system is described only in terms of its external behavior while the internal structure is unknown. Grey-box models combine these two model structures and therefore incorporate both physical system knowledge and empirical data. [25]

4. Model Formulation: Underlying Methodology and Mathematical Approach

Depending on the analytical modeling approach (Top-down or Bottom-up), generally different model formulations are utilized. For Top-down approaches, Scenario Models, Input-Output Models, Econometric Models, Computable General Equilibrium Models and System Dynamics Models are used for defining the underlying methodology [21, 22]. For Bottom-up models, however, Scenario Models, Partial Equilibrium Models, Optimization Models, Simulation Models and Multi-Agent Models are common and thus specify the underlying methodology [21, 22].

Since this work focuses on Bottom-up models, selected underlying methodologies and the mathematical approaches are described more in detail in the following: In an optimization model, a mathematical problem is formulated in which a certain number of optimization or decision variables are calculated to minimize or maximize the corresponding objective function [26]. The objective function for energy systems may refer to minimizing CO_2 emissions or costs. Additionally, certain constraints must be met, which limit the optimization problem [26]. The optimization problem can relate either to the operation of the (energy)

system or to the design of the (energy) system [20]. However, optimization models usually represent complex models and require a high level of mathematical knowledge and accordingly high quality input data [22]. A mathematically more detailed description of optimization problems is presented in Chapter 4.4, in this chapter an overview over possible optimization problems is presented, as illustrated in Figure 6.

```
                              Optimization Problems

   Linear            Real Numbers        Single-Objective     Deterministic        Approximation
   Programming       $x \in \mathbb{R}^n$    Problems
   (LP)
                     Integer Numbers      Multi-Objective      Stochastic           Heuristic
   Non-Linear        (IP)                 Problems
   Programming       $x \in \mathbb{Z}^n$
   (NLP)                                                                            Pareto-
                     Mixed-Integer                                                  Optimization
                     Numbers (MIP)
                     $x \in \mathbb{R}^n \cap \mathbb{Z}^n$

   Type of Objective   Type of Variables   Number of Objective   Objective Function   Optimization Methods
   Function & Constraints                  Functions             & Constraint
                                                                 Definition
```

Figure 6: Overview of optimization problem classifications (adapted from [27, 28])

Simulation models represent a simplified (real) system for which the behavior is to be reproduced or determined under certain conditions [22, 29]. Their purpose is to examine and compare options of system behavior with varying conditions such as costs, emissions or energy supply [26]. In contrast to optimization models which find the optimal option based on descriptive analysis, simulation models consider only the options predefined by the user and evaluate them [30]. Thus, the considered conditions for simulation models cannot be measured by one common denominator as it is the case for optimization models [26]. However, simulation models can be integrated into energy system optimization models [31] or may also be considered a type of scenario model [26]. Exemplarily, optimization models can create scenarios for simulation models, e.g., cost-optimal or exergy-optimal scenarios that are then simulated [32]. Additionally, simulation models are more flexible, allow the integration of strategic decisions and require less demanding input data compared to optimization models [21]. They can either be static representing the operation of a single time period (steady-state) or (quasi) dynamic when including system evolution over periods of time [22]. As steady-state models incorporate temporal simplifications (no description of time-dependent phenomena) for the models, they also limit computation times [32]. Therefore, steady-state models are commonly used for energy systems [32].

Typical mathematical approaches for simulation and optimization models require a common problem formulation regarding the equations describing the problem [20]. The most common model formulations use linear programming (LP), mixed-integer linear programming (MILP), mixed-integer non-linear programming (MINLP) as well as dynamic programming (DP) [33]. The most widely used mathematical method is LP as it is simple and provides time-efficient

results [22]. Additionally, mathematically the problem formulation is relatively undemanding as all equations are expressed entirely in linearized terms [22]. However, LP models are usually sensitive to input parameter variations and thus strongly depend on starting values in order reach fast convergence [22]. MILP represents an extension of LP as it allows greater flexibility in formulating the energy system model, as it limits values and therefore properly reflects real behavior, for example unit sizes of power plants which cannot reasonably take arbitrary values [22]. As neither non-linear nor dynamic programming is considered in this work, it is not described more in detail at this point. An overview of the characteristics of simulation and optimization models is presented in Table 1.

Table 1: Overview and comparison of simulation and optimization models (adapted from [26])

	Optimization Models	Simulation Models
Definition	Model that internally generates an optimal energy system design or operation over the mathematical objective function and constraints	Model that simulates the behavior of user-defined energy system design and assumptions using mathematical principles
Purpose and results	Identification of the optimal solution to a specific objective	Calculation of a set of solutions for future systems for an evaluation process
User and algorithm tasks	Design/operational decisions are made in the optimization based on limitations	Design/operational decisions are user-specific and defined outside the model
Technological detail	Detailed model of the considered system	Detailed modeling of the adapted (e.g., future) system
Computational Time	Longer computation times, but usually lower temporal resolution	Shorter computation times with higher temporal resolutions
Suited modeling perspective	Well-suited for forecasting (direct the future towards objective)	Well-suited for backcasting (discuss future pathways)

Overviews over existing models and their characteristics are described in many sources such as Kriechbaum et al. (2018) [20], Herbst et al. (2012) [21], van Beeck (1999) [22], Scheller et al. (2019) [30] as well as Grubb et al. (1993) [34]. Examples for optimization models are among others the MARKAL/TIMES model which is an optimal energy planning model as well as the energy supply optimization model MESSAGE (Model for Energy Supply Strategy Alternatives and their General Environmental Impact) [20, 21]. Exemplary, models for simulations are Long-Range Energy Alternatives Planning "LEAP", Model for Analysis of Energy Demand "MEAD" or National Impact Analysis "NIA" [21].

5. Time Horizon

Energy system models are created for different applications and thus for different time horizons [34]. Since different investigations (e.g. economic, social, environmental) affect different time scales, the time horizon thus determines the structure and the objectives of the corresponding energy system model [22]. While medium- and long-term models usually focus on allocation of available resources, short-term models in general concern (sectoral) market simulations such as detailed models of electricity or oil market simulation models [34].

6. Geographical or Spatial Coverage

This modeling aspect refers to the local extent of the system under consideration. Models can range from global considerations over national or regional systems to local or project-related dimensions. The geographic coverage is therefore an important modeling factor since the necessary spatial aggregation of the grid data depends on the grid extent. Systems with a larger geographical coverage (e.g., global, national, or even partly regional systems) often follow a top-down approach. Systems with a smaller geographical coverage (e.g. regional, local or project-related systems) often use a Bottom-up or a combined hybrid approach. [22]

7. Sectoral Coverage

Sectoral coverage refers to how many sectors are included within the models. If several sectors are represented, then the interactions of the individual sectors are usually also considered. Multiple sectors are often considered in Bottom-up or combined hybrid models, as is the case with MES, for example. [22]

8. Temporal Resolution and Spatial Resolution

In particular for modeling MES, spatial as well as temporal resolutions should be considered as energy demand and supply often occur in different locations at contrasting times [35]. Thus, the temporal resolution aspect is a critical parameter as different systems (e.g., electricity, heat, etc.) can only be adequately described for certain time resolutions (e.g. seconds, hours, etc.) [20]. Since MES models incorporate e.g., heat, natural gas and electricity systems reasonable time scales should be selected individually and optimally for the respective energy carrier system (cf. Figure 7) [35]. Additionally, MES components such as energy storages included in the MES are sensitive to the choice of timescales to enable incorporating different storage time constants (e.g., short-term battery storages and seasonal gas storages) [35]. Figure 7 provides an overview over the temporal and spatial operational and planning scales in energy system models.

Spatial resolution refers to the level of aggregation. The highest spatial resolution in energy system models are individual households or residential buildings [36]. The next resolution level is an aggregated perspective of many households, residential buildings as well as

commercial businesses in districts or businesses [20] Similarly to temporal scales, spatial dimensions in the model reflect energy transmission and distribution infrastructures to account for transfer between generation and consumption locations [35]. Thus, adequate grid models have to be included which are referred to as grid-based MES modes [20, 35].
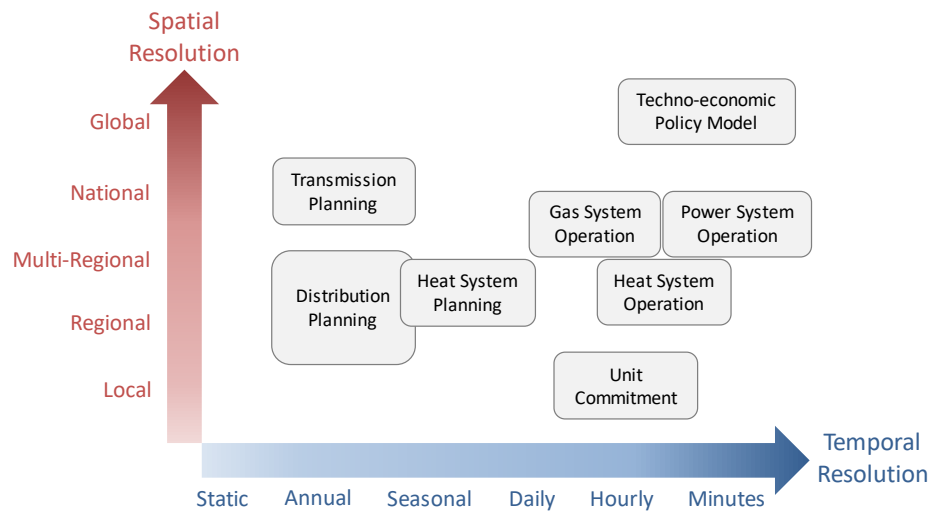
Figure 7: Spatial and temporal resolutions for MES operational and planning scales (adapted from [35, 37])

Besides the MES generation and consumption, grid-based MES models additionally include models for power flow calculations in energy grids, storage models, and models to describe synergies between different energy carrier grids (hybrid conversion technology models). There are two options for modeling grid-based MES: integrated models, in which all sub models (generation, consumption, grids, storage, etc.) are modeled in one framework, and co-simulation models, in which individual sub models are connected via a higher-level tool. [20]

For energy grid modeling there are two approaches according to Geidl et al. (2007) [8]: grid models representing Black-box models and power flow models which can be either Grey- or White-box models. Grid models provide a lossless energy transmission within the model and thus are similar for all energy carrier models (e.g., electricity, natural gas, heat) as they represent a general model without further specifications. Power flow models, however, model the electrical line losses as a function of the power flow as they are load dependent. Thus, power flow models incorporate physical laws and correlations providing accurate and detailed information. However, due to these details they present significant differences between the energy carriers, therefore, each energy carrier has to be modeled individually. [8] Power flow models can further be classified as direct current (DC) models and alternating current (AC) models [38]. DC models provide active power flows which depend on maximum power capacities and electrical line resistances [39]. Applications for DC models are exemplarily due to their simplicity long-term grid planning and expansion studies ([40]) or optimal allocation of power storages ([41]). For stability analyses or congestion analyses they are less suitable as

they do not include reactive power [42]. In contrast, AC models provide active and reactive power resulting in an additional dependency on capacitive and inductive load, generation, and electrical equipment behavior [39]. They model increased detail but are therefore also higher in complexity compared to the DC models [39]. Thus, large-scale electricity systems are more difficult to calculate as convergence problems may occur due to their high resolution making them unsuitable for real-time operation simulations [43].

Both, temporal and spatial resolution, influence the model´s accuracy [35]. However, if grid-based energy system models with high resolutions for both, time and space, are used, an immense computational effort and high demands on data are required [35]. Thus, usually a compromise between computational effort and modeling accuracy has to be reached [44]. For temporal resolution reduction a coarser temporal resolution, e.g. from 15-minute values to hourly or daily averages, can be calculated [45]. For spatial resolution reduction methods have to be applied in order to avoid loss of information within the reduced model [46, 47]. Exemplarily, for the electrical grid, smaller equivalent grid models are created using bus – aggregation or network reduction methods which aim at replicating electrical behavior from the original grid [46–48]. As network reduction methods are essential in this work for the presented modeling approach of electrical grids, they are described in detail in Chapter 4.5.

MES modeling proves to be more challenging for many of the presented aspects than modeling single energy carrier energy systems. This is because, different model boundaries as well as (temporal and spatial) resolutions and levels of detail exist for the individual energy carriers. However, to take the complexity of such MES into account, it is essential that the models reflect these differences. Thus, modeling of MES entails strict requirements for the individual (energy carrier) sub models such as power system models. [35] As this work addresses electrical grids and their modeling for MES approaches, focus is put on power system models.

Initial power system models were focused on stable energy supply as well as system costs. However, due to the necessity for transitioning into a sustainable, low-carbon energy future, climate change and corresponding policies have become essential modeling elements. Thus, the already existing and established methods for energy system modeling must adapt, so that energy system models and their corresponding grid models adequately reflect the necessary changes for energy transition. The most important resulting challenges in modeling future energy systems are the following issues: [49]

1. the decentralized and volatile RES generation and its potential estimates, which requires a higher spatial resolution in the models,
2. the increasing electrification and the associated increase in demand, which requires higher temporal resolution in the models and
3. the increasing integration of new flexibility technologies.

All modeling aspects to cover the main challenges in power system modeling for MES approaches require a suitable temporal and spatial resolutions with which a conclusive analysis of the power system can still be achieved. [49]

MES models are used to analyze a certain system under defined assumptions and developments for the future. The purpose of such energy system analysis is to develop a method that enables a measurable representation of the impacts due to changes (e.g., utilization of new technologies, operational modifications) in the energy system on a wide variety of parameters and variables (e.g., energy demand, stability variables, CO_2 emissions, energy efficiency). However, in general energy system analysis serves three purposes: [50]

1. Quantifying the performance of individual system parts or components
2. Characterizing the interactions between these system parts or components
3. Determining economic feasibility of the system

Regarding electrical energy systems within MES frameworks, the following analyses are primarily important: Power quality and stability assessment as well as assessments with regard to infrastructure expansion due to line congestion and self-sufficiency analyses using energy and power-based indicators.

3 RESEARCH OBJECTIVES AND METHODOLOGY

As presented in Chapter 2 researching MES and the incorporated infrastructures is essential to determine the impact on existing grids and to possibly derive simulation-based planning recommendations. This requires suitable grid models of the energy carrier grids considered in such a MES approach. All individual grid models must correspond to the model characteristics defined in the overall MES framework. Therefore, it is a challenge to find a suitable level of detail and corresponding spatial and temporal resolutions to achieve conclusive results for all energy carriers with reasonable calculation times. This is still a not fully researched topic in MES modelling.

In this PhD thesis, the issue of suitable level of detail is explored from several points of view on both a modeling and analysis level. Specifically, this leads to two main research objectives, which can be further subdivided.

3.1 Research Objectives

This thesis deals with the development of a suitable modeling approach that allows to create an advantageous level of detail for electrical grid models in MES applications. Therefore, the first research objective (**RO 1**) deals with a novel network reduction method for spatial resolution reduction and suitable grid structures for the validation of this method. The second overall research block (**RO 2**) addresses the impact analysis of MES on electrical grids.

RO 1: Electrical Grid Modeling Approach for MES
Which modelling approach is advantageous for electrical grid models within MES to fulfill all requirements (adequate temporal and spatial resolution as well as computation times) of MES modeling and for which applications can this approach be utilized?

> RO1.1   How can electrical grids be modeled for MES applications to enable high modeling resolution?
>
> RO1.2   What characteristics must be provided by test grid structures to develop and validate the proposed network reduction modeling approach?
>
> RO1.3   For which MES applications (voltage level, grid size, grid structure, etc.) is this novel modeling approach for electrical grid reduction suitable and offers advantages?

RO 2: Electrical Grid Analysis in MES
How can electrical grids be suitably analyzed in MES approaches in terms of power quality, infrastructure assessments and self-sufficiency?

> RO2.1   What are suitable use cases for the analysis of electrical grids in MES in terms of power quality, infrastructure assessments and self-sufficiency?

RO2.2   How do MES influence the electrical grid in terms of power quality and voltage stability, thermal line congestions as well as self-sufficiency?

Within the scope of this work, electrical grid models are developed for an already existing MES framework. This MES framework is the multi-energy carrier simulation framework HyFlow ([14, 51, 52]), which was developed at the Chair of Energy Network Technology. HyFlow thus provides the basic characteristics and requirements for the electrical grid model.

According to the energy model characterization presented in Chapter 2, HyFlow represents an integrated multi-energy, technology-based bottom-up simulation framework that considers the energy carriers electricity, natural gas, and heat as well as their interactions. The modeling approach chosen in HyFlow is a generic and modular cellular approach (Chapter 4.5), which enables the integration of each single-energy carrier model separately into the overall framework. The single-energy carrier grids cover the same geographical area with different hierarchical levels which can be chosen individually for each energy carrier model. Since bottom-up models enable changing timescales, the time horizon as well as the temporal resolution are defined before the calculation but must be equal for each energy carrier. [52]

3.2 Methodology

To answer the questions summarized in Chapter 3.1, three peer-reviewed journals and two conference papers (Appendix A) were published in the scope of this dissertation. How these publications contribute to answering the research questions and how they are connected is illustrated in Figure 8. The purpose of this chapter is to describe the methodological approach used to answer the research questions. The methodological procedures of the individual publications can be found in Appendix A.
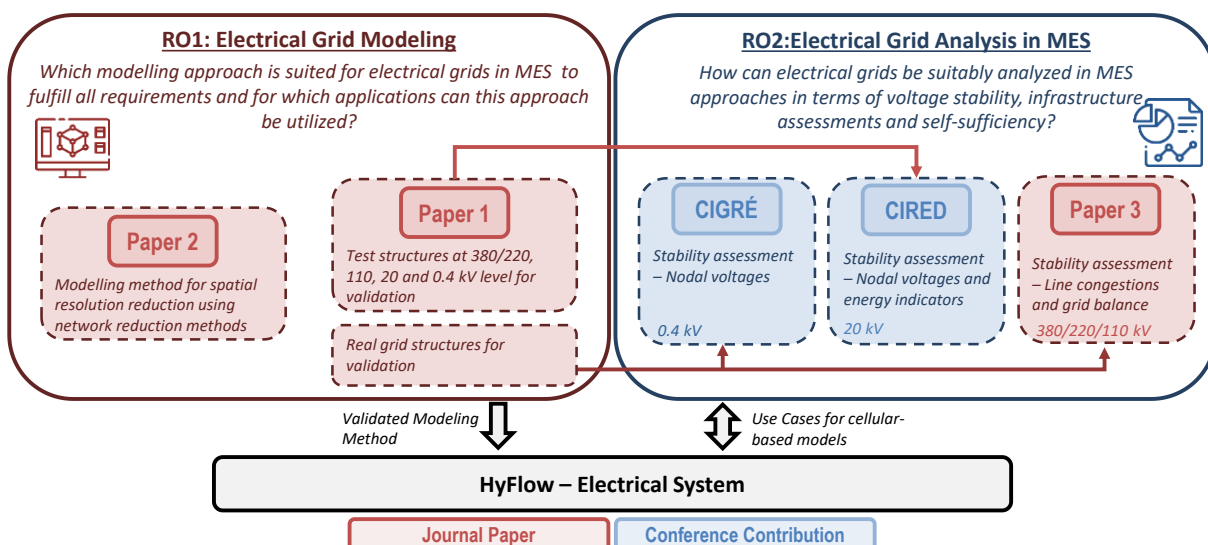

Figure 8: Overview and connections between main publications and the defined research objectives of this work (icons taken from [17])

To address **RO 1**, a comprehensive network reduction-based modeling approach is developed that allows a suitable level of detail for electrical grid models, that can also be interfaced with the other energy carrier grids. As the underlying cellular approach of the grid model is defined in the MES framework HyFlow, the electrical grid modeling approach must also correspond with it. It additionally, must enable a reasonable compromise between modeling accuracy and computation time. Therefore, a novel network reduction method specifically designed for cellular approaches is proposed in this work. Additionally, compared to network reduction methods published in literature, in many applications enhanced modeling accuracy can be achieved in the reduced grid. This novel network reduction method with enhanced modeling accuracy, in particular for reactive power, is published in Paper 2 [23].

> TRAUPMANN, A.; KIENBERGER, T., *Novel Network Reduction Method for Cellular-based Network Models with Enhanced Modeling Accuracy for Multi-Energy-System Approaches*, In: International Journal of Electrical Power and Energy Systems 2022, 137, 107827, doi.org/10.1016/j.ijepes.2021.107827.

As this method is developed in this thesis, conclusive validation has to be conducted. Therefore, test grids with customized properties are designed which are well suited for validating this novel network reduction method to create electrical grid models for MES applications. Thus, as a next step to answer **RO 1** a comprehensive database of grid characteristics within the $ENTSO - E$ ([53]) area is researched and used to develop these synthetic test grids. Publicly available data on line parameters, line lengths, grid structures, as well as research on generation and consumer profiles is used to create synthetic grids for the most common voltage levels (low-, medium-, high- and maximum-voltage). These synthetic grids do not include user-specific data, but they do replicate the behavior of real grids. The novelty behind these synthetic test grids is that they cover not only all common voltage levels, but also corresponding grid sizes, to representatively replicate the real behavior of ENTSO-E (European Network of Transmission System Operators for Electricity) power grids. Moreover, synthetic grids usually do not provide georeferenced data as they do not represent real grids. However, as the presented synthetic grids are modeled via the NEPLAN software ([54]) allowing for the provision of a graphical model which is usually not the case for synthetic grids. Additionally, the corresponding time series data are included, making them versatile and especially suitable for RES integration studies. Closer information on the data used and the approach is published in Paper 1 [55]:

> TRAUPMANN, A.; KIENBERGER, T., *Test Grids for the Integration of RES − A Contribution for the European Context*, In: Energies 2020, 13, 5431, doi.org/10.3390/en13205431.

Subsequently, the novel network reduction method is applied to all synthetic test grids and thus validated, allowing application areas and recommendations to be derived. A more

detailed description of the methodology as well as influencing factors for the best possible application are described in Paper 2.

The second overall research objective **RO 2** is answered via three individual use cases, each of which implements the developed electrical modeling approach in HyFlow and uses different analyses techniques to investigate the effects of MES on the electric grid.

In the first use case, an anonymized grid section of a real 0.4 kV low-voltage (LV) grid, which is available at the Chair of Energy Network Technology, is used for the calculation purposes. In this use case, photovoltaic (PV) power is massively expanded. Thus, the influence of the flexibility of integrating of heat pumps and distributed thermal storages in the overall MES model on power quality and stability is analyzed. A detailed description of this use case and the results obtained are described in CIGRÉ [56].

TRAUPMANN, A.; GREIML, M.; KIENBERGER, T., *Reduction Method for Planning Cross-energy Carrier Networks in the Cellular Approach Applicable for Stability Assessment in Low-Voltage Networks*, In: e&I Elktrotechnik und Informationstechnik, CIGRÉ 2020, doi.org/10.1007/s00502-020-00851-4.

The second use case performs a similar analysis, except that the considered test grid represents the synthetic test grid at the 20 kV medium-voltage (MV) level from Paper 1 for the application of the novel network reduction method from Paper 2. In this use case, both PV and wind power are massively expanded. Consequently, the influence of hybrid flexibility options in MES (integration of heat pumps and Power-to-Gas (PtG) units) is analyzed with respect to power quality and stability issues. Additionally, self-sufficiency analyses are performed and the corresponding contribution of MES. This use case is described in detail in CIRED [57].

TRAUPMANN, A.; GREIML, M.; KIENBERGER, T., *Equivalent Cellular-based Electrical Network Models for Voltage Regulation using Hybrid Conversion Technologies at the Medium-Voltage Level*, In: Conference Proceedings CIRED 2021, Paper 0304.

The last use case for the analysis of electrical grids represents a comprehensive study. It considers Austria's 110 kV high-voltage (HV) and 220/380 kV maximum-voltage (MaxV) grids to investigate hybrid conversion technologies (Gas-to-Power (GtP) and PtG units) in MES as re-purposing options at decommissioned coal-fired power plant (CFPP) sites. For this purpose, cost-optimal operating profiles are created that consider the electricity and natural gas markets as well as the system service market for balancing power. The impact of this optimized use of hybrid flexibility options on the electric grid is therefore additionally analyzed. Thermal line congestions are investigated, and power quality and stability analyses are performed. A detailed description of this use case is given in Paper 3 [58].

TRAUPMANN, A.; GREIML, M.; STEINEGGER, J.; KÜHBERGER, L.; KIENBERGER, T., *Analyzing Sector Coupling Technologies for Re-purposing Coal-Fired Power Plants in MES – Case Study for the ENTSO-E Grid Area*, In: IET Energy System Integration, John Wiley & Sons, Inc., 2022, DOI: 10.1049/esi2.12087.

4 THEORETICAL BACKGROUND

4.1 Electrical Grids – Structures, Grid Characteristics, Electrical Equipment and Parameters

In the high-voltage three-phase transmission system, electrical energy is transported in the transmission and distribution grids at hierarchical voltage levels. A grid thus includes all electrical equipment (e.g., generators, consumers, lines, transformers) that is connected to the same nominal voltage. In the electrical energy supply system, a distinction is made between the transmission grid, the subtransmission grid and the distribution grid. The transmission grid transports energy efficiently and with low losses over long distances at the 380 and 220 kV-voltage levels. The subtransmission grid transports energy trans-regionally at the 110 kV-voltage level and the distribution grid provides energy regionally or locally at the medium- and low-voltage levels (30 – 0.4 kV-voltage levels). [59]

The grid levels start at the highest level 1 designating the maximum-voltage level, where the electricity generated in the power plants and neighboring countries is fed into the transmission grid. All odd grid levels represent transmission and distribution at the respective voltage level. The even grid levels denote the transformation between the voltage levels. The lowest grid level 7 represents the distribution at the low-voltage level to the household consumers. [60] An overview over the electrical system is illustrated in Figure 9 [59].
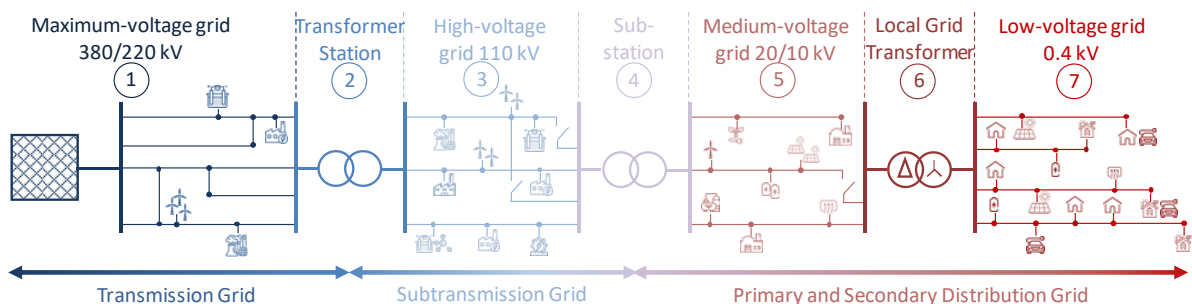
Figure 9: Overview of the structure of the electrical energy system, voltage levels and grid topologies including the grid levels in circles (adapted from [59, 60], icons taken from [17])

The grid topologies (cf. Figure 9) are categorized into 3 basic structures, the radial, ring, and mesh structures. Modifications of these 3 basic structures can occur due to different distributions of load densities. What all three structures have in common is that they have operational disconnection points which are actuated in the event of faults, during maintenance or for servicing purposes and can thus disconnect a grid part from the rest of the grid. However, this results in at least a temporary change in topology. [59]

Radial Structures: In radial grids the feeder lines form a radial structure from the feed-in point which is usually the transformer substation connected to the upper voltage level. These feeders are called tap lines. These structures usually occur at lower voltage levels primarily at the low-voltage level for supplying households. While radial structures offer advantages regarding lower requirements for grid protection, in general relatively high voltage drops occur due to higher line losses. An example of radial structures is also illustrated in Figure 9. [59]

Ring Structures: Ring structures contain openly operated ring topologies in normal operation. In contrast to radial grids, they are more complex and interconnected. However, they also require higher grid protection such as automatic disconnections of grid parts from the rest of the grid. Thus, only those grid sections affected by faults can be disconnected, while the remaining consumers continue to be provided a secure and reliable power supply. Such a ring structure is implemented mainly on higher voltage levels (medium- to high-voltage), but can also occur in the low-voltage, provided that higher load densities are present. An exemplary representation of these ring structures is also illustrated in Figure 9. [59]

Mesh Structures: Meshed grids are fully formed ring structures, in which electrical nodes and lines are supplied from several sides and thus provide the highest supply reliability. The level of grid protection is also advanced for this structure, so that faults are limited to a small grid section. As also illustrated in Figure 9, these structures are mainly implemented at the maximum- and high-voltage level (380/ 220/ 110 kV), but can also occur to some extent at the medium-voltage level. [59]

While these structures, represent the basic topologies, the actual design of the grids additionally depends on the characteristics of the area in which they are built, i.e., whether the grid is in an urban, suburban, or rural area. Since load densities and line lengths vary depending on the area (due to the number and distances of the consumers), there are also different requirements for the grids and the connected equipment. [61, 62] Generally, in urban areas there is a high load density (> 30 MVA/km^2 [62]) requiring the utilization of strong lines. Electrical line strength refers to the diameter and material of the lines, and thus ultimately to the line parameters (explained below) [61]. However, in urban grids there are short distances between the customers, therefore, line lengths are rather short. Thus, grids located in urban areas are primarily structured in ring topologies. In contrast, rural areas have lower load densities (< 5 MVA/km^2 [62]) and larger distances between grid customers. Therefore, electrical lines do not have to be as strong as in urban areas, but longer line lengths are needed [63]. Additionally, this results in mainly radial structures in such rural areas [63]. Due to these characteristics urban area grids tend to have thermal line congestion issues while rural areas usually struggle more often with nodal voltage exceeding. [64]

There is also a distinction between two different types of electrical lines: overhead lines and cables. While cables are primarily used in urban areas (at medium- and low-voltage) for safety and appearance reasons, overhead lines are mainly used at the high- and maximum-voltage levels due to their easier accessibility in case of faults. Overhead lines at the low- and medium-voltage level are only utilized in rural areas to some extent. Cables at the maximum-voltage levels are rarely used, however cables are installed in isolated cases (mostly urban areas) at the high-voltage level. [61] These are economically only feasible for short distances, but offer certain operational advantages, as their large shunt capacities attenuate harmonics [62].

The strength of electric lines depends on the diameter and thus the cross-section of the line as well as its material. Larger diameters and thus larger conductor cross-sections represent stronger electrical lines. For the conductor material, either copper, aluminum or aluminum alloys with magnesium, silicon and iron are used, whereby the alloy allows higher mechanical strength and is therefore mainly used in overhead lines. In line theory for modeling electrical lines, both diameter and material are represented by the line parameters, which also represent other physical influencing factors. [61]

The line parameters are the line resistance R', the line inductance L', the line shunt capacitance C', and the line conductance G'. The line parameters are usually represented by specific units, thus they are divided by the line length l. The specific line resistance R' accounts for the real line losses in the conductor. Thus, conductor diameter and conductor material are included in the specific line resistance R'. In general, the specific line inductance L' represents the magnetic field induced due to power transmission, while the specific shunt capacitance C' represents the corresponding electric field. [61] Overhead lines usually have a higher specific line inductance L' as a large conductor loop is created and the capacitors formed with parallel lines are small. In contrast, for cables the electrical lines form an additional capacitor with the ground, which increases the specific shunt capacitance C'. [65] The specific line conductance G' describes insulation losses and losses in the dielectric including leakage and corona currents However, this line parameter G' depends on a large number of variable factors, such as atmospheric weather conditions, conductivity properties of the surrounding material and the insulation as well as contamination on the lines. Therefore, no suitable modeling of these factors is available. As a result, the specific line conductance G' it is usually neglected. For overhead lines, the specific line conductance G' can be neglected anyway, as leakage and corona currents are relatively small compared to the other parameters. [66] Figure 10 illustrates the π-electrical line equivalent circuit including the line parameters and the line voltages and voltage losses as well as line currents for an ohmic-inductive current $\underline{I_2}$.
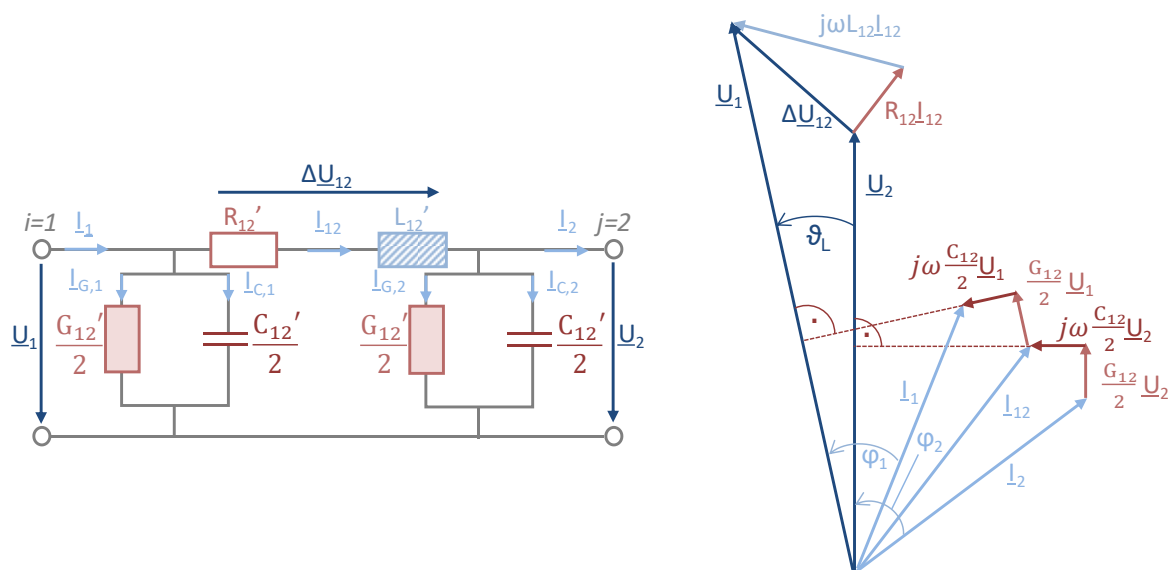
Figure 10: π-Electrical line equivalent circuit and magnetic and magnetic and electric field of two wire lines (adapted from [59, 61])

Table 2 shows the line parameters R', L', C' and usual line lengths l at the respective voltage levels for both overhead lines and cables.

Table 2: Specific line parameters of electrical lines at all voltage levels [62, 66–68]

	Line Type	R' (Ω/km)	X' (Ω/km)	C' (nF/km)	Length (km)
0.4 kV	Overhead Line	0.29-1.87	0.29-0.40	negligible	0.03-1.00
	Cable	0.14-0.86	0.08	negligible	
10-60 kV	Overhead Line	0.06-0.31	0.28-0.42	negligible	0.10-20.00
	Cable	0.12-0.31	0.11-0.21	216-456	
110 kV	Overhead Line	0.06-0.41	0.18-0.40	9-14	0.30-65.00
	Cable	0.06-0.15	0.14-0.22	112-144	
220 kV	Overhead Line	0.01-0.09	0.26-0.42	8.49-14.23	1.50-125.00
380 kV	Overhead Line	0.01-0.17	0.25-0.39	11.64-21.25	0.20-165.00

When modeling electrical lines, the electrical length of the line is also a factor. If a line is *electrically short*, then it can be modeled by a single π-equivalent line circuit element. If a line is *electrically long*, it can be described in approximation by a series of several π-elements. [59] In general, overhead lines at the low- and medium-voltage can always be modelled by electrically short lines. At higher voltage levels and for cables at the high- and maximum-

voltage level, the assumption validity of an electrically short line must be verified. [62] The maximum length of electrically short overhead lines is about 250 km, for cables it is about 50 km [61].

The equivalent circuit of electrical lines corresponding to Figure 10 is a two-port, i.e., an electrical circuit which has two terminals or connectors each at the input and output. Thus, due to this structure the two-port can be described by various matrix forms which simplify calculations. [69] Exemplarily, the chain matrix form offers advantages when calculating several consecutively connected two-ports i.e., electrical lines within a grid. By multiplying the individual chain matrices of the consecutively connected two-port lines, all two-ports can be represented by one two-port element in the grid model. Thus, this matrix form for two-ports is suitable primarily for an accurate calculation of voltage drops and line losses. [61] In Figure 11 voltage drops and line losses using the equivalent circuit are illustrated.
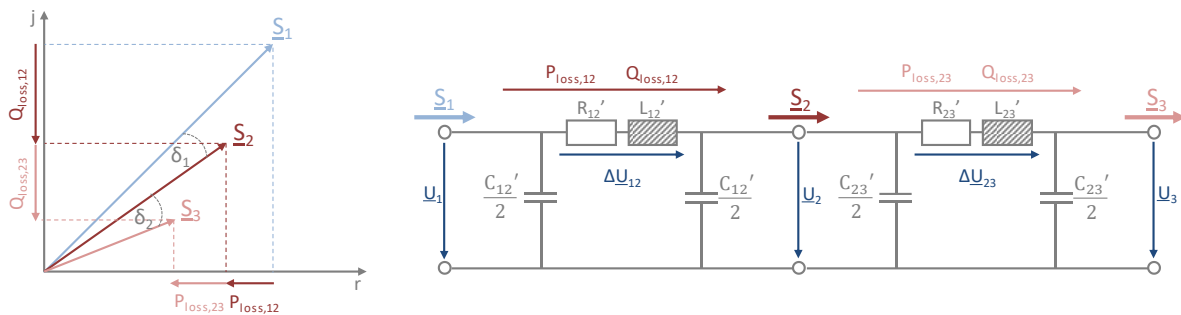
Figure 11: Voltage drop and line loss calculation for the equivalent line circuit (adapted from [61])

4.2 Reactive Power in the Grid

A transmission line can only transfer electrical energy if its own reactive power demand is provided to allow the necessary magnetic and electric fields to build up [70]. To describe this operating behavior (voltage behavior, power behavior, compensation, transmission capacity) of electrical lines, the characteristic (or surge) impedance is used, which is calculated according to Equation (1). As can be seen in Equation (1), the characteristic impedance is in general complex. [71]

$$\underline{Z}_W = \sqrt{\frac{R' + j \cdot \omega \cdot L'}{G' + j \cdot \omega \cdot C'}} \tag{1}$$

However, as the real component of the characteristic impedance is only relevant when determining the line losses, a lossless line is often assumed for studies of the operating behavior of real electric lines. In this case, the effective resistance R' is negligible ($R' = 0$) and the insulation resistance is infinitely high ($R_{is}' \to \infty$ resulting in $G' = 0$). This results in an active characteristic impedance, which simplifies the calculations of electrical line operating

behavior. The calculation of the characteristic impedance of a lossless line is illustrated in Equation (2). [59]

$$Z_W = \sqrt{\frac{L'}{C'}} \qquad \qquad \textbf{(2)}$$

If the line is loaded at the end by the characteristic impedance Z_W, the inductive reactive power due to the line inductance and the capacitive reactive power due to the shunt capacitance are equal. This electrical power is referred to as natural power P_{nat} (cf. Equation (3)) and thus represents an active power. The transmission of natural power entails a constant voltage profile (voltage at the end of the line corresponds to the nominal voltage $\underline{U}_{nN}$ [72]) and thus is associated with most efficient power transmission. However, for physical reasons, the natural power cannot always be transmitted because the thermal, voltage and active power stability is exceeded. [61]

$$P_{nat} = 3 \cdot \left(\frac{\underline{U}_{nN}}{\sqrt{3}}\right)^2 \cdot \frac{1}{Z_W} = \frac{U^2{}_{nN}}{Z_W} \qquad \qquad \textbf{(3)}$$

In normal operation P_{nat} is rarely transmitted. Mainly in long lines it is the aim to remain in natural operation, as no reactive power has to be transmitted and the voltage drop can be kept at a minimum. [59]

If lines are operated below the natural power, exemplarily in low-load operation or in open-loop operation ($S_2 < P_{nat}$), they behave like a capacitive load at the beginning of the line. This can lead to voltage increases at the end of the lines. If lines are operated above the natural power ($S_2 > P_{nat}$), as is the case with shorter lines, they behave like an inductive load at the beginning of the line. This results in a larger voltage drop at the end of the line. [59, 72]

Overhead lines are usually operated above the natural power since their rated thermal power S_{th} is higher than their natural power. In contrast, cables are usually operated below their natural power, as their natural power is higher than the corresponding rated thermal power S_{th} which presents as the limiting factor. [72] The rated thermal power S_{th} of a cable is lower than for an overhead line due to the higher insulation and the resulting impeded removal of heat [61]. Cables therefore behave like a capacitor over their entire operating range, while overhead lines behave like an inductor under greater loads [61]. Figure 12 shows the corresponding reactive power consumption Q_{loss} of an overhead line and a cable with equal cross-section und thus equal active power losses P_{loss} dependent on the transmitted power [61]. This shows that the reactive power demand Q of a line depends on the transmitted power S_2. The mathematical correlation for this demand Q is provided in Equation (4) which is valid for electrically short lines up to 250 km of line length [71].

$$Q = Q_L - Q_C = 3 \cdot \omega \cdot L \cdot I^2 - \omega \cdot C \cdot U^2 = Q_C \cdot \left[\left(\frac{S_2}{P_{nat}}\right)^2 - 1\right] \qquad \textbf{\textit{(4)}}$$

For an average 380 kV line (cf. Table 2) with a natural power of 605 MW and a characteristic impedance of 240 Ω and an assumed transmitted power S_2 of 1.5·P_{nat}, the inductive charging power or reactive power demand Q of the line is about 80 Mvar/100km. [71]
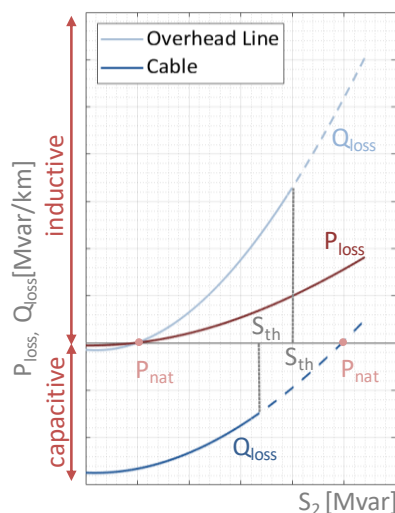
Figure 12: Reactive power losses Q_{loss} for overhead lines and cables at the same voltage level and with the same cross-section and therefore same active power losses P_{loss}, (adapted from [61, 71])

As discussed, if P_{nat} cannot be transmitted, higher losses occur, which is very common in real grid applications. Thus, accurate modeling of losses is essential to represent the grid state and maintain supply security.

4.3 Electrical Grid Analysis

4.3.1 Load Flow Calculation

One of the main tools for grid analysis is the load flow calculation, in which the steady-state voltages, currents, power flows as well as grid losses and reactive power demand are determined. These parameters define the operational state of the grid. Thus, the load flow calculation is an essential operation management and planning tool of the electrical power system for tasks such as monitoring the grid state and grid security. [72, 73]

To perform a load flow calculation, the overall grid must be described using mathematical equations. This mathematical description is provided by the nodal equation system in matrix form, which correlates nodal currents $\underline{I}$ and nodal voltages $\underline{U}$ according to Ohm's complex law. This nodal equation system in matrix form is shown in Equation (5). In this Equation (5), $\underline{Y}$ represents the nodal admittance matrix which includes the admittances connecting the nodes. [61]

$$\begin{pmatrix} \underline{I}_1 \\ \underline{I}_2 \\ \vdots \\ \underline{I}_n \end{pmatrix} = \begin{pmatrix} \underline{Y}_{11} & \underline{Y}_{12} & \cdots & \underline{Y}_{1n} \\ \underline{Y}_{21} & \underline{Y}_{22} & \cdots & \underline{Y}_{2n} \\ \vdots & \vdots & \ddots & \vdots \\ \underline{Y}_{n1} & \underline{Y}_{n2} & \cdots & \underline{Y}_{nn} \end{pmatrix} \cdot \begin{pmatrix} \underline{U}_1 \\ \underline{U}_2 \\ \vdots \\ \underline{U}_n \end{pmatrix}$$

(5)

However, for the formulation of the load flow problem, the load flow equations are expressed in terms of nodal powers rather than nodal currents as there are advantages in separating the known and unknown variables in the system [61]. An overview of known and unknown variables is illustrated in Table 3, resulting in the three different node types according to which the equations are ultimately defined [61, 71, 73].

Table 3: Classification of nodes in load flow calculations and their known and unknown variables [61, 71, 73]

Node Type	Known Variables	Unknown Variables	Definition
PQ-Node	P and Q	U and ϑ	Load Node $I < 0$
PV-or PU-Node	P and U	Q and ϑ	Generator Node $I > 0$
Slack-Node	U and ϑ	P and Q	Balance/Reference Node $I = 0$

The corresponding power equation system to Equation (5) is given in Equation (6).

$$\underline{S}_i = 3 \cdot \underline{U}_i \cdot \underline{I}_i^* = 3 \cdot \underline{U}_i \cdot \sum_{k=1}^{n} \underline{Y}_{ik}^* \cdot \underline{U}_k^* = \sum_{k=1}^{n} 3 \cdot U_i \cdot Y_{ik} \cdot U_k \cdot e^{j \cdot \left(\vartheta_{ik} - \frac{\pi}{2} - \alpha_{ik} \right)}$$

(6)

In Equation (6), ϑ_{ik} corresponds to the respective phase angle between $\underline{U}_i$ and $\underline{U}_k$ and α_{ik} is the admittance angle. It is possible to split Equation (6) into a real and imaginary component, which is also done for the load flow calculation, as reactive power is only specified at the PQ-nodes. The real and imaginary components are illustrated in Equations (7) and (8). [61]

$$P_i = \sum_{k=1}^{n} 3 \cdot U_i \cdot Y_{ik} \cdot U_k \cdot sin(\vartheta_{ik} - \alpha_{ik})$$

(7)

$$Q_i = - \sum_{k=1}^{n} 3 \cdot U_i \cdot Y_{ik} \cdot U_k \cdot cos(\vartheta_{ik} - \alpha_{ik})$$

(8)

In certain cases (e.g., medium- and high-voltage grid) it can be assumed that the admittance angle α_{ik} as well as the phase difference between the voltages due to close meshing structures $(\vartheta_i - \vartheta_k)$ is small, so that the approximations $sin(x) \rightarrow x$ and $cos(x) \rightarrow 1$ apply (cf. Equations (9) and (10)). However, in general active power is strongly dependent on the phase angle ϑ_{ik}, while reactive power is almost independent of the phase angle ϑ_{ik}, but strongly depends on voltage magnitude U. [61]

$$P_i \approx 3 \cdot U_i^2 \cdot Y_{ii} \cdot \alpha_{ii} + \sum_{k=1, k \neq i}^{n} 3 \cdot U_i \cdot Y_{ik} \cdot U_k \cdot (\vartheta_{ik} - \alpha_{ik})$$

(9)

$$Q_i \approx 3 \cdot U_i{}^2 \cdot Y_{ii} - \sum_{k=1,k\neq i}^{n} 3 \cdot U_i \cdot Y_{ik} \cdot U_k \qquad \textbf{(10)}$$

Although there are different methods for numerically solving the system of power equations, the Newton-Raphson method is presented in this work as it is generally one of the most common and efficient methods ([71]) and has been used in this work.

The basic procedure for this method is a linearization of the equation system at the respective operating point (starting value of nodal voltages), via a Taylor series approximation which is terminated after the first term. Then, the linearized system is solved resulting in an improved working point, which serve as the starting values for the next iteration. This continues until calculated nodal powers fall below an error limit and a sufficiently accurate solution is obtained. [72] The Taylor series approximation is demonstrated in Equations (11) and (12), therefore, each node is represented in the calculation via two equations [71]. The vector *x* represents the nodal phase angles and voltages within the grid divided by the voltages of the previous iteration [71].

$$\left(\frac{\partial \Delta P}{\partial x}\right)_{(v)} \cdot \Delta x_{(v+1)} + \Delta P_{(v)} = 0 \qquad \textbf{(11)}$$

$$\left(\frac{\partial \Delta Q}{\partial x}\right)_{(v)} \cdot \Delta x_{(v+1)} + \Delta Q_{(v)} = 0 \qquad \textbf{(12)}$$

Using these Equations (11) and (12) the system of equations in matrix form for the Newton-Raphson algorithm is obtained, as depicted in Equation (13). [71, 72]

$$\begin{bmatrix} \dfrac{\partial \Delta P}{\partial x} \\ \dfrac{\partial \Delta Q}{\partial x} \end{bmatrix}_{(v)} \cdot \Delta x_{(v+1)} = \begin{bmatrix} H & N \\ M & L \end{bmatrix}_{(v)} \cdot \Delta x_{(v+1)} = J_{(v)} \cdot \Delta x_{(v+1)} = - \begin{bmatrix} \Delta P \\ \Delta Q \end{bmatrix}_{(v)} \qquad \textbf{(13)}$$

The matrix *J* denotes the Jacobian or functional matrix whose entries are the change values of the starting vector for nodal voltages and voltage angles and must therefore be calculated for each iteration. The Jacobian matrix composes the sub-matrices *H*, *M*, *N* and *L*, which represent the derivatives of the known parameters (active and reactive power) with respect to the unknown parameters (voltage magnitude and voltage angle) depending on the node type. Slack nodes do not appear in the equation system of the load flow calculation, the parameters of the Slack nodes are determined via balancing of load flows and grid losses. PV nodes are only represented by one equation for active power. [74]

As soon as the calculated nodal powers P_{calc} and Q_{calc} fall below the predefined error limit ε (cf. Equation (14)), the iterations are terminated and the load flows and grid losses can be determined based on the nodal voltages and voltage angles obtained from the iteration. [72]

$$\begin{bmatrix} \Delta P \\ \Delta Q \end{bmatrix}_{(v)} = \begin{bmatrix} \left| P_{spec} - P_{calc}^{(v)} \right| \\ \left| Q_{spec} - Q_{calc}^{(v)} \right| \end{bmatrix} \leq \varepsilon \qquad (14)$$

After terminating the iterations and thus obtaining the complex nodal voltage results, the load flows, the line losses as well as the balance at the slack node still have to be determined. Generally, two load flows are defined over a line. Using the example of the line in Figure 10, one in direction $i \to j$ and one in the opposite direction $j \to i$. Load flow $i \to j$ is the load flow that enters the line at Node i and thus includes the line losses that occur in the line in order to provide the demanded power to the consumer at the end of the line. Load flow $i \to j$ is therefore the one usually obtained from load flow programs. Load flow $j \to i$ is the load flow that reaches Node j and is thus loss-free. It represents only the power that must be transferred to the consumer or is transferred to the next line $(j \to k)$. By definition, the load flow $j \to i$ results in a negative value obtained from the load flow calculation. Equations (15) and (16) describe the calculation of the complex load flow $\underline{S}_{ij}$ over a line and the resulting line losses $\underline{S}_{loss,ij}$. [66, 72]

$$\underline{S}_{ij} = \underline{U}_i^* \cdot \left(\underline{U}_i - \underline{U}_j \right) \cdot \left(-\underline{Y}_{ij} \right) + \underline{U}_i^* \cdot \underline{U}_i \cdot \underline{B}_{ij} \qquad (15)$$

The admittance $\underline{Y}_{ij}$ contains only the series components of the line (R_{ij} and L_{ij}) while $\underline{B}_{ij}$ contains the shunt elements (mostly only capacitive, only $\underline{C}_{ij}$). $\underline{U}_i^*$ represents the conjugate complex nodal voltage at the input node, which together with the line elements ($\underline{Y}_{ij}$ and $\underline{B}_{ij}$) represents the respective current. The difference between input and output voltage $\underline{U}_i$ or $\underline{U}_j$ represents the voltage drop of the line.

$$\underline{S}_{loss,ij} = \underline{S}_{ij} + \underline{S}_{ji} \qquad (16)$$

Total grid losses are calculated by summing up all individual line losses. The power at the slack node is calculated by summing all loads and generations within the grid. [72]

4.3.2 Power Quality and Voltage Stability

The power quality within the grid includes parameters such as voltage stability, flicker, or harmonics. Voltage stability is the main focus of this work. It can be defined as the ability of an electric grid to maintain the nodal voltages at all grid nodes within this range [75]. Voltage stability also depends on a number of parameters, including voltage magnitude which is defined by the voltage range ([76, 77]) [78]. Violations of the admissible voltage range can occur due to sudden high loads, grid disturbances (e.g. line outages or power plant failures) or high (distributed and volatile) energy generation [79]. The admissible voltage range for the medium- and low-voltage grid is illustrated in Figure 13. Nodal voltage stability or static (loads are assumed to be constant) reactive power stability describes the ability of a power system to maintain balanced voltages at grid nodes after a major disturbance has occurred in the system, disrupting normal operating conditions [80]. A voltage collapse occurs if voltages drop

significantly below the lower limit of the voltage range, thus endangering grid stability [79]. If the voltage range is considerably exceeded electrical equipment (e.g., generators, electric motors, transformers, end-user devices, inverters, etc.) in the grid is damaged leading to reduced availability and impeding both energy generation and power transmission [79, 81].
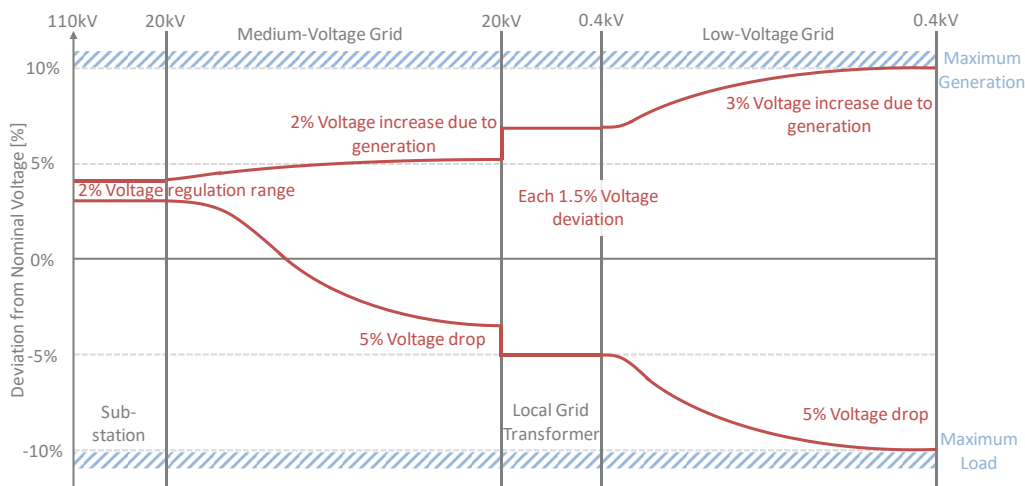

Figure 13: Admissible voltage range in the grid (adapted from [82])

Both cases strongly depend on the reactive power present in the grid [70]. The cause of voltage instabilities and thus of exceeding the admissible voltage range is an unbalanced reactive power balance in the grid, i.e., between required and available reactive power [75]. As loads and generation units evolve and increase in the future power system, the stress on the grid and thus the grids become more susceptible to voltage stability issues [75, 83]. This increasingly high utilization of the grids can lead to operation points above the natural power of the lines and results in increased reactive power demand [84]. To compensate for this, reactive power must be provided locally, as transporting reactive power puts additional stress on the grid [75]. A lack of reactive power has the same effect as grid loads, thus a voltage drop occurs, whereas a surplus of reactive power affects the grid like a generation unit and results in a voltage increase [85].

The correlation between voltage and active or, in particular, reactive power transmission can be illustrated as follows: As a result of the transmitted active and reactive power (cf. Equations (17) and (18)) of a line, a correlation is established after eliminating the phase angle ϑ_L including nodal voltage, active and reactive power (cf. Equation (19)). If this Equation (19) is expressed in p.u. values, Equation (20) is obtained which describes the grid characteristics regarding static active and reactive power stability. [86, 87]

$$P = \frac{U_1 \cdot U_2}{X} \cdot sin\vartheta_L \qquad (17)$$

$$Q = -\frac{U_2^2}{X} + \frac{U_1 \cdot U_2}{X} \cdot cos\vartheta_L \qquad (18)$$

$$U_2{}^2 = \frac{U_1}{2} - X \cdot Q \pm \sqrt{\frac{U_1{}^4}{4} - X^2 \cdot P^2 - X \cdot Q \cdot U_1{}^2} \qquad (19)$$

$$u = \sqrt{\frac{1}{2} - q \pm \sqrt{\frac{1}{4} - p^2 - q}} \qquad (20)$$

A graphical representation of Equation (20) is illustrated in Figure 14 (a). In addition, Figure 14 (b) shows the cross-section of Figure 14 (a) for a constant active power (constant power factor $\cos\varphi$) and describes how the stability can be assessed here.
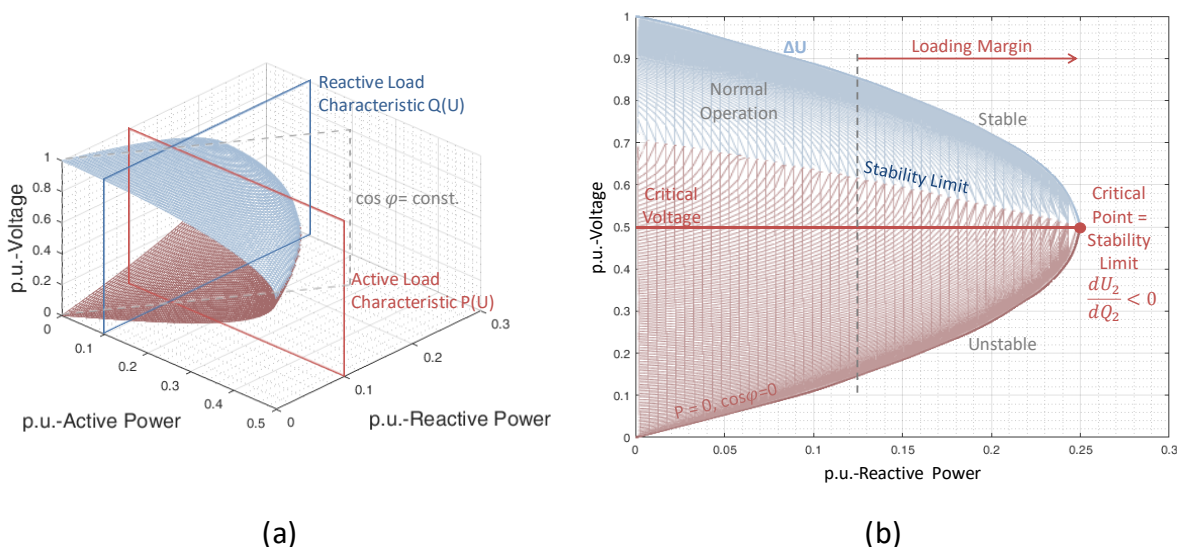

| (a) | (b) |

Figure 14: (a) Grid characteristics (P(U) and Q(U)) regarding static active and reactive power stability and (b) Voltage behavior visualized in the QU-diagram (adapted from [83, 88])

As demonstrated in Figure 14 and discussed in section 4.3.1, the voltage (magnitude) within the grid strongly depends on the reactive power and therefore underlines the importance of reactive power and its balance in the grid regarding voltage drops. [88]

4.3.3 Thermal Line Congestions

Line overloads occur when the grid´s distribution lines are no longer capable of transmitting the necessary power due to exceeding thermal limits [89]. The previously mentioned higher utilization of the grids due to increasing energy demand and RES generation leads to an additional reactive power demand [84]. As a result, congestion management and corresponding strategies become increasingly important [90]. At the same time this results in a higher current load on the grid components [91]. Higher current loads on the electrical equipment such as electrical lines can lead to a temperature rise that damages their material above a certain temperature [92]. The electrical parameters of the grid components (e.g. line parameters for electric lines) therefore limit the maximum transmittable operating currents

and powers [92]. Table 4 provides an overview over maximum currents and operating temperatures for commonly utilized electrical lines:

Table 4: Maximum line currents and operating temperatures of electrical lines [62, 93, 94]

	Line Designation	Line Type	$I_{r,max}$ (A)	T_{max} (°C)
0.4 kV	NAYY 4 x 150 SE	Cable	270	70
	94-AL1/15-ST1A	Overhead Line	350	80
10-60 kV	NA2XS2Y 1 x 240 RM/25	Cable	422	90
	184-AL1/30-ST1A	Overhead Line	535	80
110 kV	N2XS(FL)2Y 1 x 300 RM/35	Cable	588	90
	305-AL/39-ST 1A	Overhead Line	740	80
220 kV	382-AL1/49-ST1A	Overhead Line	840	80
380 kV	679-AL1/86-ST1A	Overhead Line	1150	80

Consequences of these current overloads are forced load-shedding by cutting off grid customers or planned outages for supply reliability and security protection [89]. Current measures to prevent line congestions are grid expansion, utilization of protection relays as well as dynamic thermal rating [89]. Dynamic thermal rating of electrical lines factors in weather conditions such as temperature, wind speed and direction and thereby allows for a dynamic adaption of line capacities which is currently used at critical grid points [89, 95, 96]. Another possibility to increase the transmission capacity of electrical (overhead) lines and thus avoid grid expansion is the usage of high-temperature conductors [97]. These allow up to 90% higher current carrying capacity compared to standard cables, but at the same time have a higher reactive power requirement and generate higher losses [97]. However, high-temperature conductor cables can withstand temperatures of up to 200 °C without significant operational restrictions (sagging) [98]. Additionally, Re-dispatch is a measure to prevent congestions. For Re-dispatch, the transmission system operator (TSO) intervenes in situations with line congestion and gives instructions to power plant operators to change their planned power plant dispatch accordingly to avoid grid congestions [99].

4.3.4 Short-Circuit Analysis

Primarily, a short-circuit analysis examines for different grid topologies if the potential short-circuit powers can be controlled by the circuit breakers within the grid. It is therefore an important tool in operational grid management and is already determined during grid planning. The short-circuit power $S_{k,N}''$ (cf. Equation (21)) at a certain grid node N is calculated from the nominal voltage U_N and the initial short-circuit current $I_{k,N}''$. [59]

$$S_{k,N}'' = \sqrt{3} \cdot U_N \cdot I_{k,N}'' = \frac{1.1 \cdot U_N}{\sqrt{3} \cdot Z_N} \tag{21}$$

The short-circuit power is a measure of the internal resistance of a grid. Therefore, the grid or short-circuit impedance $\underline{Z}_N$ is also determined at the respective grid point. This impedance results from the series impedance of the electrical equipment located in the short-circuit path of this grid node and can thus consist of generator impedances $\underline{Z}_G$, overhead line and cable impedances $\underline{Z}_O$ and $\underline{Z}_K$ as well as transformer impedances $\underline{Z}_T$. Figure 15 (a) shows an example of the single-phase equivalent circuit of the short-circuit current path with equipment impedances. [59]

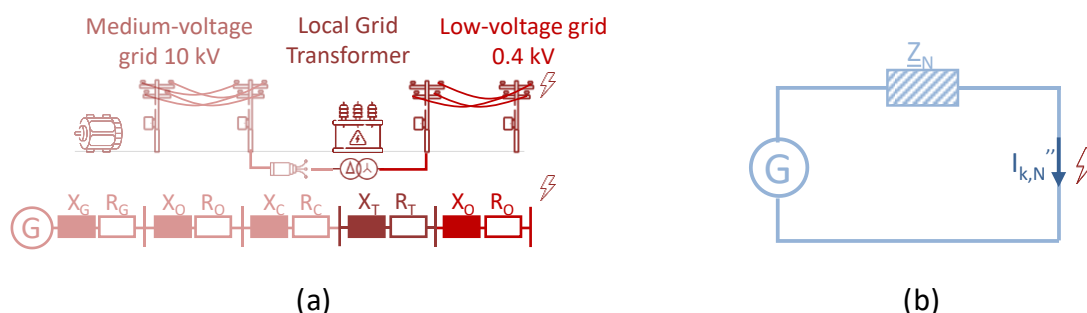(a)   (b)

Figure 15: Single-phase equivalent circuit of the (a) short-circuit current path with equipment impedances and (b) simplified equivalent circuit for short-circuit calculations (adapted from [59], icons taken from [17])

Equation (22) shows the corresponding calculation of the total impedance at grid node N where r_t represents the transformation ratio between the voltage levels This consideration enables representing the grid simplified by a source voltage and a grid impedance (cf. Figure 15 (b)). [59]

$$\underline{Z}_N = \frac{\underline{Z}_G}{r_t{}^2} + \frac{\underline{Z}_O}{r_t{}^2} + \frac{\underline{Z}_C}{r_t{}^2} + \underline{Z}_T + \underline{Z}_O = \sum R + j \cdot \sum X = R_N + j \cdot X_N \tag{22}$$

As the short-circuit power is a function of the short-circuit impedance $\underline{Z}_N$, it is thus also a measure of voltage quality and the interference resistance of the grid. It can be used to assess grid behavior and to analyze and evaluate structural aspects within the grid. Exemplarily, parallel lines have significant influence on the short-circuit impedance; the more parallel lines (and thus the higher the meshing) in the grid, the higher the short-circuit power. Other factors influencing short-circuit power are the number of synchronous machines in the grid, the degree of meshing and the switching state, as well as line lengths and the presence of inductance coils for power factor correction. [62]

4.3.5 Energy and Power-Based Indicators

The energy and power-based indicators are a way of analyzing energy systems within a defined area and provide information about the efficiency regarding energy use within that area. These energy and power-based indicators include the degree of energy self-sufficiency

ε_{ESS}, the degree of power self-sufficiency ε_{PSS}, and the self-consumption ratio ε_{SCR}. [100] The parameters necessary for the calculation of the energy and power-based indicators are presented exemplarily in Figure 16 and include power and energy values for consumption and generation ($P_L(t)$, E_L, $P_G(t)$ and E_G) within the respective area for the chosen time frame as well as the self-consumption E_{SC}. E_L represents the area under the consumption power curve $P_L(t)$, E_G equally represents the area under the generation power curve $P_G(t)$.
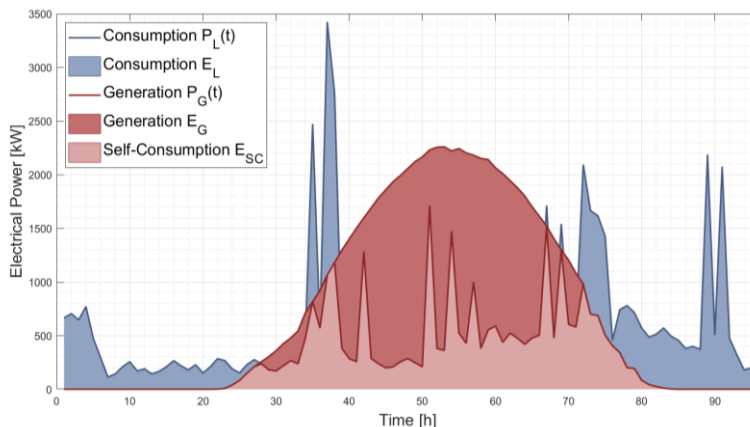

Figure 16: Exemplary illustration of consumption, generation, and self-consumption for the calculation of energy and power-based indicators

The self-consumption is calculated from the intersection of the momentary generation and the corresponding consumption (cf. Equation (23)). [101]

$$E_{SC} = \int min\{P_L(t), P_G(t)\}\, dt \qquad (23)$$

The degree of energy self-sufficiency ε_{ESS} describes the ratio between generation and consumption and thus indicates what share of the total generation can be consumed over the considered period in this area (cf. Equation (24)). If the degree of energy self-sufficiency is high, generation and consumption are balanced completely or to a large extent over the considered period. However, it cannot be ensured that the generation can effectively be consumed, as a temporal correlation is not covered. The degree of energy self-sufficiency can also assume values above 100 %, as it is possible to generate excess energy. [100]

$$\varepsilon_{ESS} = \frac{E_G}{E_L} = \frac{\int P_G(t)\, dt}{\int P_L(t)\, dt} \qquad (24)$$

To account for this temporal component between generation and consumption, the degree of power self-sufficiency ε_{PSS} (*0% $\leq \varepsilon_{PSS} \leq$ 100%*) is used which is calculated according to Equation (25). It represents an evaluation parameter of the direct usability of generation to cover local consumption. [101] This energy indicator only represents the share of the generated energy that is directly consumed and therefore does not have to be fed into the grid. [102]

$$\varepsilon_{PSS} = \frac{E_{SC}}{E_L} = \frac{\int min\{P_L(t), P_G(t)\}\,dt}{\int P_L(t)\,dt} \qquad (25)$$

The self-consumption ratio ε_{SCR} ($0\% \leq \varepsilon_{SCR} \leq 100\%$) describes the share of the directly consumed energy of the total generation in the considered period (cf. Equation (26)) [101, 102]. A low self-consumption ratio thus indicates that a high amount of the total generation in this region cannot be consumed and must therefore be fed into the grid putting additional stress on the grid [100].

$$\varepsilon_{SCR} = \frac{E_{SC}}{E_G} = \frac{\int min\{P_L(t), P_G(t)\}\,dt}{\int P_G(t)\,dt} \qquad (26)$$

High values for the power self-sufficiency and the self-consumption ratio not only have positive local effects in terms of self-sufficiency, but indicate the impact on the grid. [101]

4.4 Operational Optimization

In general, optimization represents a mathematical problem that describes a system, process, or element [103]. The optimization is responsible for finding the best solution for this problem under certain conditions or constraints [104]. Finding a solution of the problem corresponds with the determination of the decision or optimization variables x [105].

The problem formulation and the components of the optimization as well as their mathematical correlations are described in Equations (27) − (30). The main component is the objective function $f(x)$, which is to be either minimized or maximized (cf. Equation (27)). The problem can have only one optimization variable x, or several $x = [x_1, x_2, ..., x_n]$ which is called multivariable optimization. [103, 105]

$$\max f(x_1, x_2, ..., x_n) = -\min(-f(x_1, x_2, ..., x_n)) \qquad (27)$$

To further specify the optimization problem, constraints are defined to limit the solution scope. There are equality constraints (cf. Equation (28)) and inequality constraints (cf. Equations (29)). [105, 106]

$$h(x_1, x_2, ..., x_n) = b_{eq} \qquad (28)$$

$$g(x_1, x_2, ..., x_n) \leq b \qquad (29)$$

Since usually also the optimization variables are not permitted to take all values arbitrarily, usually upper ub and lower bounds lb of the variables are set (cf. Equation (30)), which restrict the value range of the variables. [103]

$$[lb_1, lb_2, ..., lb_n] \leq x_1, x_2, ..., x_n \leq [ub_1, ub_2, ..., ub_n] \qquad (30)$$

Figure 17 illustrates the structure of a numerical optimization problem as described before and its correlation to the appropriate energy model.
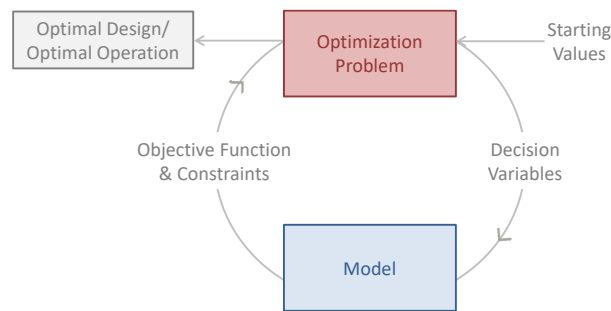
Figure 17: Illustration of a numerical optimization framework and the interaction between optimizer and model (adapted from [105])

How the optimization models are categorized has already been described in Chapter 2. In energy system optimization, a distinction is made between operational optimization and design optimization [107]. While operational optimization serves to define an optimal operation strategy of a component or a system (e.g. dispatch optimization), with design optimization the optimal dimensions of components or systems are determined (e.g. structural optimizations of grids, plant sizes of components) [107].

Predominantly, energy system optimizations represent linear problems which can be solved efficiently [107, 108]. The objective function as well as the constraints each represent linear functions in the case of linear optimization [105]. Objective functions of such complex energy systems thus usually are linear cost functions (environmental, social or economic), through which the influence of all components can be summarized [107–109]. Exemplarily, Haikarainen et al. (2014) [107] use a combination of investment and operating costs for structural and operational optimization of distributed energy systems. Wang et al. (2015) [109] use a combination of operating and environmental costs as the objective function. The constraints are customized specifically to the respective optimization problem. These can be, for example, operating ranges of plant components or start-up and powering-down behavior of the plants (ramp rates for start-up and powering-down behavior) but also supply contract conditions to be met [105, 107–109]. Often, energy system modeling also poses a MILP problem, where certain optimization variables can only take integer values, while others can have double values [110–113].

4.4.1 Electricity Markets and Price Developments

As the objective function for energy system optimization mostly refer to minimizing costs or maximizing profits, the energy markets and their design are relevant for establishing the objective function as well as the constraints. Figure 18 shows an overview of the electricity markets, since this thesis focuses on the electric energy system in the context of MES. The wholesale market for electric energy and the system services market for balancing energy are particularly significant.
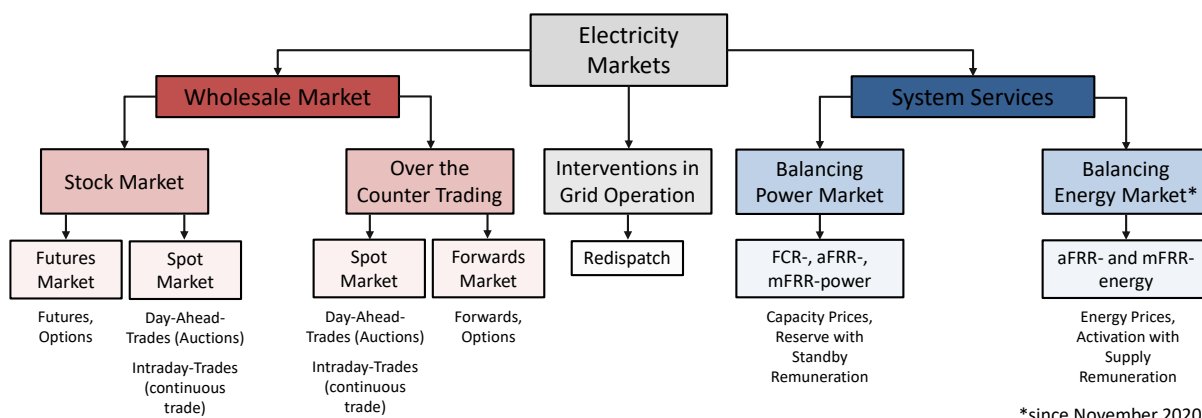
Figure 18: Overview Electricity Markets (adapted from [114])

The most significant difference between the wholesale market and the system services market is the operating principle for price formation. While the wholesale market operates according to the "pay-as-cleared" principle (cf. Figure 20 (a)), the system services market is based on the "pay-as-bid" principle (cf. Figure 20 (b)) [115]. The price formation on the wholesale market is based on the merit order, illustrated in Figure 19, representing the sorted sequence of power generation units ranked according to their generation costs, starting with the cheapest [116].
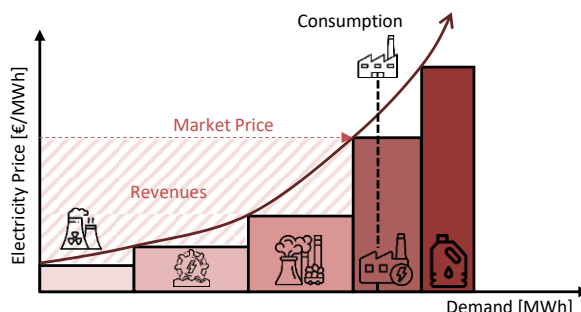
Figure 19: Original Merit-Order (adapted from [116, 117], icons taken from [17])

The current market price on the pay-as-cleared market then results from the intersection of the amount of electricity consumption (e.g., for the next day) and the electricity generation costs as demonstrated in Figure 20 (a). All power plants whose electricity generation costs are below the market price are accepted and used to generate power. [115]

Similarly, the current market price on the pay-as-bid market is formed. However, here the offers made by power plant operators are ranked according to their bids, starting again with the lowest offer. The intersection with the current consumption for balancing power and energy results in the maximum price. [115]

(a)

(b)
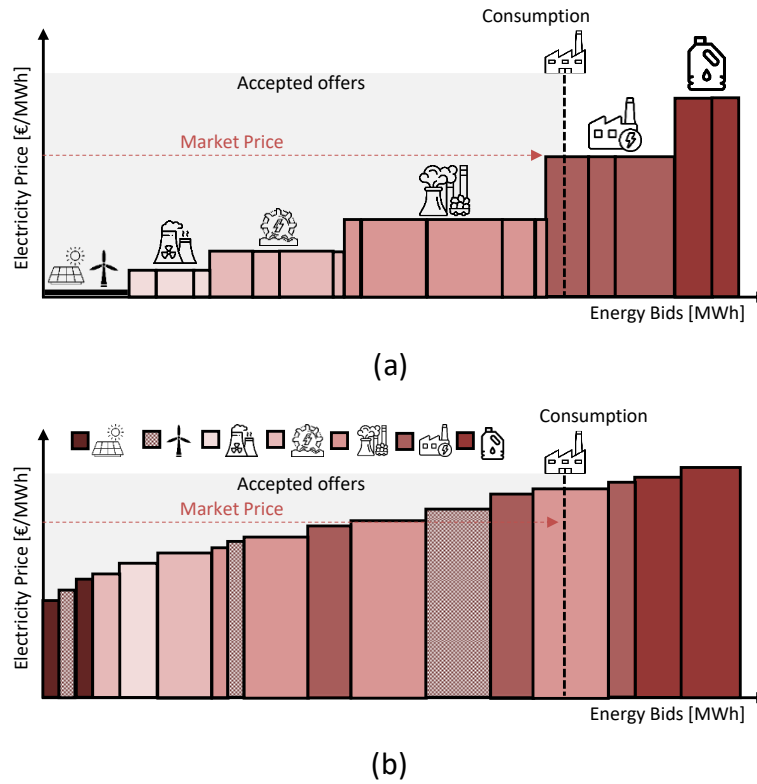
Figure 20: Comparison (a) pay-as-cleared and (b) pay-as-bid market principles (adapted from [115], icons taken from [17])

All power plants whose offers are below the maximum price are accepted and used. The actual price with which the capacity reserve or the activation is remunerated is the bid price. The market price is obtained by averaging all bids. As can be seen from the comparison between Figure 20 (a) and (b), currently higher prices tend to be obtained on the pay-as-bid market. [115] Future developments for the Merit-order are illustrated in Figure 21 [116, 118].

(a)

(b)
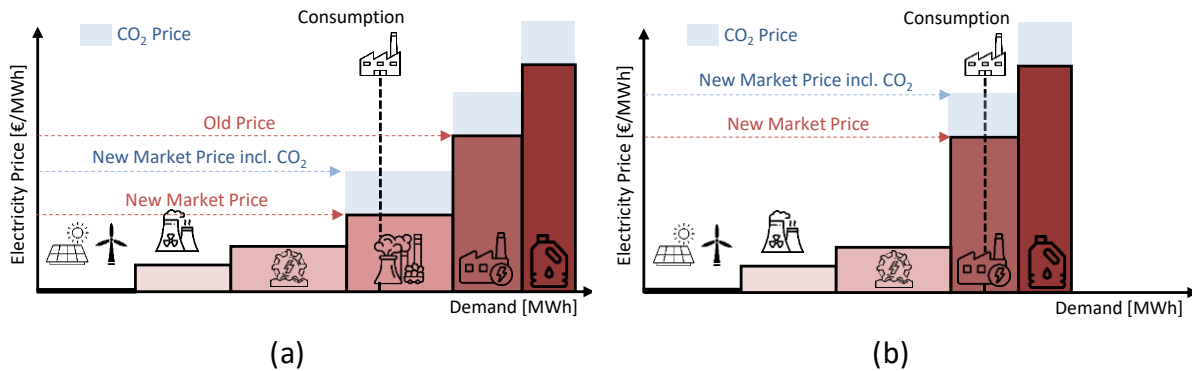
Figure 21: Merit-Order and electricity price development: (a) Market integration of RES including CO_2 prices and (b) Coal Phase-Out including CO_2 prices (adapted from [116, 118], icons taken from [17])

However, due to the future developments in power generation structures compared to Figure 19, i.e., the integration of RES as well as the coal phase-out and CO_2 pricing, prices on the pay-as-cleared market will also increase in the future. This is exemplified in Figure 21. [118]

4.5 Network Reduction Methods

Since grid-based energy system models represent highly complex models whose calculation and simulation produce a high computational effort, it is essential to find a compromise between modeling accuracy in the energy system model and its computation time. Therefore, network reduction methods are applied to model grid-based energy systems. These methods allow to reduce the spatial accuracy of the grid model without causing much loss of information and, at the same time, reduce the computation time. [44, 48]

This requires an underlying approach that also allows for such a compromise. Since the grid-based model calculations of this work are carried out in HyFlow, a cellular approach is implemented as the underlying approach, and thus serves as a basis. Cellular approaches support spatial resolution reduction of grid infrastructures, as illustrated in Figure 22.
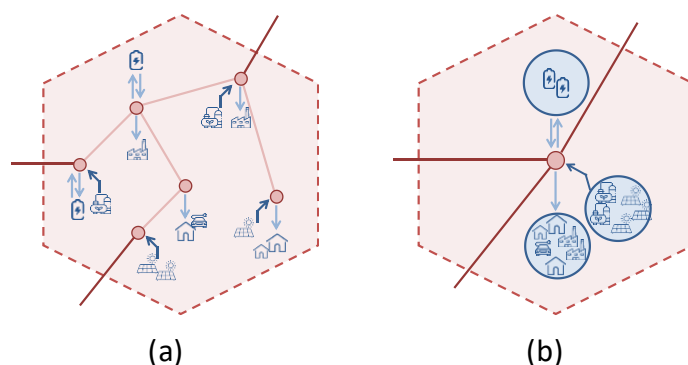

(a)   (b)

Figure 22: Cellular Modeling Approach for the (a) unreduced real grid model and (b) aggregated grid model (adapted from [23], icons taken from [17])

This cellular approach allows for a level of detail in the energy system model that achieves a suitable compromise between computation time and spatial resolution for the corresponding application. In this process, geographic grid areas or regions are divided into energy cells (cell division process). All nodes located within this cell are aggregated into a common node in the cell center. As a result, the consumers within the cell can be modeled without loss of information, but only in an aggregated form. Additionally, each cell is represented only by a small set of parameters – the cellular residual load and the tie lines between the cells. [44, 119] The cellular residual load $P_{res}(t)$, described by Equation , is defined as the difference between load $P_L(t)$ and (volatile) generation $P_G(t)$ for each time step [52].

$$P_{res}(t) = P_L(t) - P_G(t) \qquad (31)$$

All lines that are located within the cells are eliminated, whereby their losses are also no longer replicated in the reduced grid model. To represent them correctly nevertheless, network reduction methods are used. These methods have the task to reproduce these losses as closely as possible, resulting in a reduced grid with equivalent behavior to the real grid. [23] The basic idea of network reduction is that increased attention is paid to a specific grid section (internal

area), which is considered in detail. The rest of the grid (external area) only has to provide the relevant information to the area of interest over a boundary system, but does not have to be mapped completely. [120]

For the application of network reduction methods within the presented cellular approach, this basic idea of network reduction has to be adapted. For the cellular approach, all areas within the cells are reduced to an equivalent grid model and in this sense, there is no area that is represented in detail. The property of the grid that must be preserved is the overall electrical behavior, which includes load flows and line losses across the remaining lines, line losses within each cell, Slack-power and overall power losses. Particularly difficult to model are the reactive power losses in the grid.

Static network reduction methods published in literature that can be adapted to this problem are the Ward reduction method ([121, 122]) and the REI (radial equivalent independent) reduction method ([123, 124]). Both are numerical methods and use Equation (5) as a basis. The elimination of the grid nodes is performed numerically by applying Gaussian Elimination ([121]) for both methods. Thus, the lines are automatically eliminated as well. This reduces the system from Equation (5) to Equation (31) (b) and simultaneously also the grid model itself. To compensate for this elimination and thereby achieve equivalent grid behavior, compensation lines are calculated in these numerical methods. The calculation of these compensation lines differs for the two methods slightly. The index e in Equation (31) (a) (before reduction) designates the external system, which is to be reduced, index b describes the boundary system which is modified in the reduction ($\underline{I}'$ and $\underline{Y}'$) and thus contains the compensation lines. Index i denotes the internal system that is modeled in detail and not reduced. The individual entries of the matrices in Equation (31) represent smaller submatrices corresponding to the respective grid size. [46, 121]

$$\begin{pmatrix} \underline{I_e} \\ 0 \\ \underline{I_i} \end{pmatrix} = \begin{pmatrix} \underline{Y_{ee}} & \underline{Y_{eb}} & 0 \\ \underline{Y_{be}} & \underline{Y_{bb}} & \underline{Y_{bi}} \\ 0 & \underline{Y_{ib}} & \underline{Y_{ii}} \end{pmatrix} \cdot \begin{pmatrix} \underline{U_e} \\ \underline{U_b} \\ \underline{U_i} \end{pmatrix} \qquad \begin{pmatrix} 0 \\ \underline{I}' \\ \underline{I_i} \end{pmatrix} = \begin{pmatrix} 0 & 0 & 0 \\ 0 & \underline{Y}' & \underline{Y_{bi}} \\ 0 & \underline{Y_{ib}} & \underline{Y_{ii}} \end{pmatrix} \cdot \begin{pmatrix} \underline{U_e} \\ \underline{U_b} \\ \underline{U_i} \end{pmatrix} \qquad \textbf{\textit{(32)}}$$

$$\text{(a)} \qquad\qquad\qquad\qquad\qquad\qquad\qquad \text{(b)}$$

However, disadvantages of these numerical methods concern the achieved modeling accuracies in terms of reactive power [46]. The modeling accuracy refers to the deviation of electrical parameters between the reduced and the unreduced original grid model [23]. Static grid reduction methods strongly depend on the initial operating point through which the losses within the reduced grid are replicated. However, the losses in the reduced grid cannot adapt to changing load situations in the grid model. However, since the line losses are load-dependent (cf. Chapter 4.2), high deviations occur, which mainly affects reactive power losses. [23, 46, 125, 126]

5 RESULTS AND DISCUSSION

This chapter summarizes the main results of the publications within this thesis and discusses the individual results. First Chapter 5.1, addresses the first research objective **RO 1** by presenting the results for the developed modeling approach and its validation (Paper 2) using representative test grid structures (Paper 1) are presented. From these results, application recommendations are derived for the developed modeling approach. Then Chapter 5.2, addresses the second research objective **RO 2** by using the presented recommendations for the modeling approach for calculations within the MES framework HyFlow. Electrical grids (real grids and test structures) are considered at all four voltage levels. They are analyzed within the MES framework in terms of power quality and voltage stability issues as well as thermal line congestions and self-sufficiency analyses (published in CIGRÉ, CIRED and Paper 3).

5.1 Electrical Grid Modeling Approaches for MES (RO 1)

As discussed in Chapter 2 it is one of the biggest challenges in energy system modeling for MES applications to find a suitable level of detail including appropriate temporal and spatial resolution. Many of the presented modeling aspects in Chapter 2 are more difficult to realize for MES models than for other energy models as there are substantial differences between the individual energy carrier grids. When it comes to problems like… . A cellular modeling approach as described in Chapter 4.5 thus offers advantages since it is a generic and modular approach enabling a decoupling between the energy carrier grids to a certain extent. Cellular approaches additionally support spatial resolution reduction. As temporal resolution must be similar for all the energy carrier grids considered within the MES framework (in case of HyFlow 15-minute average values), a suitable compromise can only be achieved by a lower spatial resolution.

Thus, **RO 1.1** (*How can electrical grids be modeled for MES applications to enable high modeling resolution?*) is addressed with the results obtained in Paper 2. As Chapter 4.5 discusses, due to eliminated lines, information regarding electrical line losses can no longer be retained when applying network reduction within the cellular approach. Thus, conventional network reduction methods published in literature use compensation lines to account for this information loss. However, this compensation does not account for the load dependency of the electrical line losses. Thus, the presented method for reduction of cellular-based electrical grid models uses compensation modules added at the cell nodes instead of compensation lines. These modules represent a complex impedance replicating the electrical line within one cell (besides those connecting two cells) by using the sum of their electrical line parameters (R_{RLC}, L_{RLC} and C_{RLC}) and interconnecting them in an equivalent circuit. Their calculation for each

cell z is presented in Equations (33)-(35) where n designates the total number of affected electrical lines within cell z.

$$R_{RLC,z} = \sum_{i=1}^{n} R'_i \cdot l_i \tag{33}$$

$$L_{RLC,z} = \sum_{i=1}^{n} \frac{X'_{L,i} \cdot l_i}{2 \cdot \pi \cdot f} \tag{34}$$

$$C_{RLC,z} = \sum_{i=1}^{n} C'_i \cdot l_i \tag{35}$$

Thereby, it is essential that the chosen structure of the compensation module's equivalent circuit correctly depicts the relations within an electrical line meaning that series parameters (R_{RLC}, L_{RLC}) and shunt parameters (C_{RLC}) must be represented as such. This equivalent circuit structure can be achieved via different voltage potentials for the series parameters and the shunt parameters. Thus, C_{RLC} has a ground connection with a 0 V potential, while R_{RLC} and L_{RLC} are connected to a fictitious potential $\underline{U}_{fic}$ specific for each cell determined via its residual load. The equivalent line circuit of the compensation module is depicted in Figure 23.
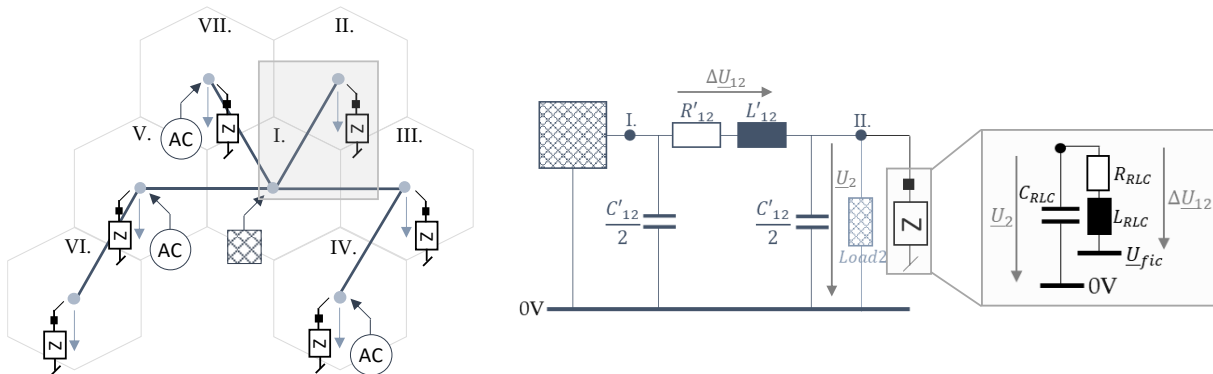
Figure 23: Compensation module application and its structural equivalent circuit for one exemplary cell [23]

This modeling approach using a novel network reduction method thus improves the weaknesses of the conventional numerical network reduction methods (cf. Chapter 4.5) regarding line loss modeling accuracy. Within this novel network reduction method, the compensation modules particularly enhance modeling accuracy of reactive power and reactive line losses as the load dependency of the electrical line losses is retained within the compensation module.

As newly developed methods need to be properly validated to ensure the desired effect and impact of the method, appropriate grid models must be available. As real grids can rarely be used due to user-specific information, they are subject to data protection and thus not publicly available. Synthetic grid models may however fail to properly replicate grid behavior and can thus not be regarded as representative. Additionally, they usually only contain grid data without time-series data for generation and consumption, and can hence only be used for

static analysis. Therefore, synthetic grid models usually serve to represent a certain purpose. The grid models used to validate the novel network reduction method are developed in this work and have to replicate real grid behavior of the grids within the ENTSO-E and they need to be able to adopt increased RES expansion. Additionally, as the load dependency of the compensation module needs to be accurate consumer and generation data have to be time-series data. Thus, to address **RO 1.2** (*What characteristics must be provided by test grid structures to develop and validate the proposed network reduction modeling approach?*) four generic test grids at each common voltage level are developed to fit these criteria. Table 5 provides an overview over the test grid characteristics regarding the overall grids. The load and generation data are either publicly available data (e.g., standard load profiles, measurements from the Austrian control area [127]), anonymized measured data available at the Chair of Energy Network Technology (e.g., load profiles at substations) or synthetically calculated data (e.g., synthetic load profiles [128, 129]).

Table 5: Overview over the developed test grids representing European structures [55]

Parameter	LV	MV	HV	MaxV	
Voltage level (kV)	0.4	20	110	220	380
Number of feeders	14	18	6	5	5
Number of network nodes	92	74	70	12	7
Number of consumer units	91	64	69	12	2
Number of generation units	39	15	18	5	5
Transformer power (MVA)	0.63	50	800	1200	10000
Vector group	Yz5	Dy5	Yy0	Ynyn0	Yy0
Topology	Radial	Radial, open rings	Closed rings	Mesh	Mesh
Number of lines	92	75	77	12	7
Total line length (km)	5.93	730.98	1477	566.50	364.70
Maximum feeder length (km)	0.81	95.90	319.08	-	-
Specific resistance R' (Ω/km)	0.063-0.249	0.133	0.176	0.076	0.043
Specific reactance X' (Ω/km)	0.079-0.080	0.146	0.408	0.230	0.220
Specific susceptance B' (µS/km)	0.000	71.314	2.796	3.770	4.398
Maximum electrical current (A)	535	422	735	840	1150

To ensure the representativeness of the developed test grids, the short circuit power and current (cf. Chapter 4.3.4) are used as validation parameters for this purpose. Thus, literature value ranges for European grids were researched and compared to the corresponding values calculated (cf. Equation (21)) for the test grids. As these value ranges are generally adhered to or slightly deviate by less than 7 % with reasonable cause (unclear assumptions about grid structures, parameters, etc. for the literature values). Hence, the developed test grids can be regarded as representative for European grids within the ENTSO-E. Thus, the grids can also ensure a conclusive validation of the novel network reduction method presented above.

Therefore, the novel network reduction method is applied to all four generic test grids for validation. As validation parameters relative deviations (cf. Equation (36) exemplary depicted

for active power) for Slack-node power and electrical tie line power flows and power losses between the original grid and the reduced equivalent grid model are used to assess overall grid behavior.

$$\Delta P_{rel,n}(t) = \frac{P_{original,n}(t) - P_{reduced,n}(t)}{P_{original,n}(t)}$$

(36)

These deviations describe the achieved modeling accuracies for each time step (15-minute values). To enable a comparison of these modeling accuracies across voltage levels the average relative deviations over the considered time and the entire grid are evaluated. The derived trends from this evaluation are illustrated in Figure 24. As the relative deviations presented in Figure 24 increase over the voltage levels for both electrical tie lines and Slack-node power, it can be assumed that this novel reduction method cannot offer advantages for all applications.

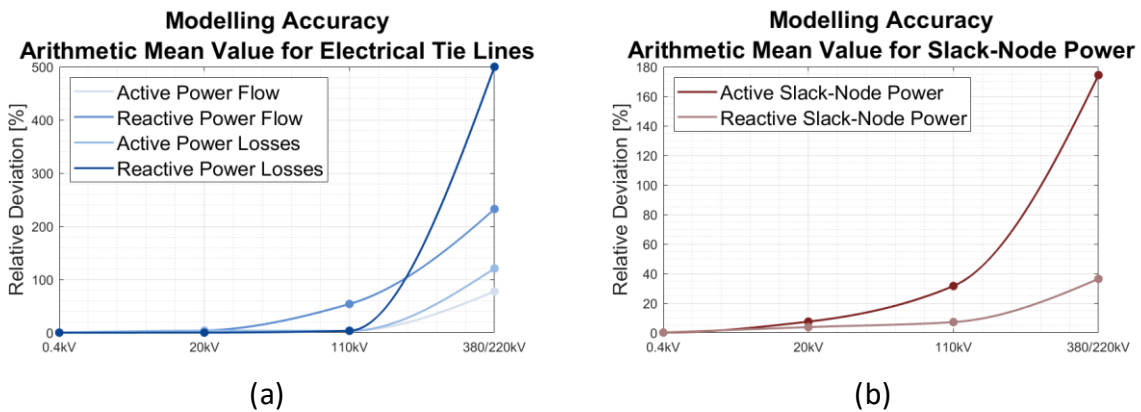(a)   (b)

Figure 24: Trends in relative deviations for (a) power and power losses within the electrical tie lines and (b) Slack-node power at each voltage level [23]

Therefore, these trends in modeling accuracy enable identifying influencing parameters as well as application recommendations for the presented novel network reduction method addressing **RO 1.3** (*For which MES applications (voltage level, grid size, grid structure, etc.) is this novel modeling approach for electrical grid reduction suitable and offers advantages?*). Influencing factors regarding modeling accuracy are voltage level, cell division (and cell size) as well as geographical load and generation distributions within the cells.

The voltage level presents as an influencing parameter since generated active and reactive line losses become higher at higher voltage levels which therefore results in a larger amount of power to be compensated by the compensation module. The compensation module is no longer fully capable to compensate the electrical line losses at higher voltage levels, in particular in terms of reactive power. This is due to the determination of the fictitious potential, which is based on the residual load within the corresponding cell. As in addition to the residual load, the nodal voltages depend on electrical line losses, this factor is missing

when determining the fictitious potential. Thus, the losses replicated in the compensation module are underestimated.

Cell division and corresponding cell sizes influence modeling accuracy as they refer to the topology of the reduced grid model. Due to cell division grid topology is altered (cf. Chapter 4.5) in the reduced model, therefore, if more intertwined (ring or meshed) structures occur in the reduced grid, modeling accuracy decreases significantly as the compensation modules show interdependencies. Thus, a compensation module can replicate line losses and therefore adapt line power flows more accurately if a cell has minimal connections to other cells. However, if ring structures occur within the cells and are eliminated during cell aggregation, they do not influence the model or its accuracy. This structural influence is due to interdependent effect of the compensation module between the electrical ring lines. Thus, radial structures in the reduced grid model present the best results regarding modeling accuracy, which occur mostly at lower voltage levels (cf. Chapter 4.1). Additionally, larger cell sizes meaning more grid nodes aggregated into one cell also decrease modeling accuracy as this again results in higher electrical line losses to be compensated by the compensation module. Also modeling accuracy can be increased if critical lines or nodes can be defined prior to the cell division process. As this process is arbitrary according to the task at hand, critical lines (at risk for thermal line congestions) can be designated as tie lines between cells and critical nodes (at risk for voltage violations) can be defined as one cell.

Regarding load and generation distribution within the cells, best modeling accuracies can be achieved if there is an even distribution within the cell due to the generated voltage drops or increases. These influence the assumed fictitious voltage potential $\underline{U}_{fic}$ and thus the accuracy of the compensation module. Table 6 presents the results for which applications this modeling approach (cellular approach with presented novel network reduction) is suitable.

Table 6: Overview over the applicability of the presented novel network reduction based on validation using the generic test grids

	Voltage Level			
	LV	MV	HV	MaxV
Radial Structure in the Reduced Grid	✓	✓	~	✗
Significant Calculation Time Savings	✓	✓	✓	✗
Low Grid Losses	✓	~	✗	✗
Applicability Recommendation	Very well suited	Well suited	Suited depending on application	Not suited

The main benefits of this modeling approach are achieved for low- and medium-voltage grids as it offers additional advantages regarding the usage of standard load profiles. These are only valid to represent consumer behavior for a larger number of consumers (> 150 consumers [130]) which is often achieved due to the aggregation process of the cellular approach.

Due to the obtained results from the validation of the presented modeling approach the network reduction method is particularly well applicable at the low- and medium-voltage level, where it offers various advantages. In contrast, at the high-voltage level it depends on the application (original grid, topology, grid expansion), if the discussed influencing parameters can be chosen beneficially reasonable modeling accuracies can be achieved. At the maximum-voltage level this method is not applicable as deviations become too high to properly replicate the original grid behavior. Additionally, at this voltage level grids are usually less expanded in terms of number of grid nodes, therefore, calculation time savings due to spatial resolution reduction is low.

As this validation is limited solely to the electrical grid, the impact of MES on cellular-based reduced grid models has to be further analyzed.

5.2 Electrical Grid Analysis in MES (RO 2)

For the impact analysis of MES expansion scenarios for RES are established and then implemented in real and synthetic grid structures. This work considers three use cases at different voltage levels and analyzes how MES can influence power quality and voltage stability as well as thermal line congestions and self-sufficiency within the electrical grid. To provide an overview over the use cases performed within this work as well as their characteristics and the analyses conducted for each use case, Table 7 is presented below. The results of the individual use cases are presented afterwards in detail.

Table 7: Overview over the use cases within this work and their analysis

Use Case		CIGRÉ	CIRED	Paper3
Type of Grid		real	synthetic	real
Voltage Level		0.4 kV	20 kV	110/220/380 kV
Time frame		One Day	One Day	One Year
Expansion Scenario		PV expansion	PV and Wind expansion	PV, Wind, EV and HP expansion
Flexibility Options		HP and Thermal Storages	HP and Thermal Storages, PtG	GtP, PtG and combined unit
Operating Strategy		Determined in HyFlow	Determined in HyFlow	Separately Optimized Operation
Type of Analysis	Power Quality and Stability	✓	✓	No issues
	Thermal Line Congestions	No issues	No issues	✓
	Self-Sufficiency Analysis		✓	

5.2.1 Use Case 1: Low-Voltage Grid (CIGRÉ)

As briefly described in Chapter 3.2 this use case is based on an anonymized real 0.4 kV low-voltage grid section of an Austrian grid available at the Chair of Energy Network Technology. In its original state only very few PV units are installed. Thus, for this use case a PV expansion scenario is created which is based on considerations of possible and suitable areas for increasing the share of PV within the grid. For this grid a reduced equivalent cell model according to the approach described in Chapter 5.1 is created. To assess the influence of MES hybrid flexibility options (HP and thermal storages) are implemented at each cell node. The grid section for this use case including the assumed PV expansion is illustrated in Figure 25 (a). The corresponding equivalent cell model is presented in Figure 25 (b). This cell model includes the compensation modules calculated according to Equations (33)-(35).

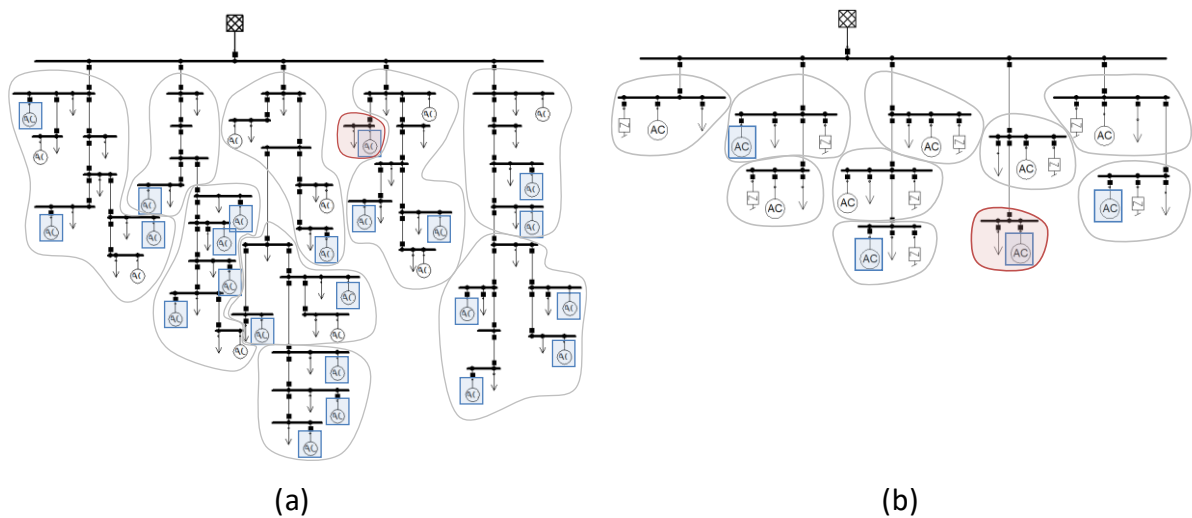(a)   (b)

Figure 25: Cell division in use case 1 including the PV expansion scenario for (a) the original 0.4 kV low-voltage grid section and (b) the reduced equivalent cell model (adapted from [56])

The red marked cell in Figure 25 represents the cell to be analyzed in this use case as the massive PV expansion in this cell leads to a violation of the upper voltage limit (cf. Figure 13). The voltage profile for the corresponding red marked cell node within the reduced grid is presented in Figure 26 (a).

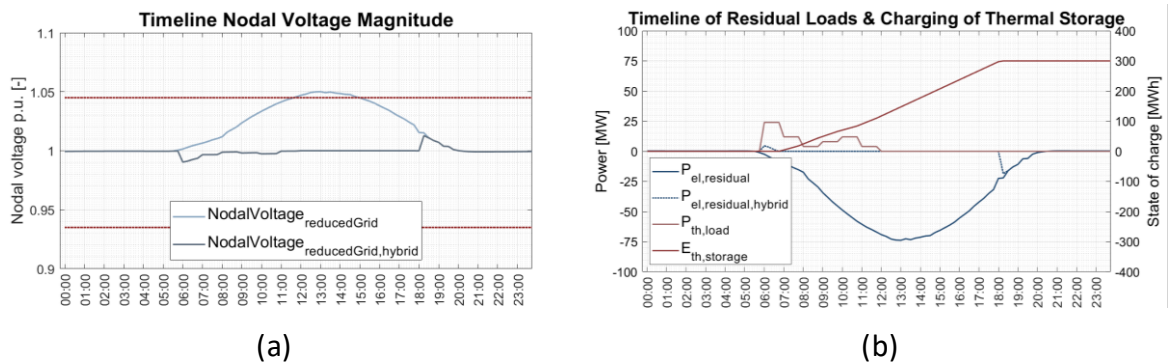(a)   (b)

Figure 26: (a) Voltage profile for the PV expansion in the reduced grid with and without hybrid flexibilities and (b) residual loads and charging state of the thermal storage of the marked cell (adapted from [56])

Figure 26 (b) additionally illustrates the operation of the HP unit and the thermal storage unit, which is determined within HyFlow. The HP units operate in a cell-serving way. Thus, they only operate if there is a heat demand or if there is surplus energy available from the installed PV unit at the corresponding cell node to balance the power within the cell [14]. As can be seen in Figure 26 the implementation of the hybrid flexibility options results in a relatively even voltage profile around the nominal voltage, thus, creating high voltage stability in the grid. Only at the beginning of the generation period of the PV unit the nodal voltage drops below nominal voltage as the HP requires additional electricity to operate. At this point there is already a heat demand, but not enough energy generated in the PV unit, thus electricity must be taken from the grid. Then again, at the end of the PV unit´s generation period the nodal voltage rises slightly as the thermal storage unit is already fully loaded while the PV unit still

generates electricity. Therefore, the surplus energy that cannot directly be used at the consumer is fed into grid leading to a slight increase of the nodal voltage.

Thermal line congestions are not an issue for this use case as high line loading due to consumption are actually reduced by the PV expansion to a certain extent.

5.2.2 Use Case 2: Medium-Voltage Grid (CIRED)

The second use case, as briefly outlined in Chapter 3.2, performs a similar analysis on a 20 kV medium-voltage synthetic test grid (as presented in Paper 1, cf. Chapter 5.1). As in use case 1 RES expansion in the grid´s original state is relatively low. Therefore, an expansion scenario for PV and wind power is established. For this scenario each commercial consumer unit is equipped with a corresponding PV system. Additionally, existing wind sites are expanded, and new ones (with appropriate conditions regarding surroundings) are added. The grid used for this use case is presented in Figure 27 including the expansion of wind and PV as well as the reduced equivalent cell model.

☐ Expansion of photovoltaic power ☐ Expansion of wind power ☐ Expansion of wind and photovoltaic power

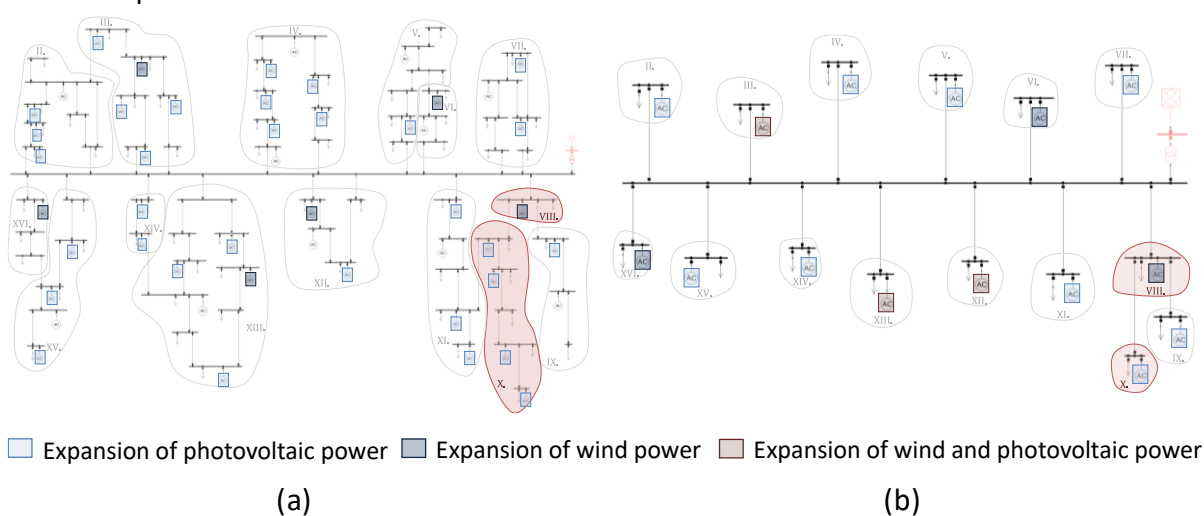(a)   (b)

Figure 27: Cell division in use case 2 including the PV and wind expansion scenario for (a) the original 20 kV medium-voltage test grid and (b) the reduced equivalent cell model (adapted from [57])

To perform an impact analysis of how grid-based MES can contribute to a stable energy distribution within the electrical grid, hybrid flexibility options are integrated into the system. In this use case, the flexibility options are HP units as well as PtG units. These flexibility options are allocated accordingly to the RES expansion: each commercial consumer requiring heat receives a HP unit and an oversized thermal storage unit to ensure maximum stability support, while PtG units are implemented in cells where only wind is expanded. Regarding the operation of the flexibility options, HyFlow uses a rule-based approach ([14]), similarly, to use case 1. While the HP units operate in a cell-serving way and thus minimize the residual load of the cell, the PtG units operate in a system-serving way. System-serving elements operate if consumption and generation within the overall system is unbalanced and thus minimize the residual load of the entire system [14]. Additionally, to ensure also maximum stability support

from the PtG unit, it is assumed that the produced natural gas is fed into the natural gas grid where storing it is considered to be unlimitedly.

For the analysis, the red marked cells in Figure 27 are considered. However, the results are exemplarily presented in Figure 28 for only Cell VIII (as designated in Figure 27) where wind is expanded.

As can be seen in Figure 28, the high RES generation results in upper voltage limit violations. Due to the hybrid conversion in the PtG unit, electrical demand increases and manages to lower nodal voltages keeping them within upper and lower limits of the voltage band. The voltage profile obtained from hybrid conversion is not as smooth as the one obtained in use case 1 (cf. Figure 26) which is due to the operating strategy chosen in HyFlow. While cell-serving elements enable very even voltage profiles within one cell, system-serving elements can bring the voltages within the allowable range, however, contribute to smoothed voltages only to a certain extent as they are directed at the entire system.
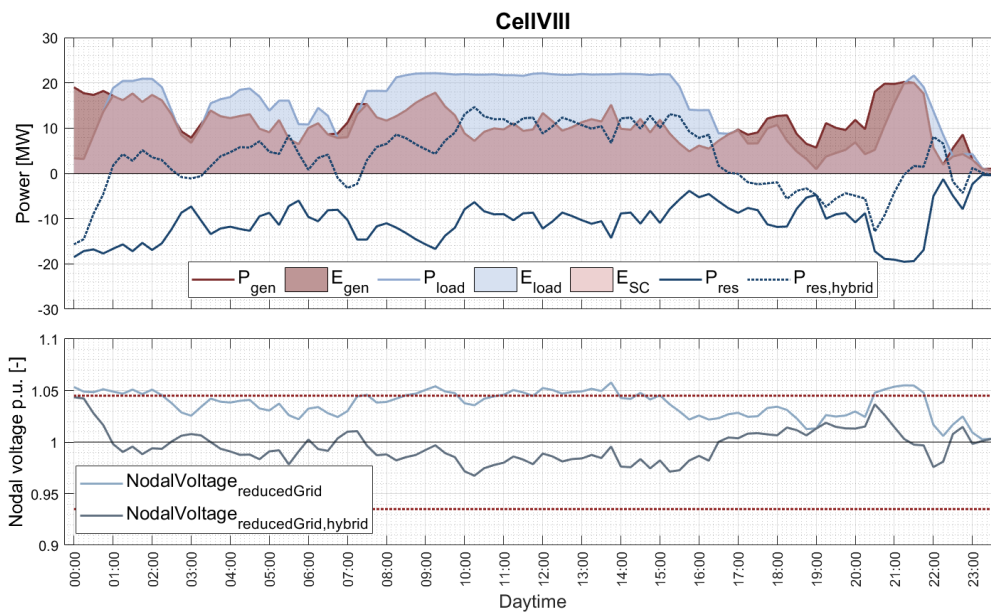

Figure 28: Power profile of Cell VIII after integrating hybrid flexibility options and a comparison between nodal voltages before and after hybrid conversion (adapted from [57])

Thus, the corresponding hybrid conversion for the entire system at the Slack-node is presented in Figure 29 which illustrates the influence of the HP and PtG units implemented in the grid.
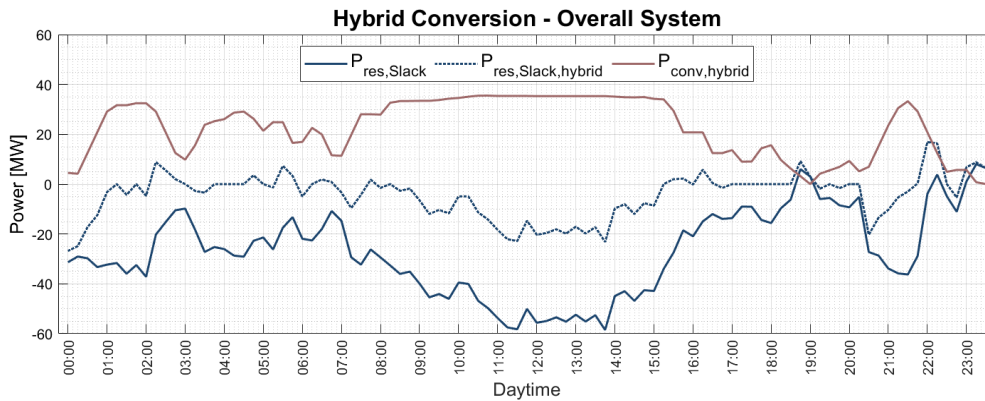
Figure 29: Residual loads and hybrid conversion within the entire system (adapted from [57])

Additionally, this use case includes a self-sufficiency analysis, therefore Figure 30 presents the energy and power-based indicators before and after hybrid flexibilities are implemented into the grid. As can be seen in Figure 30 (a), the degree of energy self-sufficiency ε_{ESS} is extremely high due to massive wind expansion within Cell VIII, therefore a large amount of energy cannot be used within the cell. Thus, an enormous amount of energy must be fed into grid putting additional stress on electrical distribution lines. After hybrid conversion the degree of energy self-sufficiency is almost 78 % as the PtG unit causes higher consumption within the cell relieving the grid.

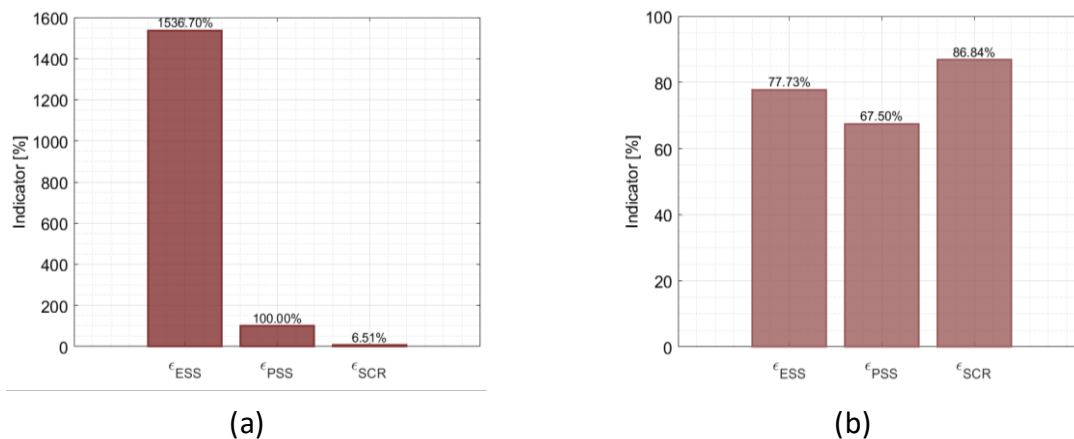(a)   (b)

Figure 30: Energy and power-based indicators for the self-sufficiency analysis (a) before and (b) after implementing hybrid flexibility options for Cell VIII (adapted from [57])

The power self-sufficiency ε_{PSS} before hybrid conversion is 100 %, meaning all the demand can be covered directly by generated power within the cell. Therefore, only the surplus energy is fed into the grid. This indicator decreases to 67.50 % after hybrid conversion due to the PtG consumption. As a result, there are some temporal discrepancies so that some of the generated power cannot be used directly within the cell as there is not enough consumption. The self-consumption ratio ε_{SCR} increases from about 6 % to almost 87 % therefore most of the generated energy can be directly consumed representing an almost self-sufficient cell. Both the power self-sufficiency and the self-consumption ratio can be significantly increased

by implementing a power storage within the cell. Higher energy and power-based indicators are also achieved if the hybrid flexibility elements are operated in a cell-serving way.

5.2.3 Use Case 3: High- and Maximum-Voltage Grid (Paper 3)

For the last use case, the entire Austrian 110 kV high- and 220/380 kV maximum-voltage levels are considered in a comprehensive study. This use case investigates sector coupling technologies as re-purposing options for decommissioned coal-fired power plants (CFPP). The expansion scenarios within this use case rely on national and European studies and expansion plans ([131–134]) for HP, EV, PV, and wind power. Thus, they represent a 2030- and 2040-scenario which is compared to the status-quo (2020). The real geo-referenced Austrian electricity and natural gas grids utilized in this use case are depicted in Figure 31. As the application recommendations for the cellular reduced grid models presented in Chapter 5.1 state, application of this method to the voltage levels within this use case is not advantageous. Therefore, each electrical grid node represents a single cell in HyFlow, thus, no network reduction is necessary as no lines are eliminated in the process.
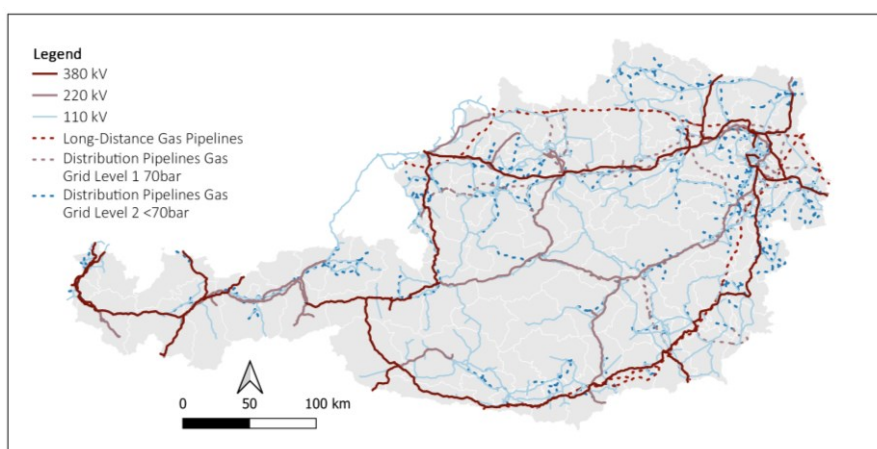

Figure 31: Incorporated and geo-referenced Austrian electricity and natural gas grids for use case 3 [58]

Re-purposing refers to dedicating existing plant equipment at the decommissioned CFPP sites to sustainable utilization, thus, supporting the coal phase-out by retaining valuable assets, as well as jobs [135, 136]. The re-purposing options chosen for investigation within this use case are Gas-to-Power (GtP) units, Power-to-Gas (PtG) units as well as combined PtG-GtP units. Therefore, they represent the hybrid flexibility options whose influence is to be researched in the electrical grid analysis. In this use case, the chosen operating strategy is not defined within HyFlow, but uses a profit-optimal operational optimization developed for this use case. This operational optimization represents a multi-variable MILP problem. It includes operational expenditures (OpEx), arbitrage transaction on the energy markets (electricity and natural gas) as well as stock market trading for balancing power in the objective function. Additionally, it considers price developments for each scenario for the spot market prices of electricity and

natural gas as well as for balancing power reserve and balancing energy activation prices. The constraints include start-up and power-down ramp rates, district heating supply contracts of the original CFPP which the re-purposing technology has to adhere to as well as lower and upper bounds for each variable. The CFPP sites considered in this use case represent the decommissioned Austrian sites Mellach and Dürnrohr and the still operating gas power plant Simmering. To set up the optimization problem, extensive research on publicly available data on the sites and the previous power plants as well as on sector coupling technologies and their characteristics and energy market price developments was conducted. An exemplary operating profile for the combined PtG-GtP unit for the 2030 scenario at the Mellach site is illustrated in Figure 32. As can be seen in Figure 32 the operational optimization consists of six variables where x_1 designates normal operation with participation in arbitrage transactions on the energy markets, x_2 designates positive and negative Frequency Control Reserve (FCR), x_3 and x_4 designate positive and negative automated Frequency Restoration Reserve (aFRR) and x_5 and x_6 describe positive and negative manual Frequency Restoration Reserve (mFRR).
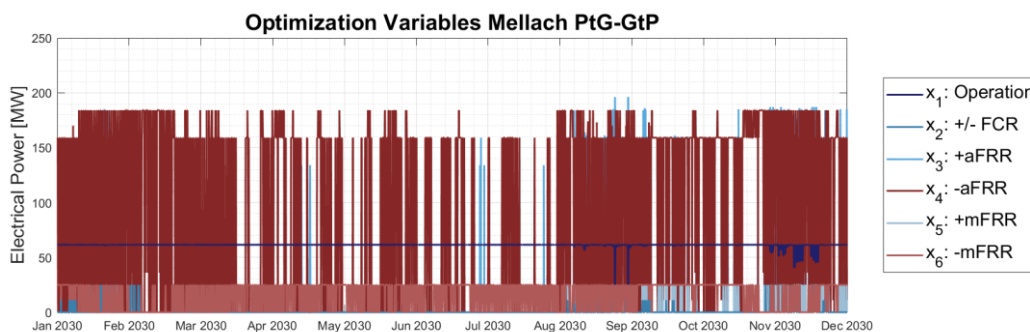

Figure 32: Cost-optimal operation profiles for combined PtG-GtP unit at the Mellach site in 2030 [58]

As discussed in Chapter 4.4.1 prices on the pay-as-bid markets (balancing power) are usually higher than on the pay-as-cleared markets (electricity). Therefore, the main contribution for the operation profile comes from the most expensive balancing power product (in this case negative aFRR (x_3)). Normal operation with participation on the energy markets (x_1) only serves to fulfill the heat supply contracts of the previous CFPP site. Due to the assumed price developments for natural gas and electricity, natural gas prices rise higher than the electricity prices in the future. Thus, PtG integration becomes more feasible so that the combined PtG-GtP unit operates mostly as a PtG unit (2038.5 full load hours for the PtG and 142.6 full load hours for the GtP).

The obtained profiles are then used to calculate the plant's revenues for participation in the energy markets (x_1) and the optimal combination of bid balancing power (x_2-x_6). In addition, the revenues for the activation of the balancing energy are also factored in. A techno-economic analysis is conducted afterwards for these re-purposing technologies at each site and for each scenario. This analysis shows that particularly high revenues are generated for

the combination plant. The capital expenditures (CapEx) are included in this analysis using a Return-On-Investment (ROI) calculation, which shows that a GtP unit alone is the most profitable, although the highest revenues are generated from the combined PtG-GtP unit. This is a result of the combined unit's significantly higher CapEx. More detailed results on this analysis can be found in Paper 3.

As this use case considers a very large grid with approximately 400 grid nodes and a long calculation time frame of one year, the grid analysis results are presented in an aggregated form. As power quality and voltage stability is not an issue for this use case, the grid analysis focuses on thermal line congestions due to expansion and determines the impact of the cost-optimal hybrid flexibility options at the decommissioned CFPP sites. Figure 33 presents the exemplary results for the GtP unit implemented at all CFPP sites for the 2030 scenario.
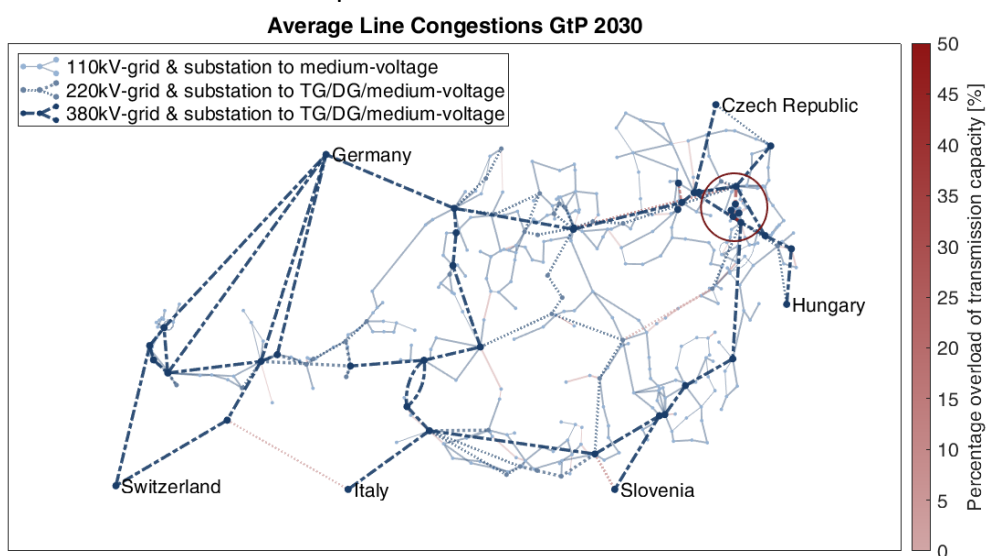

Figure 33: Hybrid load flow calculation results from HyFlow: Location of average highest and most frequent line congestions for the 2030 GtP scenario for the Austrian transmission (TG) and distribution grids (DG) [58]

Since the hybrid flexibility options are implemented at fixed locations within the grid and are operated at optimal profits, their impact on limiting renewably induced line congestion is small. Thus, also the number of congested lines within the grid is independent of the use of any of the hybrid flexibility option and does not change compared to unused CFPP sites (no hybrid flexibility options). What is achieved by the sector coupling technologies, however, is a reduction in the time steps in which overloaded lines occur. The greatest potential can be seen in the PtG units, as they can compensate for negative residual loads, i.e., overloads due to excess RES feed-in. The GtP units, on the other hand, tend to increase the overload duration. This suggests that PtG units in particular show significant potential to act as temporal flexibility options within the grid. As can be seen in Figure 33, congestions occur mainly in areas with high consumption, i.e., cities or also in areas with particularly concentrated RES expansion potential (cf. [137]). Since the flexibility options can only influence congestions locally in their surroundings, they could have greater impact if they were also placed at the corresponding

congestion centers in the grid. Nevertheless, sector coupling technologies offer a high re-purposing potential for the CFPP sites, as these sites represent optimal grid nodes for hybrid technologies due to the existing infrastructures and assets.

6 CONCLUSION AND OUTLOOK

This thesis focuses on modeling and analysis aspects of electrical grids within MES approaches and thereby addresses not fully solved research within this field. It becomes evident that **MES considerations for future energy system research need to include grid structures as they present one of the limiting factors of energy transition.** However, one of the greatest challenges in MES modeling is providing a suitable temporal and spatial resolution as time frames vary immensely between the different energy carriers.

Therefore, they require a generic and modular approach, that enables combining all considered energy carrier models. This work proposes a comprehensive novel network reduction method to provide conclusive and efficient electrical grid models as one solution for this challenge. This novel network reduction method uses the underlying methodology of a cellular approach and instead of compensation lines defined compensation modules applied to the remaining grid nodes in the reduced equivalent grid model. It thereby, enhances modeling accuracy significantly compared to network reduction methods from literature, in particular for reactive power within the grid and provides major advantages. **Therefore, the appropriate design for modeling electrical grids within the cellular approach is to calculate compensation elements applied at the grid nodes to accurately replicate electrical line losses in the reduced model (RO 1.1).** As the validation process showed, there are minimal deviations between the original grid and the reduced equivalent cell model, in particular, at the low- and medium-voltage level. However, loss replication using the compensation modules lacks accuracy at higher voltage levels and should be enhanced in future works exemplarily by an improved determination of the fictitious potential. Additionally, further validation using real grid applications should be performed as so far validation at higher voltage levels was performed based on synthetic test grids due to the limited openly available grid structures for such purposes. However, as these customized synthetic test grids have proven to replicate real grid behavior due to a short-circuit power and current comparison to literature values, it can be assumed that a conclusive validation process was performed. **Thus, the necessary characteristics of test grid structures are accurate representation of real grid behavior (RO 1.2).**

However, the advantages provided by utilizing the presented novel network reduction method show certain limitations. They can only be achieved for designated application purposes and if the derived and provided application recommendations are adhered to. **Most benefits can be achieved for expanded low- and medium-voltage grids with even load and generation distribution within the defined cells that can be turned into a radial structure within the reduced cell model (RO 1.3).** For higher voltage levels (110/220/380 kV) however, the method tends to fail in fully replicating grid losses due to a larger amount of losses that

has to be compensated and more intertwined grid structures. For the validated synthetic test grids at that voltage level, time savings due to reduction were smaller as the grid was less expanded. Nevertheless, depending on the geographical coverage (e.g., national, international, etc.) also these grids can assume larger grid sizes for which computational time savings can become significant. Therefore, further developments of this method at higher voltage levels could be beneficial to widen the scope of advantageous applications for this method.

As this method was developed to be used within MES approaches, this thesis provides three different use cases which utilized the application recommendations deduced for the proposed novel cellular-based network reduction and performs hybrid load flow calculations within HyFlow. Each use case presents a different voltage level and introduces an expansion scenario of RES and modern loads (HP, EV, and PtG) into the grid. To provide more flexibility to these assumed scenarios hybrid flexibility options are added. Each use case aims at analyzing the influence of MES on the electrical grid. Thus, these use cases are suitable for impact analyses of MES on electrical grids as they present future expansion scenarios causing issues within the electrical grid and then present hybrid flexibility options as countermeasures. **The electrical grid analysis within MES approaches needs to include power quality and voltage stability analyses as well as thermal line congestion analysis. Preferably, to fully exploit the advantages of MES also self-sufficiency studies are performed (RO 2.1).** As the presented use cases are usually complex even for the rather simple problems, there are only certain aspects that were included. Thus, further and more comprehensive use case analyses of applying this method to perform hybrid load flow calculations have to be performed.

As a result of the analysis, MES provide solutions and many benefits for the challenges the electrical grid faces during energy transition. They contribute to enhancing temporal flexibility as well as improving power quality and voltage stability. Additionally, they may provide support against line congestions. However, to exploit their full potential they have to be allocated in load or generation centers within the grid. They also contribute to self-sufficiency within defined areas as improved utilization of the decentrally and fluctuating generated energy. Thus, grid relieve can be achieved as less energy has to be transmitted or distributed over electrical lines. **Generally, MES provide additional flexibilities for the electrical grid and manage to avid nodal voltage violations as well as line congestions if these sector coupling technologies are allocated properly. Additionally, MES can improve self-sufficiency significantly, e.g., on cell-level or system-level, if the operating strategy is chosen accordingly (RO 2.2).** However, as HyFlow is still under further development at the Chair of Energy Network Technology, loop-flows transitioning through Austria as part of the European transmission grid are not included in the use cases. Taking these flows into consideration may

lead to different results. Additionally, to provide more information on MES and how these approaches cause interactions between the energy grids, the other energy carrier models must be analyzed accordingly as well. Thus, use cases that incorporate analysis of heat and natural gas grids should be researched as well to obtain conclusive and comprehensive results. Additionally, different operating strategies should be investigated, that are developed for other specific objectives such as CO_2 emissions reduction or grid support.

7 REFERENCES

[1]   EUROPEAN ENVIRONMENT AGENCY: *Climate change puts pressure on Europe's energy system*.
      URL https://www.eea.europa.eu/highlights/climate-change-puts-pressure-on. –
      Aktualisierungsdatum: 2019-12-10 – Überprüfungsdatum 2022-05-02

[2]   ANDRYCHOWICZ, Mateusz: *RES and ES Integration in Combination with Distribution Grid
      Development Using MILP*. In: *Energies* 14 (2021), Nr. 2, S. 383

[3]   PAPADIS, Elisa ; TSATSARONIS, George: *Challenges in the decarbonization of the energy
      sector*. In: *Energy* 205 (2020), Speciale 1, S. 118025

[4]   HOSSAIN, Jahangir ; MAHMUD, Apel: *Renewable Energy Integration* (2014)

[5]   BIRD, L. ; MILLIGAN, M. ; LEW, D.; National Renewable Energy Laboratory (NREL) (Mitarb.):
      Integrating Variable Renewable Energy: Challenges and Solutions

[6]   INTERNATIONAL ENERGY AGENCY: *Global Energy Review 2021: Renewables*. URL
      https://www.iea.org/reports/global-energy-review-2021/renewables –
      Überprüfungsdatum 2022-05-03

[7]   INTERNATIONAL ENERGY AGENCY: *Global Energy Review: CO2 Emissions in 2021 : Flagship
      report - March2022*. URL https://www.iea.org/reports/global-energy-review-co2-
      emissions-in-2021-2

[8]   GEIDL, Martin ; KOEPPEL, Gaudenz ; FAVRE-PERROD, Patrick ; KLOCKL, Bernd ; ANDERSSON,
      Goran ; FROHLICH, Klaus: *Energy hubs for the future*. In: *IEEE Power and Energy Magazine*
      5 (2007), Nr. 1, S. 24–30

[9]   ZACHMANN, Georg ; HOLZ, Franziska ; ROTH, Alexander ; MCWILLIAMS, Ben ; SOGALLA, Robin ;
      MEISSNER, Frank ; KEMFERT, Claudia; European Parliament (Mitarb.): *Decarbonisation of
      Energy : Determining a robust mix of energy carriers for a carbon-neutral EU*

[10] MANCARELLA, Pierluigi: *MES (multi-energy systems): An overview of concepts and
      evaluation models*. In: *Energy* 65 (2014), Nr. 3, S. 1–17

[11] BERNARDS, Raoul ; VAN WESTERING, Werner ; MORREN, Johan ; SLOOTWEG, Han: *Analysis of
      Energy Transition Impact on the Low-Voltage Network Using Stochastic Load and
      Generation Models*

[12] ENGEL, H. ; HENSLEY, R. ; KNUPFER, S. ; SAHDEV, S.: *The potential impact of electric vehicles
      on global energy systems*

References

[13] WINTER, Wilhelm ; ELKINGTON, Katherine ; BAREUX, Gabriel ; KOSTEVC, Jan: *Pushing the Limits: Europe's New Grid: Innovative Tools to Combat Transmission Bottlenecks and Reduced Inertia*. In: *IEEE Power and Energy Magazine* 13 (2015), Nr. 1, S. 60–74

[14] GREIML, Matthias ; TRAUPMANN, Anna ; SEJKORA, Christoph ; KRIECHBAUM, Lukas ; BÖCKL, Benjamin ; PICHLER, Patrick ; KIENBERGER, Thomas: *Modelling and model assessment of grid based multi-energy systems*. 7-24 Pages / International Journal of Sustainable Energy Planning and Management, Vol. 29 (2020) (2020)

[15] APPELRATH, Hans-Jürgen ; LEHNHOFF, Sebastian ; ROHJANS, Sebastian ; KÖNIG, Andreas: *Hybridnetze für die Energiewende – Forschungsfragen aus Sicht der IKT*. December 2012

[16] INTERNATIONAL ENERGY AGENCY: *Current & future energy system: hydrogen can increase flexibility of low-carbon systems* : *Twitter*. URL https://twitter.com/iea/status/615914303082901504?lang=fi – Überprüfungsdatum 2022-05-05

[17] FLATICON: *Icons taken from different authors from flaticon*. URL https://www.flaticon.com/

[18] VAHID-PAKDEL, M. J. ; SEYEDI, Heresh ; MOHAMMADI-IVATLOO, B.: *Enhancement of power system voltage stability in multi-carrier energy systems*. In: *International Journal of Electrical Power & Energy Systems* 99 (2018), Nr. 1, S. 344–354

[19] MANCARELLA, P.: *Smart Multi-Energy Grids: Concepts, benefits and challenges* (2012), S. 1–2

[20] KRIECHBAUM, Lukas ; SCHEIBER, Gerhild ; KIENBERGER, Thomas: *Grid-based multi-energy systems—modelling, assessment, open source modelling frameworks and challenges*. In: *Energy, Sustainability and Society* 8 (2018), Nr. 1, S. 244

[21] HERBST, Andrea ; TORO, Felipe ; REITZE, Felix ; JOCHEM, Eberhard: *Introduction to Energy Systems Modelling*. In: *Swiss Journal of Economics and Statistics* 148 (2012), Nr. 2, S. 111–135

[22] VAN BEECK, N.M.J.P.: *Classification of Energy Models* FEW Research Memorandum; Vol. 777; Tilburg: Operations research (1999). URL https://research.tilburguniversity.edu/en/publications/classification-of-energy-models – Überprüfungsdatum 2022-05-09

[23] TRAUPMANN, Anna ; KIENBERGER, Thomas: *Novel network reduction method for cellular-based network models with enhanced modeling accuracy for multi-energy-system approaches*. In: *International Journal of Electrical Power & Energy Systems* 137 (2022), Nr. 4, S. 107827

[24] Duun-Henriksen, Anne Katrine ; Schmidt, Signe ; Røge, Rikke Meldgaard ; Møller, Jonas Bech ; Nørgaard, Kirsten ; Jørgensen, John Bagterp ; Madsen, Henrik: *Model identification using stochastic differential equation grey-box models in diabetes*. In: *Journal of diabetes science and technology* 7 (2013), Nr. 2, S. 431–440

[25] Amara, Fatima ; Agbossou, Kodjo ; Cardenas, Alben ; Dubé, Yves ; Kelouwani, Sousso: *Comparison and Simulation of Building Thermal Models for Effective Energy Management*. In: *Smart Grid and Renewable Energy* 06 (2015), Nr. 04, S. 95–112

[26] Lund, Henrik ; Arler, Finn ; Østergaard, Poul ; Hvelplund, Frede ; Connolly, David ; Mathiesen, Brian ; Karnøe, Peter: *Simulation versus Optimisation: Theoretical Positions in Energy System Modelling*. In: *Energies* 10 (2017), Nr. 7, S. 840

[27] Özkaraca, Osman: *A REVIEW ON USAGE OF OPTIMIZATION METHODS IN GEOTHERMAL POWER GENERATION*. In: *Mugla Journal of Science and Technology* (2018), S. 130–136

[28] Schellong, Wolfgang: *Analyse und Optimierung von Energieverbundsystemen*. Berlin, Heidelberg : Springer Berlin Heidelberg, 2016

[29] Wurbs, Ralph A.: *Reservoir-System Simulation and Optimization Models*. In: *Journal of Water Resources Planning and Management* 119 (1993), Nr. 4, S. 455–472

[30] Scheller, Fabian ; Bruckner, Thomas: *Energy system optimization at the municipal level: An analysis of modeling approaches and challenges*. In: *Renewable and Sustainable Energy Reviews* 105 (2019), Nr. 7, S. 444–461

[31] Nguyen, Anh-Tuan ; Reiter, Sigrid ; Rigo, Philippe: *A review on simulation-based optimization methods applied to building performance analysis*. In: *Applied Energy* 113 (2014), Nr. 2, S. 1043–1058

[32] Mavromatidis, Georgios ; Orehounig, Kristina ; Bollinger, L. Andrew ; Hohmann, Marc ; Marquant, Julien F. ; Miglani, Somil ; Morvaj, Boran ; Murray, Portia ; Waibel, Christoph ; Wang, Danhong ; Carmeliet, Jan: *Ten questions concerning modeling of distributed multi-energy systems*. In: *Building and Environment* 165 (2019), Part 2, S. 106372

[33] Cao, Karl-Kiên ; Cebulla, Felix ; Gómez Vilchez, Jonatan J. ; Mousavi, Babak ; Prehofer, Sigrid: *Raising awareness in model-based energy scenario studies — a transparency checklist*. In: *Energy, Sustainability and Society* 6 (2016), Nr. 1, S. 519

[34] Grubb, Michael ; Edmonds, Jae ; Brink, Patrick ten ; Morrison, Michael: *The Costs of Limiting Fossil-Fuel CO2 Emissions: A Survey and Analysis*. In: *Annual Review of Energy and the Environment* 18 (1993), Nr. 1, S. 397–478

[35] Mancarella, Pierluigi ; Andersson, Göran ; Lopes, Joao Abel Pecas ; Bell, Keith Robert: *Modelling of integrated multi-energy systems: drivers, requirements, and opportunities*

Proceedings PSCC, Geneoa (2016). URL
https://www.researchgate.net/publication/305730436_Modelling_of_integrated_multi
-
energy_systems_drivers_requirements_and_opportunities_P_Mancarella_G_Andersson
_JA_Pecas-Lopes_and_KRW_Bell_Proceedings_PSCC_Geneoa_June_2016 –
Überprüfungsdatum 2022-05-10

[36] GOOD, Nicholas ; ZHANG, Lingxi ; NAVARRO-ESPINOSA, Alejandro ; MANCARELLA, Pierluigi: *High resolution modelling of multi-energy domestic demand profiles*. In: *Applied Energy* 137 (2015), Nr. 4, S. 193–210

[37] LI, Francis: *Spatial explicit techno-economic optimsation modelling of UK heating futures*. London, UCL Energy Institute, University College London. Doctoral Thesis. April 2013. URL https://discovery.ucl.ac.uk/id/eprint/1400217/1/13.07.12%20-%20FL%20PhD%20Thesis%20Final.pdf – Überprüfungsdatum 2022-05-12

[38] SCHAVEMAKER, P. ; VAN DER SLUIS, L.: *Electrical Power System Essentials*. Chichester : Wiley, 2008

[39] MEDJROUBI, W. ; MÜLLER, U. P. ; SCHARF, M. ; MATKE, C. ; KLEINHANS, D.: *Open Data in Power Grid Modelling: New Approaches Towards Transparent Grid Models*. In: *Energy Reports* 3 (2017), S. 14–21. URL https://www.researchgate.net/profile/Carsten-Matke/publication/311846414_Open_Data_in_Power_Grid_Modelling_New_Approaches_Towards_Transparent_Grid_Models/links/6040edeaa6fdcc9c7812053c/Open-Data-in-Power-Grid-Modelling-New-Approaches-Towards-Transparent-Grid-Models.pdf?origin=publication_detail – Überprüfungsdatum 2022-06-09

[40] GUNKEL, David ; MOST, Dominik: *The German transmission grid expansion in long-term perspective — What is the impact of renewable integration?*, S. 1–6

[41] MOBIUS, Thomas ; GUNKEL, David: The optimal placing of energy storages in Germany in 2020 — An implementation of a DC-load flow model. In: , S. 1–5

[42] ELDRIDGE, Brent ; O'NEILL, Richard ; CASTILLO, Anya: *An Improved Method for the DCOPF With Losses*. In: *IEEE Transactions on Power Systems* 33 (2018), Nr. 4, S. 3779–3788

[43] KILE, Hakon ; UHLEN, Kjetil ; WARLAND, Leif ; KJOLLE, Gerd: *A comparison of AC and DC power flow models for contingency and reliability analysis*, S. 1–7

[44] VOPAVA, Julia ; KOCZWARA, Christian ; TRAUPMANN, Anna ; KIENBERGER, Thomas: *Investigating the Impact of E-Mobility on the Electrical Power Grid Using a Simplified Grid Modelling Approach*. In: *Energies* 13 (2020), Nr. 1, S. 39

References

[45] Bistline, John E. T.: *The importance of temporal resolution in modeling deep decarbonization of the electric power sector*. In: *Environmental Research Letters* 16 (2021), Nr. 8, S. 84005

[46] Deckmann, S. ; Pizzolante, A. ; Monticelli, A. ; Stott, B. ; Alsac, O.: *Studies on Power System Load Flow Equivalencing*. In: *IEEE Transactions on Power Apparatus and Systems* PAS-99 (1980), Nr. 6, S. 2301–2310

[47] Ward, J. B.: Equivalent Circuits for Power-Flow Studies, Bd. 68. In: *Transactions of the American Institute of Electrical Engineers*, S. 373–382

[48] Horsch, Jonas ; Brown, Tom: The role of spatial scale in joint optimisations of generation and transmission for European highly renewable scenarios. In: *2017 14th International Conference on the European Energy Market (EEM)*, S. 1–7

[49] Pfenninger, Stefan ; Hawkes, Adam ; Keirstead, James: *Energy systems modeling for twenty-first century energy challenges*. In: *Renewable and Sustainable Energy Reviews* 33 (2014), Nr. 3, S. 74–86

[50] Simon, A. J. ; Hunt, Rebecca ; Swan, Clare ; Hermann, Weston ; Simpson, Adam: *Energy System Analysis*. URL https://gcep.stanford.edu/pdfs/i6W09tDtK-48PTmzHazOuw/5.1.Energy_Systems_Analysis.pdf – Überprüfungsdatum 2022-05-23

[51] Greiml, Matthias ; Fritz, Florian ; Steinegger, Josef ; Schlömicher, Theresa ; Wolf Williams, Nicholas ; Zaghi, Negar ; Kienberger, Thomas: *Modelling and Simulation/Optimization of Austria's National Multi-Energy System with a High Degree of Spatial and Temporal Resolution*. In: *Energies* 15 (2022), Nr. 10, S. 3581

[52] Böckl, Benjamin ; Greiml, Matthias ; Leitner, Lukas ; Pichler, Patrick ; Kriechbaum, Lukas ; Kienberger, Thomas: *HyFlow—A Hybrid Load Flow-Modelling Framework to Evaluate the Effects of Energy Storage and Sector Coupling on the Electrical Load Flows*. In: *Energies* 12 (2019), Nr. 5, S. 956

[53] European Network of Transmission System Operators for Electricity: *ENTSO-E Transparency Platform*. URL https://www.entsoe.eu/data/ – Überprüfungsdatum 2022-06-10

[54] *NEPLAN Smarter Tools*. 8700 Küsnacht Zürich Switzerland : NEPLAN AG, 2022. URL https://www.neplan.ch/ – Überprüfungsdatum 2022-06-10

[55] Traupmann, Anna ; Kienberger, Thomas: *Test Grids for the Integration of RES - A Contribution for the European Context*. In: *Energies* 13 (2020), Nr. 5431

[56] Traupmann, A. ; Greiml, M. ; Kienberger, T.: *Reduction method for planning cross-energy carrier networks in the cellular approach applicable for stability assessment in low-*

voltage networks. In: *e & i Elektrotechnik und Informationstechnik* 137 (2020), Nr. 8, S. 509–514

[57] TRAUPMANN, Anna ; GREIML, Matthias ; KIENBERGER, Thomas: Equivalent cellular-based electrical network models for voltage regulation using hybrid conversion technologies at the medium-voltage level, Geneva, 20-23-September. In: *Proceedings of the CIRED 2021 Conference*, S. 5

[58] TRAUPMANN, Anna ; GREIML, Matthias ; STEINEGGER, Josef ; KÜHBERGER, Lisa ; KIENBERGER, Thomas: *Analyzing Sector Coupling Technologies for Re-purposing Coal-Fired Power Plants – Case Study for the ENTSO-E Grid*. In: *IET Energy System Integration* (2022)

[59] SCHWAB, Adolf J.: *Elektroenergiesysteme : Erzeugung, Transport, Übertragung und Verteilung elektrischer Energie*. 3.edition : Springer Berlin Heidelberg, 2011

[60] SWISSGRID AG: *Netzbetrieb - Stromnetz - Netzebenen*. URL https://www.swissgrid.ch/de/home/operation/power-grid/grid-levels.html. – Aktualisierungsdatum: 2022 – Überprüfungsdatum 2022-05-24

[61] CRASTAN, Valentin: *Elektrische Energieversorgung 1 : Netzelemente, Modellierung, stationäres Verhalten, Bemessung, Schalt- und Schutztechnik*. 3.Edition. Berlin, Heidelberg : Springer Berlin Heidelberg, 2012

[62] HEUCK, Klaus ; DETTMANN, Klaus-Dieter ; SCHULZ, Detlef: *Elektrische Energieversorgung*. Wiesbaden : Springer Fachmedien Wiesbaden, 2013

[63] KERBER, Georg: *Aufnahmefähigkeit von Niederspannungsverteilnetzen für die Einspeisung aus Photovoltaikkleinanlagen*. Technische Universität Münschen, Fakultät für Elektrotechnik und Informationstechnik. Dissertation. October 2011. URL https://mediatum.ub.tum.de/doc/998003/998003.pdf – Überprüfungsdatum 2022-05-24

[64] KAUFMANN, Thomas ; BOTHE, Dominik ; GAWLIK, Wolfgang ; PONWEISER, Karl: Optimierung der Lastflüsse in urbanen Hybridnetzen. In: *9.International Energiewirtschaftstagung*, S. 10

[65] KIENBERGER, Thomas: *Energienetze (540.009)*. Leoben, 2017

[66] GRAINGER, John J. ; STEVENSON, William D., JR.: *Power System Analysis*. International Edition. New York : McGraw-Hill Series in Electrical and Computer Engineering, 1994

[67] AUSTRIAN POWER GRID AG: *Power Grid*. URL https://www.apg.at/en/Stromnetz/APG-Netz – Überprüfungsdatum 2022-05-24

[68] SCHEFFLER, Jörg: *Bestimmung der maximal zulässigen Netzanschlussleistung photovoltaischer Energiewandlungsanlagen in Wohnsiedlungsgebieten*. Technische Universität Chemnitz, Fakultät Elektrotechnik und Informationstechnik. Dissertation. June 2002. URL https://monarch.qucosa.de/api/qucosa%3A17912/attachment/ATT-0/ – Überprüfungsdatum 2022-05-24

[69] WEIßGERBER, Wilfried: *Elektrotechnik für Ingenieure 3* : *Ausgleichsvorgänge, Fourieranalyse, Vierpoltheorie*. 9.Edition. Wedemark, Germany : Springer Vieweg, 2015 (Elektrotechnik für Ingenieure 3)

[70] SWISSGRID AG: *Factsheet Spannungshaltung*. URL https://www.swissgrid.ch/dam/swissgrid/about-us/newsroom/positions/220519-factsheet-spannungshaltung-de.pdf – Überprüfungsdatum 2022-06-01

[71] OEDING, Dietrich ; OSWALD, Bernd Rüdiger: *Elektrische Kraftwerke und Netze*. Berlin, Heidelberg : Springer Berlin Heidelberg, 2011

[72] SCHÄFER, Karl Friedrich: *Netzberechnung*. Wiesbaden : Springer Fachmedien Wiesbaden, 2020

[73] OSWALD, Bernd R.: *Berechnung von Drehstromnetzen*. Wiesbaden : Springer Fachmedien Wiesbaden, 2013

[74] HOSEMANN, Gerhard: *Elektrische Energietechnik*. Berlin, Heidelberg : Springer Berlin Heidelberg, 2001

[75] ENARGUS: *Spannungsstabilität*. URL https://www.enargus.de/pub/bscw.cgi/d11886-2/*/*/Spannungsstabilit%C3%A4t.html?op=Wiki.getwiki – Überprüfungsdatum 2022-06-15

[76] E-CONTROL: *Technische und organisatorische Regeln für Betreiber und Benutzer von Netzen (TOR)* : *Teil D2*. URL https://www.e-control.at/marktteilnehmer/strom/marktregeln/tor – Überprüfungsdatum 2022-06-01

[77] EN 50160 (29.020). 2011-03-01. *Merkmale der Spannung in öffentlichen Elektrizitätsversorgungsnetzen*

[78] E-CONTROL: *Spannungsqualität*. URL https://www.e-control.at/industrie/strom/versorgungssicherheit/spannungsqualitaet – Überprüfungsdatum 2022-06-01

[79] ENARGUS: *Spannungsbandverletzung*. URL https://www.enargus.de/pub/bscw.cgi/d11834-2/*/*/Spannungsbandverletzung.html?op=Wiki.getwiki – Überprüfungsdatum 2022-06-01

References

[80] KUNDUR, P. ; PASERBA, J. ; AJJARAPU, V. ; ANDERSSON, G. ; BOSE, A. ; CANIZARES, C. ; HATZIARGYRIOU, N. ; HILL, D. ; STANKOVIC, A. ; TAYLOR, C. ; VAN CUTSEM, T. ; VITTAL, V.: *Definition and Classification of Power System Stability IEEE/CIGRE Joint Task Force on Stability Terms and Definitions*. In: *IEEE Transactions on Power Systems* 19 (2004), Nr. 3, S. 1387–1401

[81] VOLTIMUM: DAS INFORMATIONSPORTAL FÜR ELEKTROTECHNIKER: *Spannungsspitzen (zer-)stören die Energieversorgung*. URL https://www.voltimum.de/sites/www.voltimum.de/files/fields/attachment_file/de/others/W/201006082389760.pdf – Überprüfungsdatum 2022-06-15

[82] BÜCHNER, Jens ; KATZFEY, Jörg ; FLÖRCKEN, Ole ; MOSER, Albert ; SCHUSTER, Henning ; DIERKES, Sebastian ; VAN LEEUWEN, Tobias ; VERHEGGEN, Lukas ; USLAR, Matthias ; VAN AMELSVOORT, Marie; Bundesministerium für Wirtschaft und Energie (BMWi) (Mitarb.): *Moderne Verteilnetze für Deutschland*. Forschungsprojekt Nr. 44/12. September 2014

[83] LARIK, Raja Masood ; MUSTAFA, Mohd Wazir ; AMAN, Muhammad Naveed: *A critical review of the state-of-art schemes for under voltage load shedding*. In: *International Transactions on Electrical Energy Systems* 29 (2019), Nr. 5, e2828

[84] RENNER, Herwig: *Kapitel 5: Spannungsstabilität* (Lecture: Regelung und Stabilität elektrischer Energiesysteme)

[85] ENARGUS: *Spannungsband*. URL https://www.enargus.de/pub/bscw.cgi/d11828-2/*/*/Spannungsband.html?op=Wiki.getwiki – Überprüfungsdatum 2022-06-15

[86] CHAKRABARTI, S.: *Notes on Power System Voltage Stability* (2011). URL https://www.researchgate.net/publication/260661284_Notes_on_power_system_voltage_stability – Überprüfungsdatum 2022-06-01

[87] CUTSEM, Thierry ; VOURNAS, Costas: *Voltage Stability of Electric Power Systems*. Boston, MA : Springer US, 1998

[88] CRASTAN, Valentin: *Chapter: Spannungsregelung und Spannungsstabilität. In: Elektrische Energieversorgung 2*. Pages 563-601 : Springer, Berlin, Heidelberg, 2008

[89] ZAFRAN, Muhammad ; ARBAB, Muhammad Naeem ; AHMAD, Imtiaz ; KHAN, Muhammad Usman Karim: *A case study on alleviating electric transmission congestion using dynamic thermal rating methodology*, S. 1–6

[90] STAUDT, Philipp ; RAUSCH, Benjamin ; GARTTNER, Johannes ; WEINHARDT, Christof: *Predicting Transmission Line Congestion in Energy Systems with a High Share of Renewables*, S. 1–6

[91] RINK, Steven ; OLIVERAS, Henri ; TÄNZER, Guillem ; LEVACHER, Ralf ; RINK, Jörg; Technical University Vienna (Mitarb.): Netzautomatisierung in der Niederspannungsebene als

Bottom-Up-Ansatz zur Stabilisierung des zukünftigen Energieversorgungssystems. In: *Proceedings of 11. Internationale Energiewirtschaftstagung*, S. 15

[92] MOHRING, Alexandra ; MICHAELIS, Julia; Fraunhofer ISI (Mitarb.): *Techno-ökonomische Bewertung von Stromspeichern im Niederspannungsnetz*. 2013

[93] HAASE GESELLSCHAFT M.B.H.: *Leiterseile aus Aluminium/Stahl (AL1/ST1A) nach EN 50182:2001*. URL https://haase.at/downloadfiles/haase_en_prodtab_AL1-ST1A_de.pdf – Überprüfungsdatum 2022-08-08

[94] ESTRALIN HVC: *Power cables and cable systems 110-220 kV: Modern solutions for power cables*. URL http://estralin.com/files/catalogues/estralinHVCeng.pdf – Überprüfungsdatum 2022-08-08

[95] WANG, Yanling ; SUN, Zidan ; YAN, Zhijie ; LIANG, Likai ; SONG, Fan ; NIU, Zhiqiang: *Power Transmission Congestion Management Based on Quasi-Dynamic Thermal Rating*. In: *Processes* 7 (2019), Nr. 5, S. 244

[96] SCHMARANZ, Robert: *Teil 3 Operative Betriebsführung* (Betriebsführung elektrischer Verteilnetze). Technical University Graz, 2020

[97] VDE VERBAND DER ELEKTROTECHNIK ELEKTRONIK INFORMATIONSTECHNIK E.V.: *VDE FNN (Forum Netztechnik/Netzbetrieb) : Einsatz von Hochtemperaturleitern*. URL https://www.vde.com/de/fnn/arbeitsgebiete/innovation/freileitungen/hinweis-hochtemperaturleiter – Überprüfungsdatum 2022-08-08

[98] VDI VERLAG GMBH 2022: *Netzbetreiber zögern bei neuer Leiterseiltechnik*. URL https://www.vdi-nachrichten.com/technik/energie/netzbetreiber-zoegern-bei-neuer-leiterseiltechnik/. – Aktualisierungsdatum: 2014-01-10 – Überprüfungsdatum 2022-08-08

[99] AUSTRIAN POWER GRID AG: *Price driver - redispatch : Why does grid expansion reduce electricity costs?* URL https://www.apg.at/en/Energiezukunft/Redispatch – Überprüfungsdatum 2022-06-15

[100] PFLEGER-SCHOPF, Kerstin: *Kommunale Abwasserreinigungsanlagen mit optionaler thermischer Klärschlammverwertung als Flexibilitätsdienstleister in elektrischen Netzen*. Leoben, Montanuniversity Leoben, Chair of Energy Network Technology. Dissertation. 2021

[101] GAWLIK, Wolfgang ; GROIß, Christoph ; LITZLBAUER, Markus ; MAIER, Christoph ; SCHUSTER, Andreas ; ZEILINGER, Franz ; KANN, ALEXANDER, MEIROLD-MAURER, INGO ; GÜNTHER, Gerhard ; EUGSTER, Christian ; NENNING, Reinhard ; SCALET, Johannes ; ÖSTERLE, Philipp ; JUSSEL,

Heinrich ; Karner, Christoph ; Wolfram, Gernot ; Petschauer, Helmut: *Final Report aDSM - Aktives Demand-Side Management durch Einspeiseprognosen* (834612)

[102]   Böckl, Benjamin ; Kienberger ; Thomas: Nutzergruppenabhängiger Photovoltaik-Heimspeicherbedarf. In: *Proceedings 15.Symposium Energieinnovation 2018*, S. 6

[103]   Adby, P. R. ; Dempster, M. A. H.: *Introduction to Optimization Methods*. Dordrecht : Springer Netherlands, 1974

[104]   Kochenderfer, Mykel J. ; Wheeler, Tim A.: *Algorithms for Optimization*. Cambride, Massachusetts, London, England : The MIT Press

[105]   Diwekar, Urmila M.: *Introduction to Applied Optimization*. Cham : Springer International Publishing, 2020 (22)

[106]   Schellong, Wolfgang: *Analyse und Optimierung von Energieverbundsystemen*. Berlin, Heidelberg : Springer Berlin Heidelberg, 2016

[107]   Haikarainen, Carl ; Pettersson, Frank ; Saxén, Henrik: *A model for structural and operational optimization of distributed energy systems*. In: *Applied Thermal Engineering* 70 (2014), Nr. 1, S. 211–218

[108]   Ma, Shixi ; Zhou, Dengji ; Zhang, Huisheng ; Weng, Shilie ; Shao, Tiemin: *Modeling and Operational Optimization Based on Energy Hubs for Complex Energy Networks With Distributed Energy Resources*. In: *Journal of Energy Resources Technology* 141 (2019), Nr. 2, S. 430

[109]   Wang, Xiaonan ; Palazoglu, Ahmet ; El-Farra, Nael H.: *Operational optimization and demand response of hybrid renewable energy systems*. In: *Applied Energy* 143 (2015), Nr. 1, S. 324–335

[110]   Cheng, Yu ; Tai, Yufeng: *A MILP Model for Optimizing Distributed Resource System with Energy Storage and PV Considering Energy Storage Life Loss*. In: *2018 2nd IEEE Conference on Energy Internet and Energy System Integration (EI2), Beijing, China* (2018-10-20), S. 1–6

[111]   Gabrielli, Paolo ; Gazzani, Matteo ; Martelli, Emanuele ; Mazzotti, Marco: *A MILP model for the design of multi-energy systems with long-term energy storage* 40, S. 2437–2442

[112]   Haikarainen, Carl ; Pettersson, Frank ; Saxén, Henrik: *An MILP Model for Distributed Energy System Optimization*. In: *Chemical Engineering Transactions* 35 (2013). URL https://www.aidic.it/cet/13/35/049.pdf – Überprüfungsdatum 2022-06-10

[113]   REN, Hongbo ; GAO, Weijun: *A MILP model for integrated plan and evaluation of distributed energy systems*. In: *Applied Energy* 87 (2010), Nr. 3, S. 1001–1014

[114]   NEXT KRAFTWERKE GMBH: *Was ist der Strommarkt?* URL https://www.next-kraftwerke.de/wissen/strommarkt – Überprüfungsdatum 2022-05-20

[115]   DOLNA-GRUBER, Christoph ; KNAUS, Karina ; ZWIEB, Lukas: *Stromgroßhandel - Preisentwicklung und wesentliche Einflussfaktoren*. March 2022

[116]   NEXT KRAFTWERKE GMBH: *Was bedeutet Merit-Order?* URL https://www.next-kraftwerke.de/wissen/merit-order – Überprüfungsdatum 2022-05-20

[117]   SAUVAGE, Jehan ; BAHAR, Heymi: *Cross-Border Trade in Electricity and the Development of Renewables-Based Electric Power: Lessons from Europe* (July 2013). URL https://www.researchgate.net/publication/290391278_Cross-Border_Trade_in_Electricity_and_the_Development_of_Renewables-Based_Electric_Power_Lessons_from_Europe – Überprüfungsdatum 2022-05-20

[118]   MENTOR EBS ENERGY BUSINESS SCIENCE: *What affects elelctricity prices in Slovenia*. URL http://www.mentor-ebs.si/ARTICLES – Überprüfungsdatum 2022-05-20

[119]   VOPAVA, Julia ; BÖCKL, Benjamin ; KRIECHBAUM, Lukas ; KIENBERGER, Thomas: *Anwendung zellularer Ansätze bei der Gestaltung zukünftiger Energieverbundsysteme*. In: *e & i Elektrotechnik und Informationstechnik* 134 (2017), Nr. 3, S. 238–245

[120]   PAPAEMMANOUIL, A. ; ANDERSSON, G.: *On the reduction of large power system models for power market simulations* (2011). URL http://citeseerx.ist.psu.edu/viewdoc/download?doi=10.1.1.723.5598&rep=rep1&type=pdf – Überprüfungsdatum 2022-06-10

[121]   HOUSOS, E. ; IRISARRI, G. ; PORTER, R. ; SASSON, A.: *Steady State Network Equivalents for Power System Planning Applications*. In: *IEEE Transactions on Power Apparatus and Systems* PAS-99 (1980), Nr. 6, S. 2113–2120

[122]   DECKMANN, S. ; PIZZOLANTE, A. ; MONTICELLI, A. ; STOTT, B. ; ALSAC, O.: *Numerical Testing of Power System Load Flow Equivalents*. In: *IEEE Transactions on Power Apparatus and Systems* PAS-99 (1980), Nr. 6, S. 2292–2300

[123]   GAVRILAS, Mihai ; IVANOV, Ovidiu ; GAVRILAS, Gilda: *REI Equivalent Design for Electric Power Systems with Genetic Algorithms*. In: *WSEAS Transaction on Circuits & Systems* 7 (2008), S. 11. URL https://www.researchgate.net/publication/234756309_REI_equivalent_design_for_electric_power_systems_with_genetic_algorithms – Überprüfungsdatum 2022-06-10

[124]   SHAYESTEH, E. ; HAMON, C. ; AMELIN, M. ; SÖDER, L.: *REI method for multi-area modeling of power systems*. In: *International Journal of Electrical Power & Energy Systems* 60 (2014), October, S. 283–292

[125]   ASHRAF, Syed Mohammad ; RATHORE, Bhavna ; CHAKRABARTI, S.: *Performance analysis of static network reduction methods commonly used in power systems*, S. 1–6

[126]   RAO, Shruti ; TYLAVSKY, Daniel: Nonlinear network reduction for distribution networks using the holomorphic embedding method. In: , S. 1–6

[127]   AUSTRIAN POWER GRID AG: *Generation per Type*. URL https://www.apg.at/en/markt/Markttransparenz/erzeugung/Erzeugung%20pro%20Typ – Überprüfungsdatum 2022-06-09

[128]   PFLUGRADT, N. ; TEUSCHER, J. ; PLATZER, B. ; SCHUFFT, W.: *Analysing low-voltage grids using a behaviour based load profile generator* International Conference on Renewable Energies and Power Quality (ICREPQ), Bilbao (Spain) (2013). URL https://www.researchgate.net/profile/Noah-Pflugradt/publication/316724031_Analysing_low-voltage_grids_using_a_behaviour_based_load_profile_generator/links/592f0bab0f7e9beee7521a29/Analysing-low-voltage-grids-using-a-behaviour-based-load-profile-generator.pdf?origin=publication_detail – Überprüfungsdatum 2022-06-09

[129]   PFLUGRADT, N.: *Online Load Profile Generator*. URL https://www.loadprofilegenerator.de/ – Überprüfungsdatum 2022-06-09

[130]   ESSLINGER, Peter ; WITZMANN, Rolf: Entwicklung unf Verifikation eines stochastischen Verbraucherlastmodells für Haushalte. In: *12.Symposium Energieinnovation*, S. 11

[131]   DEUTSCH, Matthias: *Wärmewende 2030: Schlüsseltechnologien zur Erreichung der mittel- und langfristigen Klimaschutzziele im Gebäudesektor*. Febuary 2017

[132]   STATISTA: *Annual amount of heat pumps in operation in the European Union (EU) from 2013 to 2020*. URL https://www.statista.com/statistics/739745/heat-pumps-in-operation-eu/ – Überprüfungsdatum 2022-06-13

[133]   EUROPEAN COMMISSION: *EU Reference Scenario 2016: Energy, transport and GHG emissions - Trends to 2050*. URL https://ec.europa.eu/energy/sites/ener/files/documents/20160713%20draft_publication_REF2016_v13.pdf – Überprüfungsdatum 2022-06-13

[134]   PÖTSCHER, Friedrich ; WINTER, Ralf ; LICHTBLAU, Günther: *Elektromobilität in Österreich Szenario 2020 und 2050*. 2010

[135]   QVIST, Staffan ; GŁADYSZ, Paweł ; BARTELA, Łukasz ; SOWIŻDŻAŁ, Anna: *Retrofit Decarbonization of Coal Power Plants — A Case Study for Poland*. In: *Energies* 14 (2021), Nr. 1, S. 120

[136]   STOLL, H. G. ; SMITH, R. W. ; TOMLINSON, L. O.; GE Power Systems (Mitarb.): *Performance and Economic Considerations of Repowering Steam Power Plants.* Schenectady, NY, USA, 1996

[137]   SEJKORA, Christoph ; KÜHBERGER, Lisa ; RADNER, Fabian ; TRATTNER, Alexander ; KIENBERGER, Thomas: *Exergy as Criteria for Efficient Energy Systems — A Spatially Resolved Comparison of the Current Exergy Consumption, the Current Useful Exergy Demand and Renewable Exergy Potential*. In: *Energies* 13 (2020), Nr. 4, S. 843

8 APPENDIX A: PEER-REVIEWED PUBLICATIONS AND COMPLEMENTARY CONFERENCE CONTRIBUTIONS

Paper 1 (Status: Accepted)

TRAUPMANN, A.; KIENBERGER, T., *Novel Network Reduction Method for Cellular-based Network Models with Enhanced Modeling Accuracy for Multi-Energy-System Approaches*, In: International Journal of Electrical Power and Energy Systems 2022, 137, 107827, doi.org/10.1016/j.ijepes.2021.107827.

Table A. 1: Author statement to first peer-reviewed publication (Paper 1)

Activity	Contribution authors (main author is mentioned first)
Conceptualization	A. Traupmann, T. Kienberger
Methodology	A. Traupmann, T. Kienberger
Data Curation	A. Traupmann
Software Development and Validation	A. Traupmann
Modeling	A. Traupmann
Visualization	A. Traupmann
Writing (Original Draft)	A. Traupmann
Writing (Review and Editing)	A. Traupmann, T. Kienberger

Test Grids for the Integration of RES—A Contribution for the European Context

Anna Traupmann *[ORCID] **and Thomas Kienberger**

Chair of Energy Network Technology, Montanuniversitaet Leoben, Franz-Josef-Straße 18,
A-8700 Leoben, Austria; Thomas.kienberger@unileoben.ac.at
***** Correspondence: anna.traupmann@unileoben.ac.at; Tel.: +43-3842-402-5414

Abstract: A long-term sustainable energy transition can only be achieved by technological advancements and new approaches for efficiently integrating renewable energies into the overall energy system. Significantly increasing the share of renewable energy sources (RES) within the overall energy system requires appropriate network models of current transmission and distribution grids, which, as limiting factors of energy infrastructures, confine this share due to capacity constraints. However, especially regarding electrical network models, data (e.g., geographical data, load and generation profiles, etc.) is rarely available since it usually includes user-specific information and is, therefore, subject to data protection. Synthetically obtained electrical networks, on the other hand, may not be representative and may fail to replicate real grid structures due to the heterogeneous properties of currently operated networks. To account for this heterogeneity, this paper offers a contribution for the European electrical energy system and presents the development of four synthetic test networks at different voltage levels which are representative and include non-confidential time-series data. The test network development is based on an extensive literature research on a multitude of different network parameters for grids within the ENTSO-E (European Network of Transmission System Operators for Electricity) interconnected system in Europe. These parameters are then used to design the networks in NEPLAN®. Then, these networks are provided with load and generation profiles for enabling time-series calculations. To validate the representativeness of the test networks, a short-circuit analysis is conducted and the obtained results are compared to short-circuit parameters common for Austrian and German literature values as well as for value ranges for European ENTSO-E grids. The analysis shows that the presented test networks replicate European electrical network behavior accurately and can, therefore, be utilized for various application purposes to assess technological impacts on European ENTSO-E grids.

Keywords: transmission grids; distributions grids; test networks; voltage levels

1. Introduction

In order to facilitate long-term sustainable energy generation, significant changes within the energy system have to be accomplished to enable infrastructures that are mainly or even entirely based on renewable energy sources (RES). Solutions to successfully achieve the transition to a sustainable energy future aim at efficiently integrating renewable energies into the grid or using available energy within the overall energy system more efficiently. For many of these solutions, more research is needed, especially regarding infrastructural impacts as well as grid bottlenecks, in order to enable an efficient implementation [1–3].

One of these solutions is the multi-energy system (MES), which enables the use of energy across energy carriers, thus facilitating a more efficient use as well as a better integration of renewable energy sources. These systems require major changes in the structure and operation of current energy networks

which transport and distribute grid-bound energy individually to customers. Thus, present-day electrical networks are operated as independent network structures without utilizing possible connections and synergies to other energy carrier networks. Since the integration of RES into current structures burdens mainly electrical networks, intersectoral load shifts into other energy carrier networks could reduce or even avoid excessive strains. Energy exchange between different energy carrier networks, therefore, may stabilize electrical networks as well as the entire energy system. This enables a more flexible reaction to volatile, decentralized and unpredictable generation of RES. Thus, it is easier to preserve the balance between energy generation and energy consumption at all times within the grid. Significant advantages regarding primary energy use due to utilizing cascaded energy chains and exergetic potentials can, additionally, be achieved. However, in order to ensure the above mentioned benefits of multi-energy systems, efficient planning within the entire energy system is required. Therefore, a hybrid load flow modelling framework, HyFlow [4], was developed at the Chair of Energy Network Technology at the Montanuniversitaet Leoben, which aims at evaluating the influence of hybrid networks within the Austrian energy system and their potential contribution for decarbonizing the energy sector [4].

For developing and improving innovative tools, such as HyFlow, appropriate test networks including an extensive data basis of all network components are of great importance. These test networks aim at reproducing the behavior of a real network [5] and can either be used to investigate the effects of different new technologies on the network structures (impact studies on grids) or to test algorithms and program structures. Additionally, test networks also allow one to consistently compare different algorithms. Since transmission and distribution network data of a country is usually not publicly available to be used as test cases due to data protection regulations, only a few real networks are available for research purposes. Therefore, generic test networks have been continuously created and published in literature to provide test cases to the research community. For developing test networks, there are four different approaches [6]:

1. Feeder anonymization: removing private and/or sensitive data from real networks resulting in real test networks.
2. Cluster and Combine: using clustering techniques to group together a number of real networks and then assemble the pieces to a synthetic test network.
3. Manual design: focusses on specific network features resulting in a very complex process for creating the synthetic test network.
4. Planning tools: tools that are designed to create realistic networks by considering technical and economic criteria.

The most important criterion for obtaining conclusive results from test networks, e.g., regarding RES integration, is representativeness which refers to the ability of a test network to reproduce the characteristics of a real network [6]. Usually it is not explicitly clear for every available test network in the literature whether this feature is fully achieved. Additionally, only very few European test networks are available in the literature and even fewer offer appropriate data for the included network elements. The presented networks, therefore, provide a basis for European test networks within the ENTSO-E (European Network of Transmission System Operators for Electricity) interconnected system for the integration of renewable energy sources and can be extended or adapted for other or more detailed applications. This paper, thus, offers a contribution to the research community regarding European structures by addressing the following research questions:

- Which qualities do the test networks available in the literature offer (in general and specifically for European structures)?
- What are the gaps in these test networks, especially regarding RES integration, and how can comprehensive test networks be obtained without these gaps?

The first research question refers to identifying the qualities (available voltage levels, number of feeders, available load and generation data, grid representation, network size, adaption to other

application purposes) regarding the representation of the overall energy system, especially for integrating RES in European grids. The second research question, then, assesses which of the available test networks in the literature have gaps regarding the necessary qualities for RES integration, which will reveal the need for further test networks. Subsequently, this paper develops test networks which fill these gaps. Thus, the paper is divided in the following sections.

In Section 1.1, currently available test networks or test feeders are comprehensively reviewed to provide an overview. Section 1.2 then addresses these research questions and shows the limitations of the available networks, which will lead to the conclusion why specific test networks for the integration of RES in European infrastructures are required. This section is followed by Section 2, which presents the development of the generic test networks for each voltage level common in the European ENTSO-E interconnected system and addresses the used methodology of manual design. Section 3 then shows the results obtained from performing a short-circuit analysis, where the maximum short-circuit power and the maximum short-circuit current are determined for each test network to validate their representativeness. In Section 4, these results are discussed in detail. Additionally, Section 4 reviews the test network limitations from the literature addressed in Section 1.2 to show the improvements achieved for the developed test networks and their remaining limitations. Section 5 then summarizes the presented work and provides an outlook.

1.1. State of Research in Test Networks

In the following, current publicly available test feeders, which are usually comprised of only one feeder, as well as test networks, which are comprised of several feeders and therefore more closely replicate real grids, and their design approaches are presented. This section shows the characteristics of different test networks and enables the need for test networks to be derived, specifically representing European structures for networks within the ENTSO-E interconnected grid, such as Austrian grids, in detail.

1.1.1. IEEE (Institute of Electrical and Electronics Engineers) Test Feeders

The first set of test feeders was published in 1991 [7]. These first four test feeders are models of real radial distribution networks in the United States [5]. Over the years, more test feeders were added to include different features within the networks [5]. All of the added networks are also representative for the US; only in recent years have low-voltage networks and one network based on European electrical energy system structures been published [5]. A total of 11 test feeders can be found on the IEEE PES (IEEE Power and Energy Society) website [8] and are summarized in Table 1. The table shows total line lengths, voltage levels as well as application purposes for each test feeder.

Table 1. Overview over the IEEE (Institute of Electrical and Electronics Engineers) test feeders currently available.

ID	Total line Length (km)	Primary Voltage (kV)	Application Purpose
13 Node [7]	2.49 [8]	4.16 [8]	Testing power-flow convergence problems for highly unbalanced systems [6–8]
123 Node [7]	11.96 [8]	4.16 [8]	Analysis of voltage drop problems, implementation of voltage management with voltage regulators [6–8]
34 Node [7]	93.91 [8]	24.9 [8]	Testing power-flow convergence problems due to long line lengths and unbalanced feeders [6–8]
37 Node [7]	5.50 [8]	4.8 [8]	Testing algorithms for uncommon configurations [6–8]
4 Node [7]	1.30 [6]	12.47 [7]	Analysis of available three-phase transformer connections, of step-up (24.9kV) or step-down (4.16 kV) operations and balanced/unbalanced loads [6,7]
NEV [8,9]	1.82 [6]	12.47 [6]	Load modeling studies [6,10–12] and harmonic analysis [6,13]
8500 Node [14]	170.00 [8]	12.47 [6]	Testing of algorithms on realistic large-scale reference systems [6,8,14]
CTF [15]	81.67 [8]	12.47/ 24.90 [6]	Software testing issues [6], often for smart grid analysis [6,16]
342 Node [17]	15.20 [6]	13.2 [17]	Evaluation of algorithms in non-radial distribution networks [6,17], distributed energy resources (DER) studies [18], communication planning analysis [19]
European LV [8]	1.43 [8]	0.416 [8]	Studies of low-voltage feeders common in Europe and their mid- to long-term dynamic behavior [8]

The IEEE 13 node test feeder presents a highly loaded 4.16 kV network including one substation regulator as well as overhead and underground lines, shunt capacitor banks, in-line transformers and unbalanced spot or distributed loads [7].

The IEEE 123 node test feeder operates at a nominal primary voltage of 4.16 kV, which is not common, but provides voltage drop problems. Therefore, the application of voltage regulators and shunt capacitors can be tested. Additionally, due to spot loads and a multitude of switches within the test feeder, optimal configuration procedures as well as load allocations can be studied [7].

The IEEE 34 node test feeder represents a real feeder in Arizona with long and highly loaded lines and three in-line regulators, of which two are used to maintain a smooth voltage profile, and the third is used to reduce the voltage to 4.16 kV for a short section of the feeder [7].

Similarly, the IEEE 37 node test feeder represents a real feeder located in California with a nominal voltage of 4.8 kV. Electrical lines all represent underground lines and spot loads with highly unbalanced loadings occur in this test feeder [7].

For testing all possible three-phase transformer connections with the possibility for step-up (secondary voltage of 24.9 kV) as well as step-down (secondary voltage of 4.16 kV) operations, the IEEE four node test feeder can be used. The load can either be balanced or unbalanced [7].

The purpose of the neutral-to-earth voltage test case (NEV) is solving the neutral-to-earth voltage problem [8], also called stray voltage, which is a result of electrical current flowing through a neutral conductor. In addition to other test feeders, which are capable of modelling NEV problems, this test feeder is for distribution system analysis including all aspects of steady-state frequency-domain analysis in distribution networks [8]. Therefore, this test feeder can be used for load modeling studies [6,10–12]. Since NEV problems basically represent third order harmonics as well as fundamental frequency voltage, which requires a solution of the system at two different frequencies [8,20], the test network can also be used for harmonic analysis [6,13].

The IEEE 8500 node test feeder is based principally on a real network in the USA and contains common features of North American networks such as a high number of voltage regulators (load tap changer at the substation and multiple feeder regulators and switched capacitor banks), per-phase capacitor control, low-voltage secondaries, as well as centered-tapped transformers. This network enables testing of the application of algorithms, e.g., for distribution system analysis on large systems. Therefore, it is used primarily for power flow solutions but also for distribution automations (voltage and var control simulations) as well as annual load shape simulations for evaluating energy efficiency options, renewable energy generation and electric vehicle impacts [14].

The CTF (comprehensive distribution test feeder) includes most of the available configurations as well as electrical equipment and, therefore, represents a detailed network [15]. The components within the feeder include overhead lines, underground cables, transformer connections, center tapped transformers, step voltage regulators, switches, induction machines, distributed and spot loads as well as switched capacitor banks and center tapped loads and transformer substations [15]. Therefore, the model can be used to test the models of all distribution components as well as their convergence qualities [15]. Due to the included switching devices a wide range of network configuration possibilities can be created [6]. Outside of software testing issues, the results obtained from this network can be unrealistic [6].

The IEEE 342 node low-voltage network test feeder represents a moderately sized, unbalanced and highly meshed urban system. This 120/208 V network is fed by primary feeders from the 13.2 kV-voltage level. Additionally, to facilitating the assessment of non-radial, highly meshed systems, it is also possible to test systems with numerous parallel transformers and parallel low-voltage lines [17].

Since the above presented IEEE test feeders are based on North American network infrastructures, which differ from European grids regarding the distribution system configuration, the EuropeanLV (Low-Voltage) test feeder focuses on European grid infrastructures [8]. Additionally, this circuit introduces quasi-static time series power flow solutions, which are provided for this feeder using the electric power distribution system simulator OpenDSS (EPRI (Electric Power Research Institute),

Palo Alto, CA, USA) [21] and the power distribution analysis tool GridLAB-D (U.S. Department of Energy (DOE) at Pacific Northwest National Laboratory (PNNL), Washington, DC, USA) [22]. On the IEEE PES Resources online site [8], the load profiles used in the feeder with a one-minute time resolution over 24 h are provided as well [8]. This feeder can be used for distributed energy resources (DER) studies in low-voltage networks with European distribution system configurations [23].

1.1.2. PNNL (Pacific Northwest National Laboratory) Taxonomy Feeders

A big barrier for smart grid technology integration into present-day grids is the lack of adequate assessment possibilities of their impact on electrical infrastructures [24]. Besides others, this refers to the lack of distribution test feeders for such purposes. Therefore, the PNNL (Pacific Northwest National Laboratory) collected 575 distribution feeder models in the US and analyzed regional differences in feeder design and operation. Since nominal voltage level, climate region, and load composition are not sufficient characteristics for the feeders in the US, graph theory was used to identify designs that additionally characterize the feeders, such as overhead circuit length, feeder ratings and connected apparent power profile type (residential, commercial, industrial, agricultural). In total, 35 statistical and electrical properties were studied. Based on this analysis and the utilization of hierarchical clustering algorithms, a taxonomy of 24 prototypical feeder models was created that is representative of a class of distribution feeders found in each of the climate regions in the US. These feeders were then modelled in GridLAB-D and, since utility specific information was removed from the feeders, unrestrictedly distributed [24]. Further, more detailed information about the creation and description of the PNNL taxonomy feeders can be found in the report [24], and a short summary of the test feeders can be found in Table 2.

Table 2. Overview over the PNNL (Pacific Northwest National Laboratory) taxonomy feeders currently available [24].

Climate Region	Feeder ID	Primary Voltage (kV)	Feeder Description
Region 1: Temperate climate	R1-12.47-1	12.50	Moderately populated suburban and rural area
	R1-12.47-2	12.47	Moderately populated suburban and lightly populated rural area
	R1-12.47-3	12.47	Moderately populated urban area
	R1-12.47-4	12.47	Heavily populated suburban area
	R1-25.00-1	24.90	Lightly populated rural areas
Region 2: Cold climate	R2-12.47-1	12.47	Lightly populated urban area
	R2-12.47-2	12.47	Moderately populated suburban area
	R2-12.47-3	12.47	Lightly populated suburban area
	R2-25.00-1	24.90	Moderately populated suburban area
	R2-35.00-1	34.50	Lightly populated rural area
Region 3: Hot and arid climate	R3-12.47-1	12.47	Heavily populated urban area
	R3-12.47-2	12.47	Moderately populated urban area
	R3-12.47-3	12.47	Heavily populated suburban area
Region 4: Hot and cold climate	R4-12.47-1	13.80	Heavily populated urban (with primary feeder extension) into lightly populated rural area
	R4-12.47-2	12.50	Lightly populated suburban area with moderately populated urban area
	R4-25.00-1	24.90	Lightly populated rural area
Region 5: Hot and humid climate	R5-12.47-1	13.80	Heavily populated suburban area and moderate urban center
	R5-12.47-2	12.47	Moderate suburban with a heavy urban area
	R5-12.47-3	13.80	Moderately populated rural area
	R5-12.47-4	12.47	Moderately populated suburban and urban area
	R5-12.47-5	12.47	Moderately populated suburban are with lightly populated urban area
	R5-25.00-1	22.90	Heavily populated suburban with a moderately populated urban area
	R5-35.00-1	34.50	Moderately populated suburban with a lightly populated urban area
All regions: General feeder	GC-12.47-1	12.47	Load supply through a single large transformer or a group of smaller units

The loads within these test feeders are either residential (single- or multi-family households), commercial (light, moderate or heavy), industrial (light, moderate or heavy) or agricultural (light, moderate or heavy). The feeders consist of a maximum of 2000 network nodes and a minimum of 52 network nodes. The general feeder (GC-12.47-1) can exist in any of the five climate regions. Therefore, the feeder consists of only 27 network nodes [24].

The application purpose of the PNNL-taxonomy feeders is the analysis of new technologies for distribution systems, especially, for DER studies [25,26] and reliability analysis [26–28], since they assume that the solution method for power flow calculations is valid [6,29].

1.1.3. EPRI (Electric Power Research Institute) Representative Feeders

The test feeders published by the EPRI (Electric Power Research Institute) are obtained from real networks and, therefore, include bus relative coordinates as well as time-series data in order to offer more realistic test cases for the US-continental area [6]. The first three feeders (feeder J1 [30], feeder K1 [31] and feeder M1 [32]) are focused on distributed photovoltaic (PV) monitoring and feeder analysis in order to assess the impact of different levels of distributed photovoltaic penetration [6]. The application purposes of the last three feeders (feeder Ckt5, feeder Ckt7 and feeder Ckt24) are investigations of smart grid issues [33]. Table 3 shows a short summary of the EPRI test feeders:

Table 3. Overview over the EPRI (Electric Power Research Institute) test feeders currently available [30–33].

Feeder ID	Total line Length (km)	Primary Voltage (kV)	Feeder Description
Feeder J1 [30]	93.32	12.00	1.7 MW load of customer-owned photovoltaic (PV) systems and there are problems with overvoltage
Feeder K1 [31]	45.05	13.00	1 MW load of customer-owned PV systems
Feeder M1 [32]	20.92	12.47	Secondary voltage network with detailed modelling of reactive power compensation and power factor setting
Feeder Ckt5 [33]	77.23	12.47	Large-scale electric power distribution grid with 96% residential load
Feeder Ckt7 [33]	12.87	12.50	Large-scale electric power distribution grid with 39% residential load
Feeder Ckt24 [33]	119.07	34.50	Large-scale electric power distribution grid with 87% residential load

Feeder J1 is located in the northeastern US and supplies the nearest town as well as surrounding rural areas and farms [30]. Since voltage violations are caused by very fast ramp rates of the PV, voltage regulators are not capable of operating quickly enough to compensate or mitigate these effects [30]. Therefore, this feeder aims at finding solutions for areas exceeding the voltage limits [6].

Feeder K1 is located in the southeastern US and supplies commercial units and residential customers [31]. Within this feeder there are no dedicated voltage regulators; voltage regulation is provided by a load tap changer (LTC) at the substation [31]. Consequently, this feeder enables grid calculations for analyzing grids with high PV penetrations and without voltage regulators [6].

Feeder M1 contains a substation transformer to a secondary lower voltage level, which is modelled in detail including the installed radio controlled capacitor banks for reactive power compensation [32]. These capacitor banks manage to maintain a set power factor at the low-voltage level [32]. The intention of this feeder is to study capacitor bank management strategies for setting a suitable power factor [6].

Feeder Ckt5, Ckt7 and Ckt24 are test feeders for power flows in smart grids and mainly aim to study Volt/VAr control strategies in grids with high PV penetration to compensate overvoltage problems [6,33–36].

1.1.4. PG&E (Pacific Gas and Electric Company) Prototypical Feeder Models

The PG&E (Pacific Gas and Electric Company), the largest energy supplier in the US, provides 12 prototypical feeder models, which are obtained from a k-means cluster analysis of 2700 primary distribution feeders of PG&E's supply area [37]. The k-means cluster analysis forms a previously known number of k group from a large set of similar objects [6]. The resulting 12 feeder models are statistically representative of the entire supply area of PG&E [37]. The PG&E prototypical feeders represent different network structures, various sizes (ranging from approximately 100 to 200 network nodes) as well as a mix of different consumers [6]. The feeder models are available in GridLAB-D [37]. The application purpose of these feeders are studies regarding the impact of DER within different scenarios [6]. The six feeder models with primary medium-voltage are described more in detail in [38], and their characteristics can be found in Table 4 [38]. Additionally, the PG&E prototypical feeder models provide detailed low-voltage secondary networks, which connect the customers to the transformer terminals at the substations, making these test feeders distinctive from other test feeders [38].

Table 4. Overview of the six medium-voltage PG&E (Pacific Gas and Electric Company) prototypical feeder models [38].

Feeder ID	Total Line Length (km)	Primary Voltage (kV)
Feeder B	9.65	4.16
Feeder L	9.65	12
Feeder M	114.24	12
Feeder N	43.44	20.78
Feeder S	80.45	12
Feeder W	297.56	12

1.1.5. Benchmark Models

A benchmark model is an electrical network model that maintains the important technical characteristics of real grids, but is less complex than the actual network, in order to permit efficient modelling and simulation of network operation [39].

North-American Low-Voltage Distribution Benchmark Network

This North-American low-voltage distribution benchmark test feeder was developed by the CIGRÉ (Conseil International des Grands Réseaux Électriques) Task Force C6.04.02, originally, for the evaluation of methods and techniques for efficient network integration of DER [40]. Therefore, this test feeder aims at reproducing the characteristics and behavior of real low-voltage networks [6]. The topology of this feeder is comprised of three subnetworks, each subnetwork designed to supply different load types (residential, light industrial and light commercial) [40]. The primary voltage of this feeder is 12.47 kV (60 Hz), and the total line length is 0.59 km [40]. The application purpose is network management analysis, such as power management, to effectively decouple real and reactive power flows to increase system stability [41,42] or transient time-domain simulation studies for protection strategies [43].

European Low-Voltage Distribution Benchmark Network

Due to the increasing penetration of DER in the low-voltage grid (PV-units, CHP (combined heat and power)-micro turbines, small wind turbines and possibly fuel cells), future grid operation has to change compared to present-day networks. Since microgrids present possible options to operate efficiently for such conditions, this feeder model represents a low-voltage microgrid test network for European grids. For the creation of this test feeder, it was important to preserve the technical characteristics of real networks while simplifying the complexity of real networks. This allows for efficient modelling and simulation of operation within microgrids while simultaneously providing

conclusive results. Therefore, the focus was primarily on infrastructural and technical network parameters, not on connected network elements or applied control concepts. In order to obtain a benchmark model, a simple low-voltage microgrid test network is used and expanded. This low-voltage test network has a primary voltage of 0.4 kV supplied from the 20 kV-medium-voltage level. It represents a suburban area with single- and multi-residential consumers as well as apartment buildings. The total line length corresponds with 0.54 km and as line types, underground cables as well as overhead lines are used. For all consumers a power factor of 0.85 is assumed, and aggregated daily load curves are provided for this test network by Papathanassiou et al. (2005) [39]. The benchmark model is expanded by two circuit breakers for possible sectionalizing, a flywheel storage/batteries, a microturbine, a wind turbine, two PV-units as well as a fuel cell. These elements can be specified with suitable models individually for application studies. Therefore, this test network model is suitable for steady state and transient simulations for microgrids [39].

This low-voltage test network was first developed within the EU project "Microgrids" [44] and later adopted by the CIGRÉ Task Force C6.04.02 [39]. The CIGRÉ Task Force also provides an extended multi-feeder version with three individual low-voltage microgrids [39,45]. The first subnetwork is the 0.4 kV line-to-line residential test feeder described above [39,45]. The second subnetwork is a 0.4 kV line-to-line industrial test feeder with only one consumer and a total line length of 0.20 km [45]. The third subnetwork is a 0.4 kV line-to-line commercial test feeder with 15 consumers and a total line length of 0.57 km [45]. This extended multi-feeder version is used for dynamic simulations such as frequency response analysis [46].

European Medium-Voltage Distribution Benchmark Network

CIGRÉ Task Force C6.04.02 developed this medium-voltage test network in order to study various aspects of integrating DER into the medium-voltage network. This test feeder model is capable of retaining the characteristics of a real network since it is based on a German medium-voltage distribution grid within a rural area supplying a small town as well as the surrounding rural area. The nominal voltage of the network is 20 kV supplied by a transformer substation from the 110 kV-high-voltage level. For the test network model, the German reference model is separated into two subnetworks connected over the common substation. In this configuration, the distribution benchmark test network represents a radial network structure. Additionally, there is the possibility to couple the two feeders within the model using a medium-voltage direct current coupler (MVDC). This optional configuration enables also a closed ring network structure. The total line length of the benchmark test network is 15 km comprised mostly of cables, with some overhead line sections. In order to facilitate an adaption of the benchmark model to regionally varying parameters, the original values of the German reference grid were transferred into the per unit system. The loads within the test network are either industrial or residential consumers. There are various application purposes regarding distributed generation (DG) integration for this benchmark test network that include studying the impact of DG units on power flows, voltage profiles and transmission capability, as well as investigating distributed energy management systems (DEMS), small signal stability, system protection and power quality issues (harmonics, flicker, frequency and voltage variations). Additionally, the impact of MVDC coupling on power flows and voltage profiles can be assessed [47].

Additionally, to this basic medium-voltage distribution benchmark network, there are two extended versions of this benchmark network. First, there is a medium-voltage distribution network with PV and wind DER, including nine supplementary distributed energy resources (PV and wind generation units) [45]. Second, there is a medium-voltage distribution network with all DER [45]. This network includes an additional 15 DER, including PV units, wind turbines, batteries, residential fuel cells, CHP diesel units and CHP fuel cells [45].

European High-Voltage Transmission Benchmark Network

The CIGRÉ Task Force C6.04.02 also published a high-voltage level transmission benchmark network model, which consists of two different voltage levels, namely the 380 kV-voltage level and the 220 kV-voltage level. The network topology represents a closed ring structure. The total line length within this benchmark network is 2100 km, where 600 km of electrical line length belong to the 380 kV-voltage level and 1500 km belong to the 220 kV-voltage level. There are no consumer units at the 380 kV-voltage level, only at the 220 kV-level. Two transformers connect the two voltage levels. Just like the other above presented CIGRÉ test networks this benchmark model facilitates the analysis and validation of new methods and techniques aiming at enabling the economic, robust and environmentally responsible integration of DER into the European grids [45].

1.1.6. Agent-Based Distribution Test Feeders

Agent-based test feeders refer to the characteristic that the distribution feeder components are modeled as interacting agents, acting based on individually specified objectives or purposes due to financial and/or physical constraints [48]. Agent-based modelling usually addresses different application purposes, where a system is investigated on its ability to adapt to changing boundary conditions. However, with grid modelling for smart grid applications, this modelling approach may be supported by this technique for analyzing impacts of smart grid technologies on distribution feeders as well as performance evaluations of smart-grid market design.

The agent-based distribution test feeder presented by Jahangiri et al. (2012) [48] is based on a real feeder in Iowa and includes detailed information about feeder equipment (fuses, switches, overhead and underground lines, as well as transformers) and residential and commercial customers. The customers are virtually equipped with various smart-grid enabled technologies (rooftop PV-units, price-responsive demands such as plug-in electric vehicles (PEV) and intelligently controlled air conditioning). For the PV generation, effects of cloud-passing are also considered as well as realistic travel pattern data for PEV load models. The application purpose of this test feeder, therefore, is the evaluation of the impacts of smart-grid market designs as well as the development of smart-grid features (demand response, dynamic-price retail contracting, distributed generation and energy storage systems) on distribution feeders. The primary voltage of the feeder is 13.2 kV. The exact geographic coordinates of the components as well as electrical data for the test feeder model are available in GridLAB-D, offering the possibility to simulate a time period with user-defined time steps [48].

This test feeder is mainly used in smart-grid studies, such as in [49], where future requirements for supporting flexible, intelligent and active power grid management is studied, and planning process analysis, such as in [50,51], where innovative distribution grid operation concepts including RES, demand side management (DSM) and storages are investigated [6].

1.1.7. Test Feeder for DG Protection Analysis

This test feeder model allows for the comparison of different DG protection analysis tools, which have to be able to calculate fault currents, voltage and other values for different fault types and resistance values [52]. This test feeder is based on an actual feeder with a 1.65 MW wind turbine [52]. Therefore, the model consists of two different generation sources—the substation from the higher voltage level and the distributed generation source [52]. The model operates at a 12.47 kV-voltage level with a substation source of 34.5 kV of nominal voltage [52]. The total line length of the test feeder is 47.52 km [52]. This feeder is used, for example, in symmetrical component calculations for single line-to-ground fault (SLGF) currents and the related over voltages for a distribution circuit with solar photovoltaic inverter-based generation [53].

1.1.8. European Representative Synthetic Distribution Test Networks

For these test networks, two categories can be defined: first, large-scale networks modelling the network from a high-voltage/medium-voltage substation to the low-voltage level including all electrical components (consumers, feeders, substation) at the medium- and low-voltage level; second, feeder type networks, which feature common topologies of medium-and low-voltage levels. There are three large-scale and six feeder type test networks openly available in MATLAB®/MATPOWER format, and they are all three-phased and balanced. The data for these test networks were collected over online questionnaires and distributed to the participating 79 European DSOs (distribution system operators), which were published in a report [54]. This database covers 74.8% of the connected customers in the European Union. Based on this data, 36 indicators were developed, providing information about structural differences as well as similarities among distribution grids throughout Europe. This analysis provides three categories, each of which includes a set of indicators, namely network structure, network design and characteristics of distributed generation. The indicators for network structure include parameters such as number of customers, amount of distributed energy, areas of supply as well as circuit length and capacities of substations. The network design indicators include typical parameters of substations and feeders used for sizing and designing distribution installations. The category of distributed generation characteristics includes installed capacities per consumer as well as percentage of distributed generation connected at each voltage level [54,55].

The voltage levels occurring in these test networks range from the high-voltage level (HV: 132 kV) over the medium-voltage level (MV: 1–36 kV) to the low-voltage level (LV: <1 kV). Table 5 provides an overview of the available networks, both large-scale as well as feeder types [54,55].

Table 5. Overview of the available European Synthetic Distribution Test Networks [54,55].

Category	Degree of Urbanization	Description	Voltage Level (kV)	No. Feeders	Degree of Cabling (%)	Total Line Length (km)
Large-scale test networks	Urban	Fed from the 132 kV level	20/0.4	5	LV: 86 MV: 100	LV: 53.87 MV: 31.20
	Semi-urban	Fed from the 132 kV level	20/0.4	10	LV: 42 MV: 74	LV: 114.96 MV: 50.40
	Rural	Fed from the 132 kV level	20/0.4	6	LV: 4 MV: 15	LV: 211.46 MV: 131.12
Feeder type networks	Urban	2 substations	20	4	100	17.80
		1 substation, 1 switching station	20	3	100	13.16
		Short feeders	0.4	3	100	0.25
	Semi-urban	Substation ring	20	2	74	14.05
		Long feeders	0.4	1	100	1.15
	Rural	Openly operated ring structure	20	8	15	81.03

The application of these networks aims at supporting research on future distribution grids, and, therefore, they have already been used in several studies [55]. The large-scale distribution networks are used in optimal power flow studies [56] as well as data-driven approaches to reconstruct medium- and low-voltage grid topologies from smart meter data [57]. The feeder type networks have been used to investigate the impact of electric vehicle recharging strategies in combination with high PV-penetration on the grid [58]. These test networks have also been used for single-phase real-time simulations testing the impact of distributed generation [59] as well as performance studies of power line communications [60] and quantitative assessing impacts of different PV sizing and deployment rates on grid congestion and voltage unbalance [61].

1.1.9. European Non-Synthetic Low-Voltage Test Network

This test network represents a non-synthetic comprehensive low-voltage distribution test network, which represents the grid of a real European town. The data of this network is extracted directly

from the GIS system. The primary phase-to-phase voltage is 0.416 kV with a frequency of 50 Hz. There are 30 substations and 10,290 network nodes, resulting in a total line length of the grid lines of 45.94 km. For the loads, time series data with an hourly resolution over a 20-day period are available with the test network. The application purposes of this test feeder are developing and testing different kinds of software as well as distribution system optimization studies and state estimation techniques. The datasets for this test network are publicly available [62,63].

There are further test networks available, which address specific networks, e.g., for North England grids, which represent synthetic low-voltage residential feeders obtained from different clustering algorithms [64] or for Western Australian medium- and low-voltage distribution feeders using a taxonomy approach that combines cluster analysis with discriminant analysis [65].

1.2. Limitations of the Presented Test Networks

This section summarizes the findings about the presented test networks and test feeders and draws conclusions from the available datasets in order to show the limitations of these networks.

From the literature review presented above, it can be concluded that much work has been done for North American test feeders, but, in comparison, few studies are available for European networks. Figure 1 shows the splitting of the presented test networks into European and North American test networks.
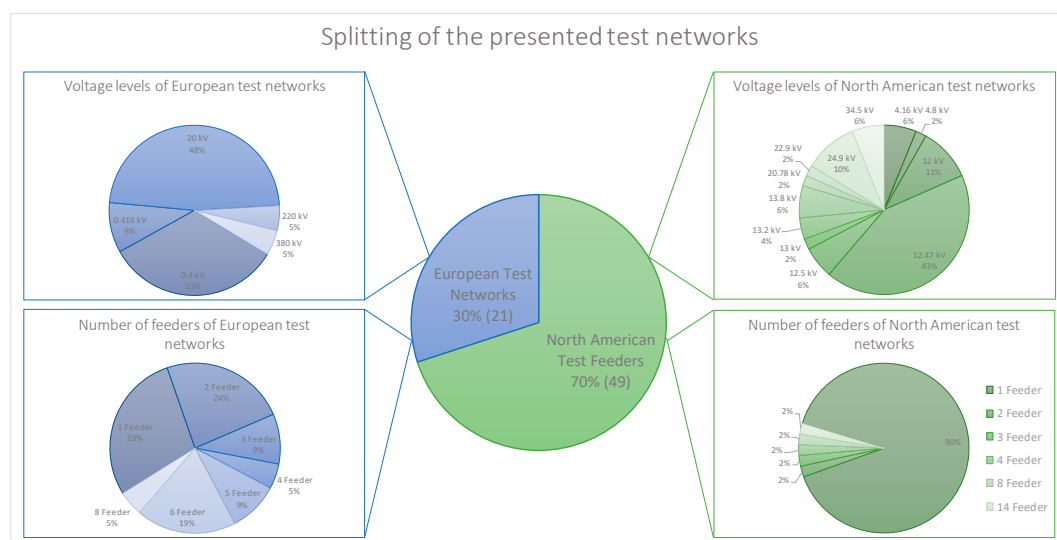
Figure 1. Splitting of the presented test networks into European and North American systems.

While many networks for the North American electrical system are available, they only include medium-voltage distribution grids ranging from 4.16 kV to 34.5 kV. For the European test networks, there are fewer systems available, but they cover most voltage levels present in European grids. Two of the presented European low-voltage networks use a voltage of 0.416 kV, which may represent previous UK networks. Today´s European low-voltage grids are usually operated at a nominal voltage of 0.4 kV. Additionally, a test network for the 110 kV-voltage level common in European structures, e.g., also in Austrian or German structures, is not available.

The described sets of test networks are only restrictedly applicable to reproduce real grids due to various limitations, some of which are common in the test networks covered by the literature review. The parameters limiting the use of these networks for some applications are described below.

1.2.1. Lack of Representativeness

The most important characteristic of a test network is the ability to reproduce actual network behavior. The representativeness depends on many different parameters which may vary in different

countries or even regions (e.g., due to geographical differences) and can possibly not be depicted. Other parameters such as technical system parameters (e.g., three- or single-phase systems, feeder lengths, load densities, electrical line types (overhead or underground), network topologies or equipment types) may influence the representativeness of a test network [6].

1.2.2. Lack of Time-Series Data

Temporally resolved load and generation profiles for consumer and (renewable) generation units are indispensable for analyzing future grid operation such as time constraints for certain network components (e.g., batteries, electric vehicles, etc.) and flexibility options, such as demand response [6]. Only some of the presented test networks also include time-series data for consumer and generation units.

1.2.3. Design and Data Specific for a Single Issue

If a test network has been designed and modelled to address a specific technical or economical problem, it may be unsuitable for other applications, since information for other issues may not be available (e.g., test feeder for DG protection) [6]. Therefore, it may not be possible to utilize one test network for multiple research questions.

1.2.4. Network Sizes

The size of the test network is an important parameter for studying real grids and obtaining conclusive and reliable results [6]. Most European test systems from the literature represent medium-sized grids, which may not be large enough to verify the performance of algorithms and the assessment of their computational effort for larger networks across voltage levels [6].

1.2.5. Missing Geographical Coordinates

Electrical calculations do not require geographical data of the network and its components [6]. However, for certain applications (e.g., expansion planning or potential reconfiguration strategies due to faults), the coordinates, which provide a graphical representation and a layout of the grid, are beneficial [6]. Most available test networks provide listed data without any information about grid layouts (except for grid connections between network nodes). Only very few of the presented test networks include geographical coordinates or at least a graphical network model for such purposes.

1.2.6. Isolated Test Feeders

This limitation refers mainly to the North American test networks, since they usually represent a single, isolated feeder. For these networks, interactions between the feeders sharing the same substation transformer cannot be assessed [6].

Due to these limitations as well as missing voltage levels in the existing test networks, it is necessary to develop comprehensive test networks with appropriate network sizes for the European ENTSO-E interconnected grids at each common voltage level. While this is possible for the 110 kV- and the 380/220 kV-voltage level, the lower voltage level test grids (20 kV and 0.4 kV) offer a contribution to the various real networks existing in Europe. Additionally, it is necessary to provide appropriate data to replicate load and generation characteristics and perform time-series calculations. Furthermore, a graphical representation of the test network as well as the possibility to adapt the networks to different applications are advantageous when using test networks for research purposes.

2. Methodology

This section presents the approach that was used to develop the test networks. Subsequently, each network is described individually in detail. The presented test networks in this work are developed for the 0.4 kV low-voltage level, the 20 kV medium-voltage level, the 110 kV high-voltage level as well

as the 380/220 kV maximum-voltage level. In Austria, for example, there are various medium-voltage levels ranging from 1 to 36 kV. However, for now there is only a 20 kV-voltage level developed in this work. Each network is modelled using the network planning and network simulation software NEPLAN [66].

The approach for test network development in this work was based on detailed literature research in order to identify the specific properties regarding European ENTSO-E electrical infrastructures, of which the Austrian structures are a part, without including sensitive user-specific information. A flowchart of the development process for the presented networks can be found in Figure 2.
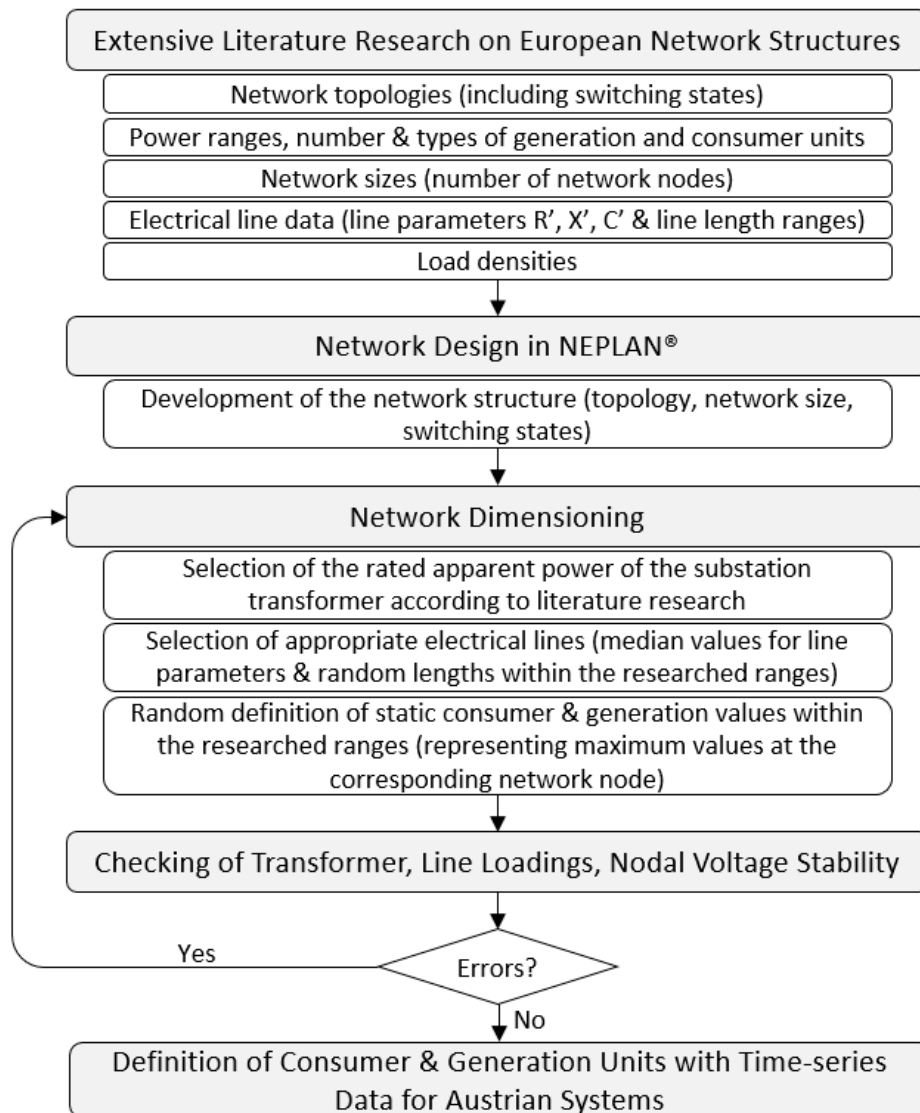
Figure 2. Method for test network development.

First, extensive literature research was conducted on European networks and their corresponding parameters. The literature values considered in this research for representing European network structures included system sizes (number of nodes), network topologies (radial, ring and meshed structures), electrical line types (overhead lines or cables), electrical line parameters (R', L', C', length) as well as generation and consumer units corresponding to the voltage level regarding their type and power range. Each parameter either represented an average value for European electrical networks (e.g., specific electrical line parameters R', L', C') or a typical range within which the values were chosen (e.g., electrical line lengths, generation and consumer power). Literature references for these

parameters were taken from a variety of sources, some of which complemented each other and some of which overlapped [67–71]. Therefore, the network parameters of the presented test networks described below represented a summary of the parameters found in the literature [67–71]. Second, the test networks were developed in NEPLAN for different network structures regarding topology, network size and switching states. This offered a graphical representation of the network. Third, based on this NEPLAN model of each voltage level, the network dimensioning could be conducted. This included the definition of a rated apparent power as well as common transformer loadings for the substation transformer. Then, static power values (momentary power values for one time step) for the consumer and generation units were randomly chosen within the power ranges derived from the literature research. They represented maximum total values of the sum of load and generation profiles connected and aggregated in one network node. The researched static values were only used for an initial dimensioning of each network, thus assessing correct line and transformer loadings as well as voltage stability. Therefore, if the previously defined transformer loadings were not exceeded due to the chosen static consumer and generation power values, the grid could be operated in normal operation without transformer congestions over time. Then, line loadings and voltage limit stability were checked. If lines were congested, stronger lines were utilized (e.g., first line at the beginning of a feeder). If voltage limit exceeding occurred at certain network nodes, either generation (upper voltage limit exceeding) or consumer (lower voltage limit exceeding) powers were reduced. If errors no longer occurred, time-series based calculations using load and generation profiles could be conducted. Regarding the time series-based calculations, corresponding load and generation profiles from Austrian grids were chosen. Figure 3 provides an overview over the test networks created in this work; they are described more in detail individually within the corresponding section. Generally, each network represented a balanced three-phase system.
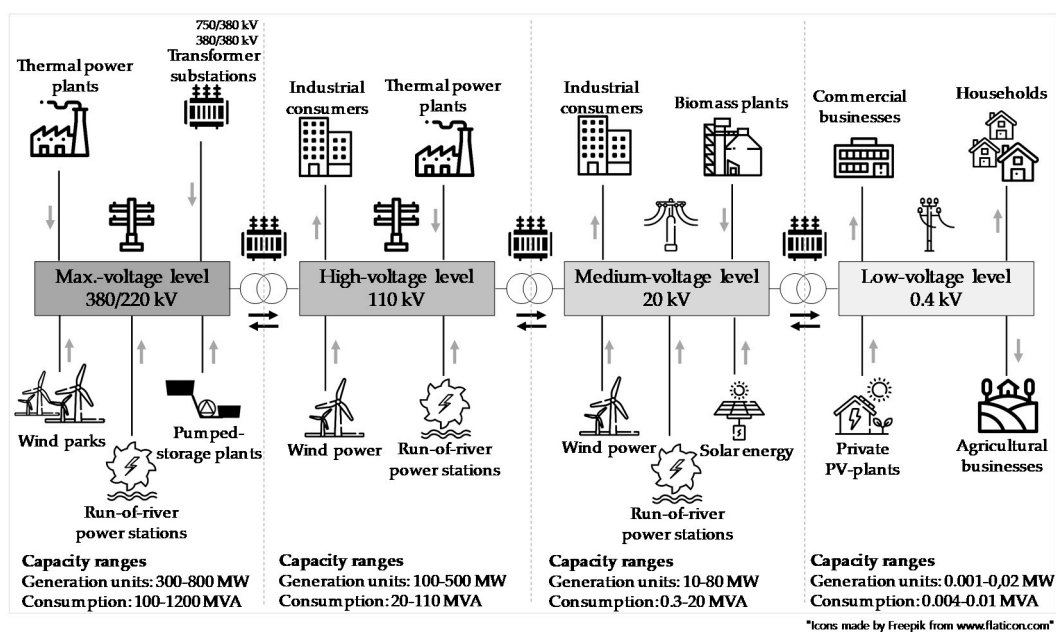
Figure 3. Overview over the test networks developed in this work according to the European interconnected grid.

2.1. Low-Voltage Level (0.4 kV)

The low-voltage test network is comprised of 92 network nodes with 91 connected consumer units as well as 39 connected generation units. The network topology represents a radial structure with 14 feeders including urban as well as suburban network structures. In the urban network structures there are shorter line lengths (0.02–0.18 km), but higher load densities, since each consumer unit

consists of several residential units. In the suburban network structures there are larger line lengths (0.15–0.5 km) and lower load densities, since each consumer unit represents only one residential unit. Residential units within the grid were either defined by synthetic load profiles (created using a load profile generator [72,73]) or standard load profiles. Which profile was used was defined by the simultaneity curves [74]. These enabled a realistic network design at the low-voltage level. Simultaneity factors take into account that the predefined static maximum load values of consumers do not occur at the same time, so that the network is not burdened with the sum of the maximum loads of all consumers in normal operation. Depending on the predefined static maximum power, the number of residential units per connection point is calculated using the given installed power of a single residential unit. The corresponding simultaneity factor can be taken from the diagram provided in [74]. This allowed realistic static values to be obtained for network dimensioning. As a result, depending on the number of residential units within one connection point, it was then decided whether standard load profiles or synthetic load profiles were utilized. In the LV test grid, there were 207 households that were represented by different synthetic profiles or the standard load profile H0 (if the number of residential units in one grid connection point was high enough), which are explained in Table 6. Additionally, there was a total of 17 commercial businesses represented by standard load profiles (4 G0, 4 G1, 1 G2, 1G3, 2 G4, 4 G5 and 1 G6) as well as a total of 6 agricultural businesses also represented by standard load profiles (2 L0, 2 L1 and 2 L0). The 39 generation units exclusively represented private PV-systems, which were defined by a synthetic generation profile created using a solar energy model developed at the Chair of Energy Network Technology, which is based on irradiation data and rooftop areas at the corresponding residential units. A more detailed itemization of the used synthetic and standard load and generation profiles can be found in Table 6.

Table 6. Load and generation profiles used at the low-voltage test network.

Profile	Description	Profile Type
CHR01 [1]	Couple both at work	Synthetic load profile
CHR03 [1]	Family with one child, both at work	Synthetic load profile
CHR051 [1]	Family with 3 children, both at work	Synthetic load profile
CHR07 [1]	Single person with work	Synthetic load profile
CHR25 [1]	Single woman under 30 years with work	Synthetic load profile
CHR27 [1]	Family with 2 children, both at work	Synthetic load profile
CHR33 [1]	Couple under 30 years with work	Synthetic load profile
CHR52 [1]	Student flat sharing	Synthetic load profile
CHR54 [1]	Retired couple	Synthetic load profile
H0	Household	Standard load profile
G0	General commercial business	Standard load profile
G1	Commercial business on weekdays 8 am to 8 pm	Standard load profile
G2	Commercial businesses with predominant consumption in the evening hours	Standard load profile
G3	Commercial businesses with continuous operation	Standard load profile
G4	Shop/Hairdresser	Standard load profile
G5	Bakery with baking room	Standard load profile
G6	Commercial businesses with operation on weekends	Standard load profile
L0	General agricultural businesses	Standard load profile
L1	Agricultural businesses with dairy/secondary livestock farms	Standard load profile
L2	Other agricultural businesses	Standard load profile
PV profile	Private PV-systems in different sizes	Synthetic load profile

[1] Load profile generator [72,73].

Within the low-voltage test network, there were 92 electrical lines with a total electrical line length of 5.931 km and single line lengths ranging from 0.02 to 0.45 km. Regarding the electrical line types within the test network, three different cable types were applied. Since the first line section supplying each feeder had to enable transmission of high loads and normal operation did not provide closed ring structures to partially supply consumer units at the end of the feeder, a stronger line type (NYY 4 × 300) was selected for some feeders. The remaining line sections within the test network corresponded with a cable type with average specific line parameters (NAYY 4 × 185 for urban structures and

NAYY 4 × 150 SE for suburban structures) for European grids at the low-voltage level. Table 7 shows the used cable types and their electrical line parameters.

Table 7. Electrical line data, 0.4 kV.

Line Designation	Type	R' (Ohm/km)	X' (Ohm/km)	B' (µS/km)	$I_{r,max}$ (A)
NYY 4 × 300	Cable	0.063	0.079	-	535
NAYY 4 × 185	Cable	0.167	0.080	-	313
NAYY 4 × 150 SE	Cable	0.249	0.080	-	270

The transformer in the local substation was a three-phase transformer with a rated apparent power of 630 kVA feeding the low-voltage network from the 10 kV-medium-voltage level. The vector group chosen for the substation transformer was Yz5, which is common for smaller distribution transformers, since unbalanced loads can occur, especially on the lower-voltage side, and balancing is achieved due to the neutral point. Table 8 shows the parameters of the transformer used.

Table 8. Transformer data, 10 kV/0.4 kV.

	U_n (kV)	U_r (kV)	$I_{r,max}$ (A)
Higher voltage side	10	10	36.4
Lower voltage side	0.4	0.4	909.3

Figure 4 shows the described low-voltage test network developed in NEPLAN.
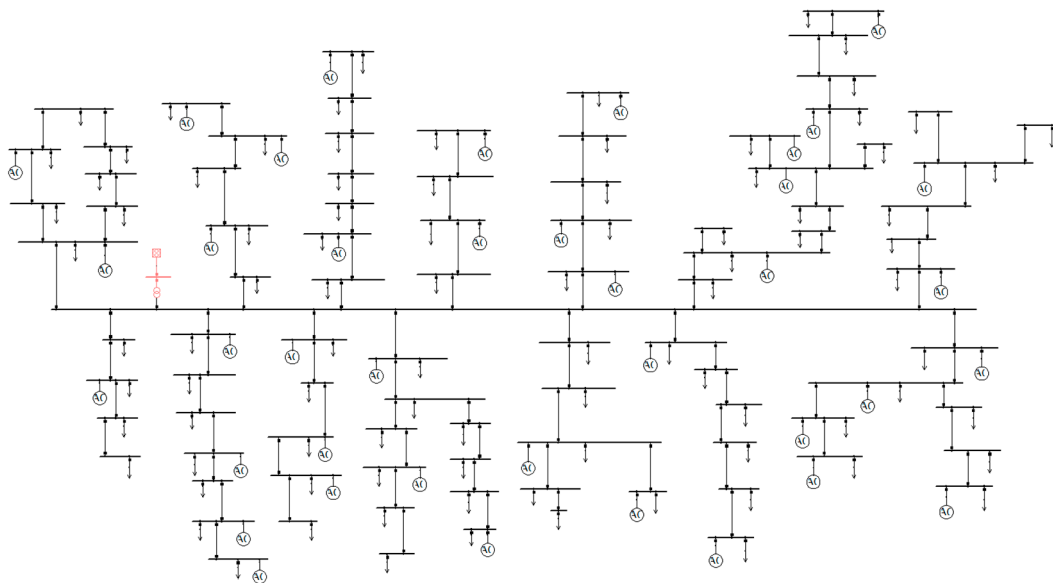
Figure 4. Low-voltage test network.

2.2. Medium-Voltage Level (20 kV)

The medium-voltage test network represented a public power distribution grid comprised of 74 network nodes with 64 consumer units and 15 generation units. Consumer units were represented by the load profiles of 7 different local substations available at Chair of Energy Network Technology, as well as commercial standard load profiles with higher annual energy consumption, since, for example, large feeding water pumps may also be directly connected at the medium-voltage level (standard load profiles G2, G3 and G6; cf. Table 6). The generation units either represented wind power units, solar power plants, biomass plants, geothermal power plants or run-of-river power stations. The data

for these generation units, except for the wind data, originated from measurements of the Austrian control area operated by the APG (Austrian Power Grid), publicly available at the APG homepage [75]. These data were then scaled down to represent a generation unit at this voltage level, since the original data represent a cumulative generation profile of each generation type for Austria. The wind data represent measured data from parts of Austria. Since the measured wind data from APG were aggregated data for all wind plants in Austria, fast start-up rates were no longer displayed within the profile due to this aggregation. Therefore, this data would no longer represent the real strain wind generation puts on the grid, since there are no fast load changes due to the flattened profile of the aggregated wind power plants. To represent real grid burdens, the measured data were used for only a couple of wind power units within the test networks.

The network topology of the medium-voltage grid is a radial structure with 2 permanently closed rings during regular operation and 11 open ring lines, which do not transmit power during normal operation. These electrical lines can be closed in the event of a fault and, thus, ensure that consumers affected by the fault are supplied via a different current path. This network topology is, therefore, referred to as an open ring structure, which is common for European medium-voltage structures. The medium-voltage test network, therefore, consists of 18 feeders.

Within the medium-voltage test network there are 86 electrical lines, of which 11 are operated in an open mode; therefore, 75 electrical lines transmit power in normal operation. This results in a total line length of 730.98 km with line lengths ranging from 1 km to 20 km. The chosen line type represented a cable that corresponded with the average specific electrical line parameters at this voltage level, which are shown in Table 9.

Table 9. Electrical line data 20 kV.

Line Designation	Type	R' (Ohm/km)	X' (Ohm/km)	B' (µS/km)	$I_{r,max}$ (A)
E-A2XHCJ2Y 1/240 RM/25 HD60	Cable	0.1329	0.1462	71.3140	422

The transformer in the transformer substation is a three-phase transformer with a rated apparent power of 50 MVA feeding the medium-voltage network from the 110 kV-high-voltage level using a Dy5 vector group, which is common for large distribution transformers in Europe. The neutral point is fully loadable, thus avoiding additional losses and neutral point shifts, which is advantageous in high current environments. Table 10 shows the parameters of the transformer used.

Table 10. Transformer data, 110 kV/20 kV.

	U_n (kV)	U_r (kV)	$I_{r,max}$ (A)
Higher voltage side	110	110	262.4
Lower voltage side	20	20	1443.4

Figure 5 shows the described medium-voltage test network for European grids designed in NEPLAN.
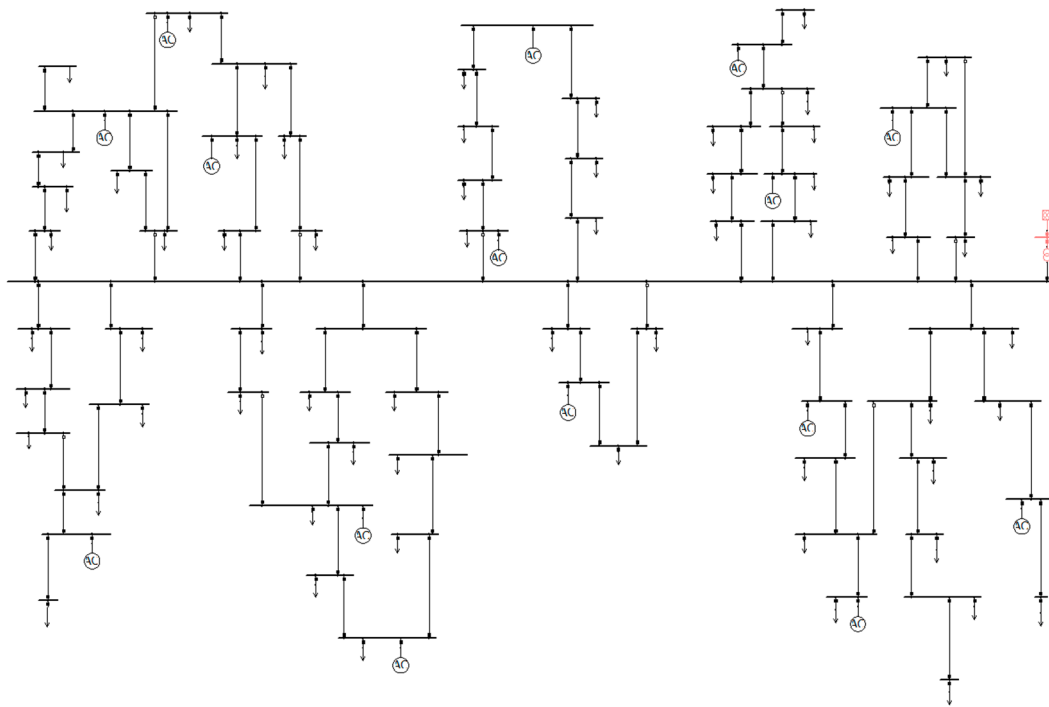
Figure 5. Medium-voltage test network.

2.3. High-Voltage Level (110 kV)

The high-voltage test grid consists of 70 network nodes with 69 consumer units and 18 generation units. The consumer units are defined by the load profiles of 27 different transformer substations available at the Chair of Energy Network Technology that supply the subordinate medium-voltage levels. The generation units represent wind power units, gas and coal power plants, as well as run-of-river power stations and discharging of storage units. The data for these generation units, except for wind power data, were also collected from measurements of the Austrian control area operated by the APG, publicly available at the APG homepage [75], and then scaled down to represent a generation unit at the high-voltage level. The wind data represent measured profiles in parts of Austria, as described within Section 2.2.

The network topology of the high-voltage test grid consists of 6 feeders and represents a closed ring structure including some redundant, open electrical lines, which can also be closed in case of a fault. Closed ring structures at this voltage level enable the transmission of larger loads and increase the security of the supply.

Within the high-voltage test grid there are 89 electrical lines, of which 12 lines are operated in an open mode during normal operation; therefore, the remaining 77 lines transmit power in normal operation with a total line length of 1477 km that includes electrical line lengths ranging from 8 km to 30 km. The electrical line type chosen for this test network was an overhead line with average specific line parameters. In this test grid, no underground cables were considered. Table 11 shows the characteristics of the chosen overhead line type.

Table 11. Electrical line data, 110 kV.

Line Designation	Type	R' (Ohm/km)	X' (Ohm/km)	B' (µS/km)	$I_{r,max}$ (A)
3×304-Al/St 1A	Overhead line	0.176	0.408	2.796	735

The transformer in the transformer substation is a three-phase transformer with a rated apparent power of 800 MVA feeding the high-voltage network from the 220 kV-maximum-voltage level.

The chosen vector group for this transformer was Yy0, which is common in European transportation grids. Table 12 shows the parameters of the transformer used.

Table 12. Transformer data, 220 kV/110 kV.

	U_n (kV)	U_r (kV)	$I_{r,max}$ (A)
Higher voltage side	220	220	1215.5
Lower voltage side	110	110	4198.9

Figure 6 shows the described European high-voltage test network designed in NEPLAN.
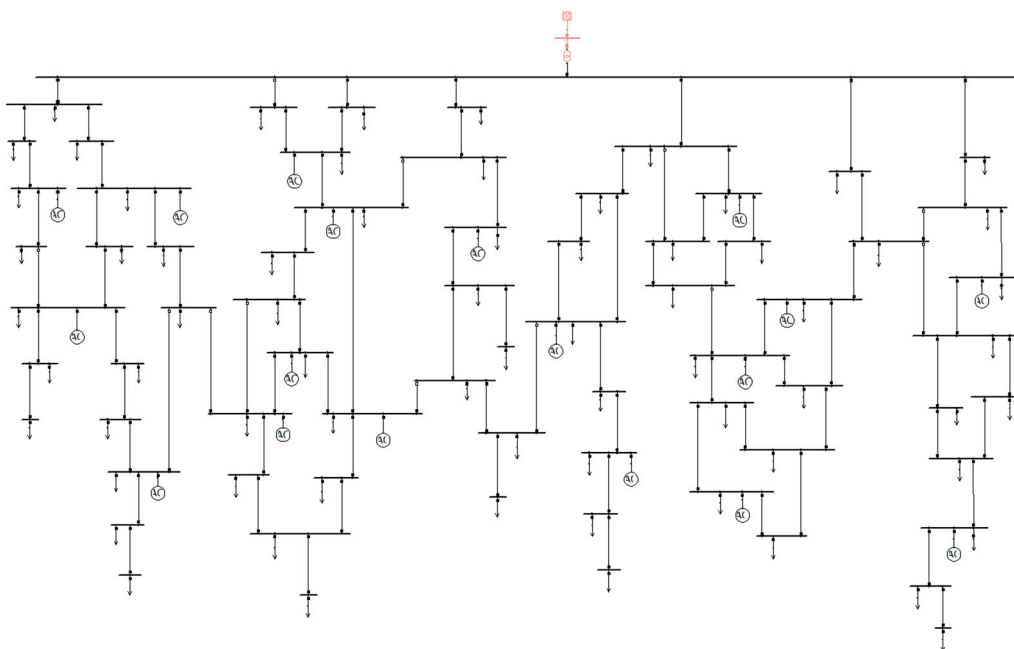
Figure 6. High-voltage test network.

2.4. Maximum-Voltage Level (380/220 kV)

The maximum-voltage test network consists of 19 network nodes, of which 7 belong to the 380 kV voltage level and the other 12 belong to the 220 kV voltage level. There are 2 consumer units within the 380 kV voltage level, which represent substations feeding the 110 kV voltage level. Within the 220 kV voltage level network there are 12 consumer units also representing substations feeding the 110 kV voltage level network. In total there are 10 generation units, 5 at the 380 kV voltage level and 5 at the 220 kV voltage level. The data for the consumer units represent the sum of a different number of load profiles of transformer substations feeding the medium-voltage level from the 110 kV voltage level available at the Chair of Energy Network Technology. The generation units represent wind power generation, gas or coal power plants, run-of-river power stations as well as pumped-storage plants. The data for the generation units were also taken from the APG homepage [75]. The wind data represent measured wind data from parts of Austria, as well as at the medium- and high-voltage level.

The network topology for the maximum-voltage grid represents a meshed structure with only very few open ring structures. This enables the transmission of greater loads and the power supply from large power stations.

The maximum-voltage level consists of 24 electrical lines, of which 5 lines are operated in an open mode during normal operation. Of the remaining 19 lines, 7 lines belong to the 380 kV-level and 12 lines belong to the 220 kV-level. The total line length of the entire 380 kV- and 220 kV-voltage level is 931.2 km, with 364.7 km at the 380 kV-voltage level and 566.5 km at the 220 kV-voltage level.

The electrical line lengths range from a minimum of 10 km to a maximum of 75 km. The electrical line type chosen for this test network was an overhead line with average specific line parameters for the corresponding voltage level. Again at this voltage level, no underground cables occur, which is common for European electrical structures. Tables 13 and 14 show the characteristics of the chosen overhead line types.

Table 13. Electrical line data, 220 kV.

Line Designation	Type	R′ (Ohm/km)	X′ (Ohm/km)	B′ (μS/km)	$I_{r,max}$ (A)
382-AL1/49-ST1A	Overhead line	0.076	0.230	3.770	840

Table 14. Electrical line data, 380 kV.

Line Designation	Type	R′ (Ohm/km)	X′ (Ohm/km)	B′ (μS/km)	$I_{r,max}$ (A)
679-AL1/86-ST1A	Overhead line	0.043	0.220	4.398	1150

Since there are two voltage levels within this test network, there are also transformer stations that connect the two voltage levels. There are 5 transformer stations connecting the 380 kV-level with the 220 kV-level. Each transformer station represents a three-phase transformer with a rated apparent power of 1200 MVA using a YNyn0 vector group. This vector group is commonly used for large dome transformers. Table 15 shows the parameters for each transformer substation.

Table 15. Transformer data, 380 kV/220 kV.

	U_n (kV)	Ur (kV)	$I_{r,max}$ (A)
Higher voltage side	380	380	1823.2
Lower voltage side	220	220	3149.2

Additionally, there is one transformer at the 380 kV-level representing the Slack-node, which either represents the exchange of power at the same voltage level or the exchange of power with a higher voltage level. For Austrian grids this also represents the exchange with another control zone of the surrounding country. In this test network, the Slack-node-transformer represented the exchange of power with another 380 kV-voltage level grid and was responsible for isolating the two networks. The rated apparent power of this transformer was 10 GVA, and the chosen vector group was Yy0, which are common in European transportation grids. Table 16 shows the parameters for the Slack-node transformer.

Table 16. Transformer data, 380 kV/380 kV.

	U_n (kV)	Ur (kV)	$I_{r,max}$ (A)
Higher voltage side	380	380	15,193.4
Lower voltage side	380	380	15,193.4

Figure 7 shows the described maximum-voltage test network created in NEPLAN. This test network was based on the actual Austrian maximum-voltage level grid, which can be found on the Austrian Power Grid (APG) homepage [76]. This test network consisted of 5 feeders.
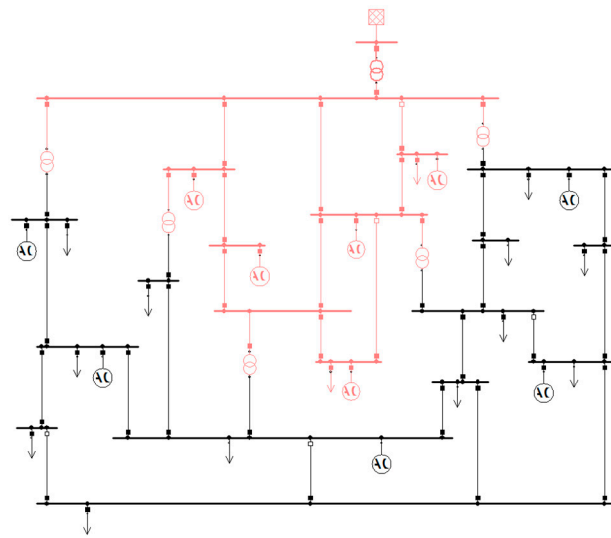
Figure 7. Maximum-voltage test network (including the 380 kV- and the 220 kV-voltage levels).

Table 17 offers an overview of the presented test networks developed in this work, including the network specific parameters.

Table 17. Overview over the developed test networks representing European structures.

Parameter	Low-Voltage	Medium-Voltage	High-Voltage	Maximum-Voltage	
Voltage level (kV)	0.4	20	110	220	380
Number of feeders	14	18	6	5	5
Number of network nodes	92	74	70	12	7
Number of consumer units	91	64	69	12	2
Number of generation units	39	15	18	5	5
Transformer power (MVA)	0.63	50	800	1200	10,000
Vector group	Yz5	Dy5	Yy0	YNyn0	Yy0
Topology	Radial	Radial, open rings	Closed rings	Mesh	Mesh
Number of lines	92	75	77	12	7
Total line length (km)	5.93	730.98	1477	566.50	364.70
Maximum feeder length (km)	0.81	95.90	319.08	-	-
Specific line resistance R' (Ohm/km)	0.063–0.249	0.133	0.176	0.076	0.043
Specific line reactance X' (Ohm/km)	0.079–0.080	0.146	0.408	0.230	0.220
Specific line susceptance B' (μS/km)	0.000	71.314	2.796	3.770	4.398
Maximum electrical line current (A)	535	422	735	840	1150

3. Results

This section presents the results obtained from performing a short-circuit analysis on each of the presented networks and comparing these results with literature data. This provides support in validating the representativeness of the networks. The short-circuit power value is a measure of voltage quality and interference resistance of a power system and, thus, the behavior of a network. As a result, the short-circuit power can be influenced by various factors, such as the number of synchronous machines within the network, the degree of meshing (including switching states) or inductance coils for power factor correction. Structural aspects of the network can be assessed via the short-circuit current, since this is mainly influenced by the number of parallel branches and, thus, directly depends on the short-circuit impedance. Therefore, this analysis showed how well the generic test networks presented replicated real network behavior [68].

For that purpose, literature values for German grids, which are very similar to Austrian grids, as well as value ranges for European grids at each voltage level were found. Therefore, Table 18 shows the researched literature value ranges for European grids regarding short-circuit power as well as short-circuit current. The value ranges presented in Table 18 are also depicted in Figure 8.

Table 18. Researched short-circuit power and current ranges for European grids.

Voltage Level		Short-Circuit Power		Short-Circuit Current	
		S_K'' Range (GVA)		I_k'' Range (kA)	
		From	To	From	To
Low-Voltage	0.4 kV	$1.22 \cdot 10^{-3}$ [77,78]	$41.12 \cdot 10^{-3}$ [78]	1.76 [78]	59.35 [78]
Medium-Voltage	20 kV	0.10 [46]	0.80 [79]	2.89 [46]	23.09 [79]
High-Voltage	110 kV	4 [80]	8 [68]	21 [80]	42 [68]
Maximum-Voltage	220 kV	5 [46]	24 [68]	13.12 [46]	63 [68]
	380 kV	5 [80]	60 [80]	7.5 [80]	90 [80]
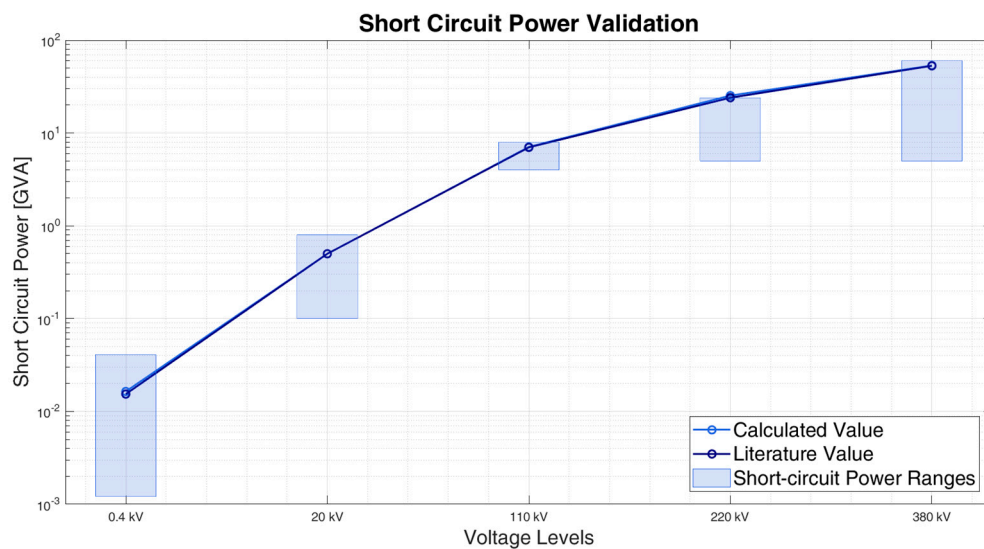
Figure 8. Short-circuit power validation for each presented test network.

Table 19 compares the calculated values of the short-circuit power for each voltage level with those found in the literature for German grids. Both are graphically depicted in Figure 8. Additionally, Table 19 shows the relative and absolute deviations between the literature values and the calculated values. The deviations were calculated according to Equations (1) and (2). A positive (absolute and relative) deviation suggests that the literature value is higher than the calculated value.

$$\Delta S''_{k,abs} = S''_{k,literature} - S''_{k,calculated} \tag{1}$$

$$\Delta S''_{k,rel} = \frac{S''_{k,literature} - S''_{k,calculated}}{S''_{k,literature}} \tag{2}$$

Table 19. Short-circuit power for each voltage level.

Voltage Level		Short-Circuit Power		Deviations	
		S_k'' Literature (GVA)	Sk'' Calculated (GVA)	Absolute (GVA)	Relative (%)
Low-Voltage	0.4 kV	$15.39 \cdot 10^{-3}$ [78]	$16.42 \cdot 10^{-3}$	−0.0011	−6.75
Medium-Voltage	20 kV	0.50 [68,81]	0.49	0.0003	0.07
High-Voltage	110 kV	7 [80]	7.08	−0.0754	−1.08
Maximum-Voltage	220 kV	24 [68,80]	25.32	−1.3169	−5.49
	380 kV	53 [68,80]	53.39	−0.3863	−0.73

In order to fully validate the developed generic test networks presented in this paper, the short-circuit currents were also taken into account. Therefore, Table 20 compares the calculated values of the short-circuit current for each voltage level with those found in the literature for German grids. Both values are graphically depicted in Figure 9. Additionally, Table 20 shows the relative and absolute deviations between the literature values and the calculated values for the short-circuit current. The deviations were also accordingly calculated as presented in Equations (1) and (2).

Table 20. Short-circuit currents for each voltage level.

Voltage Level		Short-Circuit Current		Deviations	
		I_k'' Literature (kA)	Ik'' Calculated (kA)	Absolute (kA)	Relative (%)
Low-Voltage	0.4 kV	22.21 [78]	23.70	−1.488	−6.70
Medium-Voltage	20 kV	14.43 [68,81]	14.24	0.006	0.04
High-Voltage	110 kV	36.74 [80]	37.14	−0.396	−1.08
Maximum-Voltage	220 kV	63 [68,80]	66.44	−3.440	−5.46
	380 kV	80 [68,80]	81.11	−1.112	−1.39
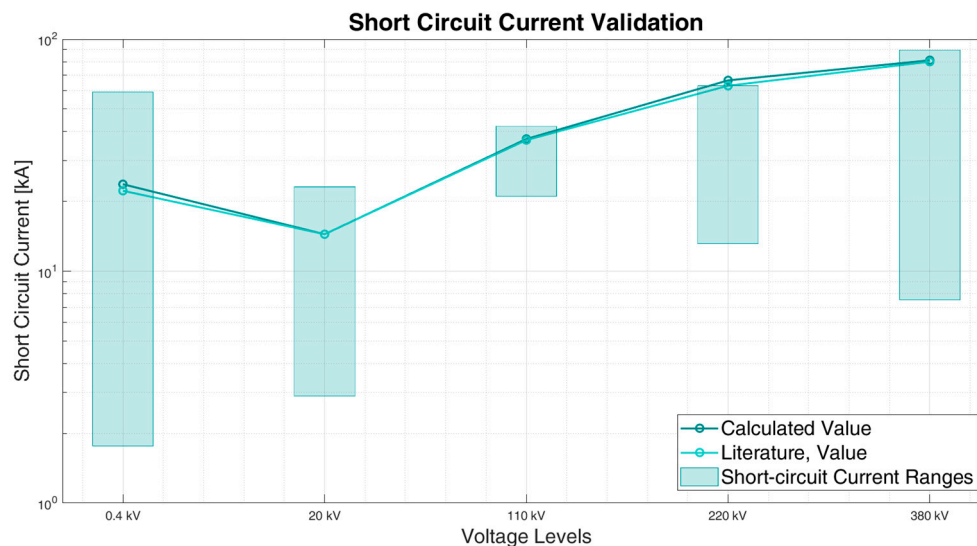
Figure 9. Short-circuit current validation for each presented test network.

4. Discussion

Within this section, first the results regarding the comparison of the short-circuit parameters presented in Section 3 are addressed. Second, the previously mentioned limitations (Section 1.2) are discussed for the presented test networks. This will show how most of the limitations for the presented test networks within the literature review can be compensated in the presented test networks, but also reveals their limitations.

4.1. Short-Circuit Results

Tables 19 and 20 as well as Figures 8 and 9 show that, in general, the presented generic test networks can be used to represent the behavior of real European networks. The reference values from the literature in Section 3 represent German grids, and the value ranges from the literature represent European grids. Since German and Austrian grids are substantially similar and no literature data was available for Austrian grids, these values were used as reference values in this work. However, this may lead to slight deviations for the short-circuit parameters, as can be seen in Figures 8 and 9.

Individually, there are some test networks that offer better replication of real network behavior than others, which will be discussed in the following.

The low-voltage test network shows a −6.75% relative deviation between the German literature value and the calculated value for short-circuit power. The relative deviation of the short-circuit current corresponds with −6.70%, therefore suggesting that the low-voltage test network may not be sufficiently representative for all applications, since both the short-circuit power as well as the short-circuit current are higher than the literature values. A higher short-circuit power, however, would suggest better voltage quality as well as greater interference resistance within the power system. Therefore, the real behavior of the grid would not be replicated properly. One parameter influencing the short-circuit values is the network structure, which for low-voltage networks mainly refers to whether they supply urban, suburban or rural areas. This network supplies mainly urban and only partially suburban as well as rural areas. Since there is no indication of the network structure for the German literature values, this may also be a cause for higher deviations. Another parameter on which the short-circuit values are dependent is the apparent power of the substation transformer feeding the network. If the rated apparent power of a substation transformer is smaller, short-circuit values are smaller as well. Since, however, there is no detailed information on the grids used for obtaining the corresponding literature values, these factors may be causes for the deviation. At the Chair of Energy Network Technology, a similar test network with primarily rural structures fed from the 10 kV-voltage level with 50 kVA rated apparent power (cf. the presented low-voltage network fed from the 20 kV-voltage level with 630 kVA rated apparent power) was developed and tested and produced short-circuit values which approximated the corresponding literature values more closely. However, the presented value range for low-voltage short-circuit power in European grids, which is between 1.2 and 41 MVA, matches the calculated values. Since the corresponding calculated value for the low-voltage grid is 16.42 MVA, the presented low-voltage test grid may replicate real network behavior of European grids sufficiently accurately.

The 20 kV medium-voltage test network shows a relative deviation of 0.07% for the short-circuit power and 0.04% for the short-circuit current. Therefore, the calculated values closely approximate German grids and, thus, also European grids. This suggests that although there is a large variety of medium-voltage grids regarding voltage levels as well as system sizes and network structures, the presented networks replicate European as well as German grids well. Therefore, they offer a valuable contribution to the research community in representing the diversity of medium-voltage grids. Since short-circuit current deviations are small (0.04%), the structure of real grids regarding parallel feeders within a medium-voltage grid is replicated especially well in this test network.

The higher voltage levels (110 kV, 220 kV and 380 kV) also show small relative deviations in short-circuit power of −1.08%, −5.49% and −0.73%. The relative deviations for short-circuit currents are similar, with values of −1.08%, −5.46% and −1.39%. Additional deviations at these voltage levels may be caused due to the lack of reactive power compensation elements (e.g., inductance coils for power factor correction). These components are important elements for energy transmission at higher voltage levels and, therefore, also influence the replication of the network behavior. Additionally, the short-circuit power at this voltage level is influenced by switching states and, thus, the resulting degree of meshing. With high degrees of meshing and fewer openly operated electrical lines, the short-circuit power increases. Since there is no detailed information on the literature values, it is possible deviations partially also occur due to different researched switching states.

4.2. Limitations of the Presented Test Networks

Since most test networks from the literature review may not be large enough for some applications, the presented generic test networks represent common network sizes for Austrian grids typical for a network of a single voltage level fed from the higher voltage level via a transformer. For the lower voltage levels (low-, medium- and partially high-voltage), common network sizes are derived from previous experiences with real grids at the Chair of Energy Network Technology. For higher

voltage levels (partially high- and maximum-voltage) the common network sizes are publicly available. Additionally, appropriate network sizes also depend on the application purpose; smaller sizes may also be sufficient to assess several research questions.

Regarding the lack of time-series data, the presented test networks include Austrian load and generation data as well as standard load profiles, which can be exchanged for different profiles for different time periods or different consumer and generation units.

The representativeness of the proposed generic test networks for European structures can be assessed from the short-circuit validation. Since the presented test networks are specifically aimed at representing European ENTSO-E structures, the mentioned parameters were researched and chosen accordingly, which is affirmed by the validation process using short-circuit parameters.

Although the presented test networks do not include geographical coordinates, since they are generically obtained from literature research, they are designed in NEPLAN and, therefore, offer a graphical representation of the network and the included components.

Another limitation addressed in Section 1.2 is that most designs and data are specific for one single issue. The test networks presented in this work are designed for replicating European network structures and their behavior, especially, for load flow calculations. If, however, other issues are addressed, these networks may be extended as required. Additionally, the fact, that these test networks are available in NEPLAN means that network parameters as well as network equipment can easily be changed or modified.

Many of the presented (mainly the North American) test feeders are limited in their use due the fact that they only represent isolated feeders and, therefore, are not capable of replicating the behavior of an entire network. On the contrary, each of the developed networks replicates one voltage level with corresponding network sizes. Therefore, each network represents more than one feeder.

5. Conclusions

This paper presents generic test networks for the European electrical distribution and transmission system. The aim is to closely replicate the network behavior of real grids at each voltage level. Since in the literature only very few representative test networks are available for European grids, new test networks with specific parameters for the European ENTSO-E interconnected system are developed, thereby ensuring a replication as accurately as possible. Since data for grids are usually sensitive due to the included consumer data and are, therefore, not disclosed by distribution and transmission system operators, only the openly available data in the literature were used to design the test networks. The researched parameters include network topologies, load densities, power ranges, types and number of consumer as well as generation units, electrical line data (line length ranges and electrical line parameters) as well as network sizes. Thus, four test networks of each voltage level common in Europe (0.4 kV, 20 kV, 110 kV, 220/380 kV) were developed.

In order to validate the presented test networks regarding their representativeness of European grids, a short-circuit analysis was performed on each test network. The results obtained from this analysis (short-circuit power and current) were then compared to literature values common in Germany and Europe. This analysis showed that the created test networks can replicate European network behavior closely. Additionally, these test networks have very few limitations and can be used for various application purposes.

References

1. Bird, L.; Milligan, M.; Lew, D. Integrating Variable Renewable Energy: Challenges and Solutions; National Renewable Energy Laboratory Technical Report NREL/TP-6A20-60451. 2013. Available online: https://www.nrel.gov/docs/fy13osti/60451.pdf (accessed on 21 August 2020).

2. Jones, L.E. *Renewable Energy Integration—Practical Management of Variability, Uncertainty, and Flexibility in Power Grids*, 1st ed.; Elsevier: Oxford, UK, 2014.

3. Hossain, J.; Mahmud, A. *Renewable Energy Integration—Challenges and Solutions*, 1st ed.; Springer: Singapore, 2014.

4. Böckl, B.; Greiml, M.; Leitner, L.; Pichler, P.; Kriechbaum, L.; Kienberger, T. HyFlow—A hybrid load flow modelling framework to evaluate the effects of energy storage and sector coupling on the electrical load flows. *Energies* **2019**, *12*, 25. [CrossRef]

5. Rodríguez Calvo, A. Scalability and Replicability of the Impact of Smart Grid Solutions in Distribution Systems. Ph.D. Thesis, Universidad Pontificia Comillas de Madrid, Madrid, Spain, 2017.

6. Postigo Marcos, F.E.; Domingo, C.M.; San Román, T.G.; Palmintier, B.; Hodge, B.; Krishnan, V.; de Cuadra García, F.; Mather, B. A review of power distribution test feeders in the United States and the need for syntheitc representative networks. *Energies* **2017**, *10*, 14. [CrossRef]

7. Kersting, W.H. Radial distribution test feeders. *IEEE Trans. Power Syst.* **1991**, *6*, 975–985. [CrossRef]

8. IEEE PES Resources. Available online: https://site.ieee.org/pes-testfeeders/resources/ (accessed on 5 June 2020).

9. Sunderman, W.G.; Dugan, R.C.; Dorr, D.S. The neutral-to-earth voltage (NEV) test case and distribution system analysis. In Proceedings of the IEEE Power and Energy Society General Meeting—Conversion and Delivery of Electrical Energy in the 21st Century, Pittsburgh, PA, USA, 20–24 July 2008; pp. 1–6.

10. Schneider, K.P.; Fuller, J.C. Detailed end use load modeling for distribution system analysis. In Proceedings of the IEEE Power and Energy Society General Meeting, Providence, RI, USA, 25–29 July 2010; pp. 1–7.

11. Schneider, K.P.; Fuller, J.C.; Chassin, D.P. Multi-state load models for distribution system analysis. *IEEE Trans. Power Syst.* **2011**, *26*, 2425–2433. [CrossRef]

12. Horton, R.; Sunderman, W.G.; Arritt, R.F.; Dugan, R.C. Effect of line modeling methods on neutral-to-earth voltage analysis of multi-grounded distribution feeders. In Proceedings of the IEEE/PES Power Systems Conference and Exposition, Phoenix, AZ, USA, 20–23 March 2011; pp. 1–6.

13. Variz, A.M.; Pereira, J.L.R.; Carneiro, S., Jr.; Barbosa, P.G. Harmonic analysis of the power distribution neutral-to-earth voltage (NEV) test case using four-wire three-phase harmonic current injection method. In Proceedings of the IEEE Power and Energy Society General Meeting, Calgary, AB, Canada, 26–30 July 2009.

14. Arritt, R.F.; Dugan, R.C. The IEEE 8500-node test feeder. In Proceedings of the IEEE PES Transmission and Distribution Conference and Exposition, New Orleans, LA, USA, 19–22 April 2010; pp. 1–6.

15. Kersting, W.H. A comprehensive distribution test feeder. In Proceedings of the IEEE PES Transmission and Distribution Conference and Exposition, New Orleans, LA, USA, 19–22 April 2010; pp. 1–4.

16. Hooshyar, H.; Mahmood, F.; Vanfretti, L.; Baudette, M. Specification, implementation, and hardware-in-the-loop real-time simulation of an active distribution grid. *Sustain. Energy Grids Netw.* **2015**, *3*, 36–51. [CrossRef]

17. Schneider, K.; Phanivong, P.; Lacroix, J.S. IEEE 342-node low voltage networked test system. In Proceedings of the IEEE PES General Meeting/Conference Exposition, National Harbor, MD, USA, 27–31 July 2014; pp. 1–5.

18. Yuan, Z.; Hesamzadeh, M.R. Hierarchical coordination of TSO-DSO economic dispatch considering large-scale integration of distributed energy resources. *Appl. Energy* **2017**, *195*, 600–615. [CrossRef]

19. Yang, T.; Huang, Z.; Pen, H.; Zhang, Y. Optimal planning of communication system of CPS for distributed network. *Hindawi J. Sens.* **2017**, 10.

20. Dugan, R.C.; Kersting, W.H.; Carneiro, S.; Arritt, R.F.; McDermott, T.E. Roadmap for the IEEE RES test feeders. In Proceedings of the IEEE/PES Power Systems Conference and Exposition, Seattle, WA, USA, 15–18 March 2009; pp. 1–4.

21. OpenDSS Page on EPRI. Available online: https://www.epri.com/pages/sa/opendss?lang=en (accessed on 10 June 2020).

22. GridLAB-D Simulation Software. Available online: https://www.gridlabd.org/ (accessed on 10 June 2020).

23.　Nousdilis, A.; Chrysochos, A.; Papagiannis, G.; Christoforidis, G.C. The impact pf Photovoltaic Self-Consumption Rate on voltage levels in LV distribution grids. In Proceedings of the 11th IEEE International Conference on Compatability, Power Electronics and Power Engineering, Cadiz, Spain, 4–6 April 2017.

24.　Schneider, K.P.; Chen, Y.; Chassin, D.P.; Pratt, R.; Enge, D.; Thompson, S. *Modern Grid Initiative Distribution Taxonomy Final Report*; Pacific Northwest National Laboratory (PNNL): Richland, WA, USA, 2008.

25.　Wu, D.; Aliprantis, D.C. Potential impacts of aggregator-controlled plug-in electric vehicles on distribution systems. In Proceedings of the 4th IEEE International Workshop on Computational Advances in Multi-Sensor Adaptive Processing (CAMSAP 2011), San Juan, Puerto Rico, 13–16 December 2011; pp. 105–108.

26.　Jahangiri, P.; Aliprantis, D.C. Distributes Volt/VAr control by PV inverters. *IEEE Trans. Power Syst.* **2013**, *28*, 3429–3439. [CrossRef]

27.　Xu, Y.; Liu, C.-C.; Gao, H. Reliability analysis of distribution systems considering service restoration. In Proceedings of the IEEE Power and Energy Society Innovative Smart Grid Technologies Conference, Washington, DC, USA, 18–20 February 2015.

28.　Jha, R.R.; Dubey, A.; Liu, C.-C.; Schneider, K.P. Bi-level Volt-VAR optimization to coordinate smart inverters with voltage control devices. *IEEE Trans. Power Syst.* **2019**, *34*, 1801–1813. [CrossRef]

29.　Schneider, K.P.; Chen, Y.; Engle, D.; Chassin, D. A taxonomy of North American radial distribution feeders. In Proceedings of the IEEE Power Energy Society General Meeting, Calgary, AB, Canada, 26–30 July 2009; pp. 1–6.

30.　Electric Power Research Institute (EPRI). EPRI Feeder J1. Available online: https://dpv.epri.com/feeder_j.html (accessed on 18 June 2020).

31.　Electric Power Research Institute (EPRI). EPRI Feeder K1. Available online: https://dpv.epri.com/feeder_k.html (accessed on 18 June 2020).

32.　Electric Power Research Institute (EPRI). EPRI Feeder M1. Available online: https://dpv.epri.com/feeder_m.html (accessed on 18 June 2020).

33.　Electric Power Research Institute (EPRRI). EPRI Smart Grid Resource Center. Available online: http://svn.code.sf.net/p/electricdss/code/trunk/Distrib/EPRITestCircuits/ (accessed on 18 June 2020).

34.　Kim, I.; Harley, R.G. A study on the effect of the high-penetration photovoltaic system on an increase in overvoltage of distribution feeders. In Proceedings of the North American Power Symposium (NAPS), Charlotte, NC, USA, 4–6 October 2015; pp. 1–4.

35.　Reno, M.J.; Coogan, K.; Grijalva, S.; Broderick, R.J.; Quiroz, J.E. PV interconnection risk analysis through distribution system impact signatures and feeder zones. In Proceedings of the IEEE PES General Meeting| Conference Exposition, National Harbor, MD, USA, 27–31 July 2014; pp. 1–5.

36.　Kim, I.; Harley, R.G.; Regassa, R.; del Valle, Y. The effect of the Volt/Var control of photovoltaic systems on the time-series steady-state analysis of a distribution network. In Proceedings of the Clemson University Power Systems Conference (PSC), Clemson, SC, USA, 10–13 March 2015; pp. 1–6.

37.　Pacific Gas and Electric Prototypical Feeder Models. Available online: http://gridlab-d.shoutwiki.com/wiki/PGE_Prototypical_Models (accessed on 19 June 2020).

38.　Hernandez, M.; Peppanen, J.; Hubert, T.; Deboever, J.; McCarty, M.; Petrenko, F.; Trinko, O. EPIC 2.03A: Test Smart Inverter Enhanced Capabilities—Photovoltaics (PV): Smart Inverter Modeling Report. Final Report. 2019. Available online: https://www.pge.com/pge_global/common/pdfs/about-pge/environment/what-we-are-doing/electric-program-investment-charge/PGE-EPIC-Project-2.03A_Modeling-Report.pdf (accessed on 13 July 2020).

39.　Papathanassiou, S.; Hatziargyriou, N.; Strunz, K. A benchmark low-voltage microgrid network. In Proceedings of the CIGRE Symposium Power Systems with Dispersed Generation: Technologies, Impacts on Development, Operation and Performances, Athens, Greece, 13–16 April 2005; pp. 1–8.

40.　Strunz, K.; Fletcher, R.H.; Campbell, R.; Gao, F. Developing benchmark models for low-voltage distribution feeders. In Proceedings of the IEEE Power & Energy Society General Meeting, Calgary, AB, Canada, 26–30 July 2009; pp. 1–3.

41.　Li, Y.; Li, Y.W. Virtual frequency-voltage frame control of inverter based low-voltage microgrids. In Proceedings of the IEEE Electrical Power and Energy Conference (EPEC), Montreal, QC, Canada, 22–23 October 2009; pp. 1–6.

42. Li, Y.; Li, Y.W. Power Management of inverter interfaced autonomous microgrid based on virtual frequency-voltage frame. *IEEE Tran. Smart Grid* **2011**, *2*, 30–40. [CrossRef]

43. Zamani, M.A.; Sidhu, T.S.; Yazdani, A. A Protection strategy and microprocessor-based relay for low-voltage microgrids. *IEEE Trans. Power Deliv.* **2011**, *26*, 1873–1883. [CrossRef]

44. CORDIS Forschungsergebnisse der EU. Large Scale Integration of Micro-Generation to Low Voltage Grids (MICROGRIDS). Available online: https://cordis.europa.eu/project/id/ENK5-CT-2002-00610/de (accessed on 24 June 2020).

45. Pandapower. CIGRE Networks. Available online: https://pandapower.readthedocs.io/en/v1.2.2/networks/cigre.html#high-voltage-transmission-network (accessed on 24 June 2020).

46. Ayaz, M.S.; Azizipanah-Abarghooee, R.; Terzija, V. European LV microgrid benchmark network: Development and frequency response analysis. In Proceedings of the IEEE International Energy Conference (ENERGYCON), Limassol, Cyprus, 3–7 June 2018; pp. 1–7.

47. Rudion, K.; Orhts, A.; Styczynski, Z.A.; Strunz, K. Design of benchmark of medium-voltage distribution network for investigation of DG integration. In Proceedings of the IEEE Power Engineering Society General Meeting, Montreal, QC, Canada, 18–22 June 2006; pp. 1–6.

48. Jahangiri, P.; Wu, D.; Li, W.; Aliprantis, D.C.; Tesfatsion, L. Development of an agent-based distribution test feeder with smart-grid functionality. In Proceedings of the IEEE Power and Energy Society General Meeting (PESGM), San Diego, CA, USA, 22–26 July 2012; pp. 1–7.

49. Vrba, P.; Marik, V.; Siano, P.; Leitao, P.; Zhabelova, G.; Vyatkin, V.; Strasser, T. A review of agent and service-oriented concepts applied to intelligent energy systems. *IEEE Trans. Ind. Inform.* **2014**, *10*, 1890–1903. [CrossRef]

50. Kays, J.; Seack, A.; Häger, U. Consideration of innovative distribution grid operation concepts in the planning process. In Proceedings of the IEEE PES Innovative Smart Grid Technologies Conference Europe, Ljubljana, Slovenia, 9–12 October 2017; pp. 1–6.

51. Kays, J.; Rehtanz, C. Planning process for distribution grids based on flexibly generated time series considering RES, DSM and storages. *IET Gener. Transm. Distrib.* **2016**, *10*, 3405–3412. [CrossRef]

52. McDermott, T.E. A test feeder for dg protection analysis. In Proceedings of the IEEE/PES Power Systems Conference and Exposition, Phoenix, AZ, USA, 20–23 March 2011; pp. 1–7.

53. Wieserman, L.; McDermott, T.E. Fault current and overvoltage calculations for inverter-based generation using symmetrical components. In Proceedings of the IEEE Energy Conversion Congress and Exposition (ECCE), Pittsburgh, PA, USA, 14–18 September 2014; pp. 1–6.

54. Prettico, G.; Gangale, F.; Mengolini, A.; Lucas, A.; Fulli, G. Distribution System Operators Observatory; JRC Technical Report. 2016. Available online: https://ses.jrc.ec.europa.eu/distribution-system-operators-observatory (accessed on 1 July 2020).

55. Mateo, C.; Prettico, G.; Gómez, T.; Cossent, R.; Gangale, F.; Frías, P.; Fulli, G. European representative electricity distribution networks. *Electr. Power Energy Syst.* **2018**, *99*, 273–280. [CrossRef]

56. Pérez-Arriaga, I.; Knittel, C. Utility of the Future—An MIT Energy Initiative Response to an Industry in Transition. Report. 2016. Available online: https://energy.mit.edu/wp-content/uploads/2016/12/Utility-of-the-Future-Full-Report.pdf (accessed on 2 July 2020).

57. Liao, Y.; Weng, Y.; Liu, G.; Rajagopal, R. Urban MV and LV distribution grid topology estimation via group lasso. *IEEE Trans. Power Syst.* **2016**, *34*, 12–27. [CrossRef]

58. Flammini, M.G.; Prettico, G.; Fulli, G.; Bompard, E.; Chicco, G. Interaction of consumers, photovoltaic systems and electric vehicle energy demand in a Reference Network Model. In Proceedings of the International Conference of Electrical and Electronic Technologies for Automotive, Torino, Italy, 15–16 June 2017; pp. 1–5.

59. Lucas, A. Single-phase PV power injection limit due to voltage unbalances applied to an urban reference network using real-time simulation. *Energies* **2018**, *8*, 15. [CrossRef]

60. González-Sotres, L.; Frias, P.; Mateo, C. Power line communication transfer function computation in real network configurations for performance analysis applications. *IET Commun.* **2017**, *11*, 897–904. [CrossRef]

61. Andreadou, N.; Jansen, L.L.; Marinopoulos, A.; Papaioannou, I. Smart Grid Laboratories Inventory. JRG Science for Policy Report. 2018. Available online: https://ses.jrc.ec.europa.eu/smart-grid-laboratories-inventory (accessed on 2 July 2020).

62. Mendeley Data—Non-synthetic European Low Voltage Test System. Available online: https://data.mendeley.com/datasets/685vgp64sm/1 (accessed on 3 July 2020).

63. Koirala, A.; Suárez-Ramón, L.; Mohamed, B.; Arboleya, P. Non-synthetic European low voltage test system. *Electr. Power Energy Syst.* **2020**, *118*, 11. [CrossRef]

64. Rigoni, V.; Ochoa, L.F.; Chicco, G.; Navarro-Espinosa, A.; Gozel, T. Representative residential LV feeders: A case study for the north west of England. In Proceedings of the IEEE Power and Energy Society General Meeting (PESGM), Boston, MA, USA, 17–21 July 2016; pp. 1–12.

65. Li, Y.; Wolfs, P.J. Taxonomic description for Western Australian distribution medium-voltage and low-voltage feeders. *IET Gener. Transm. Distrib.* **2014**, *8*, 104–113. [CrossRef]

66. NEPLAN AG (8700 Küsnacht, Switzerland). *NEPLAN-Power System Analysis*; NEPLAN AG: Zürich, Switzerland, 2019.

67. Schwab, A.J. *Elektroenergiesysteme—Erzeugung, Transport, Übertragung und Verteilung elektrischer Energie*, 3rd ed.; Springer: Berlin/Heidelberg, Germany, 2011.

68. Heuck, K.; Dettmann, K.D.; Schulz, D. *Elektrische Energieversorgung—Erzeugung, Übertragung und Verteilung elektrischer Energie für Studium und Praxis*, 9th ed.; Springer Vieweg: Wiesbaden, Germany, 2013.

69. Mahrenbach, R.; Nelles, D.; Tuttas, C. *Elektrische Energietechnik—Grundlagen, Energieversorgung, Antriebe und Leistungselektronik*, 2nd ed.; Springer Vieweg: Wiesbaden, Germany, 2013.

70. Lumpi Berndorf. Charactersitics of Aluminium Conductors Used in Austria—Technical Data According to EN50182/2001. Available online: https://www.lumpi-berndorf.at/fileadmin/downloads/Overhead_line_conductors_EN50182.pdf (accessed on 13 July 2020).

71. Strauß, S. Wirtschaftlicher und Technischer Vergleich von Energieübertragungssystemen. Master's Thesis, Institut für Technische Physik, Karlsruhe Institut für Technologie, Karlsruhe, Germany, 2011.

72. Pflugradt, N. Online Load Profile Generator. Available online: https://www.loadprofilegenerator.de (accessed on 29 May 2020).

73. Pflugradt, N.; Teuscher, J.; Platzer, B.; Schufft, W. Analysing low-voltage grids using a behaviour based load profile generator. In Proceedings of the International Conference on Renewable Energies and Power Quality (ICREPQ'13), Bilbao, Spain, 20–22 March 2013.

74. Österreichs Energie Akademie. Technische Anschlussbedingungen für den Anschluss an Öffentliche Versorgungsnetze (TAEV) mit Betriebsspannungen bis 1000 Volt, mit Erläuterungen der Einschlägigen Vorschriften. Available online: http://www.akademie.oestersenergie.at/taev.html/TAEV_Austauschblätter.pdf (accessed on 15 July 2020).

75. APG- Erzeugung Nach Typ. Available online: https://www.apg.at/de/markt/Markttransparenz/erzeugung/Erzeugung-pro-Typ (accessed on 29 May 2020).

76. APG Leitungsnetz. Available online: https://www.apg.at/de/Stromnetz/APG-Netz (accessed on 10 July 2020).

77. Kurzschlussleistung des Niederspannungsnetzes am Verknüpfungspunkt. Available online: http://www.sfv.de/lokal/mails/wvf/kurzschl.htm (accessed on 14 July 2020).

78. Kny, K.H. *Schutz bei Kurzschluss in Elektrischen Anlagen—Planen, Errichten, Prüfen*, 3rd ed.; Huss-Medien GmbH: Berlin, Germany, 2017.

79. Schorch. Elektrischer Anschluss Sicher & Problemlos. Available online: https://www.schorch.de/Cms/Media/GlobalRepositories/Schorch.Site.Allgemein/Downloads/hs/Exd-7_de.pdf (accessed on 25 August 2020).

80. Oeding, D.; Oswald, B.R. *Elektrische Kraftwerke und Netze*, 7th ed.; Springer-Verlag: Berlin Heidelberg, Deutschland, 2011; pp. 399–450.

81. Kasikci, I. *Planung von Elektroanlagen–Theorie, Vorschriften, Praxis*, 2nd ed.; Springer-Verlag: Berlin Heidelberg, Germany, 2014; pp. 61–133.

Paper 2 (Status: Accepted)

Table A. 1: Author statement to second peer-reviewed publication (Paper 2)

Activity	Contribution authors (main author is mentioned first)
Conceptualization	A. Traupmann, T. Kienberger
Methodology	A. Traupmann, T. Kienberger
Data Curation	A. Traupmann
Software Development and Validation	A. Traupmann
Modeling	A. Traupmann
Visualization	A. Traupmann, T. Kienberger
Writing (Original Draft)	A. Traupmann
Writing (Review and Editing)	A. Traupmann, T. Kienberger
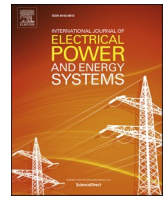
Novel network reduction method for cellular-based network models with enhanced modeling accuracy for multi-energy-system approaches

Anna Traupmann [*], Thomas Kienberger

Chair of Energy Network Technology, Montanuniversitaet Leoben, Franz-Josef-Strasse 18, 8700 Leoben, Austria

A B S T R A C T

Sustainable electricity supply can be achieved by expanding renewable energy sources (RES), which due to their volatile nature present challenges for the power grids. Modern electricity grids must be able to coordinate and balance these unpredictable generation patterns. One option for grid-friendly RES integration is multi-energy systems (MES) which enable energy use across energy carriers and, thus, relieve electrical grids. Therefore, long-term simulations of MES are indispensable and require appropriate models. Since MES have high systemic complexity due to high temporal resolution, spatial coverage, and hierarchical depth, modeling requires massive computational effort, impeding the investigations. Models with reduced complexity (spatial resolution reduction) and, thus, reduced computational effort can be created using a cellular approach. In particular, for electrical grids, reduction of complexity requires network reduction methods that create equal grid models regarding electrical behavior. Since most (numerical) network reduction methods (e.g., REI, WARD method) fail to replicate all required parameters, this work presents a novel network reduction method enhancing modeling accuracy, primarily regarding reactive power. The introduced method is based on a detailed parameter analysis to identify parameters responsible for deviations between original grid and reduced cell model. The validation of this method uses test networks at different voltage levels to reveal influencing variables that enhance modeling accuracy. This allows to derive trends for modelling accuracy of individual electrical parameters. The introduced method facilitates developing cell models for time-series-based calculations with maximum modeling accuracy and reasonable calculation effort. Additionally, this paper presents advantageous application purposes of this method.

1. Introduction

To reduce the negative impacts caused by climate change, future energy generation has to be based mainly or even entirely on renewable energy sources (RES). Since RES are usually decentralized, volatile, and, therefore, not always predictable, efficiently integrating them into existing energy systems presents a challenge. The mentioned characteristics of RES put great stress on electrical grid infrastructures and, thereby, may compromise a secure and stable energy supply. Therefore, transitioning into a low-carbon and stable future energy system requires innovative approaches and supportive tools for efficient design and operational management as well as for strategic decision-making. [1–5] One of these approaches is multi-energy systems (MES) which utilize synergies between the individual energy carrier networks to improve overall system efficiency and stability [6]. MES approaches, however, require the development of adequate network models for each energy

carrier considered, to perform spatially and temporally highly resolved and yet time-efficient and precise calculations across energy carriers and hierarchical system levels. [7–9] Therefore, the multi-energy system modeling framework HyFlow [9,10] was developed at the Chair of Energy Network Technology. Since the developed network models are integrated in HyFlow, all energy carrier models have to correspond with the frame conditions and model characterization [11–14] of HyFlow: The models have to correspond with the chosen modelling approach (cellular approach) and they have to represent bottom-up models (allow different resolutions regarding time scales and geographical areas, cf. Fig. 1).

Depending on network complexity and temporal resolution, the level of aggregation for each network model has to be defined to ensure that the computational effort for the calculation is kept at a minimum. If the temporal resolution is high, the spatial resolution has to be correspondingly lower and vice versa, to ensure minimal computational effort. Thus, a compromise between computational time and level of

---

Nomenclature

RES	Renewable Energy Sources
MES	Multi-Energy Systems
REI	Radial Equivalent Independent
TSO	Transmission System Operator
ZPBN	Zero Power Balance Network
AMV	Arithmetic Mean Value

different voltage levels and provides trends over the voltage levels. Additionally, this section shows which of the investigated parameters influences modeling accuracy most and offers improvement recommendations to enhance the modeling accuracy of this method. Subsection 5 provides conclusions regarding application purposes for which this novel reduction method is suitable.

Due to the overall subject and the methodology used, this work is relevant to the International Journal of Electric Power and Energy Systems, especially regarding Green Power and Energy Technologies and Systems.
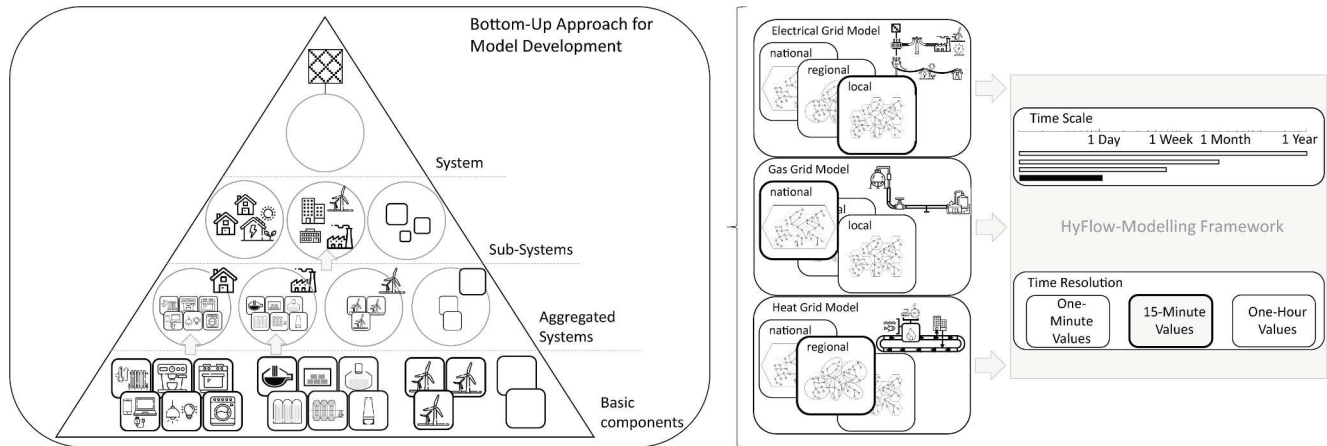
Fig. 1. Description of the HyFlow-Modeling Framework and the models implemented in HyFlow.

detail can be achieved using spatial resolution reduction (reducing size and complexity of the network model), which is supported by a cellular approach. This approach partitions the real grid into energy cells to be represented by only a small set of parameters. However, concerning electrical grids, the applied spatial resolution reduction within the cellular approach combines and eliminates network nodes as well as electrical lines, which changes the network's behavior. To obtain a smaller and less complex electrical model for the calculation with the same electrical behavior as the original grid, specific methods are necessary to compensate for this deviation. Therefore, this paper is focused on a methodical approach for the development of electrical network models corresponding to the requirements mentioned above. This leads to the following research questions:

- Which electrical parameters of the reduced grid show deviations to their original values due to applying a cellular modeling approach on the corresponding electrical grid?
- Why do these deviations (for time series-based calculations) occur, and how can they be compensated in cellular network models?
- What is the obtained modeling accuracy in the compensated cellular network model?

Section 2 reviews currently applied network reduction methods that can be used for a cellular approach. This review concludes that the achieved modeling accuracy with these methods has to be enhanced to obtain conclusive results, especially regarding reactive power. Therefore, Section 3 first presents the applied cellular modeling approach (Subsection 3.1) and then introduces a novel network reduction method specifically applicable to the cellular approach (Subsection 3.2). Additionally, Subsection 3.3 provides the test grids used to determine the modeling accuracy obtained in the reduced network model. Section 4.1 then presents results about modeling accuracy and deviations of the proposed network reduction method. Subsection 4.2 discusses the modeling accuracy of the presented network reduction method for

2. Related works – State of research in network reduction methods

Today's transmission and distribution grids are usually extended and highly interconnected networks. Therefore, TSOs cannot operate their grids individually without neglecting the influence of the interconnected grids on their control area [15]. As a result, appropriate models of electrical grids which consider the overall interconnected energy system usually exceed national borders as well as observation areas of single transmission system operator (TSO). [16,17] Analyzing such networks, especially over a long period with fine temporal resolution (e.g., 15-minute values for one year), is computationally burdening as well as time-intensive and, therefore, requires preliminary simplifications (e.g., network reduction). [17] Thus, network reduction or equivalencing of expanded grids or larger grid sections has, thus, become increasingly important. Those reduced network models (network equivalents) are smaller and less complex and replace the power system or a part of the power system. The results obtained by using network equivalents can then be transferred onto the original, unreduced, expanded grid (referred to as 'original grid' in the following). [18,19] The common characteristics of reduced network models are:

- Reliable and accurate representation of the effects of the reduced network section on the remaining network [20]
- Mathematically well-conditioned (compliance with problem-solving mechanisms such as convergence and arithmetic precision problems, predefined accuracy limits, and computational efficiency) [20]
- Wide range of applications (which may feature inter-company data exchange) [20]

The calculations performed with cellular network models can either be static (single point in time calculations) or, more commonly, time-series-based calculations, which represent a sequencing of different static operating states. Dynamic analyses of faults such as short circuits

Fig. 2. Categorization of the types of network reduction and the corresponding methods.
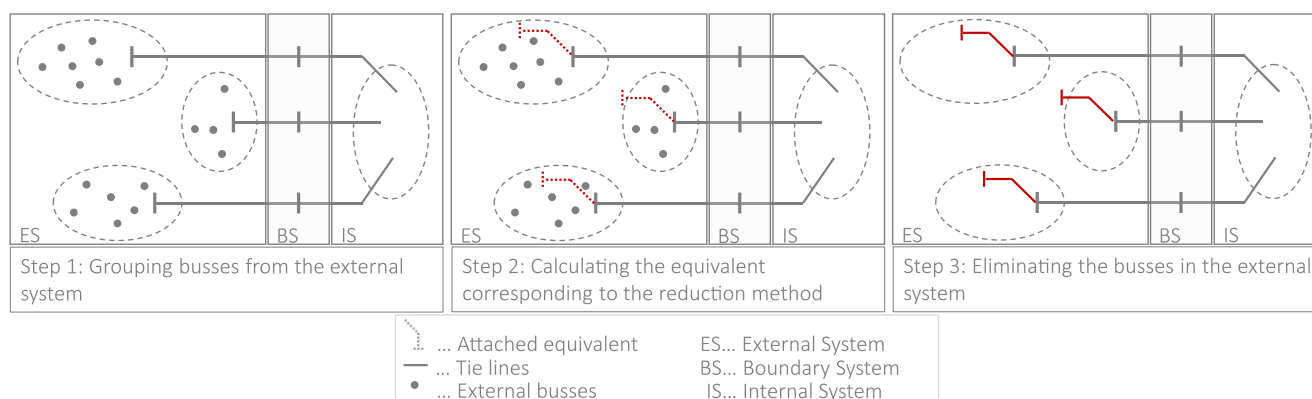

Fig. 3. Exemplary process steps for REI and WARD method for defined system boundaries of the external system, the boundary system, and the internal system for network reduction (own representation according to [19]).

are not considered in this paper. There are two different kinds of network reduction methods available in the literature. Their application depends on the type of analysis they are used for. [16] A summary of how network reduction methods are categorized is shown in Fig. 2. The corresponding network reduction method calculates the equivalent network parameters, which compensate for the deleted grid elements, according to the application requirements. [19] Due to the objective of this paper, only static or steady-state network reduction methods for engineering applications are considered.

A static network reduction performs the compensation for one single operating point. The operating point is defined by the load and generation present in the grid at a certain point in time and represents one temporally independent network state. Therefore, the reduced network model represents only this operating point of the original grid correctly. Dynamic network reduction additionally enables retaining dynamic properties of the reduced grid elements and, thus, allows investigating transient phenomena, e.g., in case of fault. [21,22] The application purpose of the reduced network model determines the network reduction method used. Therefore, for each designated utilization, only specific network reduction methods are applicable [19]. For creating reduced network models in the cellular approach, the REI method, as well as the WARD method, are appropriate.

In general, all static network reduction methods must define system boundaries for the so-called internal system (I), the external system (E), and the boundary system (B) [16]. The internal system contains the network nodes located within the area of interest, e.g., the internal network of a control zone. The external system comprises all the

network nodes, which are eliminated during the reduction and replaced by the network equivalent, while the boundary system connects the internal and the external system. [19] Fig. 3 shows exemplary system boundaries when applying a network reduction method: While the internal system is represented by a model of the original grid, the external system is represented by a model of the network equivalent after the reduction (Step 3 in Fig. 3). [20]

In real-time simulations, for example, an internal network (e.g., control zone of a TSO) has to be monitored closely in detail. On the contrary, there is no need to closely observe connected grids or grid sections (external network) as they are only minimally impacted by faults within the internal system. Therefore, they can be replaced by reduced network models as long as their electrical behavior is preserved. [16]

Steps 1 and 3 from Fig. 3 are the same for both the REI and WARD method. The implementation of the second process step, however, slightly varies. The methods use different approaches for depicting the nodal admittance matrix of the original grid. The REI method [19,23] uses a ZPBN (zero power balance network), a fictitious temporary network model, to preserve the power losses of the original grid. This network links the external busses to the equivalent REI-bus (bus to which the REI equivalent is attached) and is included in the nodal admittance matrix of the original grid. The WARD method [24,25] creates a passive network model for the external system by converting power injections of the external system to either constant currents (WARD injection method) or shunt-admittances (WARD admittance method), thus, also changing the nodal admittance matrix. This process
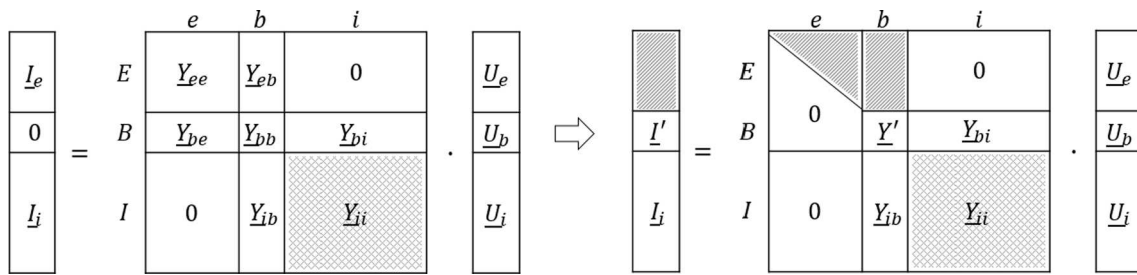
Fig. 4. Exemplary reduction of the nodal admittance matrix arranged according to the predefined system boundaries (own representation according to [20]).

for eliminating network nodes is mathematically implemented by applying a numerical solution method, the Gaussian Elimination. Gaussian Elimination gradually removes network nodes from the network by performing a triangular reduction of the nodal admittance matrix. [24] Therefore, the original grid is mathematically described by a set of equations formulated for each network node [15]. Equation (1) shows the general nodal equation system in matrix notation, where $\underline{I}$ is the complex nodal injection current vector (induced by load or generation in that node), while $\underline{U}$ is the complex nodal voltage vector and $\underline{Y}$ is the nodal admittance matrix. [16]

$$\underline{Y} \bullet \underline{U} = \underline{I} \tag{1}$$

The nodal admittance matrix $\underline{Y}$ contains information about network topology and line as well as transformer parameters. It describes which network nodes are connected via which electrical line or transformer. The specific parameters of the corresponding connection element are stored into this matrix in the form of an admittance. For the reduction, the nodal admittance matrix $\underline{Y}$ is partitioned into external (e), boundary (b), and internal (i) nodes, according to the selected system boundaries (Fig. 3). The internal nodes are only connected to the boundary busses and are, therefore, not relevant or influenced in the reduction process, which is shown in Fig. 4. [20]

After the reduction using Gaussian Elimination, a reduced matrix $\underline{Y}$ (consisting of $\underline{Y}'$, $\underline{Y}_{bi}$, $\underline{Y}_{ib}$, and $\underline{Y}_{ii}$) and the additional injected currents $\underline{I}'$ are obtained, which the REI-equivalent then provides. The values in the matrix $\underline{Y}'$ include equivalent line parameters for the connecting tie lines (compensation lines), which adapt line power flows and losses to match those in the original grid. The additional boundary bus current injections $\underline{I}'$ are added to the actual injections at the boundary busses. [20] These two parameters ($\underline{Y}'$, $\underline{I}'$) calculated using Gaussian Elimination compensate for the eliminated grid elements.

The main disadvantage of network reduction methods which use numerical methods for reducing grids or grid sections, as the WARD and REI methods, is the achieved modeling accuracy [20]. The modeling accuracy of a reduced network model refers to the deviation of electrical parameters between the original values and the reduced values. This deviation should be as minimal as possible, which can only be achieved using compensation (network reduction).

Since both methods (REI and WARD) are static reduction methods, they strongly depend on the initial operating point. The initial operating point, thus, defines the network losses of the reduced network section. Therefore, the losses for other operating states cannot be preserved after reduction leading to inaccuracies in the reduced network model. Additionally, since it can no longer be distinguished between PV- and PQ-node types for generators after the reduction, the reactive power support from the external network cannot be modeled accurately in the reduced network model. These circumstances lead to improperly preserved (mainly) reactive network behavior of the external system when these state-of-the-art numerical reduction methods are applied. Therefore, their performance varies with the extent to which the operating point changes. In addition, the presented numerical methods may lead to convergence problems when solving the reduced system using classical numerical methods (e.g., Newton-Raphson). [20,26,27]

Creating reduced equivalent network models within the cellular approach using numerical reduction methods, therefore, leads to partially inadmissible deviations and distorted electrical behavior within the cell model, as analyzed in Traupmann et al. (2019) [28]. The results of this study ([28]) obtained from applying these numerical network reduction methods (REI and WARD method) for cellular-based applications show that reactive power cannot be preserved and active power deviated significantly, as well, showing that they cannot provide sufficient modeling accuracy. [28]

A similar study to this work presenting a new static equivalent model for distribution grids with the specific purpose to model high levels of PV penetration is conducted in Samadi et al. (2015) [29]. An even more comparable study in terms of reduction areas is described in Shi et al. (2015) [30]: The presented network reduction method preserves the original grid structure in the best possible way, since it aggregates on a zonal basis, similar to the cellular approach of this work. The difference to the study in Shi et al. (2015) [30] is the compensation used, which correspond to the calculation of equivalent lines between the zones. Promising results have already been obtained, however, the computational effort for the equivalent line calculation is high. [30] Additionally, Ploussard et al. (2018) [31] also present a novel network reduction method focusing on inter-area lines for transmission expansion planning including costs, which is not the aim of the models presented in the proposed work [31]. More recent studies focus on enhanced selection of the network nodes for network reduction, such as in Huang et al. (2020) [32], where parameters from graph theory are used for improved node selection.

Thus, a new method is introduced in this paper, which deals specifically with creating reduced equivalent cellular network models for time-series-based calculations to enhance modeling accuracy. Additionally, this novel reduction method no longer depends on the initial operating state and enables an adaption to changing load and generation situations. Despite this ability to adapt to operating states, the calculation of this method must be performed only once for a defined cell division. Cell division for one application purpose remains unchanged. Thus, the reduced cell model can be used for different load and generation profiles. Due to the one-time calculation and the significantly decreased complexity of the reduced cell models, the calculation effort is minimized.

3. Problem formulation and methodology

3.1. Cellular modeling approach

This approach supports spatial resolution reduction of grid infrastructures and, thus, defines the level of detail for the network model. Thereby, it allows for a reasonable compromise between modeling accuracy and computational effort and, thus, time-efficient calculations specific for each application. Within this approach, each energy carrier network is divided into energy cells. An energy cell represents the lowest system level at which energy generation and consumption are balanced. The energy balancing is performed using time-resolved energy quantities (e.g., 15-minute values) present in each cell. [33,34] For this
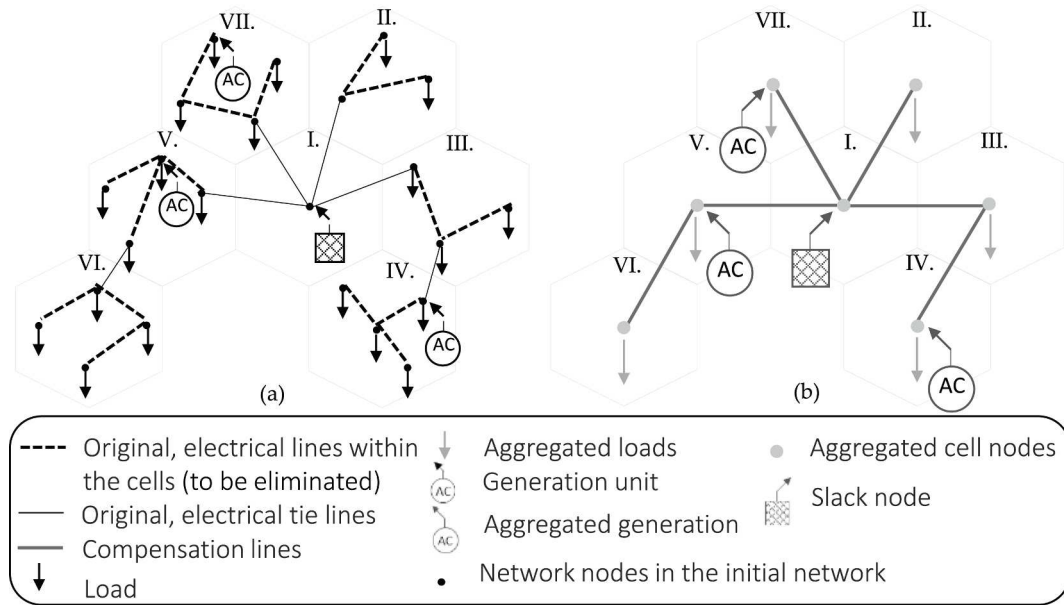
Fig. 5. Exemplary process steps of the cellular approach: (a) cell division of the original grid; (b) aggregation into energy cells.
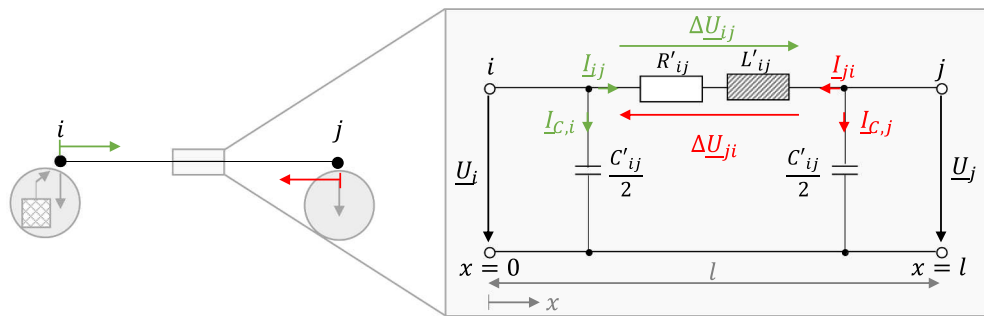

Fig. 6. Single line π–equivalent circuit of electrical transmission lines.

purpose, the residual load $P_{res}(t)$ represented in Equation (2), which is defined as the difference between load ($P_{Load}(t)$) and generation ($P_{gen}(t)$) for each time step, is calculated. [9]

$$P_{res}(t) = P_{load}(t) - P_{gen}(t) \qquad (2)$$

A positive residual load indicates that the consumed power for this time step is higher than the generated power, while a negative residual load suggests a generation surplus. [9] The residual load of each cell enables identifying the most efficient energy compensation possible using corresponding grid elements (e.g., storage or flexibility options). The residual load also assists in locating infrastructural improvement potential [34] or possible expansion measures [33] as well as beneficial cross-sector coupling points [9]. Applying the cellular approach requires two consecutive process steps, as visualized in Fig. 5.

First, each energy carrier network is partitioned into energy cells according to geographical and topological aspects (Fig. 5 a). Each energy cell represents a set of network nodes as well as generators, consumers, and storage units connected to them. The size of these energy cells corresponds to the application purpose. It can vary between state- or region-sized, or even single-household cells. In the second step, all network nodes and their connected elements are aggregated into one fictitious node in the cell center (Fig. 5 b). In this step, due to the aggregation, the network is simplified and reduced in its complexity. Thus, each cell can now be represented by only a small set of parameters. As a result, only the connecting lines between the cells and the aggregated amount of energy generation and consumption within the cells are

retained. [33,34]

During the aggregation process, the network structure of each energy carrier network is altered as a result of grid elements being eliminated. This modifies the behavior of the overall network model in a way that it is no longer equal to the original one. However, cellular network models must replicate or approximate the real grid as closely as possible. Otherwise, they cannot be utilized for planning and design purposes. Consequently, the changed behavior of the network model must be compensated for by using appropriate compensation methods, such as network reduction.

As mentioned before, all integrated energy carrier models must comply with the frame conditions of HyFlow, e.g., the chosen cellular modeling approach. However, network reduction is only necessary for electrical grids since they show significant deviations when modeled within this approach. Therefore, the presented novel network reduction method is only applicable for electrical grids.

3.2. Novel network reduction method for Cellular-Based network models

The novel network reduction method presented in this work uses tailor-made compensation elements to enhance reactive power accuracy to match the behavior of the real grid and overcome the disadvantages of numerical reduction methods. However, contrary to the numerical methods presented, these compensation elements do not change the entries within the nodal admittance matrix but rather represent ancillary nodal power added to the residual load at each cell node. This
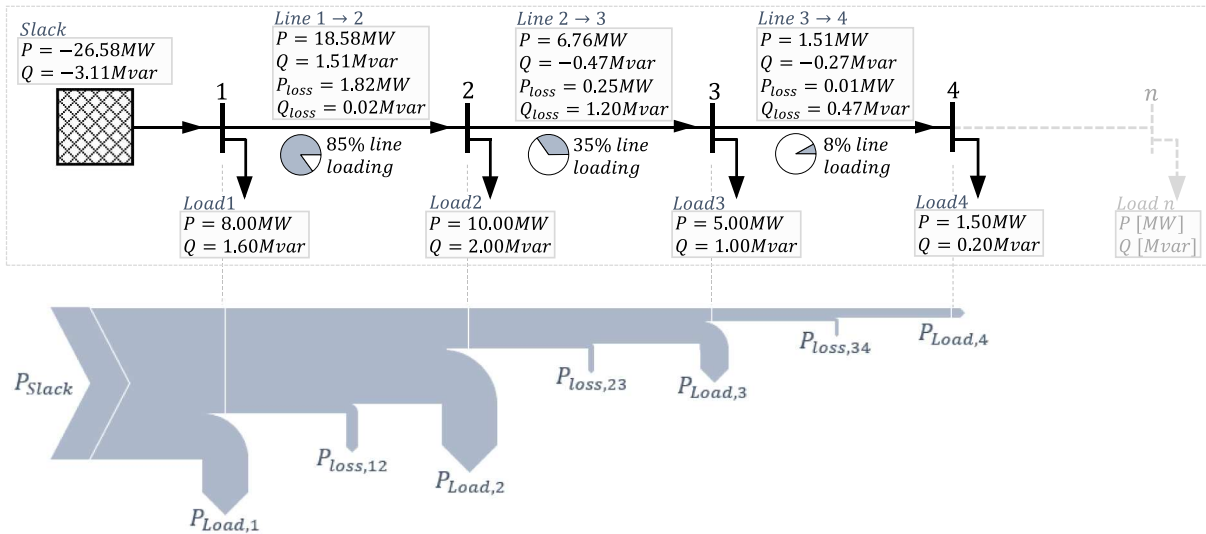
Fig. 7. Exemplary power flow diagram for active power flow over a feeder.
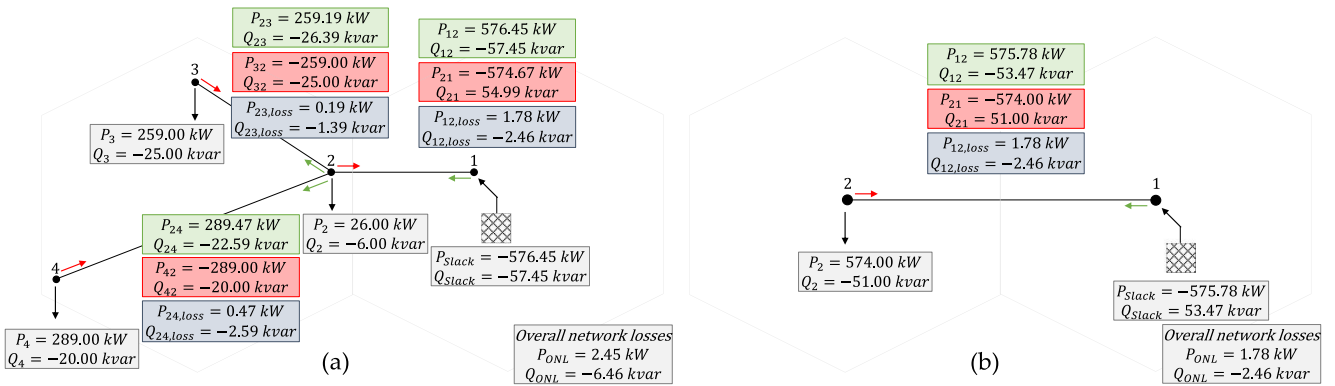
Fig. 8. Comparison of load flows (4) of the original grid and (b)after network aggregation within the cellular approach for static calculation: (a) original grid; (b) reduced network model without compensation.

additional nodal power calculation is based on a detailed analysis of the information losses (cf. Fig. 5) during the cellular aggregation process to determine which electrical parameters are modified. During the aggregation process, grid elements such as network nodes and electrical lines are modified or disappear. Therefore, the loss of information originates from these elements. Original network nodes are aggregated into the fictitious cell node. As a result, their nodal parameters (power injections and consumptions) are retained. Only information of the eliminated lines within the cells cannot be preserved. Thus, the deviation between the original grid and the reduced network model results from this elimination.

Each electrical line within a network model can be fully described and mathematically modeled using the general π-equivalent circuit in Fig. 6. In this single line equivalent circuit diagram, the physical effects occurring during energy transmission are accounted for through concentrated line parameters divided by the individual line length (specific line parameters). They also define active and reactive line losses of each electrical line. For low-voltage electrical lines (overhead lines and cables) which are, usually dominated by inductance L', the line capacitance C' is negligible. [35,36]

In general, the load flow over an electrical line, as shown in Fig. 6, consists of three shares. These shares are graphically depicted in Fig. 7, showing the power flow diagram for active power, which is equal to the reactive power diagram in principle.

The first share depends on the load at the consecutively connected

network nodes. Therefore, the active power flow over Line 1 → 2 includes the power demand at the network nodes 2, 3, and 4 ($P_{Load,2}$, $P_{Load,3}$, $P_{Load,4}$). The second share consists of the line losses within the considered electrical line ($P_{loss,12}$). Thus, at the beginning of Line 1 → 2, the active power flow includes the active power losses ($P_{loss,12}$) that occur during energy transmission over the corresponding line to enable the correct supply to the consumer at the end of that electrical line. The third share describes the electrical line losses of all the consecutively connected lines. Therefore, the active power flow over Line 1 → 2 also includes the active power losses of Line 2 → 3 ($P_{loss,23}$) and Line 3 → 4 ($P_{loss,34}$).

During the aggregation into cells, nodal loads (first share) and line losses of electrical lines that connect two cells (second share) can be retained since they do not depend on the eliminated electrical lines. The third share is lost in the aggregation process and causes load flows within the compensation lines (cf. Fig. 5) as well as Slack-node power and overall network losses to deviate from the original grid unless they are compensated for (Fig. 8).

The missing active and reactive power flow over Line 1 → 2 from Fig. 8 (b) corresponds with the sum of the line losses of Line 2 → 3 and Line 2 → 4 from Fig. 8 (a). As mentioned before, the main concern is reactive power accuracy since reactive power losses are usually much higher than active power losses and, therefore, lead to more significant deviations in load flows. This increase in modeling accuracy of reactive power quantities within the cell models is crucial for adequately
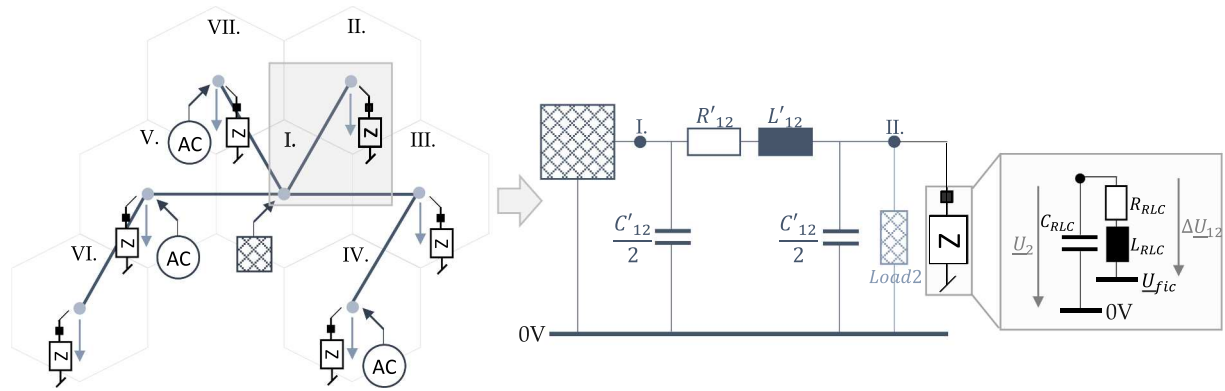
Fig. 9. Application of the compensation module and its structural equivalent circuit for one cell.
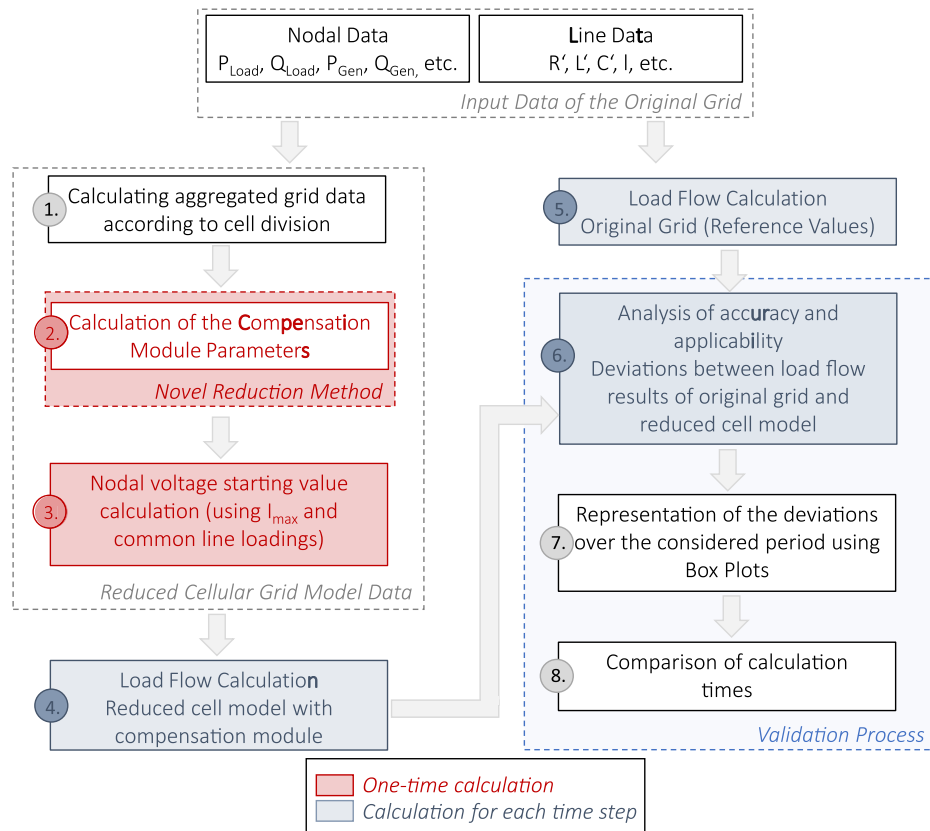

Fig. 10. Calculation scheme in MATLAB© to determine the deviations between the original grid and the reduced network model.

assessing electrical grids regarding voltage stability and line loading capacities.

Therefore, to minimize the deviation between the original (Fig. 8 a) and the reduced grid (Fig. 8 b), the line losses of the eliminated lines within the cells must be replicated in the aggregated cell model. Additionally, since line losses depend on the corresponding load flows and, therefore, the operating point, this load dependency must be recreated to be used for time-series calculations. Since load flow calculations, e.g., with the Newton-Raphson-method, use iterations that are terminated as soon as the deviation between known and calculated nodal power falls below a specific error limit, compensation can only be achieved if corresponding ancillary nodal powers are calculated for each cell and added to the residual loads of the corresponding cell node. Within the reduced network model, these ancillary nodal powers are represented by compensation elements that are attached to the fictitious cell nodes. These compensation elements replicate load-dependent active and

reactive line losses of the eliminated lines within each cell. Therefore, the parameterization of the compensation element is based on the sum of the electrical line parameters (cf. R_{RLC}, L_{RLC}, and C_{RLC} parameters in Fig. 9) of all eliminated lines within one cell. These line parameters are independent of the loads and, therefore, adapt to changing operating states. The initial concept of the compensation element published in Vopava et al. (2020) [33] was a series circuit consisting of a resistance R_{RLC}, an inductance L_{RLC}, and a capacitance C_{RLC} with a ground connection which can be seen as a variable complex resistance [33]. However, since also with this initial concept, deviations between original grid and cell model were too significant, it had to be further developed, which is now included in the presented novel method: Since the resistance R and the inductance L of an electrical line represent series elements, not shunt elements, the voltage drop and the corresponding current at the R_{RLC} and L_{RLC} would become very large due to the ground connection, unless the high-resistance capacitance C_{RLC} limits the

current. As a result, this element would not be applicable for low-voltage grids since the electrical lines at this voltage level have negligible line capacitances C. Therefore, in this novel approach, this series connection of the compensation element (compensation module) is divided so that the C_{RLC} element still has a ground connection, corresponding to the π-equivalent circuit in Fig. 6, while R_{RLC} and L_{RLC} are connected to a fictitious potential $\underline{U}_{fic}$. This leads to a voltage drop at the R_{RLC} and L_{RLC} corresponding to the voltage drop over an electrical line at the respective voltage level. The fictitious potential $\underline{U}_{fic}$ is different for each cell depending on the compensation line connecting two cells and the residual load of the cell. Using the sample network from Fig. 5, the application of the compensation module and its structural equivalent circuit and its parameters are shown in Fig. 9.

The following Equations (3) to (5) provide the calculation for each parameter of the module, where i represents the control variable for the eliminated lines within one cell, n represents the total number of eliminated lines within one cell, and z designates the cell.

$$R_{RLC,z} = \sum_{i=1}^{n} R'_i \cdot l_i \tag{3}$$

$$L_{RLC,z} = \sum_{i=1}^{n} \frac{X'_{L,i} \cdot l_i}{2 \cdot \pi \cdot f} \tag{4}$$

$$C_{RLC,z} = \sum_{i=1}^{n} C'_i \cdot l_i \tag{5}$$

One advantage of this novel method is that the compensation module requires only a small data basis, which does not depend on a previously completed load flow calculation to determine the electrical line losses of each eliminated line for each operating state. Instead, only the network parameters defined during grid planning and design are used. Equation (6) shows the calculation of the compensation module apparent power (ancillary nodal power), exemplary according to Fig. 9. The voltages used in the calculation of Equation (6) represent the results of the first voltage approximation (iteration) during a load flow calculation. This, therefore, requires no additional effort, as it is built-in within the ordinary load flow calculation (cf. step 4 Fig. 10). However, since the compensation module's apparent power has not been calculated in this first approximation step, a start value problem occurs. As a result, the nodal voltages are incorrectly approximated during this first iteration and, thus, the apparent power of the compensation module is under- or overestimated. For this purpose, an intermediate step (cf. step 3 Fig. 10) was integrated in the MATLAB© calculation scheme (cf. Fig. 10) before the load flow calculation. This step includes the solution of the start value problem and enables a more accurate approximation of this first nodal voltage iteration. This step is discussed more in detail in the description of the MATLAB© calculation scheme.

$$S_{-RLC} = \frac{\Delta U_{-12} \cdot \Delta U_{-12}^*}{(R_{RLC} + j \cdot X_{L,RLC})^*} + \frac{\Delta U_{-2} \cdot \Delta U_{-2}^*}{(j \cdot X_{C,RLC})^*} \tag{6}$$

The power imported or exported at the Slack-node is also adjusted by implementing the compensation modules since they introduce additional nodal power in the network model, which is balanced at the Slack-node. The total network losses in the reduced model ($P_{Losses,red}$, $Q_{Losses,red}$) have to be recalculated after aggregation. The losses of the lines present in the cell model (P_{Losses}, Q_{Losses}) are determined within the load flow calculation and the power of the compensation modules represent the losses of the eliminated lines due to its load dependency. However, since the modules are included into the load flow calculation as additional nodal power instead of elements that generate losses within the grid (e. g., electrical lines) they have to be added to the line losses of the present lines within the cell model (P_{Losses}, Q_{Losses}). This allocation is shown in Equations (7) and (8).

$$P_{Losses,red,t} = P_{Losses,t} + \sum_{k=1}^{z} P_{RLC,k,t} = P_{Losses,t} + \sum_{k=1}^{z} Re\left(S_{-RLC,k,t}\right) \tag{7}$$

$$Q_{Losses,red,t} = Q_{Losses,t} + \sum_{k=1}^{z} Q_{RLC,k,t} = Q_{Losses,t} + \sum_{k=1}^{z} Im\left(S_{-RLC,k,t}\right) \tag{8}$$

This compensation enables network reduction, which achieves the maximum possible accuracy for static and time-series-based analyses for each operating point or point in time.

Fig. 10 shows the calculation and validation scheme used in the paper conducted in MATLAB©. To start the calculation process, grid data of the original grid must be available. This data includes nodal data, such as active and reactive power of load and generation units (P_{Load}, Q_{Load}, P_{Gen}, Q_{Gen}) as well as node type and node number. It also includes line data, such as specific ohmic resistances R' of each line, specific inductances L', specific capacitances C', line lengths l, and the numbers of the nodes connected by the lines. This grid data is then, in the first step, converted into the aggregated data for the cell model according to the chosen cell division.

Step 2 then uses the aggregated data to parameterize the compensation module of the cellular-based network model. This step is conducted accordingly to Fig. 9, as well as Equations (3) to (5).

The next step represents the solution of the start value problem, which conducts an adjustment of the starting value of the nodal voltages (step 3). This step is necessary since calculating the apparent power of the compensation module requires a first approximation of the nodal voltages within the reduced cell model to determine the fictitious potential. Since the compensation module uses this fictitious potential to properly account for the serial line elements (R and L), this voltage potential corresponds with the voltage drop over an electrical line of the according voltage level. Thus, with a better approximation of the nodal voltages and, therefore, the determination of the fictitious potential, a more accurate compensation of the module can be achieved. This can be accomplished if nodal voltages are adjusted before the first nodal voltage approximation within the Newton-Raphson-iteration. Thus, this voltage adjustment (step 3) uses an estimation of common line loadings at the respective voltage level and maximum electrical line currents I_{max} for the corresponding electrical line type of the compensation line. Then, the compensation module is calculated accordingly to the approach shown in Fig. 9 and Equation (6) to approximate the losses within one cell. Without voltage adjustment, the miscalculation of the compensation modules occurs due to the distribution of loads within each cell and can, thus, be attributed to the load dependency of line losses. For calculating the apparent power of the compensation module (Equation (6)), each electrical line within one cell is assigned the same voltage drop or voltage increase, that of the compensation line within the cell model. If, however, smaller loads are connected at the end of a feeder, the voltage drop over that electrical line is much smaller than the voltage drop over the compensation line connecting two cells, e.g., at the beginning of a feeder. This would lead to an overestimation of the compensation module power. This is especially important at higher voltage levels due to higher absolute voltage drops or voltage increases based on higher loads and generation powers. After this adjustment (step 3) and the approximation of the nodal voltages (as part of step 4) within the cellular network model, the compensation module power calculation (also part of step 4) can be conducted according to Equation (6).

In step 4, a load flow calculation using the Newton-Raphson method of the cellular-based model can be performed. In this step, the load flow data of the reduced and compensated cellular network model can be determined using the compensation module's active and reactive power demand. The load flow data includes nodal voltages, active and reactive load flows, active and reactive line losses, active ad reactive overall network losses, and active and reactive Slack-node power.

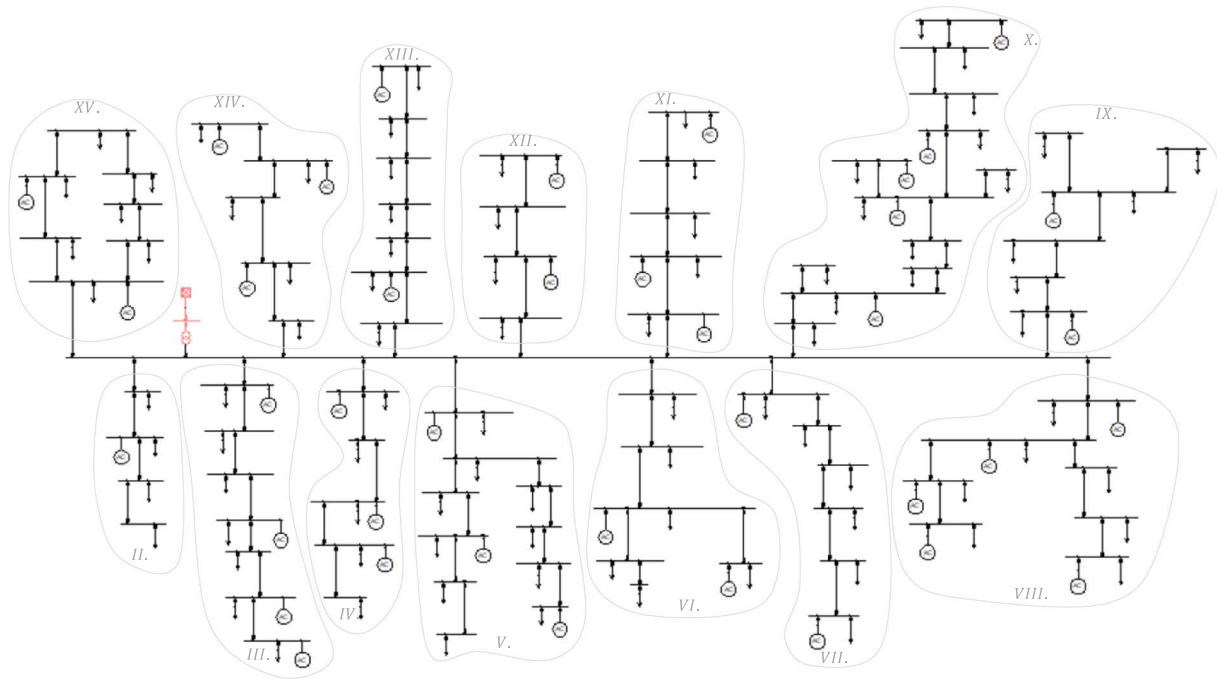To validate the load flow results obtained from the reduced and

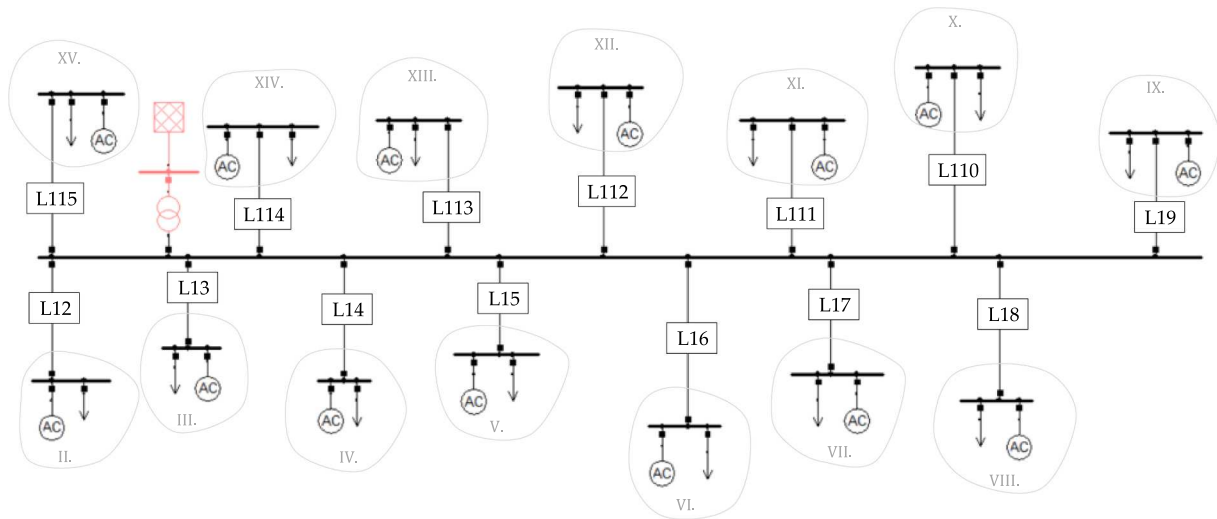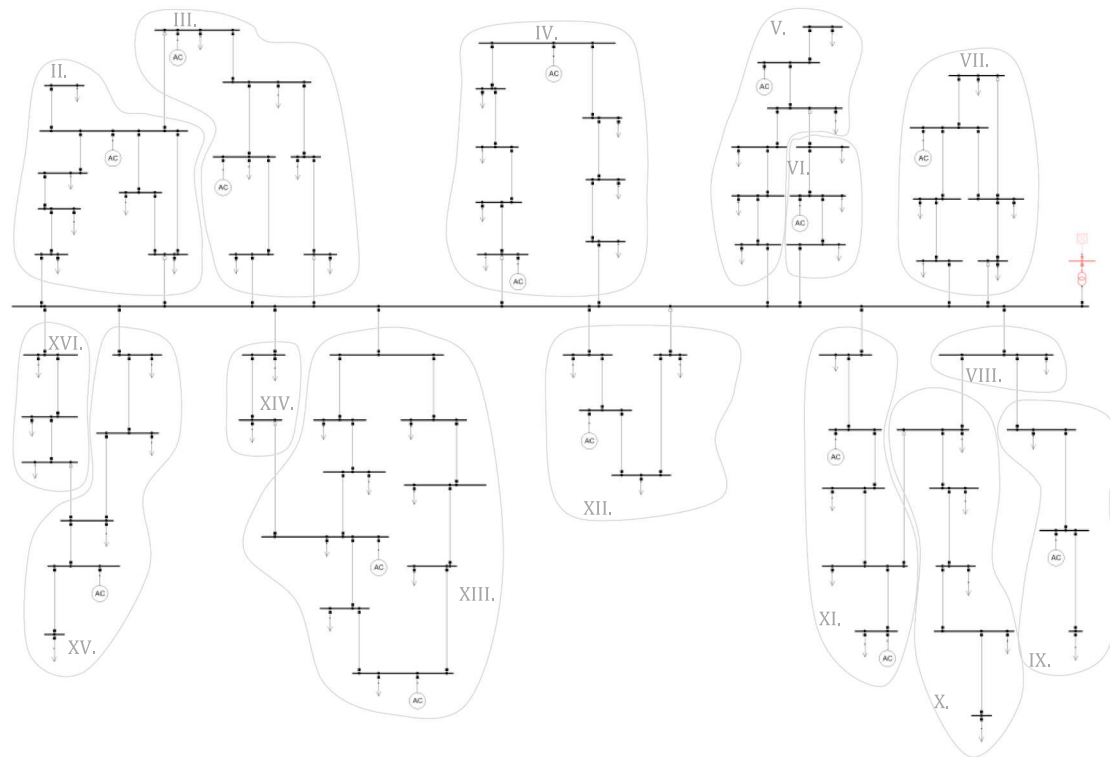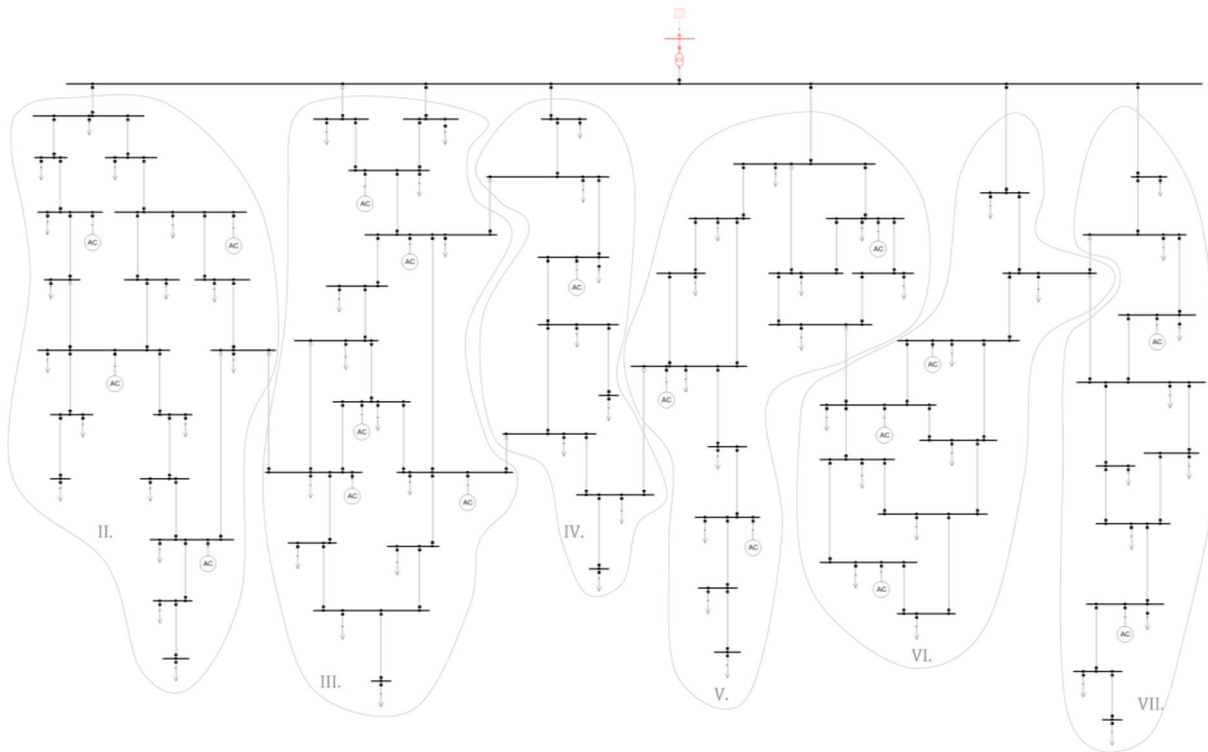**Fig. 11.** Low-voltage test grid and the corresponding cell division.

Fig. 12. Reduced network model of the low-voltage test grid.

compensated cell model, a load flow calculation of the original grid is conducted to create the reference values (step 5). The load flow results of the reduced cellular-based model are then compared to these reference values, and the deviations are calculated (step 6). The relative deviations, according to Equation (11), are then displayed using box plots (step 7). Additionally, calculation time savings can be determined by using the reduced cellular model (step 8). Steps 5 to 8 are just included in the calculation scheme to facilitate the validation process and can, therefore, be discarded for other applications.

As can be seen in Fig. 10, when using this reduction method, the parameterization of the compensation module as well as the start value adjustment has to be done just once, then it can be used for different load and generation profiles over an arbitrary time frame as long as the cell division stays the same. If, however, cell division changes, the compensation module parameters must be recalculated for the different cell settings.

3.3. Test grids for validation of the novel network reduction method for Cellular-Based network models

To ensure the applicability regarding the accuracy of the developed grid reduction method, a validation using synthetically developed test grids at different voltage levels is conducted. The test grids are based on literature values. Therefore, they do not include consumer-specific data but still replicate real-life network behavior. These grids and their parameters are described in detail in [37]. The time frame for the load and generation profiles investigated in this work is 24 h temporally resolved in 15-minute time steps using data suitable for the grids. The test grids were developed in NEPLAN© and are depicted in the following figures (Figs. 11–18). Each test grid is described in the following regarding their cell division used for validating the proposed network reduction method. Cell division for all test grids is chosen according to geographical aspects and is specific for this application purpose.

Fig. 13. Medium-voltage test grid and the corresponding cell division.
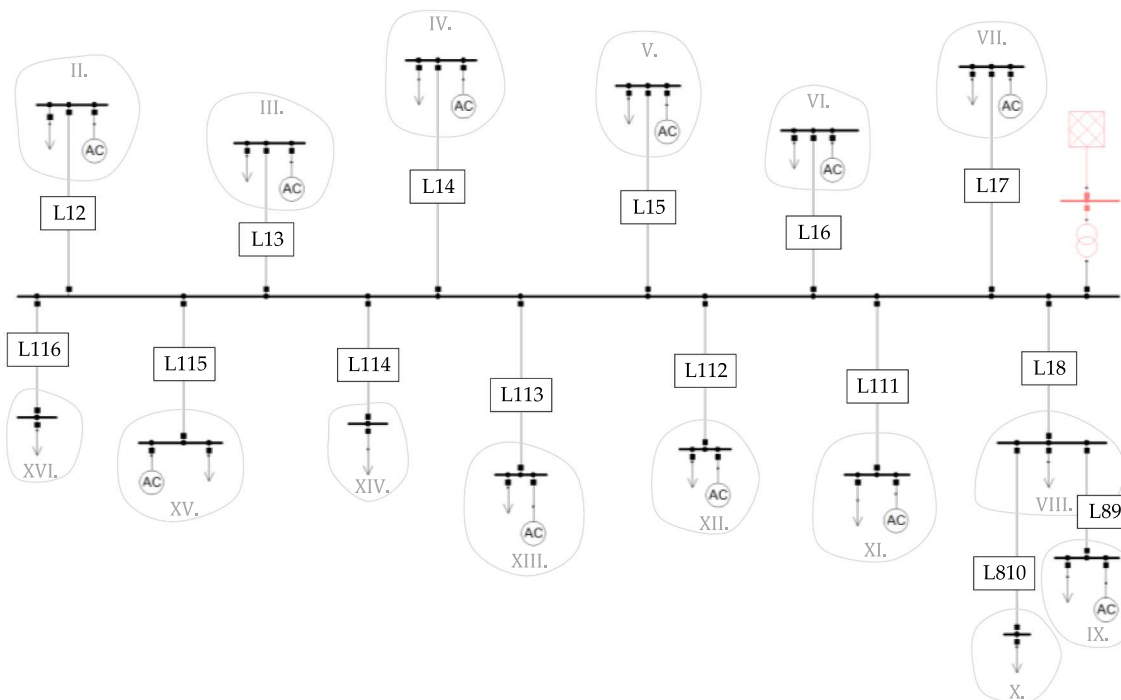
Fig. 14. Reduced network model of the medium-voltage test grid.

However, during the process of developing this method, guidelines for defining cell division to achieve maximum modeling accuracy have also been developed that will be presented in Subsection 4.2. Therefore, the chosen cell division also adheres to these division guidelines. Since these guidelines cannot be fulfilled at the maximum-voltage level due to the highly meshed structure, an attempt was made to find the best possible division for this grid to approximates these guidelines as closely as possible. To describe by which percentage the original grid is reduced in the cellular network model, a reduction factor is introduced (Equation (9)). The reduction factors calculate the percentage of the reduced network nodes of the original grid and, therefore, also describe the decreased complexity of the reduced cell model compared to the original grid.

Fig. 15. High-voltage test grid and the corresponding cell division.
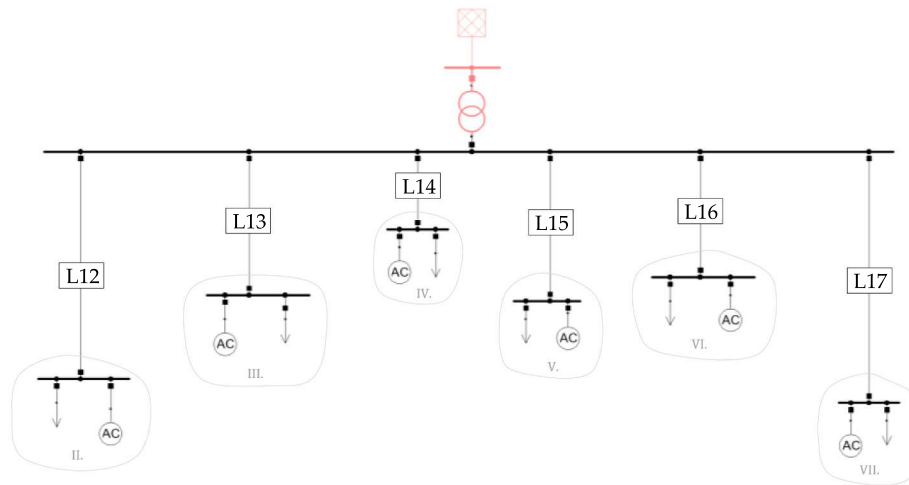
Fig. 16. Reduced network model of the high-voltage test grid.

$$reduction factor = \left(1 - \frac{number of fictitious cell nodes in reduced cell model}{number of network nodes in original network}\right) \cdot 100$$

$$(9)$$

3.3.1. Low-voltage level (0.4 kV)

The low-voltage test grid comprises 92 network nodes with 14 feeders [37]. Fig. 11 shows the low-voltage test grid topology and the corresponding cell division for the network reduction process. Each feeder is represented by one cell. Therefore, the grid is divided into 15 cells since the first cell is defined as the Slack-node, including the transformer, which is not separately marked in the figure.

Fig. 12 shows the reduced low-voltage grid, which only consists of 15 network nodes. Therefore, the grids number of network nodes is reduced by 83.7 % compared to the original grid. Due to the aggregation process,

only 14 electrical compensation lines remain, and each cell has a consumer unit as well as a generation unit.

3.3.2. Medium-voltage level (20 kV)

The medium-voltage test grid comprises 74 network nodes with 18 feeders [37], which is shown, including the corresponding cell division for network reduction in Fig. 13. Due to open connections within the test grid, which are included in the ring structures of the grid, a division into 16 separate cells is achieved, where the first cell is defined as the Slack-node including the transformer, which is not separately depicted.

Fig. 14 shows the reduced medium-voltage grid, which only consists of 16 network nodes. Therefore, the grids number of network nodes is reduced by 78.4 % compared to the original grid. Due to the aggregation process, only 15 electrical compensation lines remain.
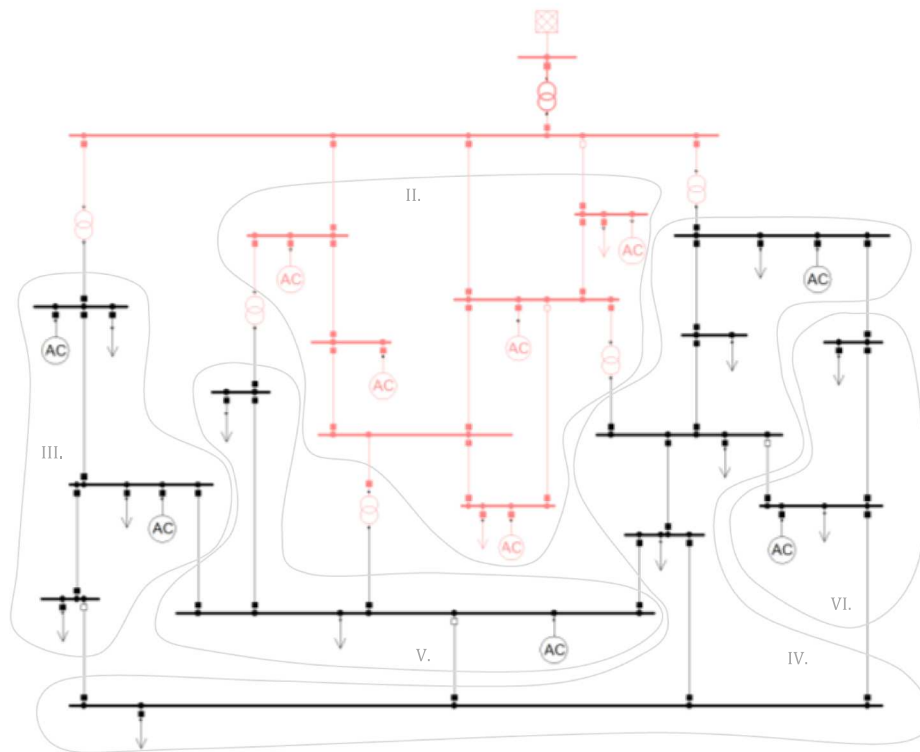
Fig. 17. Maximum-voltage test grid (including the 380 kV- and the 220 kV-voltage level) and the corresponding cell division.
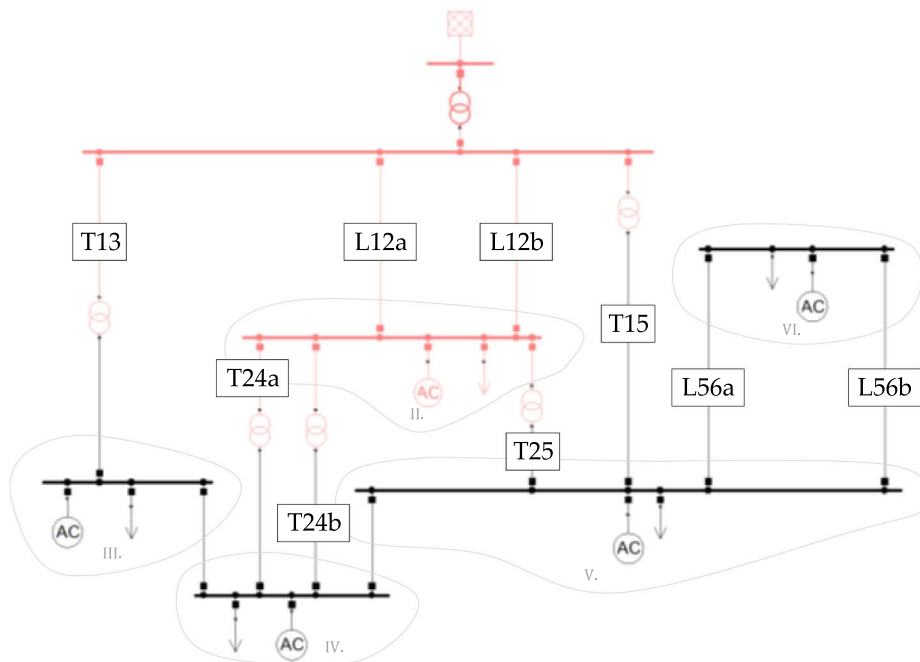
Fig. 18. Reduced network model of the maximum-voltage test grid (including the 380 kV- and 220 kV-voltage levels).

3.3.3. High-voltage level (110 kV)

The high-voltage test grid consists of 70 network nodes with six feeders connected via switched-off electrical lines forming an open ring structure [37]. Fig. 15 shows the high-voltage test grid and the corresponding cell division for network reduction. Since there are six feeders within the grid, it is possible to represent each feeder by one cell. Therefore, the grid is divided into seven cells since the first cell is defined as the Slack-node, including the transformer, which is not separately shown in the figure below.

Fig. 16 shows the reduced high-voltage grid, which only consists of 7 network nodes. Therefore, the grid's number of network nodes is reduced by 90.0 % compared to the original grid. Due to the aggregation process, only six electrical compensation lines remain.
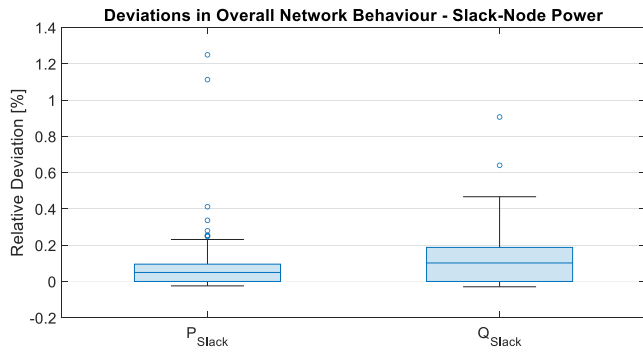
Fig. 19. Deviation of Slack-node power for the low-voltage test grid.
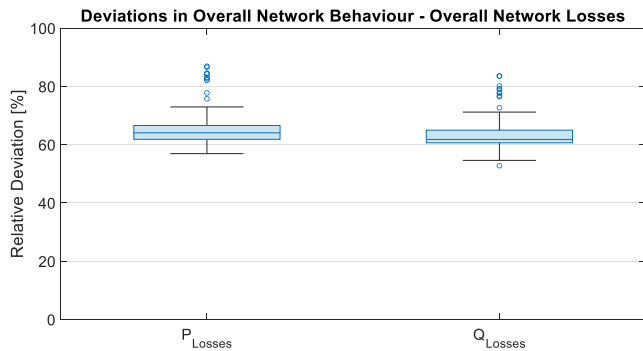
Fig. 20. Deviation of overall network losses for the low-voltage test grid.

3.3.4. Maximum-voltage level (380 kV/ 220 kV)

The maximum-voltage test grid consists of 19 network nodes, of which seven belong to the 380 kV voltage level, and the other 12 belong to the 220 kV voltage level [37]. Fig. 17 shows the maximum-voltage test grid and the corresponding cell division for network reduction. Since the network structure at this voltage level is a complex meshed grid, selecting a suitable cell division is challenging. For all voltage levels previously analyzed, it was possible to divide the cells in such a way that individual feeders are represented separately by one cell, ensuring that the reduced cellular network model is created in a radial structure. Due to the high degree of meshing, this division is not possible for the maximum-voltage level. Instead, the cell division process at this voltage level leads to a meshed structure in the reduced network model as well. Thus, the grid is divided into six cells. The 380 kV-voltage level is represented by two cells, while the 220 kV-voltage level is represented by four cells. The 380 kV-level cells include the first cell, which is defined as the Slack-node, including the transformer, which is not separately shown in the figure below.

Fig. 18 shows the reduced maximum-voltage grid, which has been reduced to six network nodes. Therefore, the grid's number of network nodes is reduced by 68.4 % compared to the original grid. Due to the cellular-based aggregation process, six electrical lines remain, and all five transformer substations connecting the 380 kV-voltage level with the 220 kV-voltage level.

4. Analysis of results

In this section, the presented test grids are used to validate the modeling accuracy for the presented novel network reduction method within the cellular approach. The modeling accuracy at each voltage level can be analyzed by calculating the deviation between the original grid and the reduced network model. This analysis shows the obtained deviations and thus, for which voltage levels this novel method presents as a practical application (low deviations) and for which the method does not provide benefits (high deviations).

4.1. Results

Deviations are calculated for active and reactive power flows (P_{line}, Q_{line}) as well as active and reactive power losses ($P_{loss,line}$, $Q_{loss,line}$) within the compensation lines and active and reactive Slack-node power (P_{Slack}, Q_{Slack}) as well as active and reactive overall network losses (P_{Losses}, Q_{Losses}). Equations (10) and (11) show an exemplary calculation for absolute and relative deviation of active power flows (ΔP_{abs}, ΔP_{rel}) for one compensation line n and a single time step t. All other deviations are calculated accordingly, as depicted in Equations (10) and (11).

$$\Delta P_{abs,n}(t) = P_{original,n}(t) - P_{reduced,n}(t) \tag{10}$$

$$\Delta P_{rel,n}(t) = \frac{P_{original,n}(t) - P_{reduced,n}(t)}{P_{original,n}(t)} \tag{11}$$

If the examined electrical parameter of the reduced cell model is higher than the corresponding value in the original grid, this results in a negative deviation. In this case, the cell model overestimates the respective parameter for that time step and vice versa. As can be seen in Equations (10) and (11), the deviations are calculated for each time step. To simplify the illustrations and ensure better comparability of the resulting deviations, box plots are used in the following analysis. These plots enable a condensed representation of the deviations occurring over the entire considered period. Thus, they show the 25 %- and 75 %-quartiles of the deviations over the period within the box edges and the 5 %- and 95 %-quantiles within the whiskers of the box plot. Additionally, the median value can be found in the plot depicted as the blue line within each box. The plotted circles outside the quantiles represent outliers. Outliers of the deviations represent time steps within the considered period when the load flow over the corresponding compensation line is very low (e.g., inversion of load flow due to higher generation). In these cases, the absolute deviation is about the same as for other time steps, but the relative deviation becomes high due to the small reference value of the original grid.

To ensure better comparability between the grids, only relative deviations are considered for creating the box plots. In the comprehensive work, all electrical parameters mentioned above (P_{line}, Q_{line}, $P_{loss,line}$, $Q_{loss,line}$, P_{Slack}, Q_{Slack}, P_{Losses}, Q_{Losses}) are considered. However, in this chapter, only deviations of Slack-node power and overall network losses are analyzed.

For a better explanation of the results, arithmetic mean values (AMV) of the deviations over the examined period are also presented in this paper. This ensures better comparability and increased understanding of the obtained deviations. However, for application purposes such as MES, the deviations from each time step have to be considered.

The deviation of overall network losses represents the sum of the deviations of individual line losses, including the line losses of the eliminated lines within the cells, which are taken into account via the calculation of the compensation modules (Equations (7) and (8)). The deviation of Slack-node power includes the deviation of electrical power flows within the individual compensation lines and overall network losses. Therefore, the difference between the deviations in Slack-node power and the deviations between overall network losses represents the sum of deviations of electrical load flows. The analysis of the deviations of the electrical parameters in individual compensation lines can be found in Appendix A. However, overall considerations of the trends of the deviations across all examined voltage levels are made in Section 4.2.

4.1.1. Low-voltage level (0.4 kV)

In Fig. 19 the box plot shows the relative deviation between the original grid and reduced cell model for active and reactive Slack-node power over the considered period at the low-voltage level. Median values of active and reactive Slack-node power depicted in Fig. 19 are 0.05 % for active Slack-node power P_{Slack} and 0.10 % for reactive Slack-node power Q_{Slack}. Arithmetic mean values of relative deviations for
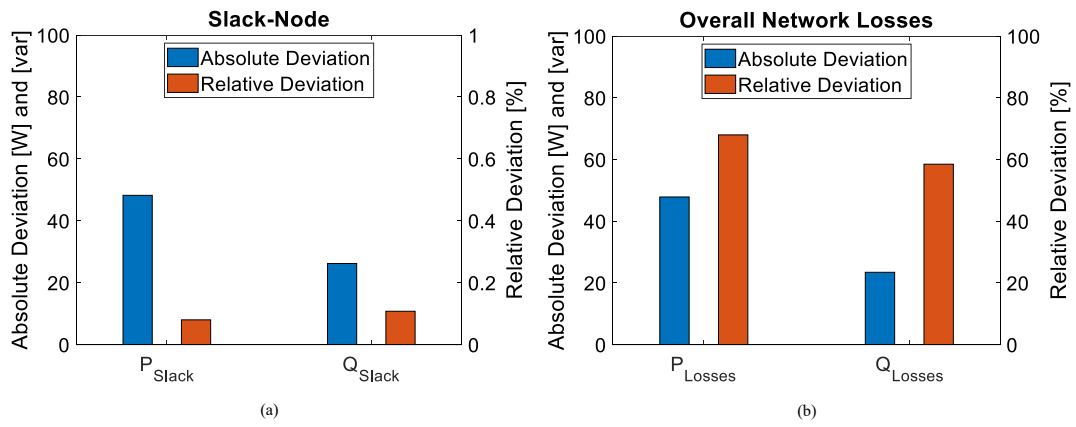
Fig. 21. Arithmetic mean values over the considered period of the deviations of (a) Slack-node power and (b) overall network losses for the low-voltage test grid.
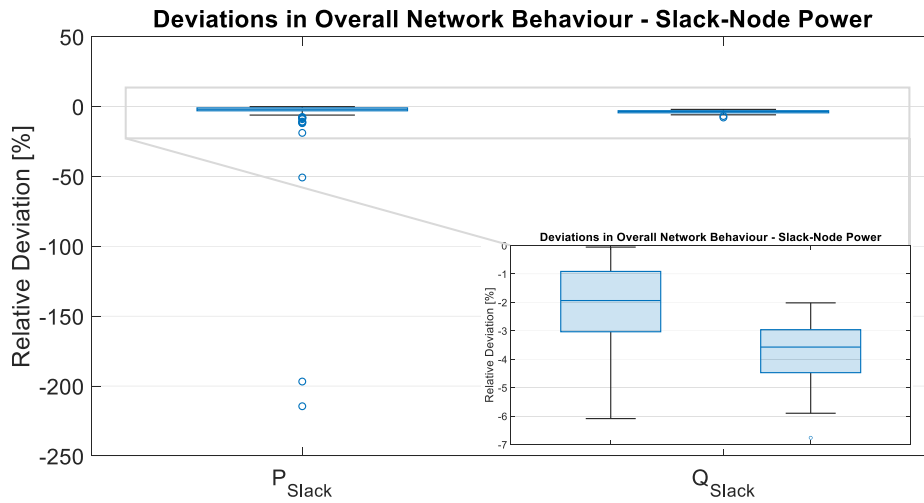

Fig. 22. Deviation of Slack-node power for the medium-voltage test grid.
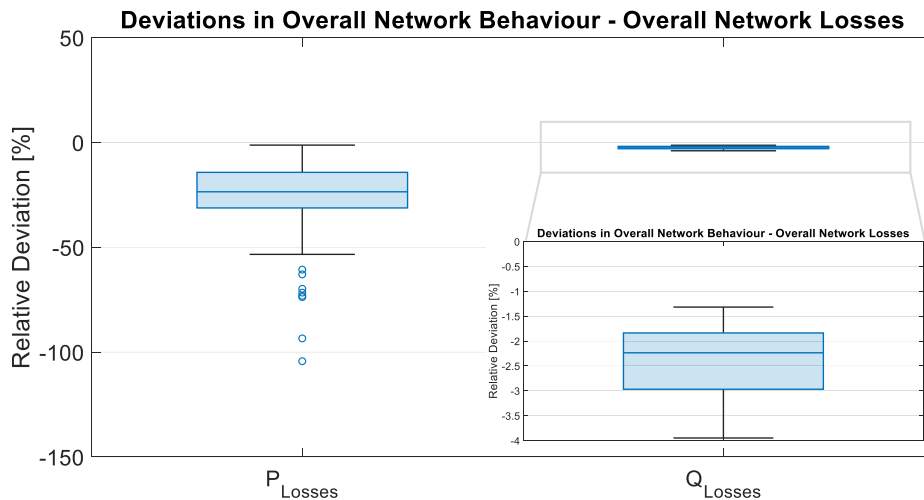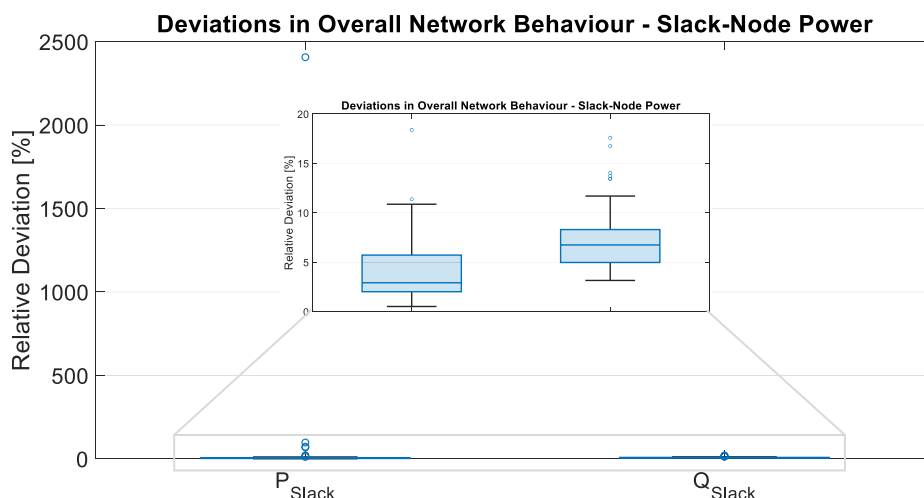

Fig. 23. Deviation of overall network losses for the medium-voltage test grid.

Slack-node power show a minimal deviation of 0.08 % for active power P_{Slack} and 0.11 % for reactive power Q_{Slack}. These relative arithmetic mean value deviations correspond with an absolute of 48.20 W of active power deviation and 26.18 var of reactive power deviation. Since median values and arithmetic mean values are close to each other, the distribution of the deviations over the considered period at the low-voltage level corresponds with a normal distribution. Therefore, there are very few outliers within the considered time frame.

In Fig. 20, the box plot depicts the relative deviation of active and reactive overall network losses (P_{Losses}, Q_{Losses}) over the considered

Fig. 24. Deviation of Slack-node power for the high-voltage test grid.
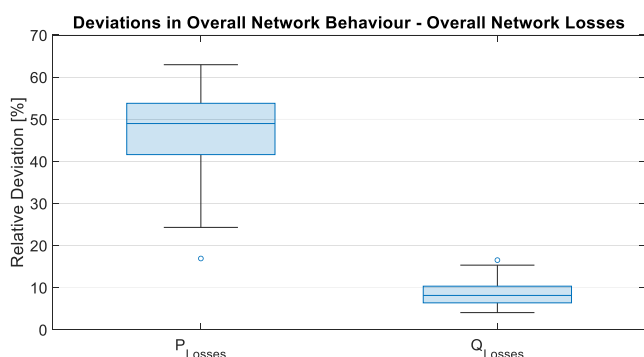
Fig. 25. Deviation of overall network losses for the high-voltage test grid.

period. The relative deviations of these electrical parameters in Fig. 20 seem high compared to those of the Slack-node powers, while absolute arithmetic mean value deviations of overall network losses (47.83 W and 23.42 var) are actually smaller than those of Slack-node powers (48.20 W and 26.18 var). This results from the fact that the reference values (original grid values) for the overall network losses are small (arithmetic mean values of 81.00 W active and 46.00 var reactive overall network losses) at the low-voltage level.

This can be seen in Fig. 21, where the arithmetic mean values over the examined period for the absolute and relative deviations of Slack-node power and overall network losses are presented.

This illustrates that absolute deviations for Slack-node powers and overall network losses are similar while their relative deviations vary due to their different reference values. Therefore, although relative deviations in overall network losses appear high, they are minimal. The arithmetic mean values are 67.95 % for active and 58.44 % for reactive overall network losses, respectively, while the median values are 71.87 % for active and 60.96 % for reactive overall network losses. Again, median values and arithmetic mean values are similar. Therefore, only a few outliers occur over the examined period.

4.1.2. Medium-voltage level (20 kV)
Applying the presented novel network reduction method for cellular-based network models on the previously described medium-voltage test grid (Fig. 14) produces the following results. Fig. 22 shows the deviations for active and reactive Slack-node power over the considered period. Since the active Slack-node power deviations show some more significant outliers, better visibility of the box plots can be achieved by zooming closer into the plot, as has been done in Fig. 22.

Fig. 22 shows that the median values of the relative deviations are −1.94 % for active Slack-node power P_{Slack} and −3.57 % for reactive Slack-node power Q_{Slack}, respectively. Corresponding arithmetic mean values are −7.48 % for active and −3.75 % for reactive Slack-node power. Since the median and arithmetic mean values are close to each other for relative reactive Slack-node power deviation, the distribution of these deviation values can be considered a normal distribution. The median and arithmetic mean values for relative active Slack-node power deviation are further apart, indicating a skew distribution with many outliers, which can also be seen in the box plot in Fig. 22. Arithmetic mean values for absolute deviations are −125.06 kW for active and −492.70 kvar for reactive Slack-node power. Fig. 23 shows relative deviations for overall network losses of the medium-voltage test grid.

Median values illustrated in Fig. 23 are –23.51 % for active overall network losses P_{Losses} and −2.24 % for reactive overall network losses Q_{Losses}, respectively. In comparison, the arithmetic mean values are −26.39 % for active and −2.38 % for reactive overall network losses. Since median and arithmetic mean values for the relative deviations of both active and reactive losses are close to each other, both follow a normal distribution. Therefore, it is indicated that the main deviation results from (active) power flows within individual electrical compensation lines. Corresponding absolute arithmetic mean value deviations for overall network losses are −125.08 kW for active power losses and −492.72 kvar for reactive power losses.

4.1.3. High-voltage level (110 kV)
Fig. 24 shows the modeling accuracy of Slack-node power for applying the presented network reduction method at the high-voltage test grid. Since there is one significant outlier for relative active Slack-node power deviation, better visibility can again be achieved using an additional zoomed-in plot.

The median value for the relative deviation of active Slack-node power is 2.92 %, while the median value for the relative deviation of reactive Slack-node power is 6.75 %. The arithmetic mean value for the relative active Slack-node power deviation shows a value of 31.59 % (1955.34 kW absolute deviation) and 7.15 % (3517.54 kvar) for relative reactive Slack-node power. This illustrates that while the median value for active Slack-node power shows only a small relative deviation from the original grid, the comparison to the corresponding arithmetic mean value shows that there are many outliers with high deviation values in the active Slack-node power distribution. This corresponds with a skew distribution of the relative active Slack-node power deviation distribution. Contrary to this, reactive Slack-node power median and arithmetic mean values are close to each other, suggesting a normally distributed profile of the relative reactive Slack-node power deviation. Hence,
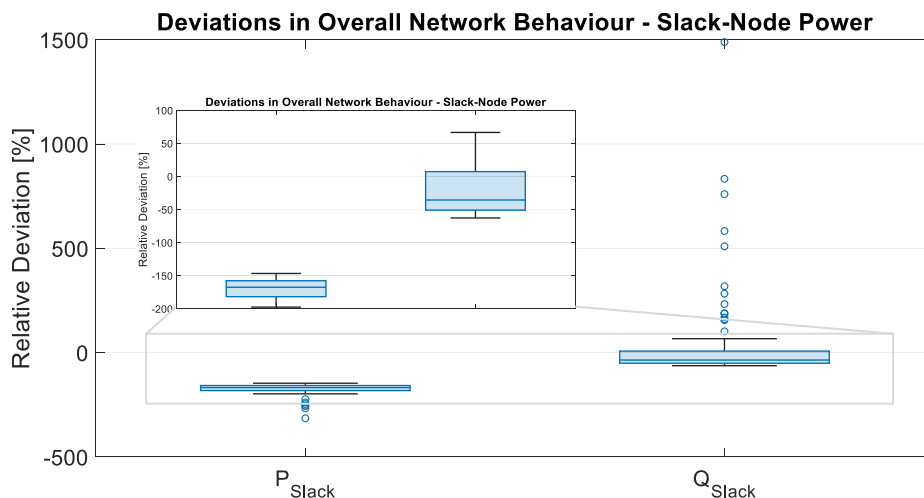
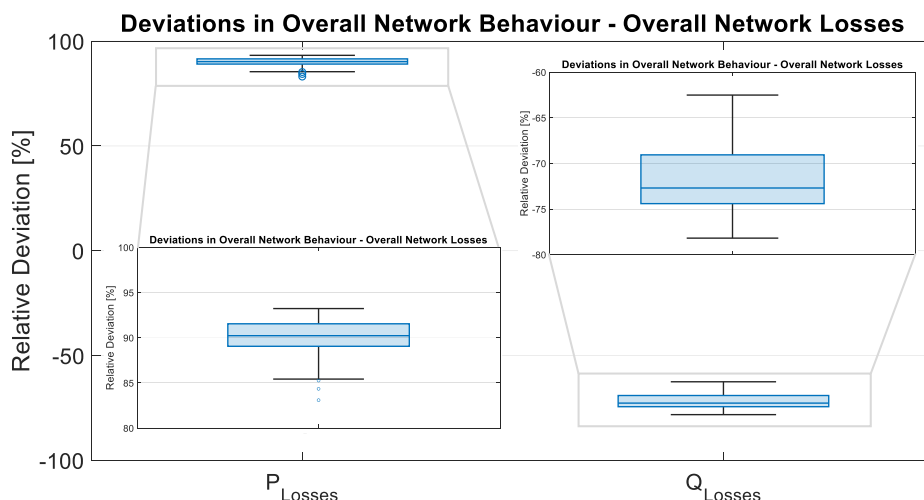**Fig. 26.** Deviation of Slack-node power for the maximum-voltage test grid.

Fig. 27. Deviation of overall network losses for the maximum-voltage test grid.

reactive Slack-node power shows very few outliers.

Fig. 25 illustrates relative overall network loss deviation over the considered period. As can be seen in this figure for both relative deviation profiles, there are very few outliers. This indicates a normally distributed profile and, therefore, median and arithmetic mean values close to each other. Relative active overall network loss deviation shows a median value of 48.97 % and an arithmetic mean value of 47.25 % (1955.08 kW absolute deviation) over the considered time frame. Relative reactive overall network loss deviation shows a median value of 8.13 % and an arithmetic mean value of 8.56 % (3517.28 kvar absolute deviation).

4.1.4. Maximum-voltage level (380 kV/ 220 kV)

For the maximum-voltage level test grid, the results of applying the presented network reduction method can be found in Fig. 26 and Fig. 27. Fig. 26 displays the relative Slack-node power deviation. For better visibility of the median values, a zoomed-in plot is added to the figure. Median values are −167.48 % for relative active Slack-node power deviation and −35.55 % for relative reactive Slack-node power deviation. However, arithmetic mean values are − 174.31 % for relative active Slack-node power deviation and 36.41 % for relative reactive Slack-node power deviation. The corresponding absolute arithmetic mean value deviations for active and reactive Slack-node power are 2051.55 MW and 45.96 Mvar. Comparing the median and the arithmetic mean values

concludes that relative active Slack-node power deviations are normally distributed with only a few outliers, while the relative reactive Slack-node power deviation distribution is skew with many more significant outliers. Deviations at this voltage level are higher compared to the other voltage levels investigated in this work. The reason for this will be discussed in the next chapter.

Fig. 27 displays the relative overall network loss deviation. A zoomed-in plot is added to the figure for better visibility of the boxes and the median values.

The median value of relative active overall network losses is 90.23 %, while the arithmetic mean value is 89.94 % (14.64 MW absolute deviation). For the relative reactive overall network losses over the considered period, the median corresponds with a value of −72.70 %, and the arithmetic mean with a value of −72.00 % (131.17 Mvar absolute deviations). In both cases, median values and arithmetic mean values are close to each other, indicating a normally distributed profile of the relative overall network deviation profiles.

4.2. Discussion

4.2.1. Trends in modeling accuracy

In this section, the previously presented relative deviations obtained at each voltage level are analyzed, and general trends in modeling accuracy are derived to compare results across voltage levels. This shows
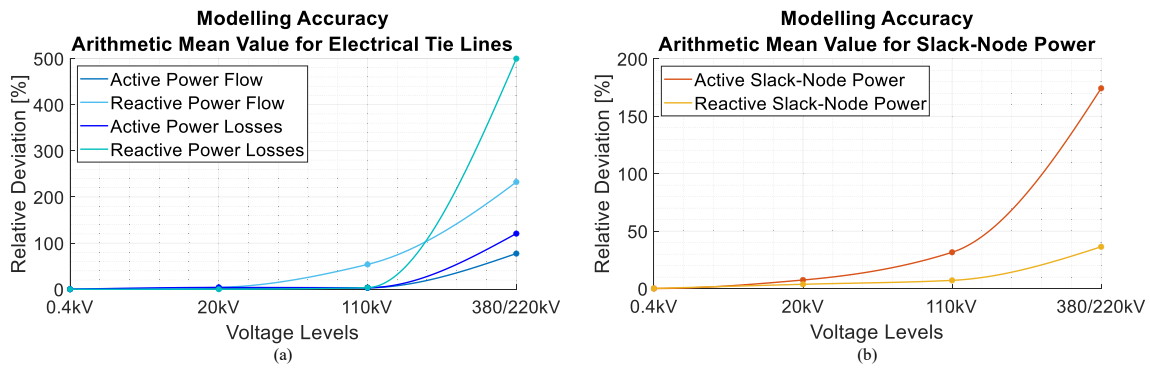
Fig. 28. Trends in relative deviations for electrical compensation lines (a) and Slack-node power (b) at each voltage level.

Table 1
Arithmetic mean values for each voltage level – electrical compensation lines.

Voltage level	Active Power Flow [%]	Reactive Power Flow [%]	Active Power Losses [%]	Reactive Power Losses [%]
0.4 kV	0.03	0.10	0.06	0.06
20 kV	1.54	4.08	3.96	0.12
110 kV	3.17	53.89	3.44	3.57
380/220 kV	77.45	232.46	120.73	499.79

Table 2
Arithmetic mean values for each voltage level – Slack-node power.

Voltage level	Active Slack-power [%]	Reactive Slack-power [%]
0.4 kV	0.09	0.12
20 kV	7.48	3.75
110 kV	31.59	7.15
380/220 kV	174.31	36.41

that the presented novel reduction method is better suited for certain voltage levels due to their specific characteristics.

These trends are depicted in Fig. 28. Fig. 28 (a) shows the arithmetic mean values of relative deviations of all compensation lines and transformer units within each of the test grids. Fig. 28 (b) shows the arithmetic mean values of relative deviations of the corresponding active and reactive Slack-node power. For calculating these values, e.g., the arithmetic mean values for relative deviation of active and reactive power flows over the considered period, and the corresponding line losses of each compensation line within each test grid are averaged (Equation (12)). These values depicted in Fig. 28 represent the arithmetic mean values for each electrical parameter separately over the entire period and grid (e.g., over all the compensation lines of one voltage level grid). In Equation (12), the parameter t represents a single time step within the considered period, and n represents the one electrical connection element between cells at one voltage level. T presents the total number of time steps and N the total number of electrical compensation lines.

$$(\Delta P_{rel})_{AMV} = \frac{\sum_{n=1}^{N}\left(\frac{\sum_{t=1}^{T}\Delta P_{rel,n}(t)}{T}\right)}{N} \tag{12}$$

These arithmetic mean values, according to Equation (12), are used in order to ensure the comparability of results and to derive trends for each voltage level. For other considerations regarding the application of this method, the results from the box plots over the entire considered period in Section 4.1 have to be taken into account. However, the trends in the obtained deviation for the presented novel method applied to the test grids can be taken from Fig. 28.

Table 1 shows the calculated arithmetic mean values depicted in Fig. 28 (a) for each test grid considered in this work regarding the compensation lines to better assess the trends.

For each considered parameter, the arithmetic mean value relative deviations increase from the low-voltage level to the maximum-voltage level. In general, deviations increase at higher voltage levels due to higher network losses that must be balanced. As shown in Fig. 28 and Table 1, the relative arithmetic mean value deviations increase substantially at the maximum-voltage level. This high increase results from the existing network topologies of each test grid which will be discussed more in detail in the next section. While it is possible to choose a cell division to create a radial structure in the reduced cell model at the low-, medium- and high-voltage level, it is not possible to do so at the maximum-voltage level due to its highly meshed structure. The reduced cell model, therefore, also has a meshed structure. Due to the mechanism of the compensation module, mutual influences of the compensation modules occur, increasing the deviations between the original grid and the reduced cell model.

The reason why reactive power flow deviations are higher at the 110 kV-voltage level compared to the low- and medium-voltage grid is due to larger cell sizes which have to be chosen to create a radial structure for the reduced network model at this voltage level. Cell size influences modeling accuracy, especially for reactive power flows since more electrical lines are eliminated within each cell. Therefore, more significant amounts of power have to be compensated. These higher deviations occur because information about the geographical load and generation distribution within the cells has a more significant impact at higher voltage levels. To account for this geographical distribution in the compensation module, the voltage adjustment step is conducted before the load flow calculation. However, despite the nodal voltage start value adjustment, this still leads to an incorrect calculation of the nodal voltages (step 3 in Fig. 10) and, therefore, a miscalculation of the compensation modules causing higher deviations at this voltage level. Since it is assumed in the calculation scheme of Fig. 10 that voltage drops over the eliminated lines within the cells are all the same, different magnitudes of loads and generations within the cells (and thus, varying voltage drops over the lines to be eliminated within the cell of the original grid) cause more significant deviation. Therefore, if the voltage drops over electrical lines within the cells are close to each other, which is mainly the case for low- and medium-voltage grids, modeling accuracy is higher.

At the medium-voltage level, deviations increase due to larger active and reactive losses compared to the low-voltage grid. However, the reduced model offers a good approximation of the original grid at this voltage level with deviations below 5 %.

The values in Table 2 for Slack-node power within the overall network at each voltage level (except for the low-voltage level) show that active power deviates more than reactive power. This is because starting from the medium-voltage level up, electrical line capacitance C' shows an increasing influence on reactive power and reactive losses
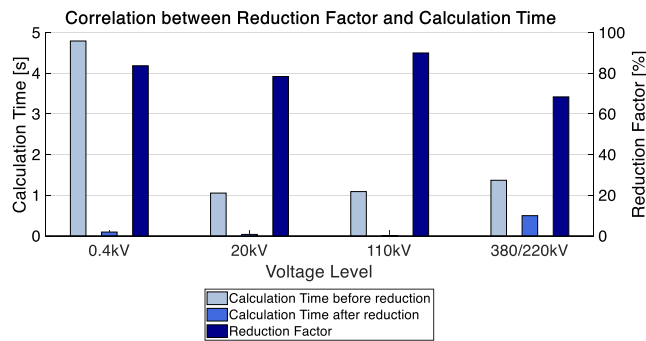
Fig. 29. Correlation between reduction factor and calculation times before and after network reduction.

within the grid. For the compensation module (Fig. 9), the influence of shunt elements (such as *C'*) can be simulated more accurately than serial elements (such as *R'* and *L'*), leading to a closer approximation for reactive power. This is also an effect of the load and generation distribution within the cells since they affect the calculation of the compensation module power. Thus, in the calculation scheme, voltage drops are assumed to be equal for each eliminated line causing deviation for the series elements' share of the compensation module (R_{RLC} and L_{RLC}), while nodal voltages can be approximated closely (shunt element share of the compensation module) due to the solution of the start value problem corresponding to Fig. 10. Since at the low-voltage level, there is no capacitive influence from electrical lines and line losses are minimal, both, active and reactive Slack-node power deviation, are in the same range.

4.2.2. Identified influencing parameters on modeling accuracy and improvement recommendations

Modeling accuracy can be enhanced using compensation methods specifically applicable to the application purpose. However, there are other influencing parameters on modeling accuracy that such methods cannot compensate. Therefore, this section addresses the influence of network parameters and provides guidelines for achieving maximal approximation between the original grid and the aggregated cellular-based network model.

Based on the discussion above, three influencing parameters are substantial for the modeling accuracy in the reduced cell network model:

1. The voltage level
2. The cell division (including cell size)
3. The geographical distribution of loads and generations within each cell

Modeling accuracy is influenced by the voltage level (cf. Fig. 28) since the generated absolute active and reactive power losses within the electrical lines during energy transmission are higher at higher voltage levels. Thus, the compensation module has to compensate for a larger amount of power. The compensation module is then no longer capable of fully compensating the power line losses despite the voltage adjustment step of the calculation scheme (cf. step 3 of Fig. 10), which becomes less accurate the higher the voltage level. However, this presents a numerical problem rather than an electrical one. Additionally, network topologies become more intertwined at higher voltage levels, which influences cell size and cell division of the original grid.

Modeling accuracy is significantly influenced by cell division. This parameter mainly refers to the topology of the reduced cell model, which is defined by the cell division process. Since this process is arbitrary and solely depends on the application purpose, it can be chosen according to the geographical and topological parameters of the original grid. If ring structures occur in the topology of the original grid, they

only influence the modeling accuracy if they are still present in the reduced network model. If ring structures of the original grid "disappear" within one cell, they do not influence modeling accuracy. Therefore, the network topology within one cell is not an influencing parameter. However, the network structure within the reduced network model is an influencing parameter and can either correspond with a radial structure, a ring structure, or a meshed structure. As network topologies within the reduced cell model become more intertwined and complex, deviations increase considerably (Fig. 28). For a radial network structure in the reduced cell model, it is possible to adapt single line load flows by implementing the corresponding compensation module at the fictitious cell node. This leads to smaller deviations between the original grid and the reduced cell model since no mutual influences of the compensation modules can occur due to the lack of connections between other fictitious cell nodes. This influencing factor has already been described in Jasmon et al. (1991) [38], where they identified the reduction to a single-line equivalent of a radial grid structure as the key factor for enhanced performance of the model.

Cell size refers to the number of network nodes assigned to one cell and, therefore, corresponds with the reduction factor between the original grid and the aggregated cellular-based network model, which can be calculated according to Equation (9). Fig. 29 shows these reduction factors, which are already provided in Section 3 in the description of the corresponding test grids with the calculation times for the entire time frame before and after reduction.

With a larger number of network nodes assigned to one cell, a larger number of electrical lines are eliminated during the aggregation process. Therefore, the compensation module has to balance a larger amount of power resulting from line losses over many different electrical lines. This compensation is more difficult since the effects of different load and generation distributions within the cells have a more significant influence. This leads to slightly increased deviations when cell sizes are larger. The cell size parameter is closely related to the last parameter, the geographical load and generation distribution.

Only cell division and, thus, cell size can be used to increase modeling accuracy within reduced cell models. Keeping cell sizes small usually decreases the advantages reduced network models offer regarding calculation times. However, too large cell sizes decrease modeling accuracy. Using appropriate cell division to create a radial structure after aggregation has the most significant influence on modeling accuracy. While reduced cell network models with radial structures can be modeled accurately, reduced cell models with ring structures show inadmissible deviations (cf. Fig. 28). Suitable cell division may also allow for assessing the grids regarding voltage stability and grid capacity without loss of information, despite aggregation of grid sections. Thus, it is still possible to conclusively evaluate the grids with less calculation time. For these evaluations, line loadings and nodal voltages are essential. Therefore, a line that may easily be overloaded cannot be eliminated within one cell. A highly loaded line, which can usually be identified beforehand, has to be defined as a connecting tie-line between two cells (Fig. 30).

A network node that is subject to possible voltage stability issues has to be defined as one cell. This, however, is only accurate if the assessed node is close to the Slack-node (Fig. 31). This is because a specific voltage drop occurs in each line. Therefore, the total voltage drop increases with a larger number of lines. If many lines are eliminated within the cells (meaning between the Slack-node and the assessed cell node), this voltage drop cannot be accurately retained in the cell model. Therefore, this assessment may not be advantageous for some applications since nodal voltage drops usually occur at the end of a feeder.

The geographical distribution of load and generation within each cell, as discussed in Section 3.2, influences modeling accuracy since the compensation module tries to compensate for the losses of the eliminated lines within one cell using an aggregated representation of the cell. The deviation after the compensation considers that lines at the end of a feeder are less loaded than lines at the beginning. Those lines only
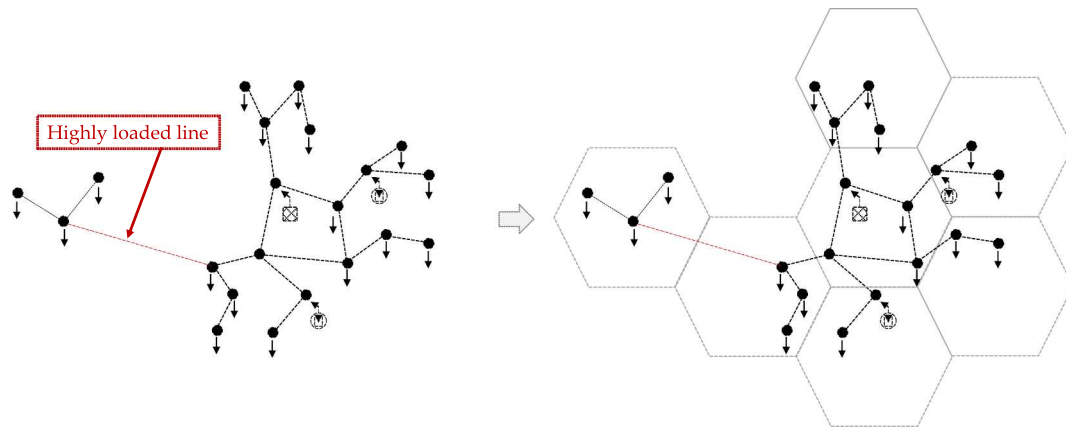
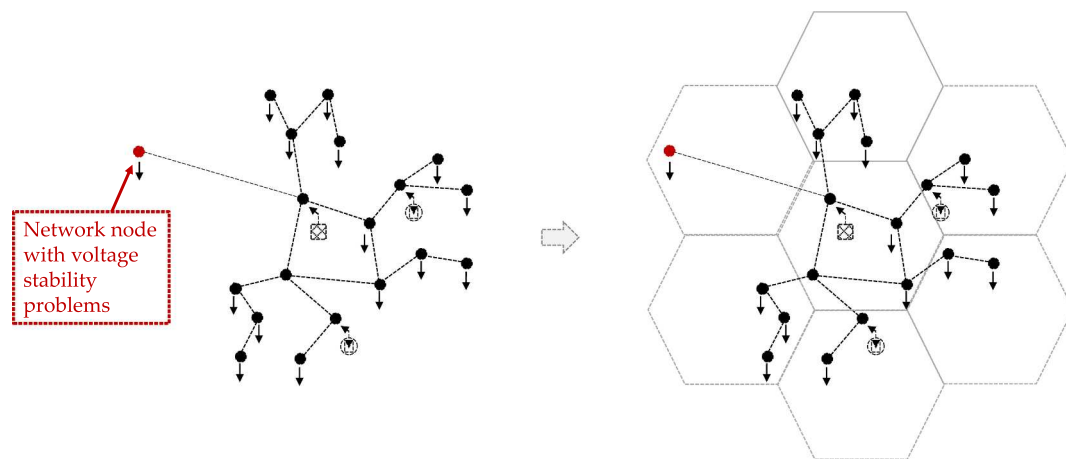**Fig. 30.** Cell division for assessing electrical line overloads.

Fig. 31. Cell division for assessing voltage stability at critical network nodes.

transmit the power, including the resulting line losses, which is also consumed at the connected network node. Electrical lines at the beginning of a feeder transmit the power needed for the entire feeder, including the generated line losses of all electrical lines connected. Since electrical line losses are load-dependent, the losses within the lines at the beginning of a feeder are higher than those within the lines at the end. To avoid a complete load flow calculation of the original grid, this information is not available or helpful for the compensation module calculation since this module aims to adapt to changing operating points. Therefore, one single voltage drop is assigned to each line within the cell (described in Section 3.2). This voltage drop results from the nodal voltage calculation in step 3 of Fig. 10 and thus, solely depends on the residual load within one cell. As a result, the line losses from eliminated lines at the end of feeders are overestimated on a cellular level. This deviation occurs at all voltage levels but causes negligible errors in the low- and medium-voltage level. However, since cell sizes are bigger at higher voltage levels to ensure a radial structure in the reduced grid, there are more electrical lines with different voltage drops than the one assigned in the calculation scheme. Therefore, this effect has more influence at higher voltage levels. The influence of this deviation is reduced due to higher transmitted power at the end of the feeder. Thus, some electrical compensation lines are modeled more accurately than others, as shown in the figures in Appendix A.

5. Conclusion

This paper presents a novel network reduction method specifically designed to maximize modeling accuracy in cellular-based network

models. By applying this method, a one-time calculation of the compensation modules of each cell for a given cell division enables a load- and generation-dependent (time-series calculations) consideration of the original network losses within the reduced cell model. Thus, depending on the application, considerable computational time savings can be achieved. Based on the results (deviations) obtained from applying the presented network reduction method on test grids, application purposes for which the cell models offer advantages are defined.

Since it is almost impossible to achieve a radial structure within the maximum-voltage grid, network reduction at this voltage level is not suitable. Additionally, grids at this voltage level usually are not largely expanded. Therefore, network reduction does not offer any advantages regarding more time-efficient calculations.

Whether it makes sense to reduce high-voltage grids or not depends on the original grid, meaning its expansion, its topology, and the use of the corresponding reduced network model. At this voltage level, the presented network reduction method achieves reasonable modeling accuracies, as long as a radial structure in the cellular-based network model can be achieved by proper cell division.

In medium-voltage grids, there may be many applications for which the presented network reduction, within the cellular approach, considering the achievable modeling accuracies, is sufficient. In particular, medium-voltage urban grids because they consist of a large number of nodes. Thus, annual calculations with fine temporal resolution and complex scenario calculations (RES, battery electric vehicles, heat pumps, …), as well as their analysis, are time extensive. For example, in this case, using the presented novel network reduction method to cellular-based network models can be beneficial. Another example is
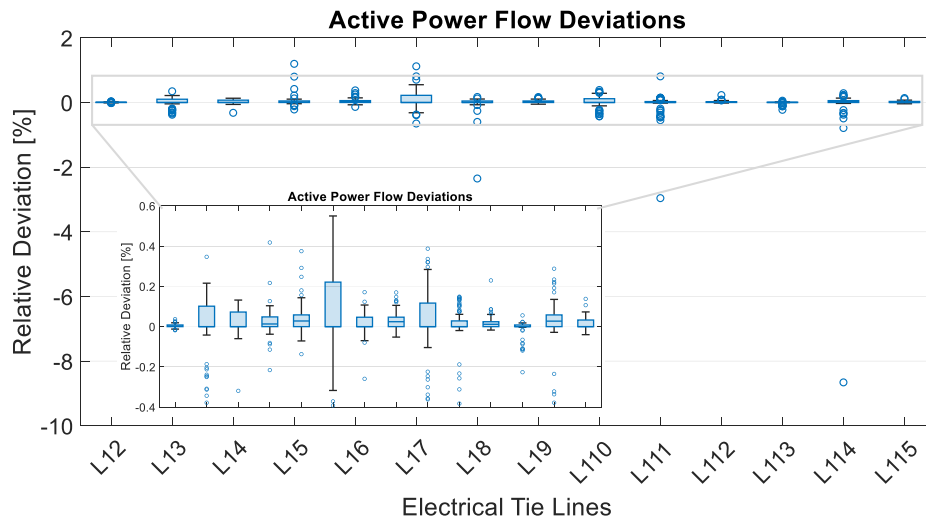
Fig. A1.1. Deviations of active power flows in the electrical compensation lines for the low-voltage test network.
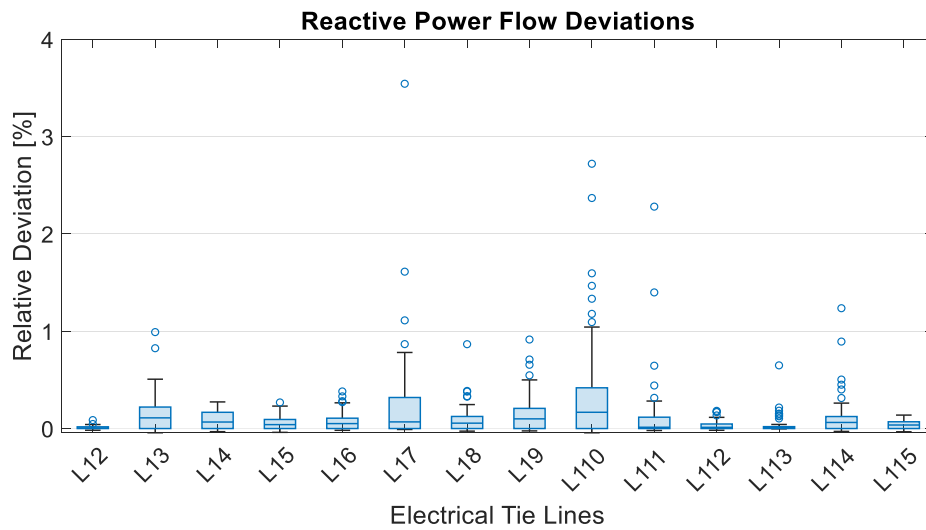

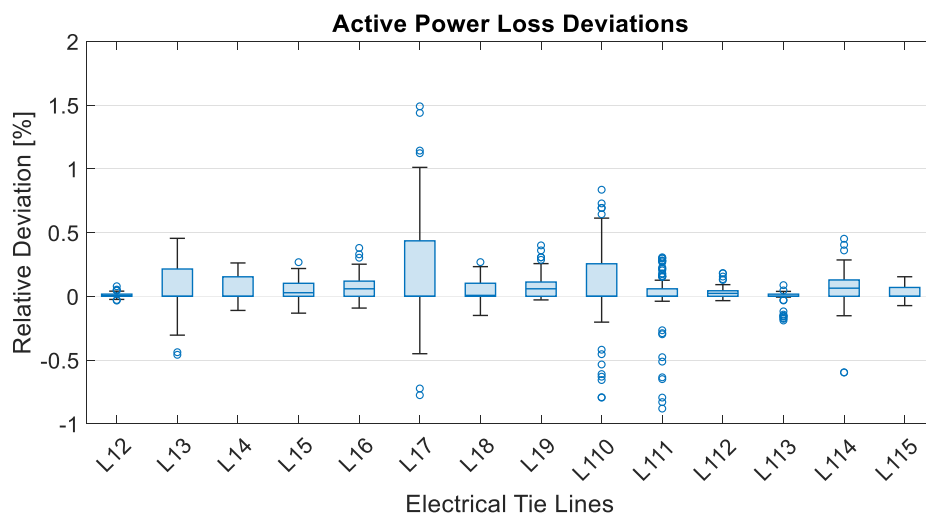**Fig. A1.2.** Deviations of reactive power flows in the electrical compensation lines for the low-voltage test network.

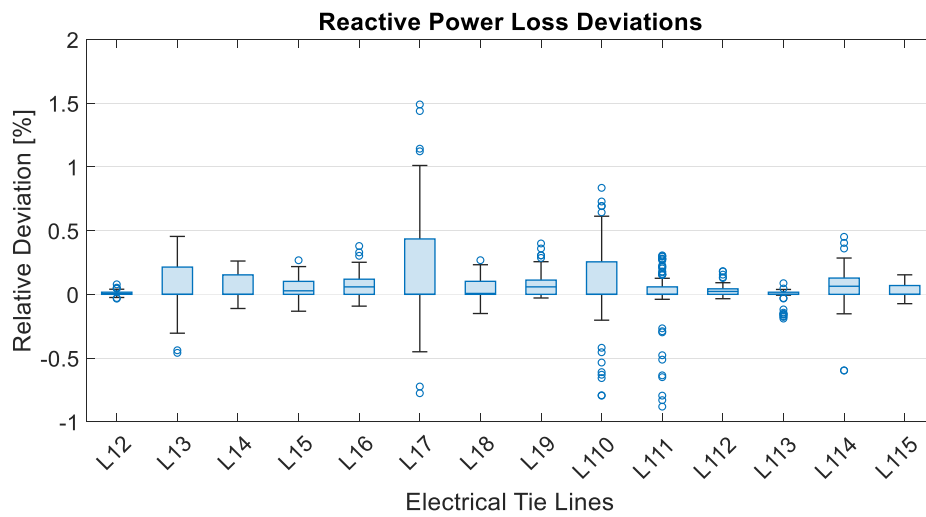**Fig. A1.3.** Deviations of active power losses in the electrical compensation lines for the low-voltage test network.
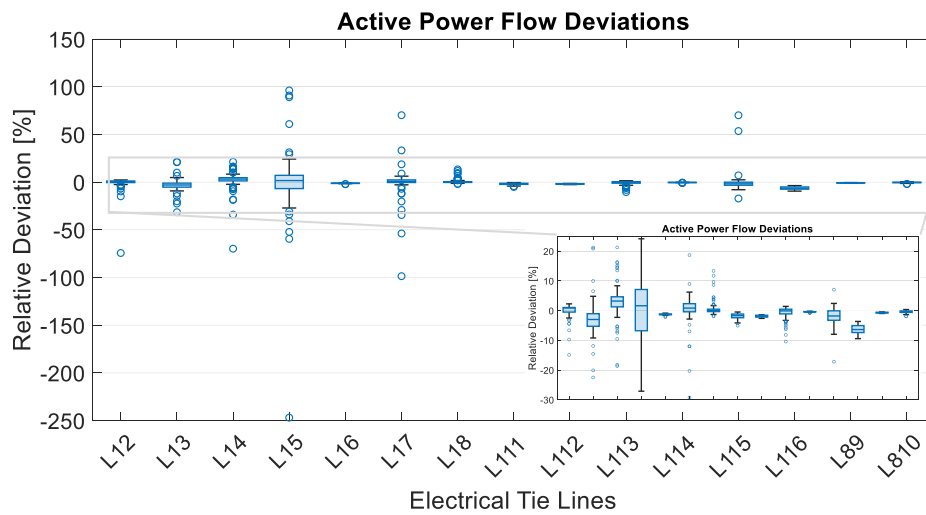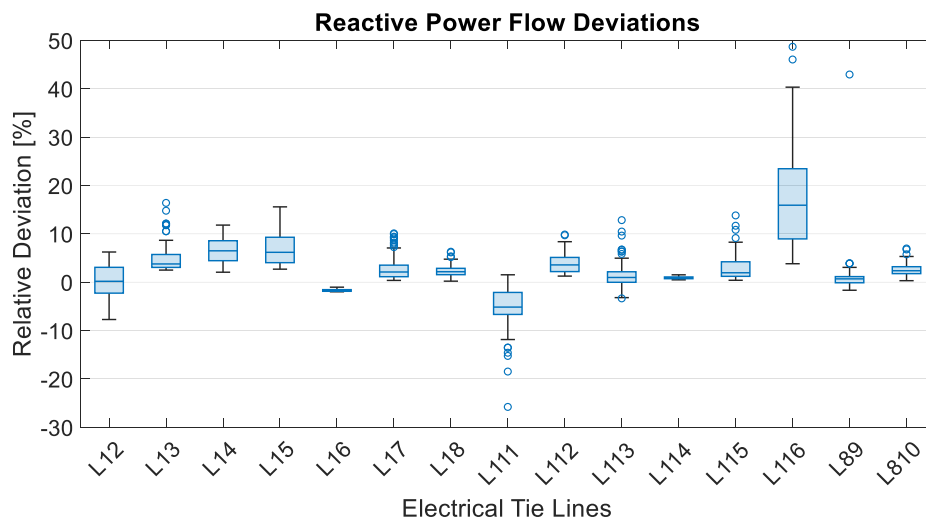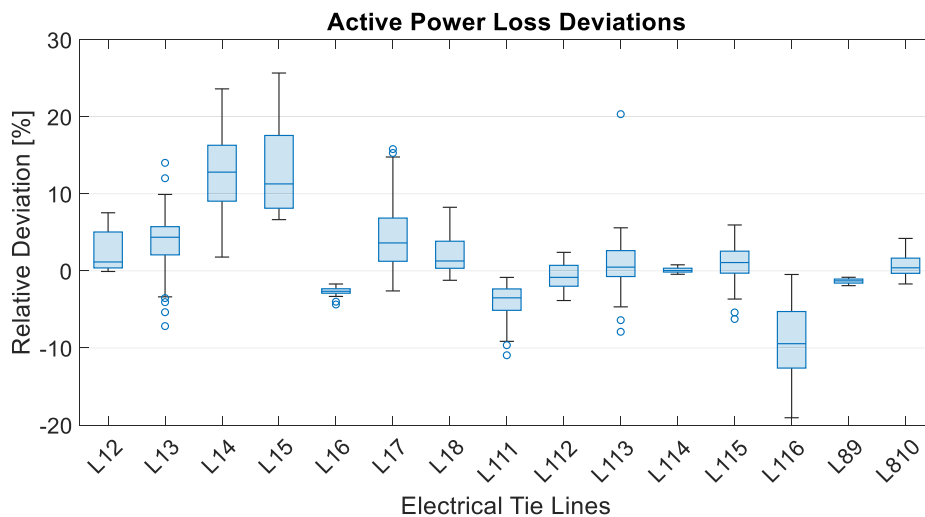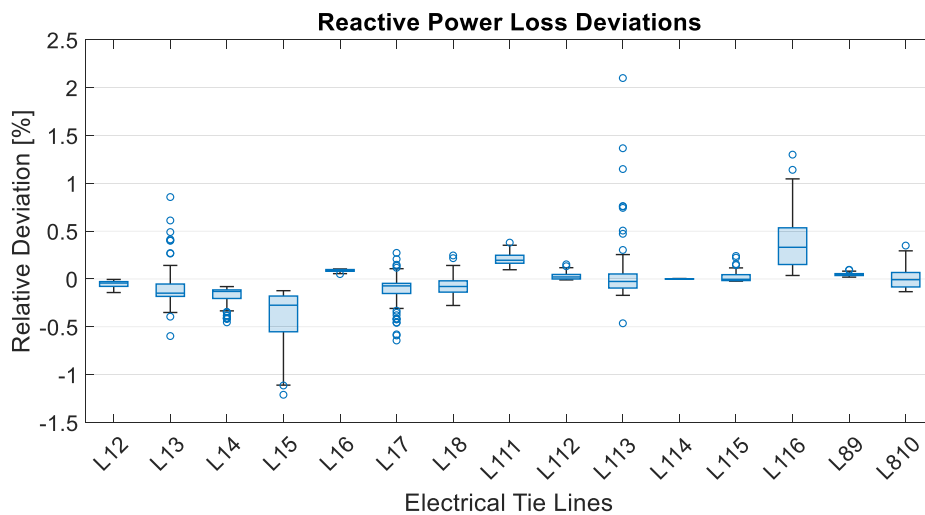
Fig. A1.4. Deviations of reactive power losses in the electrical compensation lines for the low-voltage test network.

Fig. A2.1. Deviations of active power flows in the electrical compensation lines for the medium-voltage test network.

Fig. A2.2. Deviations of reactive power flows in the electrical compensation lines for the medium-voltage test network.
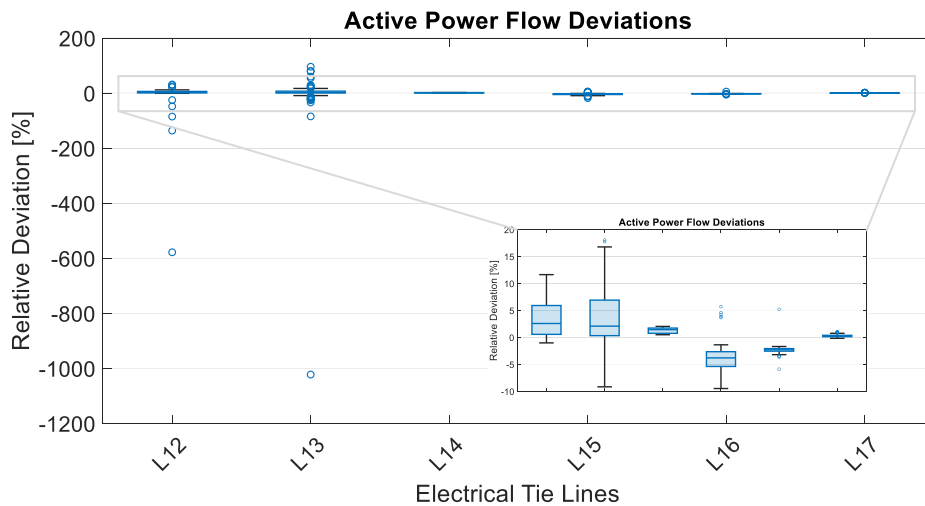
Fig. A2.3. Deviations of active power losses in the electrical compensation lines for the medium-voltage test network.

Fig. A2.4. Deviations of reactive power losses in the electrical compensation lines for the medium-voltage test network.

Fig. A3.1. Deviations of active power flows in the electrical compensation lines for the high-voltage test network.
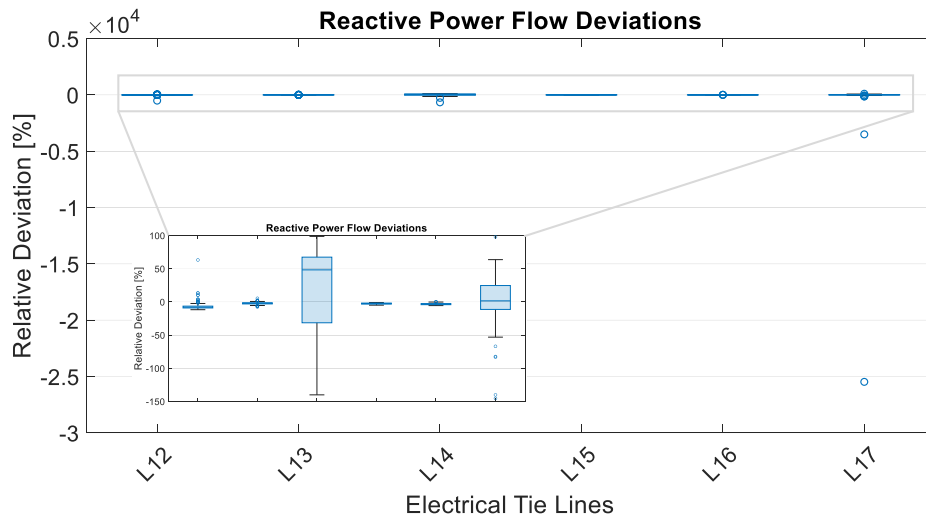
Fig. A3.2. Deviations of reactive power flows in the electrical compensation lines for the high-voltage test network.
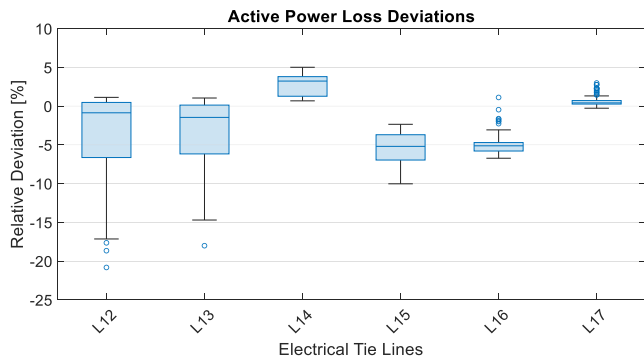

Fig. A3.3. Deviations of active power losses in the electrical compensation lines for the high-voltage test network.

particularly relevant in the hybrid modeling framework HyFlow, in which this method of developing accurate electrical cellular-based network models is embedded.

However, the most important application purposes for reduced cellular-based network models are low-voltage grids. For these grids, cellular-based models offer significant advantages due to the achieved high modeling accuracy. Additionally, if a sufficient number of residential units (about 150 households [39]) are combined within one cell, standard load profiles can be used as appropriate data for the consumers. Since standard load profiles represent an average consumption of many different residential units, they cannot properly approximate the consumption of a single or a couple of households. However, within a cell, the peaks in individual consumption cancel each other out due to asynchronicity resulting in an average profile over all considered households within one cell. Therefore, standard load profiles can simulate actual consumption within one cell accurately. In addition, high reduction factors can be achieved since a large number of consumers can be combined in one cell, which is, again, advantageous in terms of time-efficient calculations. Furthermore, during the regular operation of low-voltage grids, the first lines of a feeder extending from the Slack-node are of particular interest. For grid monitoring at the distribution system operator (DSO), those electrical lines are essential since overloads mainly occur there. The electrical lines at the beginning of a feeder can be assessed in the reduced cellular-based network model
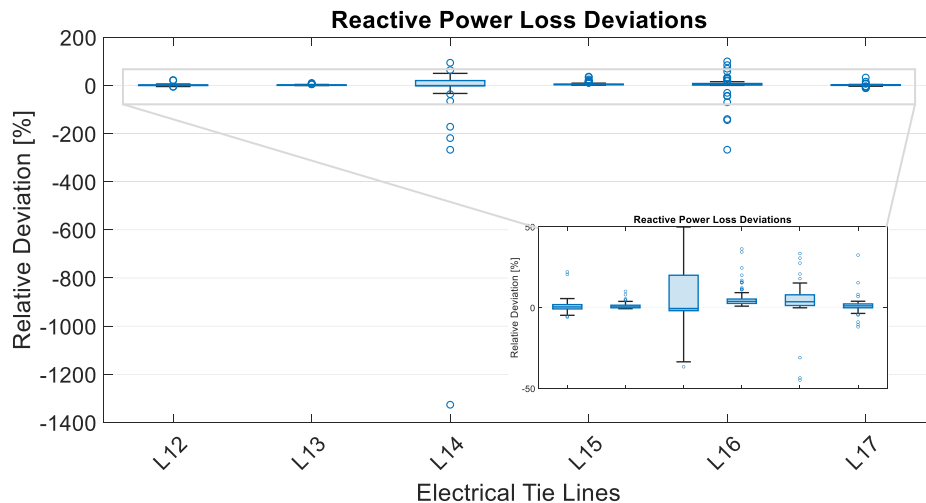
that it is possible to reduce an entire low-voltage grid connected to a local substation, enabling the additional representation of the overall network losses within the low-voltage grid. For these applications, the main advantage is faster calculations. Besides that, additional information can be included in the network, which could otherwise, without reduction, only be achieved if a cross-voltage level calculation of both fully represented grids is conducted. This hierarchical computation is

Fig. A3.4. Deviations of reactive power losses in the electrical compensation lines for the high-voltage test network.
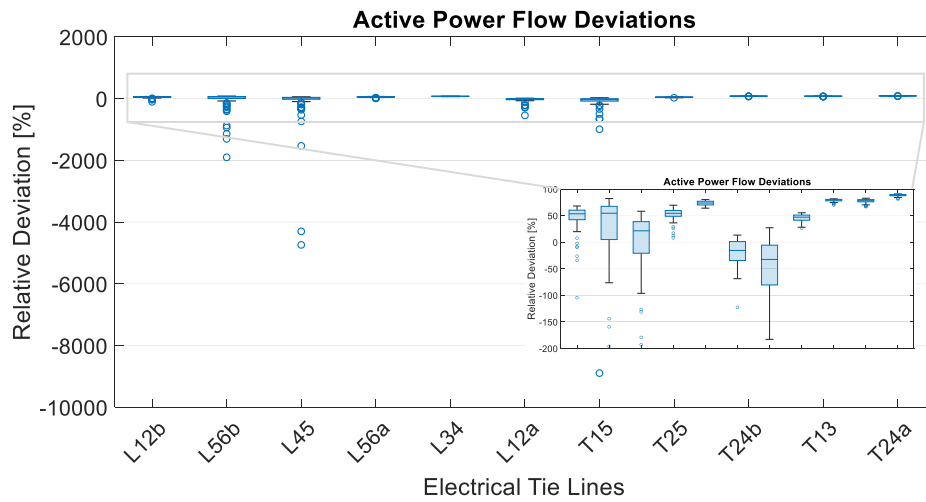
Fig. A4.1. Deviations of active power flows in the electrical compensation lines for the maximum-voltage test network.
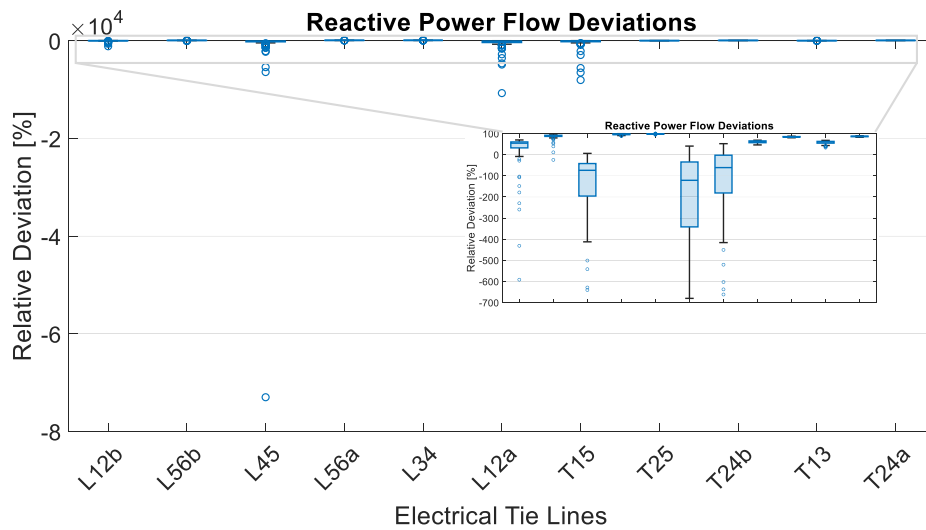

Fig. A4.2. Deviations of reactive power flows in the electrical compensation lines for the maximum-voltage test network.
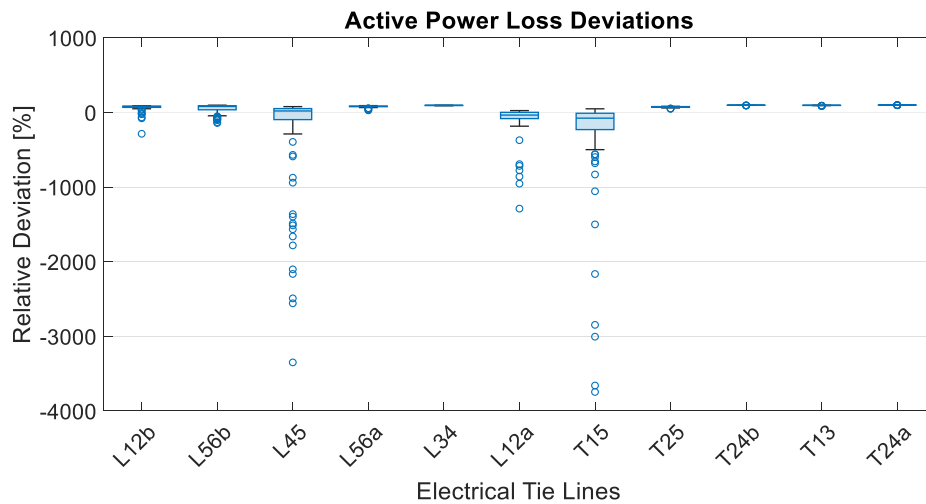

Fig. A4.3. Deviations of active power losses in the electrical compensation lines for the maximum-voltage test network.
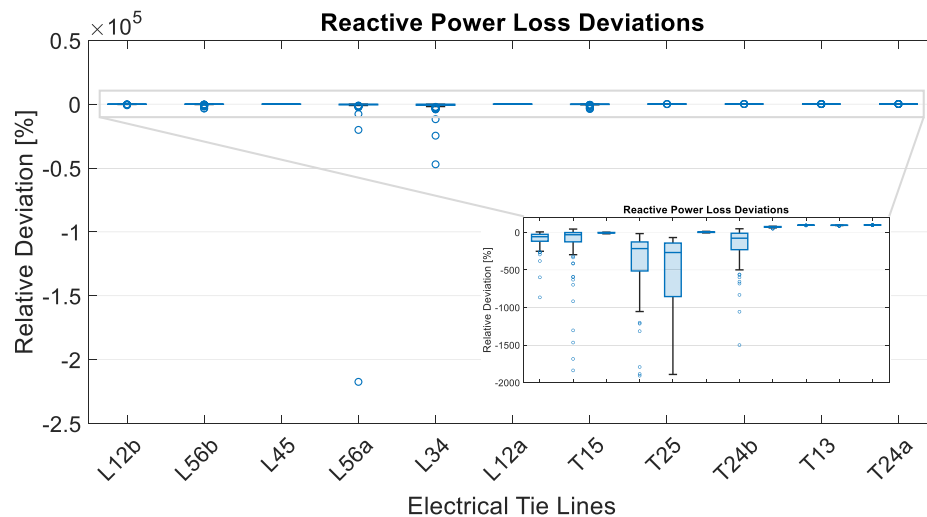
Fig. A4.4. Deviations of reactive power losses in the electrical compensation lines for the maximum-voltage test network.

with suitable cell division without any loss of information.

For real electrical grids there may also be advantages in in using geo-referencing ([40]) to enhance cell division. Since the cell division process is essential for modeling accuracy, geo-referencing may be beneficial for defining the system boundaries of each cell. However, for the synthetically developed test grids used in this work, geo-referencing is not possible due to the lack of corresponding geo-data.

The additional advantage achieved by using this cellular approach, besides more efficient calculations of extended networks over finely resolved long periods, is the identification of suitable multi-energy network nodes. Such nodes are beneficial regarding the exchange of energy between the different energy carriers. Thus, the cellular approach was chosen as the modeling approach in HyFlow which combines the energy carrier model for the electrical grid with other energy carrier network models (e.g. heat and gas).

Declaration of Competing Interest

The authors declare that they have no known competing financial interests or personal relationships that could have appeared to influence the work reported in this paper.

Acknowledgements

Appendix A. Closer examination of the deviations

shows the box plots for the relative deviations of active and reactive power flows as well as active and reactive line losses of the electrical connection elements over the considered time period.

Low-voltage level (0.4 kV)

Fig. A11 to Fig. A14 show the deviations of the low-voltage test network.Fig. A1 2.Fig. A1 3.

Medium-voltage level (20 kV)

Fig. A2 1 to Fig. A2 4 show the corresponding deviation of the medium-voltage test network.Fig. A2 2.Fig. A2 3.

High-voltage level (110 kV)

Fig. A3 1 to Fig. A3 4 show the corresponding deviations of the high-voltage test network.Fig. A3 2.Fig. A3 3.

Maximum-voltage level (380 kV/ 220 kV)

Fig. A4 1 to Fig. A4 4 show the corresponding deviations of the maximum-voltage test network.Fig. A4 2.Fig. A4 3.

References

[1] Papadis E, Tsatsaronis G. Challenges in the decarbonization of the energy sector. Energy 2020;205. https://doi.org/10.1016/j.energy.2020.118025.

[2] Jones LE. Renewable Energy Integration – Practical Management of Variability, Uncertainty, and Flexibility in Power Grids. 1st ed. Oxford, United Kingdome: Elsevier; 2014.

[3] Hossain, J. (Ed.); Mahmud, A. (Ed.) *Renewable Energy Integration – Challenges and Solutions*, 1st ed.; Springer: Singapore, 2014, DOI: 10.1007/978-981-4585-27-9.

[4] Bird, L.; Milligan, M.; Lew, D. Integrating Variable Renewable Energy: Challenges and Solutions. National Renewable Energy Laboratory Technical Report, 2013, Available online: https://www.nrel.gov/ docs/fy13osti/60451.pdf (accessed on 8th October 2020).

[5] Celata F, Dinnie L, Holsten A. Sustainability transitions to low-carbon societies: insights from European community-based initiatives. Regional Environment Change 2019;19(4):909–12. https://doi.org/10.1007/s10113-019-01488-6.

[6] Vahid-Pakdel MJ, Seyedi H, Mohammadi-Ivatloo B. Enhancement of power system voltage stability in multi-carrier energy systems. Int J Electr Power Energy Syst 2018;99:344–54. https://doi.org/10.1016/j.ijepes.2018.01.026.

[7] Mancarella P. MES (multi-energy systems): An overview of concepts and evaluation models. Energy 2014;65:1–17. https://doi.org/10.1016/j.energy.2013.10.041.

[8] Kriechbaum L, Scheiber G, Kienberger T. Grid-based multi-energy systems – modeling, assessment, open source modeling frameworks and challenges. Energy, Sustainability and Society 2018;8:35. https://doi.org/10.1186/s13705-018-0176-x.

[9] Böckl B, Greiml M, Leitner L, Pichler P, Kriechbaum L, Kienberger T. HyFlow-A Hybrid Load Flow Modeling Framework to Evaluate the Effects of Energy Storage and Sector Coupling on the Electrical Load Flows. energies 2019;12:25. https://doi.org/10.3390/en12050956.

[10] Greiml M, Traupmann A, Sejkora C, Kriechbaum L, Böckl B, Pichler P, et al. Modeling and model assessment of grid based Multi-Energy Systems. Int J Sustainable Energy Planning & Management 2020;29:7–24. https://doi.org/10.5278/ijsepm.3598.

[11] van Beeck NMJP. Classification of Energy Models. Available online: FEW Research Memorandum 1999;777:25. https://pure.uvt.nl/ws/portalfiles/portal/532108/777.pdf.

[12] Grubb M, Edmonds J, ten Brink P, Morrison M. The Costs of Limiting Fossil-Fuel CO_2-Emissions – A Survey and Analysis. Annual Rev Energy Environment 1993;18:397–478. https://doi.org/10.1146/annurev.energy.18.1.397.

[13] Herbst A, Toro F, Reitze F, Jochem E. Introduction to Energy Systems Modeling. Swiss J Economics Statistics 2012;148(2):111–35. https://doi.org/10.1007/BF03399363.

[14] Pfenninger S, Hawkes A, Keirstead J. Energy systems modeling for twenty-first century energy challenges. Renew Sustain Energy Rev 2014;33:74–86. https://doi.org/10.1016/j.rser.2014.02.003.

[15] Tleis N. Power Systems Modelling and Fault Analysis. Elsevier; 2019. p. 705–41.
[16] Papaemmanouil, A.; Andersson, G. On the reduction of large power system models for power market simulation. 17th Power Systemy Computation Conference, Stockholm, Sweden, August 22-26, 2011.
[17] Ward, J.B. Equivalent Circuits for Power-Flow. *Transactions of the American Institute of Electrical Engineers* **1949**, *68 (1)*, 10, DOI: 10.1.1.723.5598.
[18] Shayesteh E, Gayme DF, Amelin M. System reduction techniques for storage allocation in large power systems. Electrical Power and Energy Systems 2018;95: 108–17. https://doi.org/10.1016/j.ijepes.2017.08.007.
[19] Gavrilas M, Ivanov O, Gavrilas G. REI Equivalent Design for Electrica Power Systems with Genetic Algorithms. WSEAS Trans Circuits Systems 2008;10(7): 911–21.
[20] Deckmann S, Pizzolante A, Monticelli A, Stott B, Alsac O. Studies on Power System Load Flow Equivalents. IEEE Trans Power Apparatus Systems 1980;99(6): 2301–10. https://doi.org/10.1109/TPAS.1980.319798.
[21] Stadler, J.; Renner, H. Application of Dynamic REI Reduction. 4th IEEE PES Innovative Smart Grid Technologies Europe (ISGT Europe), Copenhagen, Denmark, October 6-9, 2013, DOI: 10.1109/ISGTEurope.2013.6695311.
[22] Krahmer, S.; von Haken, A.; Weidner, J.; Schegner, P. Anwendung von Methoden der Dynamischen Netzreduktion–Abbildung von 110-kV-Netzen für die Untersuchung der transienten Stabilität im Übertragungsnetz, Proceedings of the 15th Symposium Energieinnovation, Graz, Austria, 14-16th February 2018.
[23] Shayesteh E, Hamon C, Amelin M, Söder L. REI method for multi-area modeling of power systems. Electrical Power Energy Systems 2014;60:283–92. https://doi.org/10.1016/j.ijepes.2014.03.002.
[24] Housos EC, Isisarri G, Porter RM, Sasson AM. Steady State Network Equivalents for Power System Planning Applications. IEEE Trans Power Apparatus Systems 1980; 99(6):2113–20. https://doi.org/10.1109/TPAS.1980.319789.
[25] Deckmann S, Pizzolante A, Monticelli A, Stott B, Alsac O. Numercial Testing of Power System Load Flow Equivalents. IEEE Trans Power Apparatus Systems 1980; 99(6):2292–300. https://doi.org/10.1109/TPAS.1980.319797.
[26] Rao, S.; Tylavsky, D. Nonlinear Network Reduction for Distribution Networks using the Holomorphic Embedding Method, Proceedings of the North American Power Symposium (NAPS), Denver, CO, USA, 18-20th October 2016, DOI: 10.1109/NAPS.2016.7747978.
[27] Ashraf, S.M.; Rathore, B.; Chakrabarti, S. Performance Analysis of Static Network Reduction Methods Commonly Used in Power Systems, Proceedings of the 18th National Power Systems Conference (NPSC), Guwahati, India, 18-20th December 2014, DOI: 10.1109/NPSC.2014.7103837.
[28] Wien, Austria: Wirk- und blindleistungsgenaue Modellierung von reduzierten Netzen im zellularen Ansatz, 13–15th Febuary; 2019.
[29] Samadi A, Shayesteh E, Soder L, Eriksson R. Static Equivalent of Distribution Grids With High Penetration of PV Systems. IEEE Trans Smart Grid 2015;6(4):1–12. https://doi.org/10.1109/TSG.2015.2399333.
[30] Shi D, Tylavsky DJ. A Novel Bus-Aggregation-Based Structure-Preserving Power System Equivalent. *IEEE Trans Power Systems* 2015;30(4):1977–86. https://doi.org/10.1109/TPWRS.2014.2359447.
[31] Ploussard Q, Olmos L, Ramos A. An Efficient Network Reduction Method for transmission expansion planning using multicut problem and Kron reduction. IEEE Trans Power Syst 2018;99:1–10. https://doi.org/10.1109/TPWRS.2018.2842301.
[32] Huang, B.; Li, J.; Wang, J. An Evidential Reasoning Approach to Building Node Selection Criterion for Network Reduction. **2020**, https://arxiv.org/pdf/2012.13684.pdf, Accessed on: 19th October 2021.
[33] Vopava J, Koczwara C, Traupmann A, Kienberger T. Investigating the impact of e-mobility on the electrical power grid using a simplified grid modeling approach. energies 2020;39:25. https://doi.org/10.3390/en13010039.
[34] Vopava J, Böckl B, Kriechbaum L, Kienberger T. Anwendung zellularer Ansätze bei der Gestaltung zukünftiger EnergieverbundsystemeApplication of the cellular approach to design energy systems for the future. Elektrotechnik & Informationstechnik 2017;134(3):238–45. https://doi.org/10.1007/s00502-017-0501-7.
[35] Kundur, P. AC Transmission. In *Power System Stability and Control*, 1st ed.; Balu, N. J., Lauby, M.G.; McGraw-Hill Inc.: USA, 1994, pp. 199-201.
[36] Grainger, J.J.; Stevenson, Jr., W.D. Power-Flow Solutions. In: *Power System Analysis*, 1st ed.; Director, S.W.; McGraw-Hill Series in Electrical and Computer Engineering: Singapore, 1994, pp. 342-356.
[37] Traupmann A, Kienberger T. Test Grids for the Integration of RES – A Contribution for the European Context. *energies* 2020;13:29. https://doi.org/10.3390/en13205431.
[38] Jasmon GB, Lee LHCC. Distribution network reduction for voltage stability analysis and loadflow calculations. Int J Electric Power Energy Systems 1991;13(1):9–13. https://doi.org/10.1016/0142-0615(91)90011-J.
[39] Graz, Austria: Entwicklung und Verifikation eines stochastischen Verbraucherlastmodells für Haushalte, 15–17th February; 2012.
[40] Bosisio A, Berizzi A, Amaldi E, Bovo C, Morotti A, Greco B, et al. A GIS-based approach for high-level distribution networks expansion planning in normal and contingency operation considering reliability. Electr Power Syst Res 2021;190: 106684. https://doi.org/10.1016/j.epsr.2020.106684.

CIGRÉ 2020 (Status: Accepted)

TRAUPMANN, A.; GREIML, M.; KIENBERGER, T., *Reduction Method for Planning Cross-energy Carrier Networks in the Cellular Approach Applicable for Stability Assessment in Low-Voltage Networks*, In: e&I Elktrotechnik und Informationstechnik, CIGRÉ 2020, doi.org/10.1007/s00502-020-00851-4.

Table A. 1: Author statement to first conference contribution (CIGRÉ)

Activity	Contribution authors (main author is mentioned first)
Conceptualization	A. Traupmann, T. Kienberger
Methodology	A. Traupmann, T. Kienberger
Data Curation	A. Traupmann, M.Greiml
Software Development and Validation	M. Greiml, A. Traupmann
Modeling	A. Traupmann, M.Greiml
Visualization	A. Traupmann
Writing (Original Draft)	A. Traupmann
Writing (Review and Editing)	A. Traupmann, T. Kienberger

Reduction method for planning cross energy carrier networks in the cellular approach applicable for stability assessment in low-voltage networks

Anna TRAUPMANN, Matthias GREIML, Thomas KIENBERGER
Chair of Energy Network Technology
Montanuniversitaet Leoben
Austria
anna.traupmann@unileoben.ac.at

SUMMARY

Stability assessment for electrical networks is an essential research topic for sustainable energy generation and, therefore, future electrical networks. Renewable energy sources implemented in the grid in order to substitute fossil fuels as energy sources presents as a challenge for current network infrastructures since renewable energy sources are highly volatile and, therefore, not always predictable. Especially in low-voltage networks with high shares of PV penetration and extended network branches that supply customers with high consumption, power quality issues arise, since these infrastructures were historically built to transport and distribute electrical energy from local substations to the consumers. Due to further developments and new consumer groups connected to the grid, as well as generation in PV units, load flows may be reversed or enlarged leading to challenges in terms of overloads and voltage problems. In this work, a method for reducing electrical networks at the low-voltage level by applying the cellular approach is presented with special regard to power quality issues that may arise in low-voltage networks. Network reduction, in general, enables faster calculations of expanded networks with fine temporal resolution and can, therefore, be applied when handling large amounts of grid data. This methodology for network reduction within the cellular approach is implemented into a hybrid load flow calculation framework developed at the Chair of Energy Network Technology. The results obtained from the hybrid load flow calculation can then be used to show how hybrid flexibility options as well as storage units can help increase network stability (in this case regarding voltage stability).

KEYWORDS
Network Reduction - Cellular Approach - Cross Energy Carrier Network - Electrical Network Planning - Stability Assessment - Voltage Stability - Power Quality

INTRODUCTION

Substituting fossil fuels with fluctuating renewable energy sources (RES) requires the implementation of flexibility options in order to relieve the electrical distribution grid if there are generation peaks that cannot be consumed at that time. Since RES are mainly decentralized and not always predictable, they introduce a high volatility into the grid which impedes balancing electrical energy generation and consumption. As a result, the need for flexibility options arises in order to efficiently integrate renewable energy sources and simultaneously prevent exceeding of stability limits. Sector coupling allows for these flexibility options to be used across energy carriers and, thus, further increase system flexibility as well as stability. Cross energy carrier networks, additionally, facilitate increasing overall system efficiency by enabling maximum energy use (e.g. cascaded energy use) and seasonal energy storage. Furthermore, cost savings could be achieved by utilizing the most favorable storage and transport capacities depending on the network state which avoids powering down fluctuating RES. [1-2] Therefore, efficient design as well as operational management of cross energy carrier networks in order to ensure a secure and stable future energy supply requires appropriate tools. Such tools have to be able to perform efficient and accurate load flow calculations across energy carriers, in order to obtain reliable results regarding the impact of flexibility options on the grid. Therefore, the multi-energy hybrid modelling framework HyFlow for cross-energy carrier calculations was developed at the Chair of Energy Network Technology. For each energy carrier considered in this framework an appropriate model representing the grid infrastructure with high temporal and spatial resolution is required. The modelling approach shown in this work to enable these criteria is the cellular approach. Especially for electrical networks, applying this approach requires compensation methods in order to preserve active as well as reactive behavior of the original network structures and, thereby, enable appropriate stability assessment.

The main focus of this paper is to demonstrate, how an appropriate cell division can be used to create an electrical cell network that can be effectively applied for stability assessment in terms of power quality at the low-voltage level. This model is then used for a calculation within HyFlow in order to implement flexibility options as well as storage units appropriate at this voltage level. Thereby, it illustrates how hybrid flexibility options can be used in order to increase voltage stability within the grid.

METHODICAL APPROACH

The cellular approach

The cellular approach represents a modelling approach which supports spatial resolution and defines the level of detail for aggregated networks. Within this approach each energy carrier network considered is divided into energy cells, which represent a set of network nodes assigned accordingly to geographical aspects. The size and the location of the cells as well as the assigned network nodes are variable with regard to individual infrastructural parameters for each energy carrier network model. However, each cell is then aggregated in order to be represented by only a small set of parameters. In this step all consumers, generators and storage units located within one cell are aggregated in one single, fictitious node in the cell center. As a result, the physical connection lines between the cells and the aggregated amount of energy generation and consumption within the cells are retained. The energy cell level is defined to be the lowest system level at which energy balancing can occur. Depending on system configuration and network state, energy can then be balanced as efficiently as possible using time-resolved power values (e.g. 15-minute values). [3] The cellular approach, thus, allows for the application of standard load profiles (and/or synthetic load profiles) as long as a certain number of consumers is aggregated within the cells. Additionally, it enables the identification of advantageous cross-sector coupling points and the simplification of complex network structures enabling time-efficient calculations. [3] [4]

Due to the aggregation, a simplified network model is created, which allows for faster calculations of expanded networks over long periods of time [5]. However, the aggregation process changes the original network structures, and, therefore, information essential for characterizing the network is lost. This lost information leads to deviations between the original, unreduced network and the reduced, cellular based network model. Thus, compensation methods have to be applied in order to closely approximate the real network within the model, which are described in the next section.

Network reduction methods

Network reduction methods are used in order to simplify network size and complexity and account for these changes by compensating the lost information. [6-8] In this work, a network reduction method specifically applicable to the cellular approach is implemented minimizing the error between the original network and the simplified cell model. This error refers to deviations in active and reactive power flows over connecting tie lines between cells as well as the overall electrical behavior of the network including power flows over the Slack-node and overall network losses. The reason why information is lost in this process is due to electrical lines within the cells that are neglected or "deleted" when aggregating network nodes into one fictitious node in the cell center. The electrical line losses of those neglected lines change intercellular load flows as well as the Slack-node power and the overall network losses. In order to compensate for these losses elements that recreate the network losses of the neglected lines have to be implemented at the cell nodes. Compensation can only be achieved if the lost information is substituted at the fictitious nodes which is due to the calculation process of the Newton-Raphson-method. The iteration of the Newton-Raphson-method can only be terminated if the deviation between known and calculated nodal power falls below a certain error limit. Therefore, load flow adaption can only be achieved if the line losses are compensated at the nodes, thereby, modifying nodal balances. Intercellular load flows adjust accordingly to nodal voltages calculated in the iteration, which are based on nodal loads and generations as well as implemented nodal compensation elements present within the network. The process of network aggregation within the cellular approach and of implementing compensation elements into the reduced cell network using network reduction methods is shown in the figure below (Figure 1):
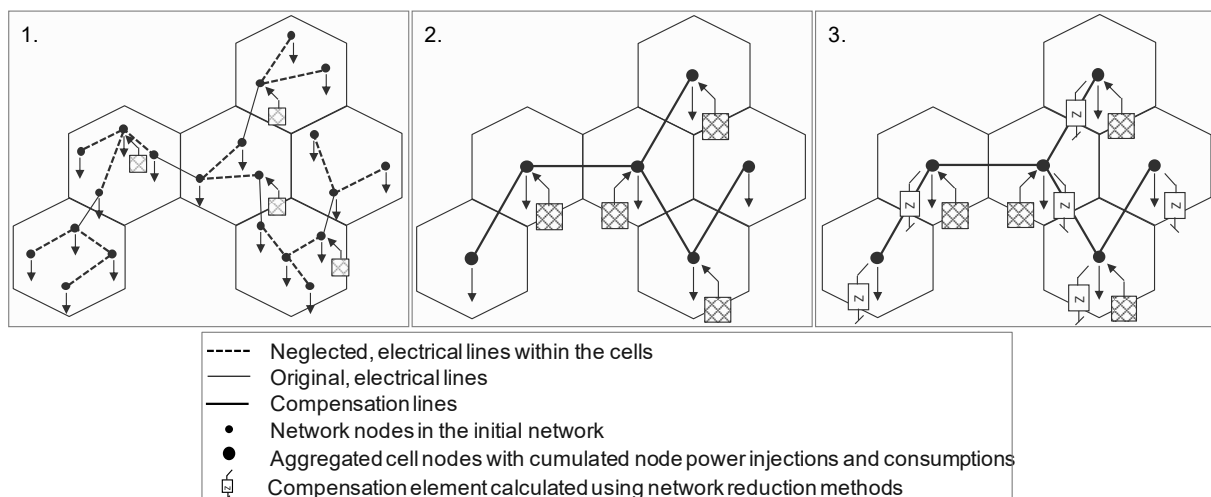

Figure 1 : Exemplary network aggregation process steps within the cellular approach: 1. Original, unreduced network, 2. Reduced network within the cellular approach (infrastructural changes), 3. Implemented compensation elements

For parameterizing these compensation elements, the electrical line parameters (according to the π-equivalent circuit) of the neglected lines within the cells are used. These line parameters characterize each electrical line in terms of conductor material, insulation as well as electromagnetic field and, therefore, active and reactive power losses within the lines.

This parameterization creates a load variable compensation element that enables adapting the aggregated cell model to equalize the original, unreduced network for each operating point (load and generation present at a certain point in time), which enables creating less complex, but accurate reduced cell models.

If, however, a network is aggregated, regardless of its accuracy, it is no longer possible to assess all nodal voltages and line conditions in terms of critical network nodes (according to EN 50160 [9]) or thermal line utilization (according to line specifications). In order to use the cellular approach due to its before mentioned advantages, this work shows how reasonable cell division enables properly assessing these criteria even after aggregation.

Cell division for stability assessment of reduced cell networks

Both, critical network nodes as well as critical lines can be identified prior to creating the cell network and can, therefore, be taken into account when dividing the network into cells. Critical network nodes refer to voltage stability and, therefore, power quality for consumer and generation units connected to that network node. Specifications about required power quality at network nodes within the medium- and low-voltage network can be found in the EN 50160 standard ([9]) which defines the permissible voltage range. Within that range nodal voltages may deviate from the nominal voltage [10]. The voltage band at the low-voltage level ranges from 0.935 p.u. (-6.5% from nominal voltage) to 1.045 p.u. ($+4.5\%$ from nominal voltage), assuming that transformation in local substations from the medium-voltage level to the low-voltage level leads to a grid voltage that does not correspond with nominal voltage and a voltage phase angle of zero [10]. Critical lines or line overloads refer to exceeding a predefined line current limit for thermal line utilization which puts the electrical line at risk of failure and, therefore, may impede security of supply. This limit is obtained from line specifications regarding maximal line current. Capacity issues due to thermal line utilization, usually, occur in urban areas and determine planning and design requirements in such areas [11].

The assessment of these criteria after network aggregation is essential in order to gain reliable and conclusive results from calculations that use these cell models, which can be facilitated by using appropriate cell division. In both cases, accurate reactive power modelling within the reduced cell model is the prerequisite for this assessment and can be achieved using the before mentioned compensation method. Regarding cell division, critical network nodes should be defined as individual cells, meaning no other nodes are assigned to this cell and the fictitious cell node in the cell center is equivalent to the original node regarding nodal voltage and power. Since compensation methods aim at equivalencing intercellular load flows in the reduced cell model to the unreduced, original network, line loadings can be assessed by defining highly loaded lines as connecting tie lines between two cells. Using these recommendations for cell division stability assessments as well as grid planning actions can also be conducted using aggregated network models since it allows for critical network sections to be represented by their real structure. These cell dividing recommendations are illustrated in the figure below (Figure 2).
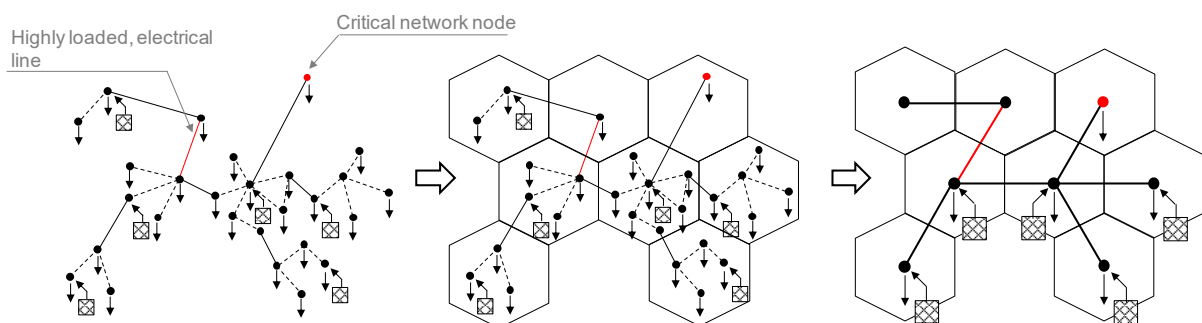

Figure 2 : Exemplary cell division for voltage stability assessment as well as line loading evaluation

Hybrid flexibility option and storage implementation

The reduced network, according to the guidelines regarding cell division in order to evaluate voltage stability shown in the last section, can be implemented in the hybrid load flow calculation framework HyFlow accounting for electricity, heat and gas grids. HyFlow allows for the use of various flexibility options (such as heat pumps at the low-voltage level) as well as storage units (e.g. heat storages) to be implemented into the grid if necessary to balance energy generation and consumption and, thereby, increase overall network stability. Each hybrid conversion element has its own operating strategy which either refers to balancing energy within each cell or balancing energy within the overall network. More precisely, energy balancing refers to keeping the residual loads within the defined system boundary (energy cell or overall system) as minimal as possible. The residual load of each cell $P_{res}(t)$ represents the difference between generated, fluctuating power $P_{gen}(t)$ and consumed power $P_{load}(t)$ within that cell for each time step (Formula (1)) [3].

$$P_{res}(t) = P_{load}(t) - P_{gen}(t) \qquad (1)$$

Within a stable electrical grid power consumption and generation are always balanced, meaning there is no residual load. If, however, there is a difference countermeasures including the implementation or activation of storage facilities as well as hybrid conversion units have to be taken. At the low-voltage level, for example, a heat pump can be used to balance energy within one cell. It operates on excessive power generated in PV units that cannot be consumed at that moment, resulting in a negative residual load of the considered cell. It may also be turned on if there is a heat demand in the corresponding cell, resulting in an additional positive residual load.

RESULTS

Low-voltage test grid

The low-voltage test grid (Figure 3 A. and Table 1) used in this work initially represents a network section of an Austrian low-voltage grid with currently only few installed PV units. It consists of 46 network nodes and 5 feeders resulting in a radial network structure. There are 41 consumer units present in the test grid which are represented by standard load profiles consisting of different customers such as households (78 H0-profiles), businesses (7 G0-, 12 G1-, 2 G3, 1 G4, 2 G6-profiles) as well as agriculture (36 L0-profiles). For the 8 PV generation units present in the unreduced grid consisting of 32 installed PV systems at individual customers measured profiles were applied. The degree of cabling for the unreduced low-voltage test grid is 95.6 % and the total electrical line length sums up to 3.3 km. The calculation time frame in this work includes 24 hours in 15-minute-time steps for a summer day in June. Figure 3 shows the initial network without PV expansion as well as the chosen cell division and the reduced cell network. The original unreduced network is reduced by 76 % from 46 network nodes to only 11 network nodes which can be seen in Figure 3 B.

Table 1: Network characteristics of the current state unreduced low-voltage grid without PV expansion

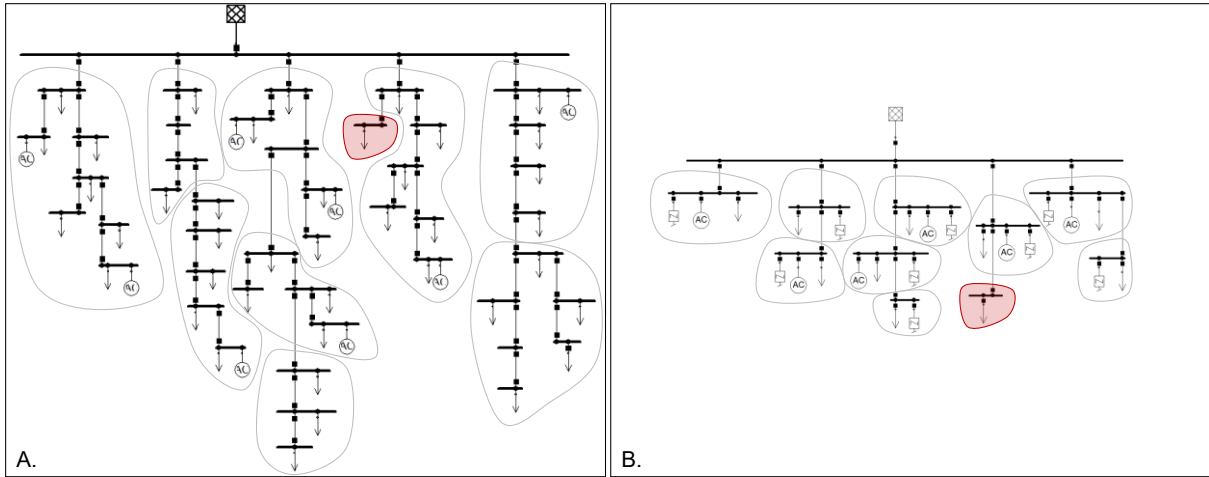| Network data	
Number of cables	43
Number of overhead lines	2
Topology	radial
Total electrical line length	3.3 km
Generation and consumer unit data	
Number of feeders	5
Number of consumer units	41
Total number of customers	138
Number of PV generation units	8
Total number of PV systems at customers	32

Figure 3: Cell division for the initial low-voltage grid A. unreduced grid, B. reduced cell network

This work presents a scenario in which the share of PV units is extensively increased compared to the current state represented in Figure 3 A. The PV expansion is based on the consideration regarding which possible areas at the customers may be suited for increasing the share of PV systems within the overall grid. For the considered network node in the marked cell, the PV expansion is enlarged to such an extent that an exceeding of the upper voltage limit could be detected. The overall increased share of installed PV units leads to negative residual loads during times with high electricity generation of the PV units. The cell division for this network is chosen accordingly to the guidelines discussed in one of the previous sections and enables reliably assessing voltage stability at the marked network node in Figure 3. Line loadings are not an issue in this test case since high line loadings in the initial network are actually reduced in the future scenario due to the extensive installation of PV units. Therefore, only voltage stability is assessed in this work.

It can be seen in Figure 4 that appropriate cell division can facilitate correct modeling of specific nodal voltages. In this example for the node in the red marked cell timelines for the nodal voltages in the unreduced grid and the reduced grid are identical.
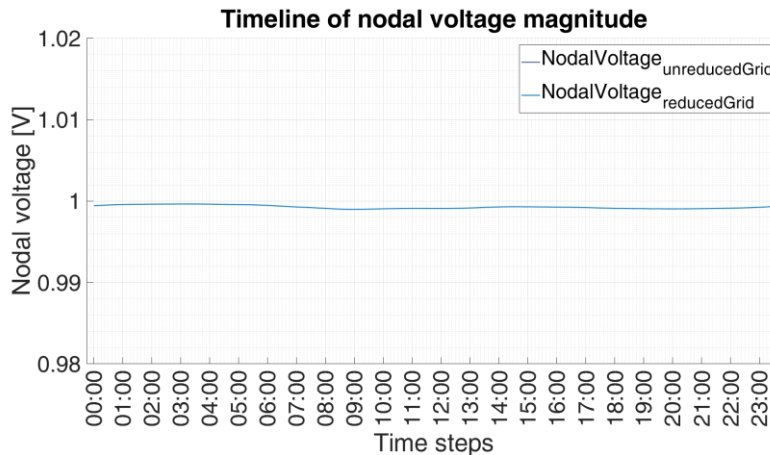

Figure 4: Timeline of the nodal voltage magnitude of the marked cell without PV expansion

The low-voltage test grid for the PV expansion scenario can be described according to Table 2. The initial grid stays the same, only the PV units are greatly expanded. Figure 5 shows the electrical network model of the future scenario for the low-voltage test grid with extensive increase in the share of PV units.

Table 2: Network characteristics of the unreduced low-voltage grid for the future PV expansion scenario

6

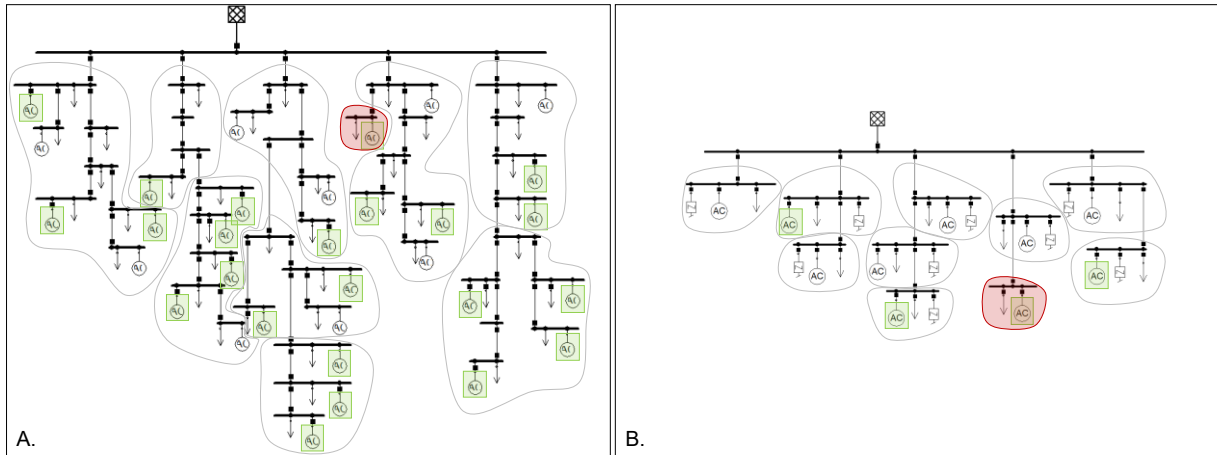| Network data	
Number of cables	43
Number of overhead lines	2
Topology	radial
Total electrical line length	3.3 km
Generation and consumer unit data	
Number of feeders	5
Number of consumer units	41
Total number of customers	138
Number of PV generation units	32
Total number of PV systems at customers	104

Figure 5: PV expansion scenario for the low-voltage grid with extensive increase in installed PV units
A. unreduced grid, B. reduced cell network

Figure 6 shows, equally to Figure 4, that using the same cell division, nodal voltages for the marked cell in Figure 5 can also be modelled correctly, even if negative residual loads at the observed network node occur. However, in this case negative residual loads lead to an increase in nodal voltage magnitude above the upper voltage limit and, thereby, compromise voltage stability.
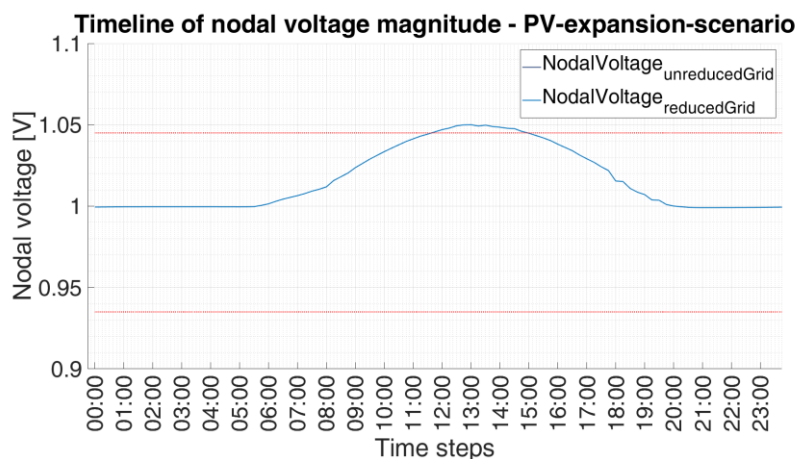

Figure 6: Timeline of the nodal voltage magnitude of the marked cell in the PV expansion scenario

In order to keep a high power quality for this PV expansion-scenario meaning that nodal voltages cannot exceed upper or lower voltage limits, counter-measures have to be taken.

Implementation of hybrid flexibility options and storage units using HyFlow

Negative residual loads and, therefore, the increase in nodal voltage magnitude, which influences overall network stability, can be balanced by implementing flexibility options such as storage facilities as well as hybrid conversion units. For the PV expansion scenario described in the previous section, heat pumps can be implemented into the low-voltage grid. Therefore, each consumer unit within the aggregated grid receives a time-dependent heat demand ($P_{th,load}$) for that summer day. The correspondingly implemented heat pump within each cell operates only if there is heat demand or if there is surplus electricity available from renewable generation at the corresponding cell node. Additionally, in order to enable maximal stability support using heat pumps there is also a heat storage unit available at each consumer unit which can store heat produced at times when there is no heat demand by the consumers. The heat storage at the considered node within the marked cell is significantly oversized for the corresponding heat demand. This is due to the fact that the generation potential of the installed PV system at this node is expanded to such an extent that it leads to exceeding voltage limits. The size of the heat storage is selected accordingly based on the expanded PV generation. Therefore, almost the entire electrical surplus energy can be converted into thermal energy, even if there is no longer a heat demand. Basically, hybrid conversion technologies in combination with storage systems are implemented in order to temporally decouple generation and consumption and, additionally, enable using other energy carriers at the same time. In this case, the storage unit would be sized for the amount of energy that cannot be used at a certain time, but can be used at later times. Then, the storage unit would be able to store the thermal energy converted from excessive electrical energy the next day. In the example given here, the storage unit is fully charged at the end of the day and could not store any more energy the following day, unless there is an additional heat demand. However, in order to assess power quality an oversized storage unit is a more suitable way to show how corresponding flexibility options affect voltage stability.

The hybrid conversion of the residual load ($P_{el,residual}$ and $P_{el,residual,hybrid}$) as well as the heat demand of the consumer ($P_{th,load}$) within the marked cell and the state of charge of the thermal storage unit ($E_{th,storage}$) at the corresponding fictitious cell node calculated within the hybrid load flow calculation framework HyFlow are illustrated in Figure 7.
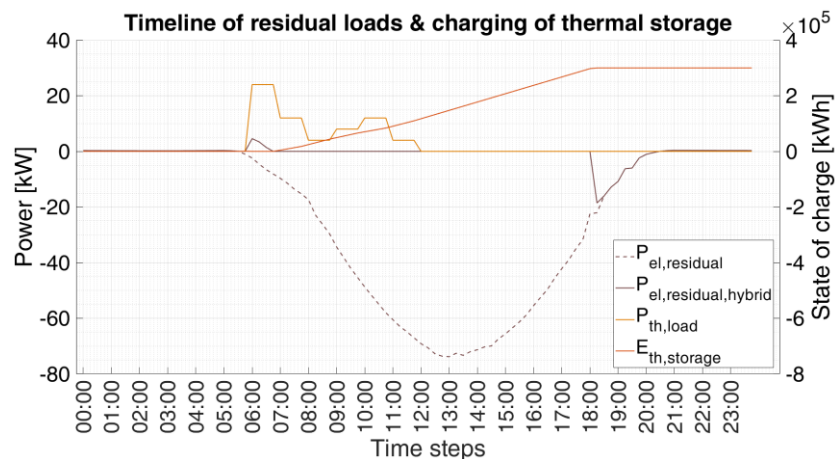

Figure 7: Time line of electrical residual loads and heat demand as well as state of charge for the marked cell in the PV expansion scenario

Evaluating the newly calculated residual load $P_{el,residual,hybrid}$ for the reduced grid in the PV expansion scenario leads to a very stable nodal voltage at the considered network node which can be seen in comparison to the previous nodal voltage in Figure 8.

The voltage drop in Figure 8 at the beginning of the hybrid conversion (~6:00) is a result of the required heat demand which occurs before a negative residual load from renewable energy generation is available at that node. Therefore, the additional electrical power required for the operation of the heat pump leads to a temporal increase in electrical

consumption until higher renewable generation can be achieved. The voltage increase at the end of the hybrid conversion (~18:00) can be avoided if the corresponding heat storage is previously sized even larger or if other flexibility options are implemented. Thereby, all the electrical excess energy from the PV unit could be utilized. In the test case presented in this work the heat storage is fully charged in the evening (~18:00), therefore, the negative residual load cannot be compensated entirely by the hybrid conversion element and, thus, nodal voltage slightly increases during that period.
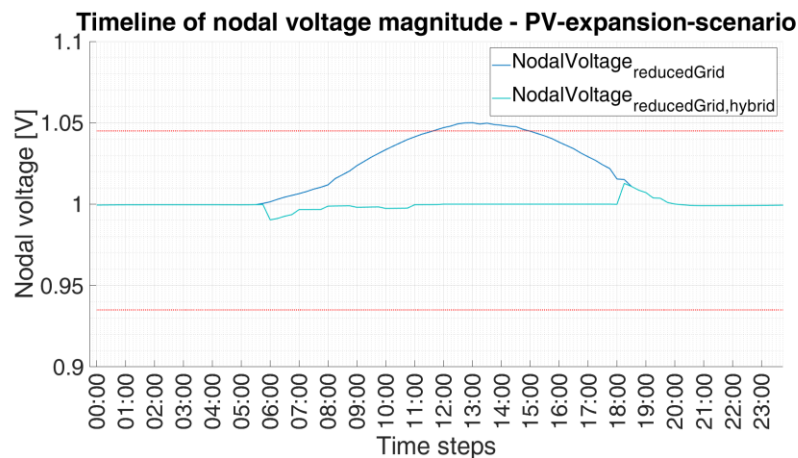

Figure 8: Timeline of the nodal voltage magnitude of the marked cell in the PV expansion scenario with hybrid conversion for voltage stability

To summarize, network reduction within the cellular approach can decrease calculation time and, with appropriate cell division, still enable adequately and accurately assessing voltage stability and, in general, power quality. Therefore, aggregated networks within the cellular approach can be used to analyze, for example, PV expansion-scenarios. As the test network in this work shows, power quality may be an issue for extensive PV expansion at certain network nodes. However, by using hybrid flexibility options in combination with corresponding storage units it is possible to maintain voltage stability within the grid and at the same time to further increase the expansion of renewable energy.

ACKNOWLEDGEMENT

BIBLIOGRAPHY

[1]   Kriechbaum, L.; Scheiber, G.; Kienberger, T. (2018): Grid-based multi-energy systems – modelling, assessement, open source modelling framework and challenges. In: Energ Sustain Soc 8 (1), S. 244. DOI: 10.1186/s13705-018-0176-x.

[2]   Appelrath, H.J.; Lehnhoff, S.; Rohjans, S.; König, A. (2012): Hybridnetze für die Energiewende – Forschungsfragen aus der Sicht der IKT. In: acatech – DEUTSCHE AKADEMIE DER TECHNIKWISSENSCHAFTEN.

[3]   Böckl, B.; Greiml, M.; Leitner, L.; Pichler, P.; Kriechbaum, L.; Kienberger, T. (2019): HyFlow – A Hybrid Load Flow-Modelling Framework to Evaluate the Effects of Energy Storage and Sector Coupling on the Electrical Load Flows. In: Energies 12 (5), S.956. DOI: 10.3390/en12050956.

[4]   Böckl, B.; Kriechbaum, L.; Kienberger, T. (2016): Analysemethode für kommunale Energiesysteme unter Anwendung des zellularen Ansatzes. In: 14. Symposium Energieinnovation (EnInnov2016).

[5]   Vopava, J., Koczwara, C., Traupmann, A., Kienberger, T.: Investigating the Impact of E-Mobility on the Electrical Power Grid Using a Simplified Grid Modelling Approach. In: Energies 13 (1), DOI: 10.3390/en13010039.

[6]   Papaemanouil, A.; Andersen, G.: On the reduction of large power system models for power market simulations. In: 17th Power Systems Computation Conference Stockholm.

[7]   Gavrilas, M.; Ivanov, O.; Gavrilas, G.: REI Equivalent Design for Electric Power Systems with Genetic Algorithms. In: WSEAS TRANSACTIONS on Circuits & Systems (October 2008), Issue 10, Volume 7.

[8]   Deckmann, S.; Pizzolante, A.; Monticelli, A.; Scott, B.; Alsac, O.: Studies on Power System Load Flow Equivalencing. In: IEEE Transactions on Power Apparatus and Systems (Nov/Dec 1980), Volume PAS-99, No.6, pp. 2301-2310.

[9]   ISO EN 50160, 2011, „Voltage Characteristics in Public Distribution Systems".

[10]   Taljan, G.; Krasnitzer, M.; Strempfl, F.; Jarz, A.: Spannungsniveau im 30-kV Netz UW Judenburg/West – Lösungsansätze mit Smart Grids. In: 12. Symposium Energieinnovation (EnInnov2012).

[11]   Kaufmann, T.; Bothe, D.; Gawlik, W.; Ponweiser, K.: Optimierung der Lastflüsse in urbanen Hybridnetzen, In: 9. Internationale Energiewirtschaftstagung (IEWT 2015).

CIRED 2021 (Status: Accepted)

TRAUPMANN, A.; GREIML, M.; KIENBERGER, T., *Equivalent Cellular-based Electrical Network Models for Voltage Regulation using Hybrid Conversion Technologies at the Medium-Voltage Level*, In: Conference Proceedings CIRED 2021, Paper 0304.

Table A. 1: Author statement to second conference contribution (CIRED)

Activity	Contribution authors (main author is mentioned first)
Conceptualization	A. Traupmann, T. Kienberger
Methodology	A. Traupmann, T. Kienberger
Data Curation	A. Traupmann, M.Greiml
Software Development and Validation	M. Greiml, A. Traupmann
Modeling	A. Traupmann, M.Greiml
Visualization	A. Traupmann
Writing (Original Draft)	A. Traupmann
Writing (Review and Editing)	A. Traupmann, T. Kienberger

Equivalent cellular-based electrical network models for voltage regulation using hybrid conversion technologies at the medium-voltage level

Anna Traupmann[1][*], Matthias Greiml[1], Thomas Kienberger[1]

[1]*Montanuniversitaet Leoben, Chair of Energy Network Technology, Franz-Josef-Straße 18, 8700 Leoben, Austria*
*anna.traupmann@unileoben.ac.at

Keywords: ELECTRICAL NETWORKS, RENEWABLE ENERGY SOURCES, NETWORK REDUCTION, CELLULAR APPROACH, HYBRID FLEXIBILITY OPTIONS

Abstract

Expanding and integrating renewable energy sources (RES) challenges today's energy systems, especially, electrical grids. Therefore, efficient RES integration methods have to be developed. This work chooses a multi-energy systems (MES) approach using the modelling framework HyFlow, developed at the Chair of Energy Network Technology. For this approach, simplified cellular-based electrical network models are developed using a specific network reduction method that enables these models to be used as an equivalent of the complex original grid since it shows equal electrical behaviour. As an example, this work uses a medium-voltage European test grid with massive volatile RES (wind and photovoltaic) expansion. This will show how this method can stabilize the grid and improve power quality using hybrid flexibility technologies (heat pumps (HP) and Power-to-Gas units (PtG)). Thus, grid expansion measures can be avoided, and self-sufficiency can be increased by this approach.

1 Introduction

Integrating renewable energy sources (RES) into electrical grids requires efficient implementation approaches, since especially volatile and unpredictable RES, such as wind and solar power, will have to increase on a large scale to meet the climate goals. The fluctuations in power generation occurring due to these RES put strain on electrical grids and may cause power quality issues as well as grid congestions. [1-3] Solution approaches for enabling grid-friendly operation and at the same time advancing RES expansion are, for example, multi-energy systems (MES), which relieve electrical grids by shifting surplus electrical energy into another energy carrier network. The MES modelling framework HyFlow [4,5] supports the integration of RES into electrical grids by using a cellular approach for the modelling of different energy carrier networks providing spatial resolution reduction to enable faster calculations and creating coupling points between energy carrier grids. [5] This paper presents a study of a medium-voltage grid, showing how hybrid technologies can be used to enhance power quality issues caused by RES and increase self-sufficiency.

2. Methodology

2.1 Cellular Modelling Approach and Network Reduction
Integrating different energy carrier models into one framework, like HyFlow, requires a modelling approach that is generic and modular in its application. A cellular approach offers this possibility and supports spatial resolution reduction to allow reasonable calculation times

of expanded networks with fine temporal resolution. By combining or deleting electrical network elements (nodes and lines) it allows for a grid representation that enables advantages for cross-energy carrier networks. The real network is divided into energy cells representing the lowest system level for which energy balancing using corresponding residual loads $P_{res}(t)$ (by e.g., 15-minute-values) can be achieved. [5-7] The residual load $P_{res}(t)$ is defined as the difference between load $P_{load}(t)$ and generation $P_{gen}(t)$, as shown in Equation (1). [5]

$$P_{res}(t) = P_{load}(t) - P_{gen}(t) \tag{1}$$

A defined set of network nodes is assigned to each cell, depending on geographical aspects. Size, location, and number of assigned nodes of each cell depend on the application purpose. For each cell consumer and generation units are aggregated into a fictitious node in the cell centre to be represented by a small set of parameters. [5-7] Thus, the level of detail of the network model is decreased, however, information influencing the electrical behaviour is lost and has to be compensated using network reduction. The lost information refers to the line losses of the neglected lines within the cells. A specifically developed network reduction method is used to replicate these losses using a compensation module to represent the total line losses of each cell. The module is parameterized using the electrical line parameters (R, L and C) of the neglected lines (Fig. 1). This method allows for the less complex cell model to be used equivalently to the real network and its use in HyFlow. Fig. 1 shows the cellular approach including the network reduction method. [8]
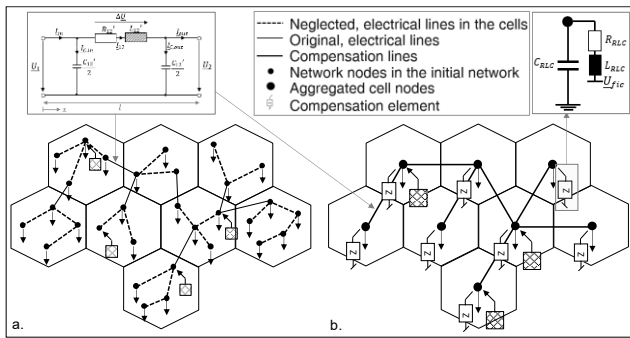
Fig 1: Cellular Modelling Approach with integrated compensation modules using network reduction

2.2 Test Network Description

The used test network represents a 20 kV-medium-voltage public power distribution grid developed from literature data. [9] Fig. 2 shows the original test network including the chosen cell division for the expansion scenario and the corresponding reduced cell model depicted in NEPLAN [10].
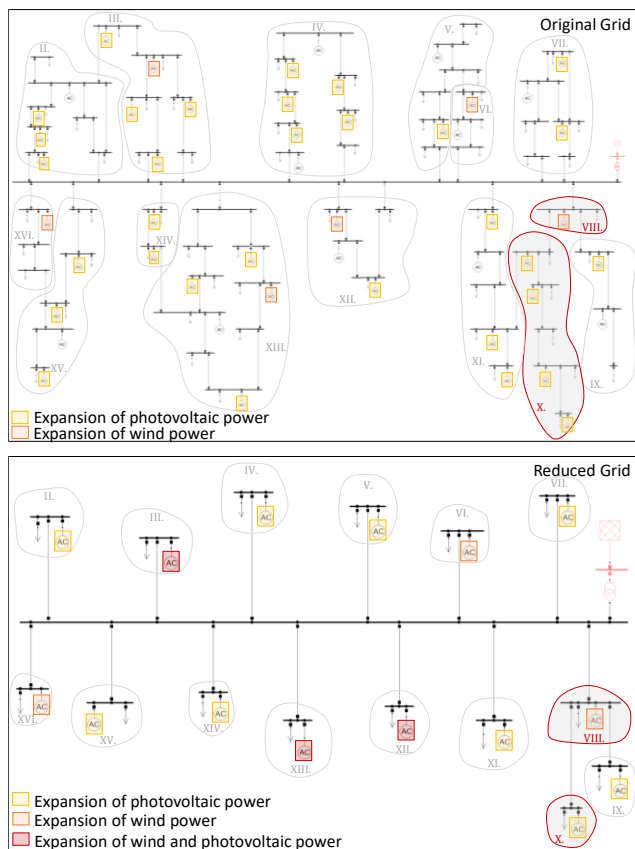

Fig. 2: Original network with cell division and PV/wind expansion and corresponding reduced model

The original network consists of 74 network nodes with 64 consumer units (local substations and commercial consumers represented by standard and synthetic load profiles) and 15 generation units (solar power, biomass plants, geothermal power plants and run-of-river power stations). A closer description of the network and its

parameters can be found in [9]. The original test network is reduced to 16 cells (reduction of network size by 78.38 %), thereby, accelerating calculation times by 96.35 %. This work develops an expansion scenario in which the share of photovoltaic (PV) and wind power units is massively increased in the test network compared to its current state described in [9]: Each commercial consumer unit is equipped with a corresponding PV system, additionally, existing wind power plants are expanded and new wind sites are added. For the analysis two cells (Cell VIII and Cell X) are chosen, which are marked in Fig. 2. While the renewable expansion in Cell VIII is an enlargement of the existing wind power plant, PV-system installations are used for the expansion in Cell X.

Due to the volatile renewable expansion a voltage increase is detected for the node in Cell VIII (Fig. 4) and Cell X (Fig. 5). However, to ensure a stable energy supply, the nodal voltages must be within the tolerance range (0.935-1.045 p.u.) of the nominal voltage. If these limits are exceeded, e.g., due to increased renewable generation, overvoltages occur which can damage electrical equipment and cause power quality issues as well as voltage instability.

2.3 Hybrid Flexibility Options

MES offer many advantages such as cascaded energy use and increased energy system efficiency as well as stability by using synergies and coupling different energy carrier networks. [2,3,5] The hybrid flexibility options implemented at the cell nodes, to achieve these advantages, are Power-to-Gas (PtG) units and heat pumps (HP). Therefore, besides PV-units (section 2.2), each commercial consumer is given a heat demand, which is covered by the corresponding HP. PtG units are implemented in cells where only wind power is expanded.

HyFlow uses a rule-based approach for the operation of hybrid flexibility units. This approach distinguishes between cell-serving and system-serving operation. Cell-serving elements aim to minimize the residual load of the corresponding cell, while system-serving elements aim to minimize the residual load of the overall system. HPs follow a cell-serving operation strategy in HyFlow, thus, they operate if there is heat demand or surplus electricity available within that cell. Therefore, to enable maximum stability support by ensuring that the electrical surplus energy of these cells can be converted to heat even if there is no heat demand at that time, a significantly oversized heat storage unit is implemented together with the HP in this work. PtG units, however, are operated in a system-serving strategy. This means that they operate if consumption and generation within the overall system is unbalanced. In this case, to ensure maximum stability support by the PtG units, the produced gas is fed into a connected gas pipeline storing the produced gas unlimitedly. [4]

2.4 KPIs for Energy Balancing in Cellular-Based Networks

In order to evaluate the efficiency of energy use and, thus, energy balancing within each cell, energy indicators are utilized. These energy indicators (energy self-sufficiency

ε_{ESS}, power self-sufficiency ε_{PSS} and energy self-consumption ratio ε_{SCR}) are explained based on the loads and generations of Cell X. In Fig. 3, $P_{gen}(t)$ represents the power that is provided from local generation in Cell X for the respective time step t. E_{gen} indicates the area under the $P_{gen}(t)$ curve representing the generated energy for the time period. $P_{load}(t)$ from Fig. 3 represents the locally consumed electrical power of Cell X, the area under this curve, therefore, indicates the consumed energy E_{load}. The intersection of E_{gen} and E_{load} represents the self-consumption E_{SC}, meaning the energy that is generated and directly consumed within that cell. The self-consumption is defined according to Equation (2). [11]

$$E_{SC} = \int min\{P_{load}(t), P_{gen}(t)\}\, dt \qquad (2)$$

The degree of energy self-sufficiency ε_{ESS} indicates how much of the locally generated energy E_{gen} can be locally consumed E_{load} (Equation (3)). Since generated energy quantities can be much higher than the consumed energy, ε_{ESS} can show values above 100 %. The degree of power self-sufficiency ε_{PSS} enables an analysis of the share of self-consumption E_{SC} in relation to the local energy consumption E_{load} (Equation (4)). ε_{PSS}, therefore, can never be higher than 100 %. Similarly, the energy self-consumption ratio ε_{SCR} allows analysing the share of self-consumption E_{SC} in relation to the locally generated energy E_{gen}, which limits ε_{SCR} to a maximum of 100 % (Equation (5)). [11]

$$\varepsilon_{ESS} = \frac{E_{gen}}{E_{load}} = \frac{\int P_{gen}(t)dt}{\int P_{load}(t)dt} \qquad (3)$$

$$\varepsilon_{PSS} = \frac{E_{SC}}{E_{load}} = \frac{\int min\{P_{load}(t), P_{gen}(t)\}\, dt}{\int P_{load}(t)dt} \qquad (4)$$

$$\varepsilon_{SCR} = \frac{E_{SC}}{E_{gen}} = \frac{\int min\{P_{load}(t), P_{gen}(t)\}\, dt}{\int P_{gen}(t)dt} \qquad (5)$$
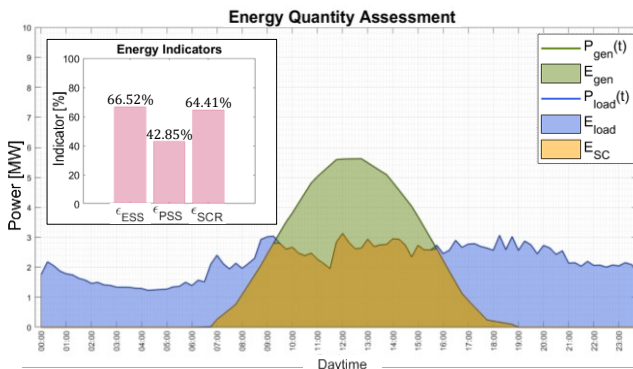

Fig. 3: Energy indicators ε_{ESS}, ε_{PSS} and ε_{SCR} on the example of Cell 10

Using storages or hybrid conversion technologies can increase the shares of the energy indicators and, thus, increase energy efficiency.

3 Results

3.1 Expansion Scenario – Base Case

The following figures, Fig. 4 and 5, show the aggregated electrical profiles, energy quantities and the resulting overvoltages for Cell VIII and Cell X discussed in section 2.2.
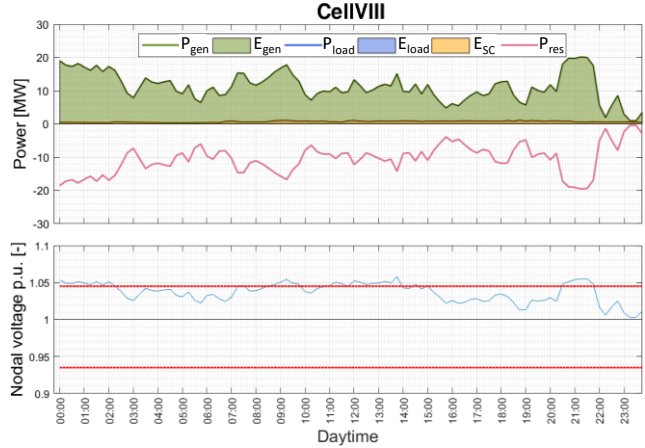

Fig. 4: Electrical profile of Cell VIII and the corresponding nodal voltage time-series before hybrid conversion
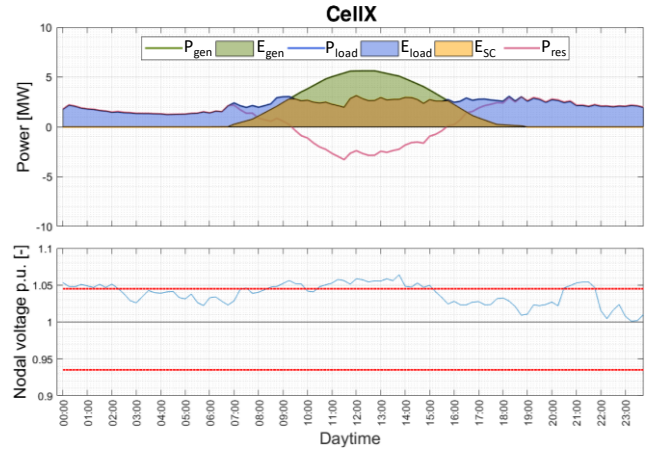

Fig. 5: Electrical profile of Cell X and the corresponding nodal voltage time-series before hybrid conversion

To compensate these voltage limit exceedings due to increased integration of RES into the electrical grid, hybrid elements are implemented at the corresponding cell nodes.

3.2 Prevention of Voltage Limit Violations

The hybrid elements described in section 2.3 implemented within the reduced cellular-based test network model are used in a hybrid load flow calculation in HyFlow. This aims to stabilize nodal voltages within the grid and increase self-sufficiency within single cells as well as the overall system. Thus, Fig. 6 shows the residual load after hybrid conversion $P_{res,hybrid}(t)$ as well as the higher electrical load $P_{load}(t)$ obtained due to the installed PtG unit within Cell VIII. Additionally, it depicts the voltage profile for the corresponding cell node. As can be seen in Fig. 6, the implemented PtG unit enables a smoothed nodal voltage

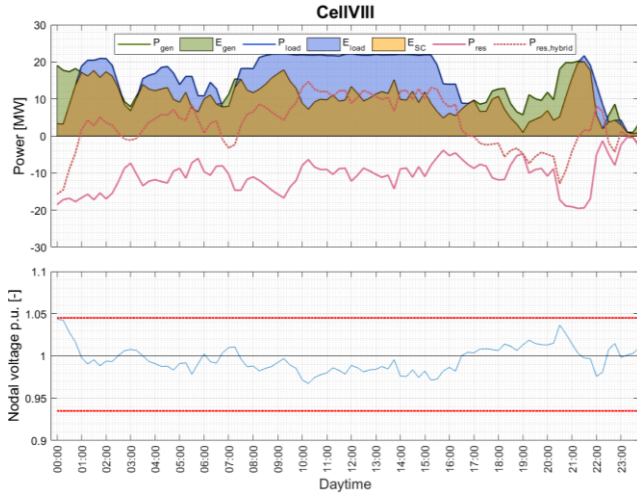profile over the examined period of time, showing no overvoltages.

Fig. 6: Electrical profile of Cell VIII and the corresponding nodal voltage time-series after hybrid conversion

Since the services of PtG units cannot be derived directly from a cell-level consideration due to its system-serving operating strategy, Fig. 7 shows how the implemented PtG units within the entire test grid can serve to reduce the residual load at the Slack-node (system boundary). The residual load $P_{res,Slack,hybrid}(t)$ in Fig. 7, however, also includes the influence caused by the implemented HPs within the overall system and is obtained using Equation (6). The load provided by PtG and HP sums up to $P_{conv,hybrid}(t)$.

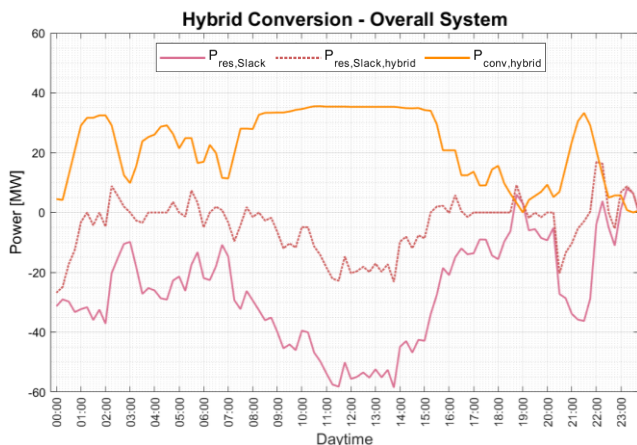$$P_{res,Slack,hybrid}(t) = P_{res,Slack}(t) + P_{conv,hybrid} \qquad (6)$$

Fig. 7: Hybrid conversion within the overall system at the system boundaries (Slack-node)

The cell-serving operating strategy of the implemented HPs can be observed directly, based on the load and generation situation present within the cell, which is shown on the example of Cell VIII in Fig. 8. Fig. 8, thus, displays the residual load after hybrid conversion $P_{res,hybrid}(t)$ as well as the additional electrical load $P_{load}(t)$ needed to produce the

demanded heat by the installed HP of Cell X. Additionally, Fig. 8 depicts the obtained voltage profile of Cell X due to the hybrid conversion. However, since Cell X is the subsequent in the feeder after Cell VIII, its voltage profile is mainly influenced by the smoothed nodal voltage of Cell VIII. Thus, it primarily shows the implications of the PtG unit on the nodal voltage of Cell VIII. Due to the HP and corresponding heat storage, the additional voltage increase caused by high PV-generation around noon can be minimized since most of the negative residual load can be compensated. As a result, violations of voltage limits can successfully be prevented.
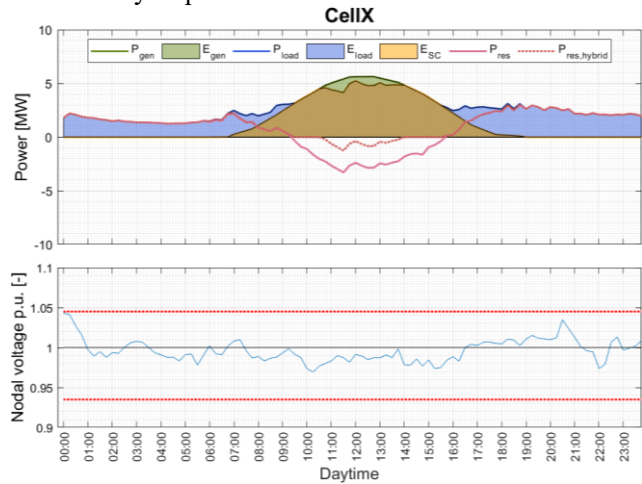

Fig. 8: Electrical profile of Cell X and the corresponding nodal voltage time-series after hybrid conversion

3.3 Energy Balancing

As discussed in section 2.1, a cellular approach can be used to enable efficient energy balancing. Additionally, section 2.3 discussed how MES can increase energy efficiency. Thus, as demonstrated in section 2.4, Fig. 9 shows the energy indicators (energy self-sufficiency $\mathcal{E}_{ESS}$, power self-sufficiency $\mathcal{E}_{PSS}$ and energy self-consumption ratio $\mathcal{E}_{SCR}$) for Cell VIII. Before hybrid conversion, the energy self-sufficiency $\mathcal{E}_{ESS}$ of Cell VIII has a high share of 1536.70 %, which is due to the expansion of wind power within that cell. While the share of power self-sufficiency $\mathcal{E}_{PSS}$ is 100 %, the energy self-consumption ratio $\mathcal{E}_{SCR}$ is very low (6.51 %). This indicates that, although $\mathcal{E}_{ESS}$ and $\mathcal{E}_{PSS}$ are high, the energy use within Cell VIII is not efficient, due to the high amount of surplus renewable energy that cannot be used locally within the cell.
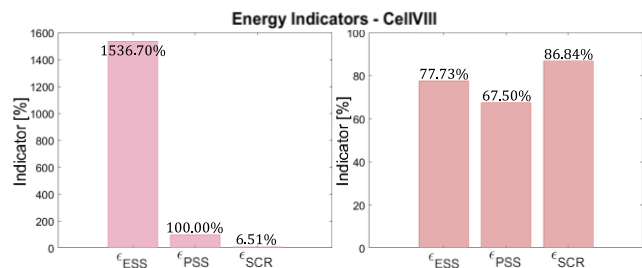

Fig. 9: Energy indicators before (left) and after (right) hybrid conversion within the energy system for Cell VIII

After the hybrid conversion (Fig. 9 (right)), the energy indicators show that the energy use within the cell has increased due to the additional power converted in the PtG unit. This shows that, although the PtG unit is operated using a system-serving strategy minimising the residual load of the overall system and, thus, increasing energy use, it also enhances energy use within single cells.

The energy indicators for Cell X before the hybrid conversion (Fig. 10 (left)) already show efficient energy use with an energy self-sufficiency $\mathcal{E}_{ESS}$ of 66.52 %, a power self-sufficiency $\mathcal{E}_{PSS}$ of 42.85 % and an energy self-consumption ratio $\mathcal{E}_{SCR}$ of 64.41 %. However, as can be seen in Fig. 10 (right), energy use within Cell X can be further enhanced due to the hybrid conversion. The lower values for the energy indicators of Cell X, compared to Cell VIII, are due to the distribution of load and PV-generation within the cell. The electrical energy demand E_{load} is distributed over the entire period of time, while the high PV-generation E_{gen} is only available during daytime. This limits the energy self-consumption E_{SC} and decreases the shares of the energy indicators.
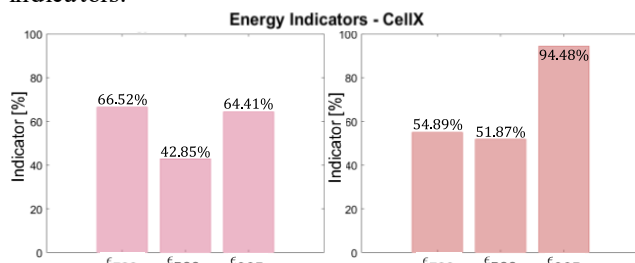

Fig. 10: Energy indicators before (left) and after (right) hybrid conversion within the energy system for Cell X

Although, the share of energy self-sufficiency is lower after hybrid conversion (54.89 %), which is due to the higher energy demand caused by the HP, the energy can be used more efficiently. Especially, the energy self-consumption ratio is very high (94.48 %), indicating that most of the generated energy within Cell X can be used directly within the cell. This reduces the residual load within the cell and, therefore, grid congestions due to energy transportation over the electrical lines between cells.

4 Conclusion

This work presents a study on how innovative approaches (multi-energy systems) and tools (cellular-based electrical networks with network reduction and the hybrid modelling framework HyFlow) can help overcome the challenges of a sustainable energy future. The results obtained from the hybrid load flow calculations show, that hybrid conversion technologies can be used to stabilize voltages and increase power quality. MES can also be used to increase the efficiency of energy use within the energy system. Therefore, the analysis of key energy indicators (energy self-sufficiency $\mathcal{E}_{ESS}$, power self-sufficiency $\mathcal{E}_{PSS}$ and energy self-consumption ratio $\mathcal{E}_{SCR}$) on cell-level shows that by

using hybrid conversion technologies, the cellular self-sufficiency can be enhanced. This suggests, that hybrid conversion technologies provide multiple advantages for the future challenges during energy transition.

5 Acknowledgements

6 References

[1] Papadis, E.; Tsatsatsaronis, G.: ‚Challenges in the decarbonization of the energy sector', Energy, 2020, 205, pp. 1-15.

[2] Kriechbaum, L.; Scheiber, G.; Kienberger, T.: ‚Grid-based multi-energy systems – modelling, assessment, open source modelling frameworks and challenges ', Energy, Sustainability and Society, 2018, 8, (35), pp. 1-19.

[3] Mancarella, P.: 'MES (multi-energy systems): An overview of concepts and evaluation models', Energy, 2014, 65, pp. 1-17.

[4] Greiml, M.; Traupmann, A.; Sejkora, C.; Kriechbaum, L.; Böckl, B.; Pichler, P.; Kienberger, T.: 'Modelling and model assessment of grid-based Multi-Energy Systems', International Journal of Sustainable Energy Planning & Management, 2020, 29, pp. 7-24.

[5] Böckl, B.; Greiml, M.; Leitner, L.; Pichler, P.; Kriechbaum, L.; Kienberger, T.: 'HyFlow - A Hybrid Load Flow Modeling Framework to Evaluate the Effects of Energy Storage and Sector Coupling on the Electrical Load Flows', energies, 2019, 12, p.25.

[6] Vopava, J.; Koczwara, C.; Traupmann, A.; Kienberger, T.: ‚Investigating the impact of e-mobility on the electrical power grid using a simplified grid modeling approach ', energies, 2020, 39, p.25.

[7] 15. Vopava, J.; Böckl, B.; Kriechbaum, L.; Keinberger, T.: ‚Anwendung zellularer Ansätze bei der Gestaltung zukünftiger Energieverbundsysteme', *e&i* Elektrotechnik & Informationstechnik, 2017, 134, (3), pp. 238-245.

[8] Traupmann, A.; Kienberger, T.: 'Novel Network Reduction Method for Cellular-Based Networks with High Modelling Accuracy for Multi-Energy System Approaches' (under submission), 2021.

[9] Traupmann, A.; Kienberger, T.: ‚Test Grids for the Integration of RES – A Contribution for the European Context', energies, 2020, 13, p.29.

[10] NEPLAN-Smarter Tools. https://www.neplan.ch/ (accessed on 18th Febuary 2021).

[11] Böckl, B.; Kienberger, T.: 'Nutzergruppenabhängiger Photovoltaik-Heimspeicherbedarf'. 15th Symposium Energieinnovation, Graz, February 2018, pp. 6.

Paper 3 (Status: Accepted)

Table A. 1: Author statement to third peer-reviewed publication (Paper 3)

Activity	Contribution authors (main author is mentioned first)
Conceptualization	A. Traupmann, T. Kienberger
Methodology	A. Traupmann, T. Kienberger
Data Curation	A. Traupmann, M. Greiml, J. Steinegger
Software Development and Validation	A. Traupmann, M. Greiml, J. Steinegger
Modeling	A. Traupmann
Visualization	A. Traupmann, L. Kühberger
Writing (Original Draft)	A. Traupmann
Writing (Review and Editing)	A. Traupmann, T. Kienberger

ORIGINAL RESEARCH

天津大学
Tianjin University

IET
The Institution of
Engineering and Technology

WILEY

Analysing sector coupling technologies for Re-purposing coal-fired power plants–Case study for the ENTSO-E grid

Anna Traupmann [ORCID] | Matthias Greiml | Josef Steinegger | Lisa Kühberger | Thomas Kienberger

Chair of Energy Network Technology, Montanuniversitaet Leoben, Leoben, Austria

Correspondence

Anna Traupmann, Chair of Energy Network Technology, Montanuniversitaet Leoben, Franz-Josef-Strasse 18, 8700 Leoben, Austria.
Email: anna.traupmann@gmx.at

Funding information

European Commission

Abstract

The high emission intensity of coal-fired power plants (CFPP) leads to the inevitable next step towards energy transition, the coal phase-out. One challenge is the subsequent use of still-functioning assets. Re-purposing these assets avoids value loss and creates new opportunities for coal regions. Therefore, this study considers the sector coupling technologies Power-to-Gas (PtG) and Gas-to-Power (GtP) as re-purposing options. First, a multi-variable Mixed-Integer Linear Programming optimisation model is established. This model includes the participation of the plant in the current (2020) and future (2030, 2040) electricity and natural gas spot-markets and the balancing power market while fulfilling existing contracts, and allows for determining the re-purposing technologies' operating profiles. By applying a techno-economic analysis, investment recovery periods of the considered re-purposing technologies are assessed, which range between two (GtP) and over ten (PtG) years. A sensitivity analysis accounting for current energy prices and technological advancements reveals capital expenditure has the highest impact on this Return-On-Investment period. Additionally, a case study considering the Austrian energy grids is performed to account for the grid impact of integrating these technologies at former CFPP sites. Thus, it is found that the investigated sector coupling technologies have the potential to compensate for grid congestions even in profit-optimised operation.

KEYWORDS

coal phase-out, combined cycle gas turbine, energy markets, mixed-integer linear programming, power-to-gas

1 | INTRODUCTION

Coal represents the most common fossil fuel resource and is the largest source for electricity generation, providing about 37% of the global electricity demand [1]. Additionally, coal electricity generation is considered reliable and cost-effective [2]. However, since coal is also the most carbon-intensive fossil fuel, currently accounting for more than 30% of global CO_2 emissions [3], coal-fired electricity generation is under political and economic pressure [2]. Therefore, the coal phase-out [4] is an inevitable next step for European countries to rapidly achieve climate neutrality of the electrical energy system [4]. To remain within the carbon budget of the Paris Agreement [5], 72% of the CFPPs operating in 2020 within the

European Union (EU) have to be shut down by 2025 [4, 6]. While more than 30% of the European countries already have coal-free power generation, the coal phase-out is not even under discussion in 24% of the European countries. A more detailed description of the coal phase-out trends in Europe can be seen in Figure 1. According to the individual national phase-out plans, 63% of the European countries are expected to generate coal-free electricity by 2030 [7].

The coal phase-out, however, leads to the early closure of existing coal-fired power plant (coal-fired power plants (CFPP)) sites before they reach end-of-life. Thus, the coal phase-out entails the risk of leaving valuable assets (e.g. infrastructure, staff etc.) and expensive commitments (e.g. supply and disposal contracts) behind [8]. These non-coal-related assets (including
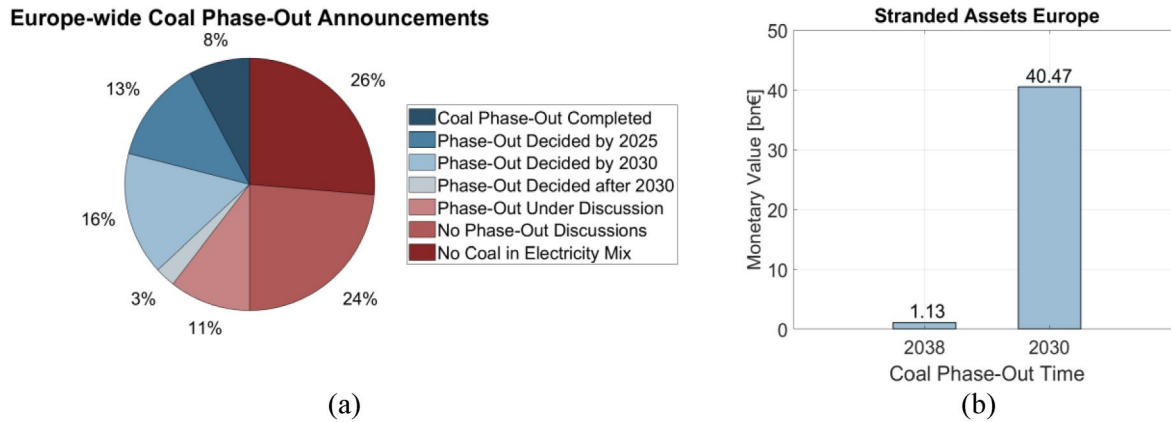
FIGURE 1 (a) Trends of the coal phase-out within the EU27 (data taken from [7]) and monetary value of stranded assets [4, 12, 13].

infrastructures such as power grid, gas grid, and district heating grid connections, road-, train, or harbour connections, and substantial industrial accessed area as well as steam turbo-generator systems, condenser cooling systems, electrical equipment, cooling towers, pump houses, and auxiliary buildings) represent the key value of decommissioned sites [9, 10]. The mentioned components have a lifetime of about 35–50 years if maintained accordingly. Therefore they are very likely to still have operating permission after decommissioning the CFPP [9]. These so-called "stranded assets" rapidly lose their value or may even become liabilities [11]. The monetary value of these stranded assets for the currently over 300 CFPPs in the European Union (EU27) [4] amounts to an estimate of € 1.13 billion (scaled-up values for Europe from the data given in Ref. [4, 12, 13] for Germany). The € 1.13 billion in stranded assets is obtained if the phase-out is accomplished by 2038, which is the goal for Germany [7], Europe's largest coal consumer [14]. However, if the European phase-out is achieved by 2030, this estimated monetary value of the stranded assets would amount to € 40.47 billion (scaled-up values for Europe from the data given in Ref. [4, 12, 13] for Germany). This estimation also strongly depends on the remaining useful lifetime of the components [9] and can be seen in Figure 1.

Due to their already mentioned infrastructures, the sites offer optimal conditions for implementing new sustainable technologies. As a result, re-purposing provides numerous advantages compared to plant decommissioning. Reusing the existing infrastructures can save local jobs and tax revenue and ensure economic stability during the energy transition [15]. This may also lower the barriers to exiting the coal industry [16]. Additionally, re-using these components prevents the stranding of assets by up to 40% of the initial investment costs of a newly built CFPP [9]. Consequently, it is the priority of the power plant operator to retain as many assets as possible [15]. Therefore, the site's available support and infrastructure represent key factors for subsequent re-purposing with sustainable technologies.

Additionally, as will be described later in the paper (cf. Chapter 2.1), CFPPs cover specific tasks that are neglected after decommissioning, for example, grid support [17, 18].

Therefore, the European coal phase-out also impacts the grids within the interconnected ENTSO-E grid area.

Since this work is focussed on further researching the re-purposing of CFPPs, it contributes to the United Nation's Sustainable Development Goals 7 (Affordable & Clean Energy), 9 (Industry, Innovation & Infrastructure), and 13 (Climate Action) [19]. Re-purposing CFPPs enables modernising energy infrastructures for a sustainable future energy generation, enhancing Renewable Energy Source (RES) expansion and supporting the regional economic development of coal regions. Thus, it is an essential instrument to advance emission mitigation and energy transition.

1.1 | State of research

1.1.1 | Re-purposing of coal-fired power plants

Re-purposing, re-powering, or retrofitting of coal-fired power plant (CFPP) assets describe the process of sustainably utilising the existing plant equipment of decommissioned or end-of-life CFPPs after their coal phase-out [9, 20]. While re-purposing entails adapting and utilising the existing assets for a new purpose, that is, for a different technology, re-powering refers to replacing parts of an old plant to extend system life. Retrofitting, however, describes adding or integrating new technology assets to an existing system [9]. However, these re-utilisation processes always entail retaining plant components with existing operating permissions for economically and environmentally sustainable applications [20]. The following retrofitting and re-purposing options are presented:

Fuel switch
So far, the most common retrofitting option is fuel switching from coal to natural gas to reduce its CO_2-emissions [9]. This is because the method is already proven, the technological challenges are known and manageable [21], and the entire existing CFPP can be re-used [9].

Retrofitting using a fuel switch to biomass [22] requires a replacement of the fuel handling and input system, the

pre-treatment, and the burning system to enable a 100% retrofit [23]. However, a partial or complete substitution of coal with biomass is currently one of the main retrofitting options for CFPPs with existing experience of co-firing biomass in the coal industry [2]. Several recent studies and projects are dealing with biomass retrofitting for CFPPs: Reumann et al. (2019) [2] present case studies for total biomass retrofitting in fossil-fired power generation and combined heat and power (CHP) units utilised for the currently ongoing Biofit project [24]. Rutz et al. (2020) [25] include a list of already retrofitted CFPPs to biomass plants, and Tzelepi et al. (2020) [23] conducted a Strength, Weakness, Opportunities and Threats analysis for the retrofitting process with biomass pointing out that the major issue with this technology is biomass availability, in particular, for large-scale CFPPs [23]. It is also possible to switch to other fuels, such as petroleum coke [21]. Retrofitting plants with fuel switch technologies is often economically sound. However, only a particular share of coal is usually replaced, which reduces but does not avoid CO_2 emissions [22]. Therefore, a fuel switch may be considered a transitioning option for CFPPs [22].

Integrated Gasification Combined Cycle (IGCC)

Integrated Gasification Combined Cycle (IGCC) is currently a widespread re-powering option for power utilities since it reduces CO_2-emissions and provides additional operational flexibility [22, 26]. In an IGCC, preliminary, there is a sub-stoichiometric fuel gasification (e.g. coal, biomass, or waste) before the main gas and steam process. This results in raw gas, which is then fed into the water-steam cycle of the power plant [26]. The conventional CFPP can be restructured into an IGCC plant, as described in the transition paths for CFPPs, according to Song et al. (2021) [22]. However, this involves high costs and can also not be considered a full re-powering technology as it only serves to mitigate CO_2 emissions to a certain extent [22].

Renewable energy sources, battery storage, and ancillary services

Re-purposing decommissioned or end-of-life CFPP can also support RES expansion as already assessed areas become available. However, more importantly, regarding the expansion of RES, the CFPP sites may provide ancillary services for the grid. Thereby, for example, the existing generator can be used as a synchronous condenser to provide reactive power support for the grid, ancillary services, or grid inertia [16, 22].

Another option is turning a decommissioned CFPP into large stationary battery storage plants using, for example, Second-Life-Batteries from electric vehicles (EV) to expand volatile RES [27]. Second-Life-Battery applications are a vital part of a circular economy. Reusing them at CFPP sites enables additional grid relieving services for grid operators while re-purposing the existing CFPP infrastructure [28].

Thermal storages for renewable energy technologies

Another re-purposing option is adding solar thermal collectors to the CFPP sites, which increase feedwater heating and lower the emission intensity of the CFPP [29]. However, this option does not qualify as a full re-purposing option since emission reductions are minimal [9]. Mills (2018) [29] outlines projects where this technology has been implemented.

A case study on the re-purposing of decommissioned CFPPs with thermal storage, storing renewable energy, which is then fed into the grid using the existing grid infrastructure at the sites, is presented in Geyer et al. (2020) [30]. This study researches how a high-temperature molten salt storage system can be integrated into a CFPP by re-using the existing Rankine steam cycle. This option provides benefits, particularly emission reduction and high flexibility to cover present residual loads and enhance system stability. This re-purposing option has not yet been implemented at a CFPP site [30].

Power-to-fuel technologies

The "Green Deployment of E-Fuels And Liquids based on CO_2 (GreenDEALCO$_2$)" project [31] supports research on the integration of power-to-fuel technologies in closed and end-of-life coal-related assets. The CO_2 needed for fuel synthesis should be provided by industrial processes near the CFPP, such as cement plants or steel mills. Thus, the GreenDEALCO$_2$ supports using stranded assets for CFPP retrofitting and CO_2 utilisation in the industrial sector. This ongoing project will provide case studies on power-to-fuel integration in Germany, Austria, and Greece, including sustainability analyses for realistic deployment prospects [31].

Tertiary utilisation

Non-technological re-purposing projects are described in Slavin et al. (2011) [32]. This report states that due to the strategic locations of CFPPs, which are mainly close to waterfronts, have railway or road connections, and (often) vicinity of urban areas, they present valuable sites for civic and private utilisation as well. This utilisation includes housing opportunities, offices, shopping buildings, parks, and other community facilities [32].

Profitability studies, accompanying measures, and initiatives

A study by the Energy Sector Management Assistance Programme (2021) [33] deals with the economic viability of CFPP re-purposing and retrofitting under consideration of a cost-benefit analysis of most of the technologies mentioned above at an exemplary site. The study concludes that there are strong economic reasons for re-utilisation, as the direct benefits outweigh the decommissioning and remediation costs of the CFPP [33].

There are also current projects focussed on further researching the re-purposing of CFPPs: The "Re-Purposing Coal Power Plants during Energy Transition (RECPP)" project [34] is funded by the European Commission. The RECPP's tasks are the mapping of coal regions as well as their sites in Europe and finding re-purposing options for the sustainable use of assets at decommissioned power plant sites [34]. The project "Just Transition Toolbox for Coal Regions (JT-Toolbox)" [35] is a German project that develops a "toolbox" for the re-purposing of CFPPs. It includes strategy development and provides recommendations for governance structures and

employment support. It also identifies technology options and highlights opportunities for the renaturation and re-purposing of CFPP lands and their infrastructure [35].

Additionally, an increasing number of initiatives addressing the issue of sustainable coal phase-out and the associated opportunities for re-purposing arise. For example, the Accelerating Coal Transition initiative as part of the Climate Investment Funds [36] provides socio-economic and infrastructural support for countries to transition away from coal [37]. Thus, it aids in tackling challenges related to national strategies, people, and communities, as well as land and infrastructure [37]. In addition, there is also the Powering Past Coal Alliance, an association of national and subnational governments, companies, and organisations working to transition from unabated coal-fired generation to clean energy [38, 39].

1.1.2 | Sector coupling integration studies

As illustrated in the previous section, the re-purposing of CFPPs to CCGTs is more common, and the operational characteristics of CCGTs are already researched in detail. Therefore, this section focuses on Power-to-Gas (PtG) and combined PtG and Gas-to-Power (PtG-GtP) applications. As no re-purposing studies are using PtG, this section summarises the state of research regarding PtG integration and modelling.

A very comprehensive study from Eveloy et al. (2018) [40] summarises different publications on deployment scenarios for PtG. These scenarios include applications on a regional or national level, as well as on a plant level, such as at industrial or power plant sites. From this summary, two studies are particularly interesting: First, Heinisch et al. (2015) [41] consider a PtG deployment application on a national level by presenting a case study for Denmark, which investigates the effects of PtG on the power grid. This study uses a PtG deployment model, which minimises the total system operation costs via a direct current (DC) optimal power flow calculation and performs a congestion analysis of the DC grid model. However, this study uses a simplified DC grid model and lacks certain boundary conditions, for example, import and export to neighbouring countries. Second, Buchholz et al. (2014) [42] investigated a study on a combined lignite CFPP and PtG unit. Thus, the original lignite CFPP is equipped with a PtG unit to increase the economic performance and viability of the CFPP. This hybridisation of the CFPP is intended to reduce the load on the CFPP during fluctuating RES supply so that the CFPP is in a constant operating state. However, this study is restricted to the power plant level, while any interactions with markets or grids are neglected.

In conclusion, Eveloy et al. (2018) [40] concluded that the following aspects are still missing in the current state of research dealing with PtG integration: [40]

- Since there is a significant potential for the integration of PtG at plant sites, such deployment scenarios must be substantiated with real-life case-by-case studies and

include synergies with industrial plants and power plant components.
- In addition, grid calculations with cross-sectoral interactions are necessary, which primarily include real-life electricity and gas and the heating grids and consider competing fuel prices (e.g. electricity and gas).
- Furthermore, it is necessary to consider a broader range of performance criteria in the deployment optimisation models of PtG, which need to include future applications like ancillary services (e.g. balancing power and grid flexibility).

Besides the deployment scenarios, recent studies differ in applied optimisation methods: A study that focuses on approaches to operational optimisation of PtG is presented by Khani et al. (2017) [43]. This study shows an operational optimisation for the day-ahead scheduling of PtG plants with a built-in gas demand forecasting algorithm. It also includes a grid consideration, but only in the case of an outage in the gas network. Ma et al. (2021) [44] present an optimal dispatch model for a CHP, PtG, and CCS system. However, the author focuses on CO_2 emission reduction rather than on enabling and analysing system integration. A more comprehensive study by Yang et al. (2020) [45] describes an integrated operational optimisation for combined cooling, heat, and power, PtG, and CCHP-PtG using an improved risk explicit interval parameter programminging approach to achieve risk minimisation and enable operational cost control. The risks considered include uncertainties in wind power output, electricity market clearing, and natural gas prices and the model also considers a microgrid.

As the previously mentioned studies only focus on arbitrage market participation, different studies also investigate application potentials for PtG units to be used for ancillary services, including balancing power and grid flexibility. Mazza et al. (2018) [46] poi out that very few papers are available in the literature considering PtG for grid service applications. However, Walker et al. (2015) [47] provide an overview of the capacity of PtG to aid in voltage and frequency regulation [48]. Witkowski et al. (2020) [49] determined the technical suitability of thermal sector coupling technologies (e.g. Combined Cycle Gas Turbine (CCGT)) for the provision of system services in selected European electricity markets and analysed expected future developments and trends. Correspondingly, Xing et al. (2018) [50] propose future research directions for modelling and optimising PtG units in terms of their potential of fulfiling grid services.

1.2 | Open research and contribution of this work

From the literature and research cited in Chapters 1.1.1 and 1.1.2, it is evident that the coal phase-out and possible re-purposing of existing CFPP assets is a current topic in current research gaining increasing traction. Although a wide variety of re-purposing options for CFPPs are already being considered in studies, projects, and implementations, few of

them [29–31] focus on sector coupling technologies. While there are many studies on sector coupling integration in general, operational optimisations rarely include the potential for balancing power provision. Most studies, particularly on PtG units, solely present the technical potential for balancing power provision instead of their actual participation in the frequency restoration (FR) markets. Additionally, the literature studies do not provide a more extensive analysis of the re-purposing options regarding their economic viability. Usually, they do not include precise simulations regarding the impact on the overall energy grid. Therefore, the following research questions have not been addressed in the literature yet:

- What is the optimal operating strategy of the selected sector coupling technologies as re-purposing options from an economic perspective considering energy and FR markets?
- What is the impact of assumed future electricity and gas price developments on the cost-optimal operation of the selected sector coupling technologies?
- What is the economic benefit of implementing the selected sector coupling technologies into existing CFPP sites with a market-optimised operation (spot-market orientated and grid service orientated)?
- What is the impact of integrating these cost-optimally operating sector coupling re-purposing technologies on the Austrian energy grids now and in the future?

To address these research questions, this work concentrates on sector coupling technologies (PtG, GtP, or a combination of both) as particularly valuable re-purposing options for CFPPs, given that infrastructural assets (primarily grid connections) are retained. Due to the limited availability of large-scale grid data, Austria is used as a case study in this work. Since the Austrian grid area is part of the ENTSO-E, the derived conclusions are also generally valid in this area and can be applied to it. This work also includes an economic analysis of the Austrian energy system for the considered re-purposing technologies.

Thus, this paper is structured as follows: Section 2 presents this paper's methodology. Subsection 2.1 characterises the Austrian CFPP sites and the selected re-purposing technologies. Subsection 2.2 then provides an overview of the energy and balancing power reserve market, the balancing energy activation market, and the assumed future energy prices. Subsection 2.3 describes the methodology for operational optimisation, the objective function, and the constraints to define the optimisation problem. Subsection 2.4 then provides a detailed description of the multi-energy system (MES) load flow simulation framework "*HyFlow*" used to assess the impact or re-purposed CFPP sites on the Austrian energy grids. Section 3 presents the results from this analysis, and Section 4 discusses them in detail. Finally, Section 5 provides the conclusions drawn from this work and offers closer insight into the advantages obtained from re-purposing decommissioned CFPPs.

2 | METHODOLOGY

This section presents this work's applied methodology, which is schematically illustrated in Figure 2. In this work, the original CFPPs are replaced with selected sector coupling technologies (PtG, GtP, or a combination of both). These technologies are designed based on the original plants' existing electrical and thermal capacities. Thus, no design optimisation is necessary in advance. In the first step, an operational optimisation of the individual technologies is carried out to maximise profits on the energy day-ahead spot market and FR reserve and activation market, as seen in Figure 2. Afterwards, the optimised operation profiles for each Austrian power plant site location Mellach, Dürnrohr, and Simmering are integrated into the MES load flow simulation framework "*HyFlow*". This program obtains and analyses the load flows in the electricity grids at the maximum- and high-voltage levels (380/220 and 110 kV). The individual components of the operational optimisation model and the load flow model shown in Figure 2 are described further in the following chapters.

2.1 | Characterisation of the coal-fired power plant sites and their re-purposing options

Besides generating electricity for customers, large CFPPs fulfil various purposes and tasks, such as providing ancillary grid services for stable electrical grid operation and grid support, waste disposal (e.g. sewage sludge firing), and heat delivery for neighbouring demand. Future sustainable re-purposing technologies (partially) have to account for these tasks. Therefore, specific requirements are demanded of the re-purposing technologies:

- Power to be generated has to be in the same capacity range as the CFPP
- Heat delivery contracts of the previous CFPP must still be fulfiled
- Central ancillary services have to be facilitated on a daily as well as a long-term basis

Austria has already ceased coal-fired power generation in the spring of 2020 and is thus one of the seven EU countries that no longer have coal in its electricity mix. Therefore, this paper focuses on the sites of Austrian CFPPs that have already been decommissioned. These include the Mellach district heating power plant [51] of the VERBUND Thermal Power GmbH & Co KG, which was closed in April 2020 [52], and the Dürnrohr thermal power plant [53] of the EVN AG, which was decommissioned in August 2019 [54]. In addition, another site is considered where a gas-fired power plant is currently in operation, the Simmering power plant of the Wien Energie GmbH [55]. Since, in the long term, CFPP and all fossil-fuelled power plants will have to be substituted with more sustainable technologies, this gas-fired power plant was also considered in this work. The same conditions and requirements exist at this
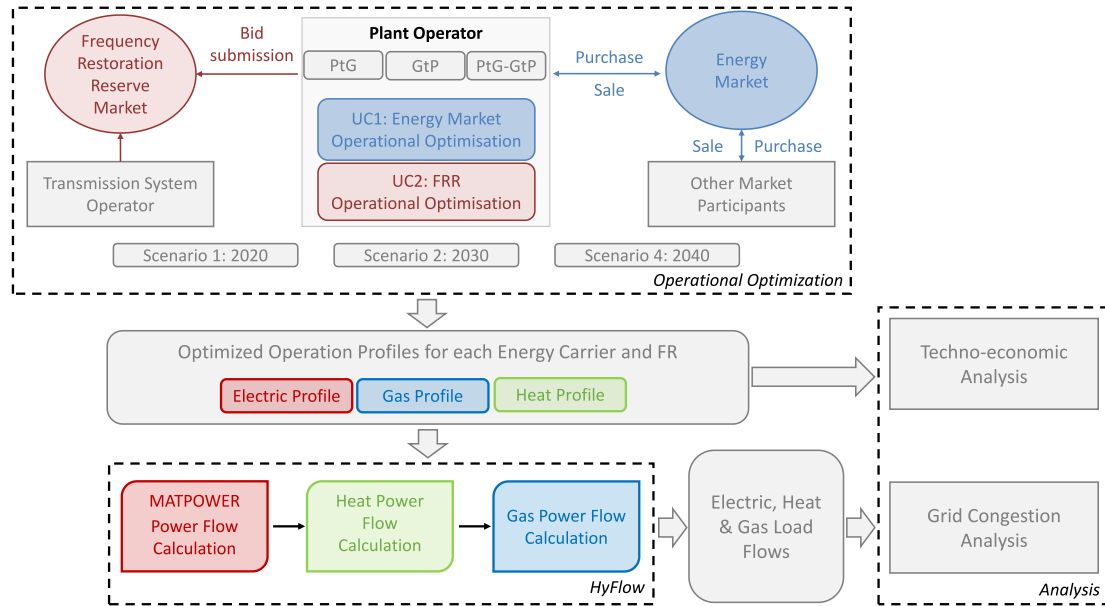
FIGURE 2 Flow chart of the performed calculations within this work

site as at the CFPP sites, which means that the same re-purposing technologies are integrated. The three sites considered in this work are presented in Figure 3, obtained from a georeferenced model of the Austrian energy system. Additionally, Figure 3 shows potential CO_2 sources from the nearby industry and biogas plants, which may provide the necessary CO_2 for the methanisation step of the PtG unit.

The selected sites are characterised in Table 1, which describes the site-specific input parameters for optimising the operating profiles.

To ensure that most tasks of the original CFPP can still be fulfiled, three re-purposing technologies are chosen for the calculations conducted in this work. These technologies enable the presented requirements to be fulfilled.

1. **Power-to-Gas (PtG),** including waste heat utilisation: The PtG unit consists of a large electrolyser and a methanisation unit to produce synthetic natural gas (SNG) from the produced hydrogen. The electrolyser has a power input corresponding to the electrical capacity of the original power plant. This work assumes that the CO_2 needed for the methanisation process is available from neighbouring industries or biogas plants in close vicinity to the site (cf. Figure 3). The produced SNG is then fed into the natural gas grid, and the waste heat of the PtG unit is utilised to supply the district heating demand of neighbouring cities.
2. **Gas-to-Power (GtP):** The GtP unit represents a CCGT power plant operated using the gas mixture provided by the natural gas grid. Since it is assumed in this work that the gas composition in the grid changes in the future (as discussed in section 2.2), the GtP unit operates with a Methane-Hydrogen (CH_4-H_2) mixture as obtained from the grid, CCGT plants allow for CHP production. Therefore the simultaneously produced heat is also utilised to supply district heating demand to neighbouring cities. CCGT
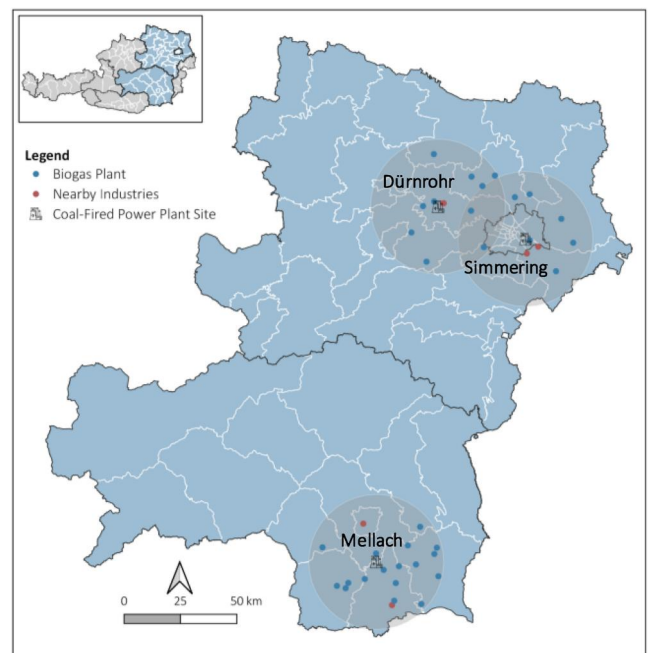
FIGURE 3 Austrian coal-fired power plants (CFPP) site locations, electricity, and natural gas grids, as well as nearby industries and biogas plants [56–58].

plants can bridge energy transition by achieving a more sustainable and less emission-intensive energy generation than FPPs [59]. Additionally, by enabling the use of a CH_4-H_2-mixture as a fuel for the GtP unit, a gradual energy-carrier transition from natural gas to climate-neutral Hydrogen can be achieved.

3. **Combination PtG-GtP:** The combined plant consists of a PtG unit and a GtP unit, as described above. Since both units are available at the site, the assumption for the

TABLE 1 Site-specific parameters for the considered power plants in Austria

Parameter		DHPP Mellach	TPP Dürnrohr	TPP Simmering
Nominal electric power	(MW$_{el}$)	246	352	760
Nominal thermal power	(MW$_{th}$)	230	405	600
District heating supply	(MWh$_{th}$)	746 658	200 000	3 327 750
		66% of the district heating demand in graz	District heating demand in St.Pölten	50% of the district heating demand in vienna

calculations within this work is that the two units cannot be operated simultaneously. Additionally, the obtained products from the units (PtG: SNG, GtP: electrical power) are fed into the grid and cannot be utilised directly as input for the other unit. However, it is possible to switch the operation between the units within each time step.

To calculate the profit-optimised operating profiles of the analysed technologies, both PtG and GtP must be defined in terms of their properties and operational characteristics. These technology parameters provided in Table 2 (PtG) and Table 3 (GtP), together with the site and energy market-specific data (cf. Chapter 2.2), then represent the input variables for the optimisation.

Using these parameters, the optimisation calculations can be set up and performed as described in more detail in chapter 2.3.

2.2 | Day-ahead energy markets, frequency restoration Reserve, and activation markets, as well as assumed future energy prices

To create economically optimised operating profiles of the individual technologies, prices of the energy purchased and supplied (electricity and natural gas) are required. "Pay-as-cleared" market prices on the day-ahead spot market are used for electricity and natural gas. For the base year 2020, corresponding electricity prices were downloaded from the Energy Exchange Austria power exchange [70]. For the years 2030 and 2040, a simplified electricity price forecast model based on literature data on expected future developments is used. The developments considered in this model are annual mean values of the electricity price [71] and the number of extreme price situations, meaning electricity prices higher than 100 €/MWh and below 0 €/MWh [72]. These developments are presented in Figure 4.

Major drivers for the electricity price development until 2040 are expected to be primary energy demand and CO_2-prices as well as feed-in from RES. As can be seen in Figure 4, it is assumed that electricity prices will increase continuously from 2030 onwards due to increasing CO_2-prices. This increase is mitigated due to higher feed-in from RES (wind and photovoltaic (PV) power) and increasingly flexible electricity demand [71]. As a result, electricity prices will become more volatile, leading to more frequent low or even negative price situations [72]. However, the Russian attack on Ukraine in

TABLE 2 Technology parameters for the optimisation of the Power-to-Gas (PtG) unit [60–63]

Parameter		Power-to-gas (PtG)		
		2020	**2030**	**2040**
Ramping rate	(%/min)	20	20	20
Power range[a]	(%)	25–100	25–100	25–100
Heat production[b]	(kWh$_{th}$/kWh$_{el}$)	0.54	0.54	0.54
Efficiency	(%)	33	47	49
Full load hours	(h)	3000–6000	3000–6000	3000–6000
Operating hours	(h)	4000–8000	4000–8000	4000–8000
System lifetime	(a)	20–30	20–30	20–30
CapEx	(€/MW)	1 543 000	1279 000	1 113 000
Annual OpEx	(€/MW)	26 470	21 995	19 290

[a]Divided by the nominal power of the unit.

[b]This value refers to waste heat generation for the Power-to-Gas units.

TABLE 3 Technology parameters for the optimisation of the Gas-to-Power (GtP) unit [64–69]

Parameter		Gas-to-power (GtP)		
		2020	**2030**	**2040**
Ramping rate	(%/min)	1.67/2.33[a]	1.67/2.33[a]	1.67/2.33[a]
Power range[b]	(%)	10–100	10–100	10–100
Heat production	(kWh$_{th}$/kWh$_{el}$)	0.60	0.60	0.60
Efficiency	(%)	55	55	55
Full load hours	(h)	7000–8000	7000–8000	7000–8000
Operating hours	(h)	Up to 8760	Up to 8760	Up to 8760
System lifetime	(a)	30–40	30–40	30–40
CapEx	(€/MW)	805 000	740 000	700 000
Annual OpEx	(€/MW)	32 200	29 600	28 000

[a]Start-up behaviour/power-down ramping rates of the technology.

[b]Divided by the nominal power of the unit.

February 2022 led to massive distortions in global energy markets. Current electricity and gas prices are higher than they are expected to be in 2050. It is unclear when and if they will return to the level before the Ukraine war. The prices used for this work are based on data published before the Ukrainian war. To also account for the current situation's impact with regard to this work's results, a sensitivity-analysis is performed.

For the development of the literature-based future electricity price time series, the annual mean values are used to calculate scaling factors for 2030 and 2040, which are then applied to scale-up the time series of electricity prices from 2020 in a quarter-hourly temporal resolution.

However, these scaled time series do not sufficiently represent the overall price situation, such as the development of extreme price situations. Therefore, a curve-fitting measure of the electricity price duration curves of the scaled 2020 curves is performed for 2030 and 2040. The curve-fitting uses the piecewise cubic Hermite interpolating polynomial, which requires fixed points (annual mean values, number of quarter-hourly time steps above 100 €/MWh and below 0 €/MWh) so that not only the annual mean values but also the number of extreme price situations match the literature values in [71, 72]. Then, the individual quarter-hourly electricity prices in the annual profile are adjusted to the fitted duration curve. The obtained electricity price curves for 2030 and 2040 and their duration curves are shown in Figure 5.

For the base year, 2020, natural gas prices were taken from the exchange data platform of the European Energy Exchange [73]. Like the electricity price, the natural gas price time series 2020 with the quarter-hourly resolution is scaled to represent the price situations in 2030 and 2040. For this purpose, calculations based on literature data [74, 75] were performed. In addition, these calculations are based on an energy mitigations scenario (MGS) of the Federal Environment Agency Austria (WEM scenario [76]) as part of a transition path to reach climate neutrality. The MGS scenario additionally assumes a future gas composition (CH_4, H_2, Bio-CH_4) for the natural gas

grid. The Bio-CH_4 is linearly increasing in the MGS, starting from 4 TWh in 2030, as foreseen in the Government Programme. The share of hydrogen is a result of the modelling. This energy share of the gas price thus serves as a scaling factor for the 2020-time series of the gas price to 2030 and 2040. The obtained time series for the gas price, including the gas composition, can be found in Figure 6. Again, gas prices are also included in the sensitivity analysis to consider the impact of the current price situation.

For the FR markets, both the balancing power market (provision of balancing power with standby remuneration via capacity prices) and the balancing energy market (supply of balancing energy with activation remuneration via energy prices) are considered. The "pay-as-bid" principle applies to both the balancing power and energy. Therefore, the total system service costs are settled via bid prices for bid time slots of 4 hours. Bids can be made for all FR products individually or in combination. The FR products are positive and negative Frequency Containment Reserve (FCR), automated Frequency Restoration Reserve (aFRR), and manual Frequency Restoration Reserve (mFRR). For the FCR, there is no balancing energy market. Activated FCR is compensated via the balancing power reserve prices.

Within this work, the balancing power reserve is included in the optimisation, while the balancing energy activation is included in the revenue calculation after the optimisation. However, the prices for the balancing power reserve and the balancing energy activation are obtained by averaging all existing offers. This price is used to reimburse the corresponding balancing power or energy [78]. This approach guarantees that
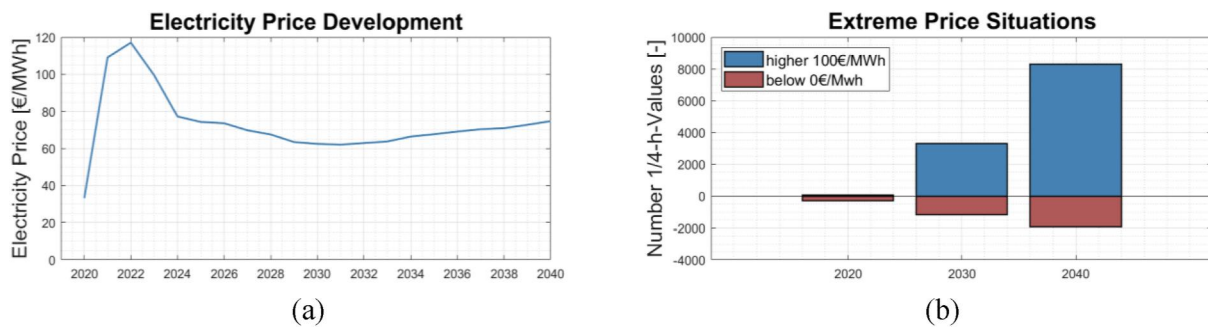

(a)

(b)

FIGURE 4 Electricity price development until 2040 (a) [71] and development of extreme price situations (b) [72].
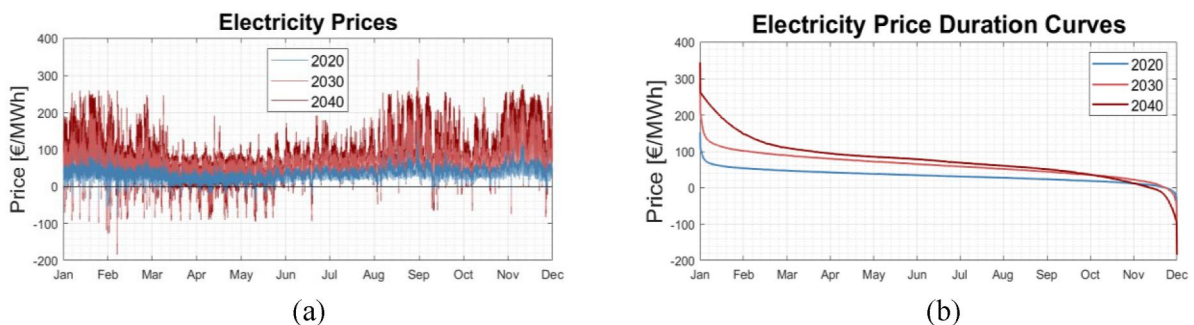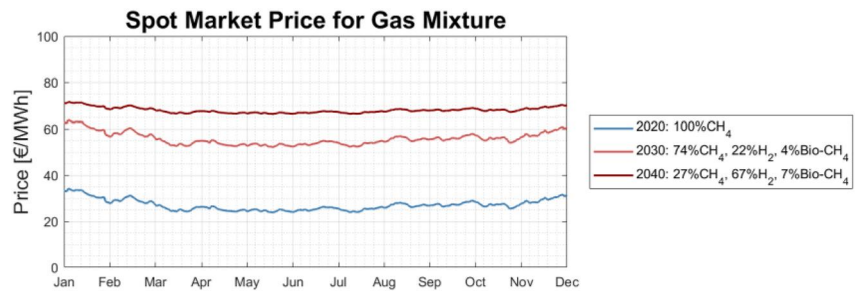

(a)

(b)

FIGURE 5 Electricity prices (left) and their duration curves (right) for 2020, 2030 and 2040

FIGURE 6 Natural gas price for 2020, 2030, and 2040 and the gas mixture in the grid (following [77])

the respective bid offers of the re-purposed CFPP operators are accepted in the merit-order [79]. Figure 7 presents the obtained time series for all FR products for 2020, 2030, and 2040.

Regarding the technologies, the respective product of balancing power is provided differently. For the GtP unit, the reservation or activation of positive balancing power or energy corresponds with an increase in power output and, thus, the electrical power supply to the grid. Therefore, negative balancing power or energy can be provided by reducing the amount of power fed into the electrical grid. On the other hand, the reservation or activation of positive balancing power or energy for the PtG unit means reducing the electrical power drawn from the grid. In contrast, an increase in consumption from the grid results in negative balancing power or energy, exemplarily to compensate for excess electricity from RES.

For the base year 2020, the data regarding the reservation and activation of FR products are openly available from the Austrian Transmission System Operator Austrian Power Grid (APG) APG [80–84]. To consider future developments, scaling factors from literature for the developments of average balancing power prices [85] and the FR demand [86] in 2030 and 2040 are used to calculate scaling factors for the available prices in 2020. These developments are based on the utilisation of wind and PV plants to provide negative balancing power in the future. As a result, the prices for negative balancing power reserve increase significantly, while the prices for the provision of positive balancing power reserve tend to increase [85]. Since this scaling was also performed for the activation prices, the same effects are evident in the time series for 2030 and 2040.

Figure 8 provides the results from the conducted sensitivity analysis regarding electricity and gas spot market prices and CapEx and balancing power reserve and energy activation prices for each re-purposing technology. As can be seen clearly, in Figure 8a and b, the input energy carrier for the respective technology (natural gas for GtP units and electricity for PtG units) shows a smaller influence on the obtained Return on Investment (ROI).

In contrast, the output energy carrier (electricity for GtP units and natural gas for PtG units) of the re-purposing technology shows a linear influence on the ROI, as higher output energy carrier costs result in correspondingly higher revenues. Similar results are obtained for combined PtG-GtP units as they show a combination of the results from the PtG and the GtP units. The balancing power reserve and

energy activation prices have a linear influence on the ROI. With increasing prices, also the revenues increase. However, balancing energy activation prices shows a more negligible effect than balancing power reserve prices. The highest impact on the ROI is offered for all the investigated re-purposing technologies by CapEx. As lower CapEx significantly increases the ROI, future economic viability of all the re-purposing technologies is mainly driven by CapEx reduction and technological advancement.

2.3 | Operational optimisation of the load and generation profiles of the Re-purposing technologies

To analyse and evaluate the current and future impact of the considered re-purposing technologies PtG, GtP, and PtG-GtP and their subsequent integration into the energy system, profiles that provide economically optimum plant operating schedules. This operational power plant optimisation depends on a large number of influencing factors: [87]

- Corresponding day-ahead market prices for electricity
- Corresponding day-ahead market prices for fuels (e.g. natural gas) and CO_2 emission allowances
- Technical parameters (minimum/maximum load, maximum ramp-up/ramp-down time etc.)
- Contractual obligations (e.g. supplying contracts for district heating)
- Corresponding prices for additional participation in the FR markets for reservation of generation capacity

The general problem definition is shown in Equation (1). The optimisation problem within this work represents a multi-variable Mixed-Integer Linear Programming problem. The objective function $f(x)$ maximises profits. Thus, the revenues (Equation (2)) and costs (Equation (3)) from participating in the energy and FR markets are included depending on the corresponding technology. The optimisation examines which operating point is optimal in the respective time step so that all balancing power market products can be optimally provided simultaneously. Thus the highest profits can be achieved collectively. As a result, the optimisation model also provides an optimal FR product combination regarding obtained profits. For the combination PtG-GtP unit, it is decided within
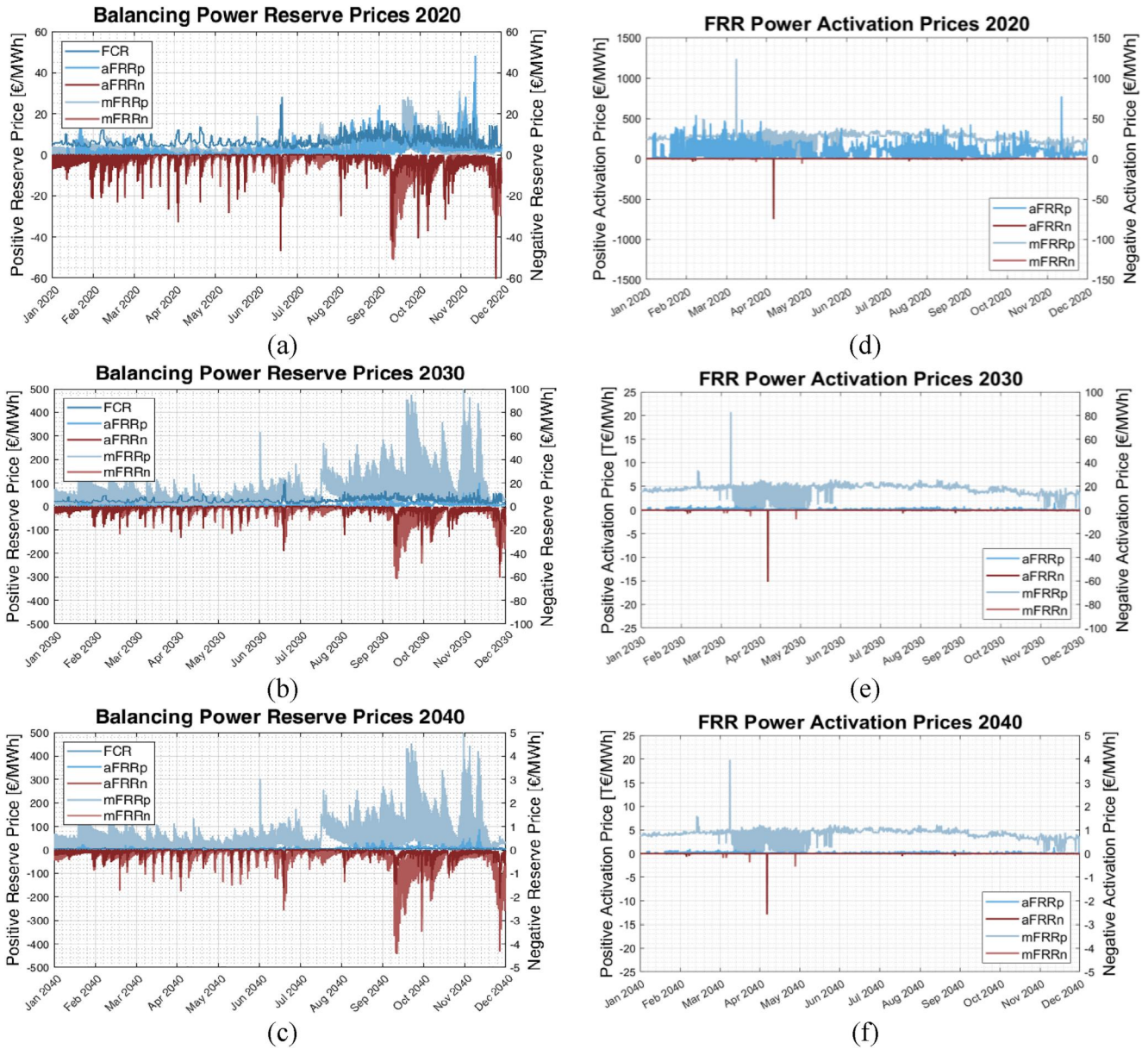
FIGURE 7 Balancing power price development (a-c) and balancing energy activation price development (d-f)
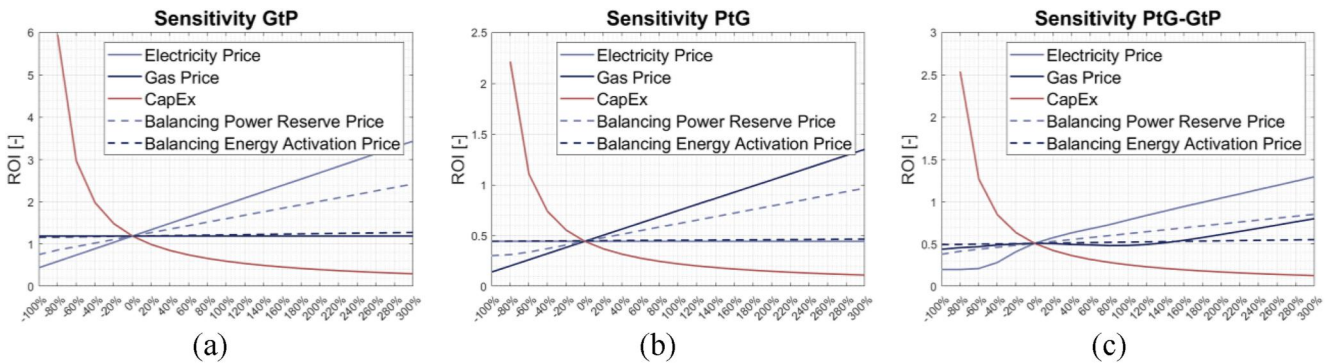

FIGURE 8 Sensitivity analysis on revenues regarding electricity and gas spot market prices as well as CapEx and balancing power reserve and balancing energy activation prices for (a) Gas-to-Power (GtP) units, (b) Power-to-Gas (PtG) units, and (c) PtG-GtP units at the Mellach site

the calculation which unit operates within which time step. However, the objective functions correspond with the respective objective function of the individual technologies.

$$\max_{x}(f(x_1,\ldots,x_6)) = \max_{x}(Profit(x_1,\ldots,x_6))$$
$$= \max_{x}(Revenues(x_1,\ldots,x_6) - Costs(x_1)) \tag{1}$$

$$Revenues(x_1,\ldots,x_6) = Revenues_{EnergyMarket}(x_1)$$
$$+ Revenues_{FRR-Market}(x_2,\ldots,x_6) \tag{2}$$

$$Costs(x_1) = Costs_{EnergyMarket}(x_1) + OpEx(x_1) \tag{3}$$

The objective function $f(x_1,\ldots,x_6)$, as described in Equation (1), includes the optimisation variables $x_1\ldots x_6$ ($x_1\ldots$ double value, x_2-$x_6\ldots$ integer values). Each optimisation variable represents the optimised electrical plant power in MW dispatched at the implemented markets in each time step (quarter-hourly values). The dispatch depends on the available day-ahead spot market energy prices (electricity p_{el} and gas prices p_{gas} in €/MWh) as well as Operational Expenditures (OpEx in €/MW) and prices for the reservation of operating capacity for positive and negative FR products ($p_{FCR,p}$, $p_{FCR,n}$, $p_{aFRR,p}$, $p_{aFRR,n}$, $p_{mFRR,p}$ and $p_{mFRR,n}$ in €/MWh). The optimisation variable x_1 represents the dispatch of the plant, which is determined by the day-ahead spot market energy prices. The other optimisation variables represent the amount of reserved power for the individual FR products. Thus, positive and negative FCR is described in the optimisation via x_2 due to the symmetry constraint for FCR reservation. In contrast, positive aFRR is represented by x_3, negative aFRR by x_4, positive mFRR by x_5, and negative mFRR by x_6. Positive and negative aFRR and mFRR can be bid separately, contrary to FCR, and are thus not subject to any symmetry constraints. The calculations also include the conversion efficiencies of the technologies $\eta_{c,PtG}$ and $\eta_{c,GtP}$ to convert between gas and electricity. The individual components comprising the objective function are listed in Table 4.

The factor 1.494 in Table 4 describes the added taxes, grid usage, and metering charges to the energy share considered for the day-ahead spot market price said for gas procurement in

the GtP unit [88]. These added costs to the energy share do not have to be paid for the procurement of electricity for the PtG units as there is a regulation in place for Austria to omit these costs for certain plants (among others PtG units) [89].

However, since the operation of the re-purposing technology must also fulfil specific requirements, for example, taking over the original tasks of the CFPP, or is subject to certain limitations, the optimisation problem is bounded by constraints. For optimising the operating point on the day-ahead energy spot market, these constraints include start-up r_{up} and powering-down r_{down} ramping rates of the respective technology, as well as minimal lb (lower bounds) and maximum operating powers ub (upper bounds). Additionally, a certain amount of district heat must be supplied to fulfil the contractual obligations to provide district heating. The district heating demand of the cities Graz, St. Pölten, and Vienna modelled using this function is shown in Figure 9.

To model this constraint correctly, the time-resolved district heating demand Qth of the respective supplied nearby city is estimated via the associated daily mean temperature values for 2020 [90] and via the corresponding annual district heating demand by using the SigLinDe-function [91]. This function combines the Sigmoid function and linear components used to create standardised heat load profiles, allowing for a simplified estimation of time-resolved heat demand [91].

The primary constraints for the optimisation regarding the combination of FR products provided for balancing power reserve are minimum and maximum bid quantities of electrical power. These constraints for the optimisation are presented in Table 5. Table 5 Pth designates the thermal power of the respective technology and P_{el} the corresponding electrical power.

While there is a maximum bid restriction of 25 MW for FCR and mFRR, aFRR can be offered without any upper limit. However, the minimum bid quantity is 1 MW for FCR and mFRR products and 5 MW for aFRR products. Trading is only allowed in whole MW increments. Therefore the FR variables ($x_2,\ldots,x_6$) represent integer values. In addition, regular dispatch operation (x_1) plus FR products ($x_2,\ldots,x_6$) must not exceed or fall below the maximum and minimum technological power limits (lb and ub). Since the optimisation is performed in quarter-hour time steps, it must also be ensured that the FR products are constant over 4 h (corresponds to 16 quarter-hour values), as provided for this time (cf. chapter 2.2).

The PtG and GtP units are primarily dispatched for participation at the energy spot markets when there is a district heating demand, as this constraint must be strictly fulfilled. Regarding their use for control reserve, the prices of the respective FR product and the capacity still available after spot market participation are relevant for dispatch at the FR reserve market. The actual dispatch time of the different units at each market is the result of the optimisation and is presented in detail in the discussion.

Based on the optimisation problem described above, optimised operating profiles for the re-purposing technologies considered in this work can be generated for each site and scenario. These are then integrated into the MES load flow

TABLE 4 Components of the objective function for each considered technology

Objective function component		PtG	GtP
Revenues (€)	Revenues$_{EnergyMarket}$	$p_{gas} \cdot \eta_{c,PtG} \cdot x_1$	$p_{el} \cdot x_1$
	Revenues$_{FR\ Market}$	$x_2 \cdot p_{FCR,p} + x_2 \cdot p_{FCR,n} + x_3 \cdot p_{aFRR,p} + x_4 \cdot p_{aFRR,n} + x_5 \cdot p_{mFRR,p} + x_6 \cdot p_{mFRR,n}$	
Costs (€)	Costs$_{EnergyMarket}$	$p_{el} \cdot x_1$	$\dfrac{p_{gas} \cdot 1.494 \cdot x_1}{\eta_{c,GtP}}$
	OpEx	$OpEx_{PtG} \cdot x_1$	$OpEx_{GtP} \cdot x_1$

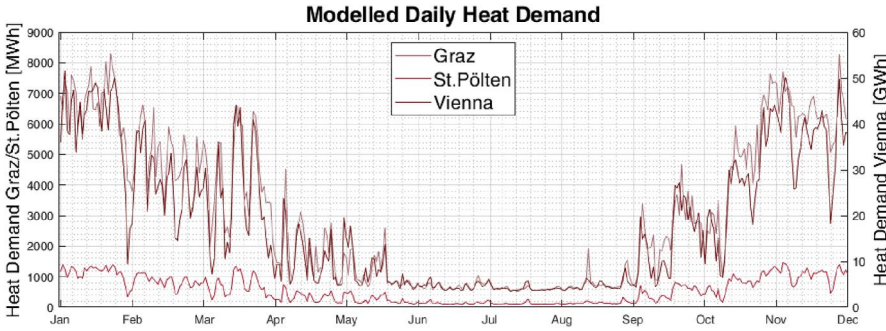Abbreviations: GtP, Gas-to-Power; PtG, Power-to-Gas.

FIGURE 9 Modelled daily heat demand for the supply of district heating in Graz, St. Pölten, and Vienna

TABLE 5 Optimisation constraints for the operating profiles of the re-purposing technologies

Constraint		PtG	GtP
Energy market	Start-up/power-down ramp	$-r_{down,PtG} \leq x_{1,k} - x_{1,k-1} \leq r_{up,PtG}$	$-r_{down,GtP} \leq x_{1,k} - x_{1,k-1} \leq r_{up,GtP}$
	Lower and upper bounds	$lb_{PtG} \leq x_{1,k} \leq ub_{PtG}$	$lb_{GtP} \leq x_{1,k} \leq ub_{GtP}$
	District heat supply	$P_{th,PtG} \cdot 0.25 \cdot \sum_k \frac{x_{1,k}}{P_{el}} = Q_{th}$	$P_{th,GtP} \cdot 0.25 \cdot \sum_k \frac{x_{1,k}}{P_{el}} = Q_{th}$
FR market	Lower and upper bounds $+/-$ FCR	$1 \leq x_2 \leq 25$	
	Lower and upper bounds $+/-$ aFRR	$5 \leq x_3, x_4 \leq ub_{PtG}$	$5 \leq x_3, x_4 \leq ub_{GtP}$
	Lower and upper bounds $+/-$ mFRR	$1 \leq x_5, x_6 \leq 25$	
	Constant power reserve 4 h	$\sum_{k=1}^{16} \frac{x_{2,\dots,6,\ k}}{x_{2,\dots,6}} = x_{2,\dots,6}$	
Sum constraint positive FR products		$lb_{PtG} \leq x_1 + x_2 + x_3 + x_5 \leq ub_{PtG}$	$lb_{GtP} \leq x_1 + x_2 + x_3 + x_5 \leq ub_{GtP}$
Sum constraint negative FR products		$lb_{PtG} \leq x_1 + x_2 + x_4 + x_6 \leq ub_{PtG}$	$lb_{GtP} \leq x_1 + x_2 + x_4 + x_6 \leq ub_{GtP}$

Abbreviations: GtP, Gas-to-Power; PtG, Power-to-Gas.

simulation framework "*HyFlow*" to assess the impact of these sector coupling technologies as re-purposing options on the Austrian energy grids.

2.4 | HyFlow–multi-energy system load flow simulation framework

Grid calculations must be performed to assess the impact of integrating re-purposing technologies for CFPPs into existing energy systems. Since this work focuses on sector coupling technologies as re-purposing options for CFPPs, a load flow simulation framework that can incorporate different energy carrier grids and their interactions is required. Therefore, this work uses the MES simulation framework HyFlow, developed by the Chair of Energy Network Technology. An exemplary structure of HyFlow is provided in Figure 10.

HyFlow is a modular and generic modelling and simulation framework that includes all grid-bound energy carrier grids (electricity, district heating, and natural gas grid) [92]. In this work, for each considered energy carrier, a specific grid model has to be developed [93, 94] based on a cellular approach. This approach provides a spatial structure of the incorporated grids by dividing them into energy cells [94]. Since the representation of the grids within HyFlow allows for considering different voltage, pressure and/or temperature levels, several grid levels account for this complexity. A transfer between grid levels is accomplished via a virtual Slack-node by which the aggregated

power values of all lower-level cells are transferred to the higher-level grid. [95] Each cell is represented by one cell node in the cell centre [94]. In this work, the central cell nodes are represented by the 110 kV high voltage power grid substations. The area of a cell results from increasing concentric circles originating from this substation until it meets the concentric circle of a neighbouring substation [96]. The other energy carriers (natural gas and heat) follow this cell division. However, a MES grid connection (grid node) is only available if there is also a grid structure within that specific cell. Thus, their cell centres allow various sector coupling technologies to be implemented to enable energy transfer across energy carriers.

HyFlow primarily aims to identify the influence of trends on the Austrian energy grids. Thus, a georeferenced model of the Austrian power, natural gas, and district heating grid is implemented and utilised for the calculations [95, 97]. To define the boundaries to the connected grids in neighbouring countries, cross-border lines are connected to a Slack-node [97]. This Slack-node represents differential load flows to these countries as imported or exported power [97]. A more detailed description of the HyFlow model of the Austrian grids and their boundaries can be found in [93, 95, 97]. The electrical model of the APG includes the 380 kV, the 220 kV, and the 110 kV grid.

In contrast, the natural gas grid comprises long-distance pipelines and distribution pipelines for grid levels 1 and 2. A qualitative representation of the power and natural gas grids within HyFlow can be seen in Figure 11. There is no

FIGURE 10 Exemplary representation of the cellular approach within HyFlow, including the considered energy carrier grids
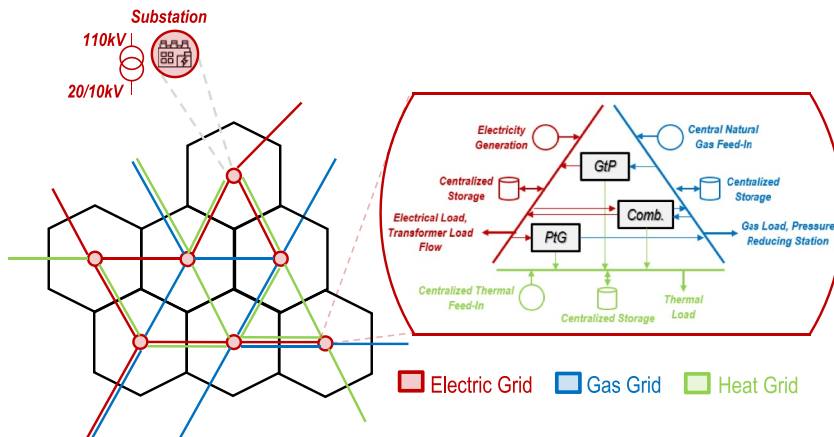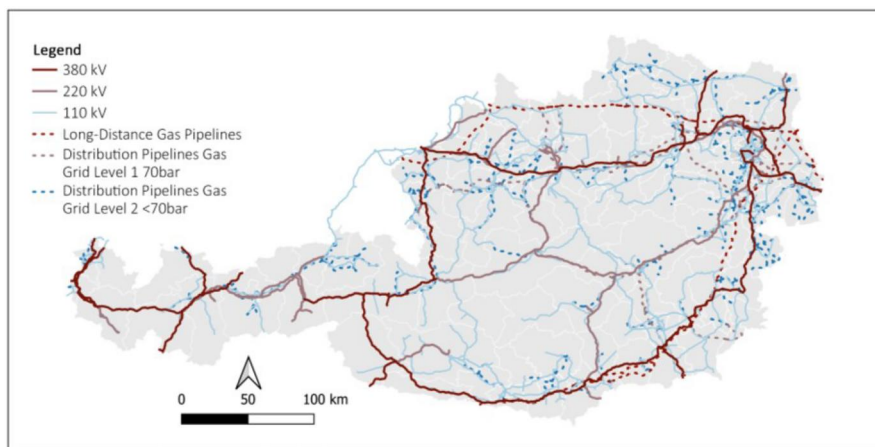

FIGURE 11 Incorporated Austrian power and natural gas grids in HyFlow [56, 99, 100].

georeferenced model for the district heating grid. However, the model was implemented in HyFlow, according to ref. [98].

The load and generation data for the calculations of this work consider 2020 as the base line for future developments of 2030 and 2040. Thus, the used data already included in HyFlow assumed expansion plans for volatile RES (wind and PV power), EV, as well as heat pumps (HP) (cf. Table 6). Using this MES load flow tool Hyflow, the aim is to analyse the obtained load flows, particularly for the power grid, and to evaluate whether, where, and to what extent overloads occur.

The local distribution of RES expansion is assumed according to Sejkora et al. (2020) [105]. In general, it can be stated that the expansion of wind focuses primarily on the east of Austria. In the west, mainly hydropower is expanded, and PV and biomass can be assumed to be equally distributed over Austria [105].

3 | RESULTS

This chapter will first show the optimised profiles of the three different re-purposing technologies. Then, the simulation results from HyFlow showing the resulting load flows in the Austrian energy system when integrating these re-purposing technologies with their optimised operating profiles are

TABLE 6 Assumptions for the HyFlow calculations for each scenario [101–104]

		2020	2030	2040
Heat pump share	(%)	2	9	13
Electric vehicle share	(%)	1	32	56
PV share	(%)	5	7	10
Wind share	(%)	14	18	21

presented. For the HyFlow calculations, selected scenarios were analysed. An overview of the performed scenarios can be found in Table 7. Additionally, reference scenarios are calculated for each year, representing scenarios with new CFPP sites and, therefore, no implemented re-purposing options. The 2020 scenario can be regarded as a representation of the current Austrian energy system.

3.1 | Optimised operating profiles for the coal-fired power plants sites in Austria

Regarding the operational optimisation, a large set of results for each investigated scenario (2020, 2030, 2040) and each

technology (PtG, GtP, PtG-GtP) and site are obtained (18 different optimised load profiles, each with individual annual profits and full load hours). Therefore, this chapter presents the optimised operating profiles for one site (Mellach) and one scenario (2030) for each re-purposing technology. However, there will be a comparison of all the results regarding profits. For

the optimisation, the input parameters of the Austrian CFPP sites (Table 1), the re-purposing technologies (Table 2 and Table 3), and the temporally resolved spot-market prices for electricity, gas as well as balancing power reserve and balancing energy activation (chapter 2.2) are considered. Using these input parameters together with the optimisation model presented in chapter 2.3, the optimised plant dispatch on the day-ahead spot market (x_1), as well as the optimal composition of the products for balancing power reserve ($x_2, \ldots, x_6$), are obtained. The optimisation results for each optimisation variable $x_1, \ldots, x_6$ are presented in Figure 12, using the Mellach site.

For the GtP unit, the optimised operation results in 1128.4 h full load hours for the year 2030, while at the Dürnrohr site, 876 h, and the Simmering site, 1395.75 h of full load hours are achieved. If the PtG technology is considered a re-purposing technology in 2030, then 2190 h of full load hours are attained at each site. For the combined PtG-GtP unit, cumulative full load hours of 2181.1 h (PtG: 2038.5 h,

TABLE 7 Performed calculations within HyFlow using the optimised profiles for the re-purposing technologies

Re-purposing technology	2020	2030	2040
Reference	(x)	(x)	(x)
GtP	(x)	(x)	(x)
PtG			(x)
PtG-GtP			(x)

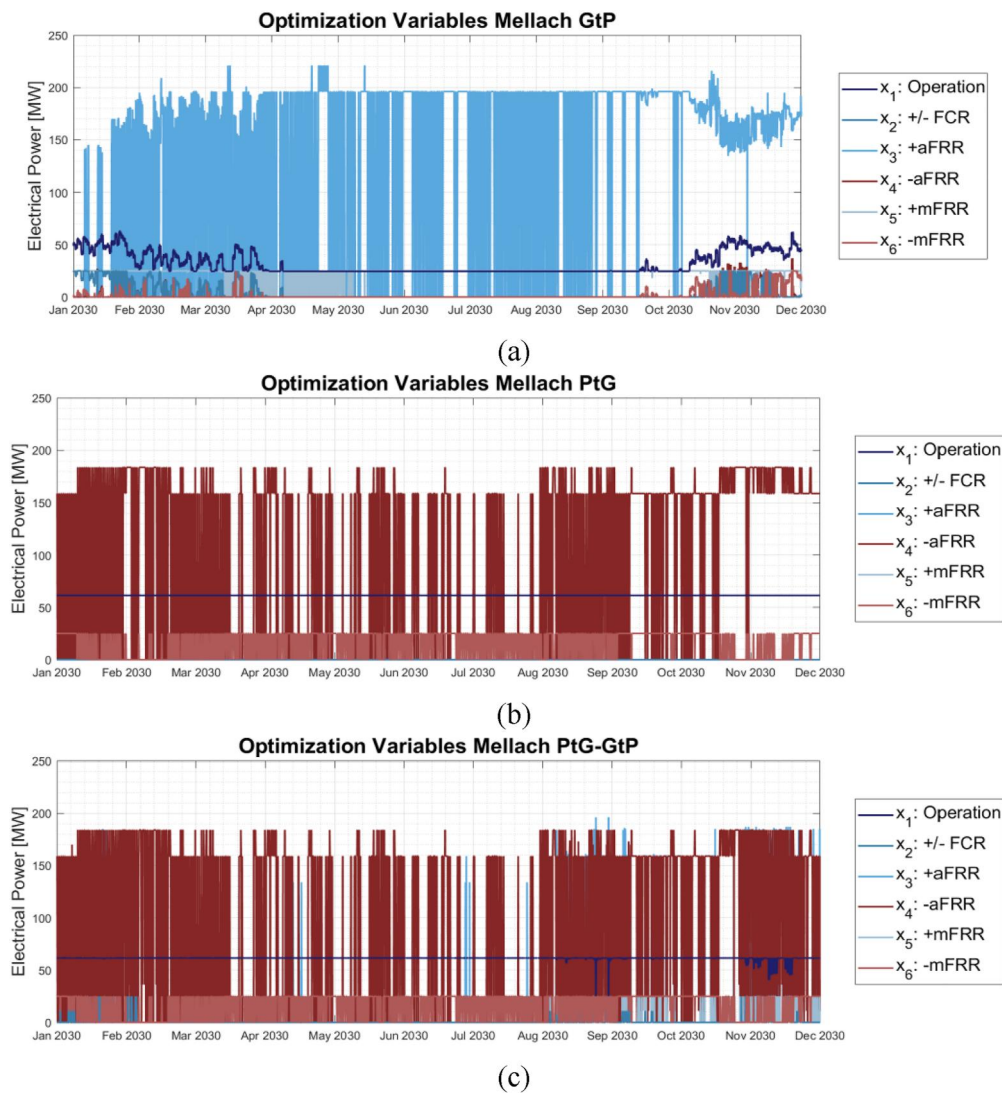Abbreviations: GtP, Gas-to-Power; PtG, Power-to-Gas.

(a)

(b)

(c)

FIGURE 12 Results for each optimisation variable for the Mellach site in scenario 2030 with (a) a Gas-to-Power (GtP) unit, (b) a Power-to-Gas (PtG) unit, and (c) a combination PtG-GtP unit

GtP: 142.6 h) at the Mellach site, 2170.6 h (PtG: 2038.5 h, GtP: 132.1 h) at the Dürnrohr site and 2188.3 h (PtG: 2038.5 h, GtP: 149.8 h) at the Simmering site can be achieved under the conditions and assumptions specified for the calculations in this work (see chapter 2.1).

Based on the optimised electrical operating profile of the respective plant, the activated balancing energy is added to the optimised operational profile resulting in an overall electrical activation profile. This is achieved by using the activation times in 2020 [81]. These electrical activation profiles and the respective gas demand and heat delivery profiles are shown in Figure 13 for the PtG, GtP, and PtG-GtP at the Mellach site for the 2030 scenario. The conversion between the energy carrier profiles is based on the assumed conversion efficiencies (between electricity and gas) and heat generation efficiencies (cf. Table 2 and Table 3). However, as the impact of the profit-

optimised operation of the re-purposing technologies is analysed in HyFlow and since the deployment of balancing energy activation is evaluated in advance so that no line or node overloads occur, only the energy carrier profiles without activations are considered in HyFlow.

Since Figure 13c depicts the combined PtG and GtP unit, negative values represent the operation of the PtG unit, while positive values represent the operation of the GtP unit.

To enable a comparison between the sites, Figure 14 shows the revenues of each technology for all three sites in the 2030 scenario. With a GtP unit replacing the original CFPP in its electrical power output, total revenues of €80.80 million at Mellach (€18.32 million from the electricity spot market, €21.89 million balancing power reserve, and €40.59 million balancing energy activation), €86.15 million at Dürnrohr (€19.18 million from electricity spot market, €26.38 million
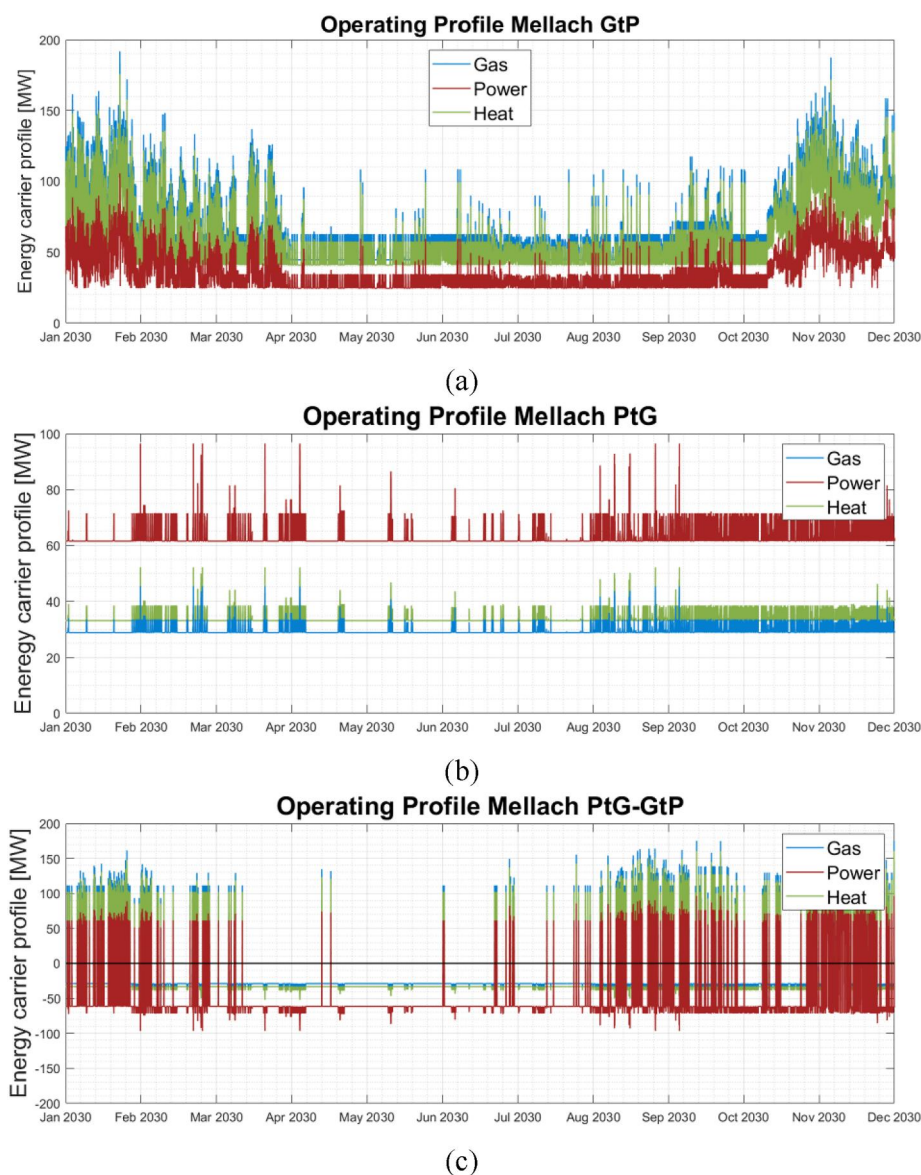

(a)

(b)

(c)

FIGURE 13   Results of the individual optimised energy carrier profiles for electricity, natural gas, and heat

balancing power reserve and €40.59 million balancing energy activation) and €152.58 million at Simmering (€70.17 million from electricity spot market, €41.85 million balancing power reserve and €40.59 million balancing energy activation) can be achieved. While the revenues of the two smaller plant sites (Mellach, Dürnrohr) are mainly obtained by balancing energy activation, the larger plant site Simmering receives most of its revenues from the sale of electricity on the electricity spot market.

The revenues from PtG units replacing the original CFPPs in the 2030 scenario correspond to €33.73 million (€30.03 million from the natural gas spot market, €3.69 million from balancing power reserve, and €0.01 million from balancing energy activation) for Mellach, €48.05 million (€42.97 million from the natural gas spot market, €5.07 million from balancing power reserve and €0.01 million from balancing energy activation) for Dürnrohr and €103.16 million (€92.77 million from natural gas spot market, €10.38 million balancing power reserve and €0.01 million from balancing energy activation) for Simmering. While most of the revenues are obtained from arbitrage activities on the natural gas spot market in the case of the PtG unit, some are obtained from balancing power reserve and only minimal revenues from balancing energy activation.

If the PtG-GtP combined unit is used as a re-purposing technology in 2030 to replace the original CFPPs, total revenues of €42.97 million for Mellach (€5.21 million in the electricity spot market, €27.89 million in the natural gas spot market, €7.14 million for balancing power reserve, and €2.73 million for balancing energy activation) can be obtained. For Dürnrohr, total revenues for PtG-GtP technology in this scenario amount to €58.83 million (€6.79 million in the electricity spot market, €39.91 million in the natural gas spot market, €9.40 million for balancing power reserve, and €2.73 million for balancing energy activation) and €123.24 million for Simmering (€17.04 million in the electricity spot market, €86.17 million in the natural gas spot market, €17.30 million for balancing power reserve, and €2.73 million for balancing energy activation). Thus, the highest revenues can be obtained in total using the combined unit.

To comply with market-rules, marginal costs were calculated. Thus, only energy costs (natural gas for the GtP unit

and electricity for the PtG unit respectively) and OpEx are included in the objective function of the optimisation. However, the CapEx is included in the ROI calculations and, thus, the total profits obtained. When achieving an ROI of 1 (payback period), the entire CapEx of the re-purposing unit has already been recouped by the profits. For a GtP unit, this is already the case after approximately 2–5 years. For a PtG unit, the payback period for unit acquisition in 2020 is over 15 years. Therefore, technological advancement in the next few years is crucial to shortening the payback period. However, with the assumed PtG technology developments (cf. Table 2), the payback period can be reduced to less than 10 years for the acquisition of a PtG unit in 2030 and 2040 respectively. A similar situation applies to the combined PtG-GtP unit. However, since very high profits are generated from the sale of electricity and natural gas, the payback time to reach an ROI of 1 is about 13 years for unit acquisition in 2020. Also, future technological developments until 2030 will reduce this time to less than 10 years for the combined technology. Due to the assumed developments regarding balancing power and energy prices, revenues from balancing power reserve and balancing energy activation regarding negative FR products will become smaller in the future. The ROI for all three re-purposing technologies at the Mellach site for 2020, 2030, and 2040 scenarios are depicted in Figure 15.

The production of SNG in the methanisation for the PtG and the combined PtG-GtP unit requires a corresponding CO_2 mass flow, as shown for each site in Figure 16. This work assumes that sufficient CO_2 sources are available in the vicinity of the respective site, which is also coarsely investigated. For this purpose, neighbouring industries or smaller biogas plants can serve as CO_2 sources. The information regarding the available CO_2 from industry was taken from the individual sustainability reports [106–113] of the industrial sites nearby. For this work, it is also assumed that the 2020 CO_2 mass flows are still available in 2030 and 2040. However, alternatively, a direct air capture (DAC) unit can be installed at each site. However, these DAC units require additional electricity and heat demand and provide comparatively small amounts of CO_2 due to the air composition. As an advantage, the DAC unit
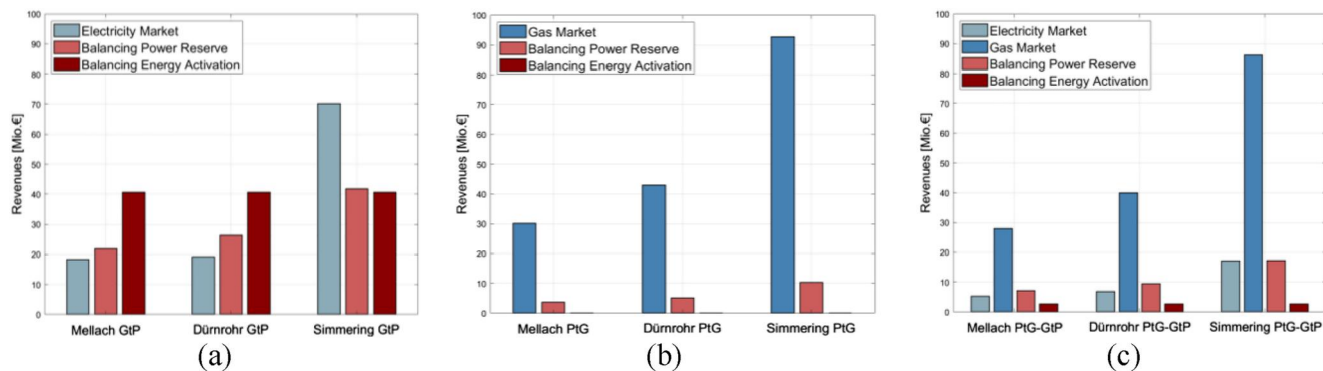

FIGURE 14 Revenues for each site in the 2030 scenario on the electricity and natural gas spot market as well as for balancing power reserve and balancing energy activation for (a) the Gas-to-Power (GtP) unit, (b) the Power-to-Gas (PtG) unit, and (c) the PtG-GtP unit
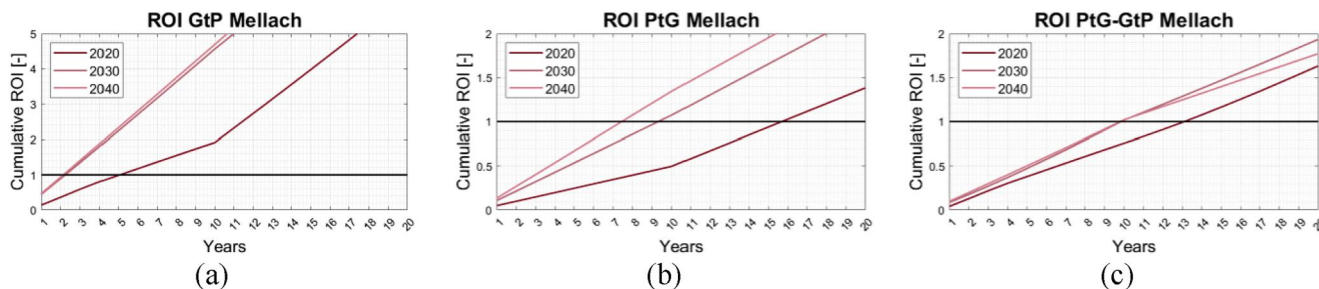
FIGURE 15   Return on investment (ROI) of each technology for the three scenarios 2020, 2030, and 2040 at the Mellach site
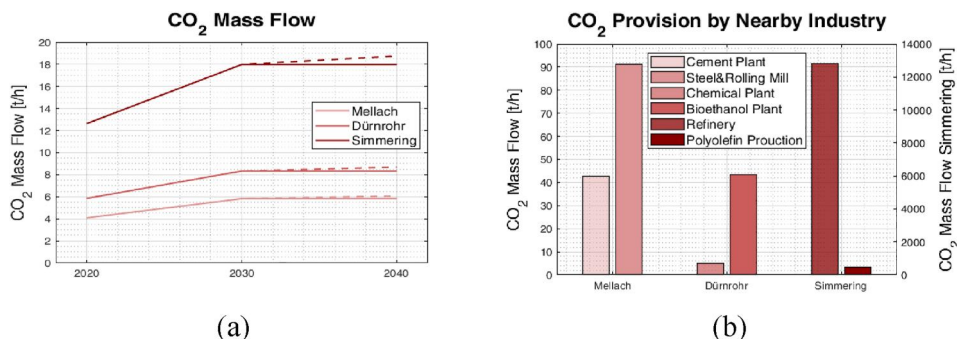

FIGURE 16   (a) CO_2 mass flows for the operation of the Power-to-Gas (PtG) unit as well as the PtG-Gas-to-Power unit at the corresponding site and (b) possible CO_2 mass flow provision by nearby industry (according to [106–113])

could provide CO_2 independent from the scheduling of industrial processes [114].

Close to the Mellach site is a cement plant (approx. 25 km) and a steel and rolling mill (also approx. 25 km), which could provide the necessary amount of CO_2. Close to the Dürnrohr site are a chemical industry site and a bioethanol plant (approx. 3 km), which could provide the required CO_2. For the Simmering site, a nearby refinery and a polyolefin production plant (approx. 8 km) could provide the necessary CO_2. For better visualisation of the nearby industry and surrounding biogas plants (30 km radius), a georeferenced representation of the Austrian CFPP sites and their surroundings is depicted in Figure 3.

3.2 | Load flows within the Austrian energy grids

A large number of results are also obtained from the load flow calculations, which is why the results are presented in an aggregated form. The average line overloads, the number of congested lines, and the number of time steps in which congestions occur are considered for this analysis. In addition, power imports and exports across Austrian borders to neighbouring countries are considered. From the set of scenarios shown in Table 7, detailed individual results are again depicted for 2030. According to the assumed expansion rates for RES, EVs, and HPs (cf. Chapter 2.4) in the grid, both the number of congested lines and the number of time steps in which overloads occur increase over time (Figure 17).

While in 2020, only two lines are congested at specific points, in 2030, there are 10, and in 2040 11 lines are congested. As can also be seen in Figure 17, the number of overloaded lines depends on the re-purposing technologies used. It, therefore, equals the number of congested lines in the reference scenarios.

In contrast, the number of time steps in which overloads occur and, therefore, the congestion duration corresponds to the re-purposing technology. Figure 17b shows that in 2020 an overload time of 9.5 h with congestions occurring for both the reference scenario without re-purposing and the GtP-scenario. In the 2030 and 2040 GtP scenarios, the number of time steps with overloads increases compared to the reference scenario. This results in a congestion duration of 133 h in 2030 (reference scenario 120 h) and 119 h in 2040 (reference scenario 125 h). However, the PtG units in the individual and combined plant in the 2040 scenario lower this number compared to the reference scenario to about 111 h of overloads.

Examining the average level of congestion in the lines (Figure 18), the overload extent decreases over the considered scenarios, although the congestion frequency (lines and time steps, cf. Figure 17) increases. For the overload extent again, a slight dependence on the re-purposing technologies can be seen in the 2040 scenario. In all scenarios, the average line overloads are very low and vary only within a range of 1%–2% overload, as illustrated in Figure 18. A spatial allocation of the overloaded lines in the 2030 GtP scenario can be taken from Figure 19.

The highest and most frequent overloads are in the marked area, which is located in the Austrian capital Vienna, where
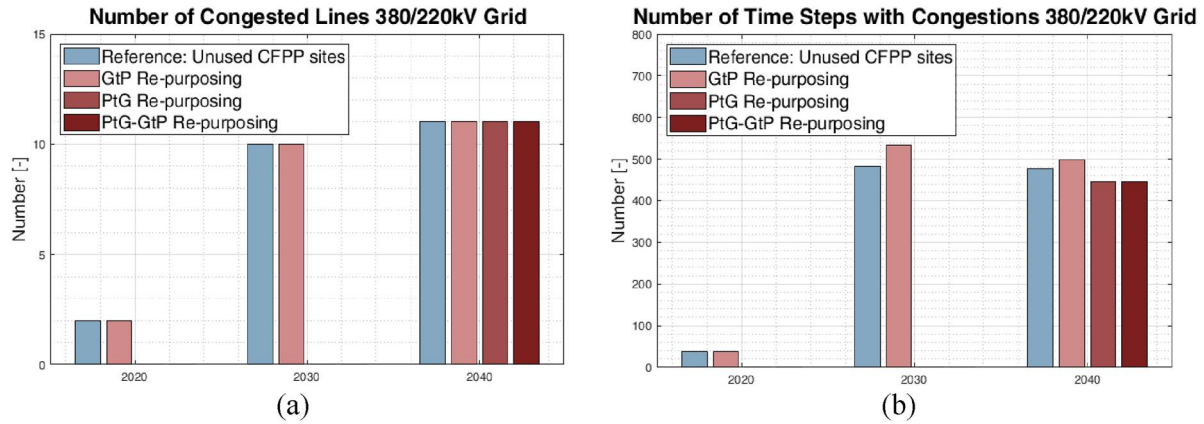
FIGURE 17 MES load flow simulation results from HyFlow: (a) Number of congested lines and (b) number of time steps in which congestions occur for the 380/220 kV grid
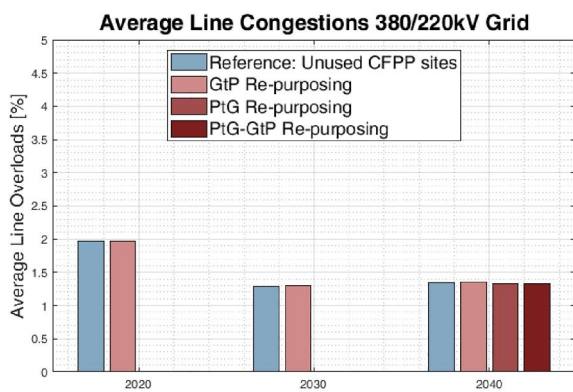

FIGURE 18 MES load flow simulation results from HyFlow: Average line congestions in the 380/220 kV grid

consumption is correspondingly high. Otherwise, there are less congested 220 kV transmission lines, while there are no overloads in the 380 kV grid. These overloads result from the RES expansion and its regional differences (e.g. the wind is expanded primarily in the east of Austria).

Since the integrated, optimised operating profiles include balancing power activated in Austria, additional import and export in and out of Austria are presented in Figure 20. Due to the high RES expansion, net exports increase over the three scenarios for all re-purposing technologies from almost 13 TWh in 2020 to about 34 TWh in 2030 and about 35 TWh in 2040. Net imports also generally increase due to additional demand for EVs and HPs and local generation unavailability. These imports are 6.67 GWh for 2020, 15.37 GWh for 2030, and 16.10 GWh in 2040 each in the reference scenario. As illustrated in Figure 20, neither exports nor imports are significantly influenced by the re-purposing technologies at the CFPP sites. Exports vary by an increase or decrease of 20–30 GWh. Imports decreased most between the reference and GtP scenarios in 2020 (by 680 GWh). Only for the PtG and the PtG-GtP unit integration scenarios, there is an increase in imports by 90 GWh due to higher electricity demand resulting from the PtG operation.

Concerning nodal stress, neither the acceptable voltage band's upper limit nor the lower limit (0.9–1.1 per unit) is violated at this maximum-voltage level.

4 | DISCUSSION

With the chosen optimisation approach, which considers arbitrage activities on the energy spot market and selling balancing power reserve on the FR market, the full load hours of the plants are below 2200 h per year. This suggests that a high share of the plant capacity is allocated to balancing power reserve as a result of the operational optimisation (cf. Figure 12). Within the scope of the work, these two objectives (operation for participation on the energy spot market and balancing power reserve at the FR market) were optimised first consecutively with two separate objective functions and then with one combined objective function to enable a comparison and to account for the first research question. For this purpose, the operating profile of the re-purposing technologies at the individual sites was optimised for participation in the energy spot market first, for which the units were almost always operated at their maximum power. Based on this, the balancing power reserve was then optimised. However, due to the primarily high power being dispatched at the spot markets, only a small capacity was available for balancing power reserve. Thus, usually, there were no combinations of different FR products, but the product with the highest bid price was used for bidding on the FR market in optimised operation. The comparison, thus, showed that the maximum profits are only achieved if the two markets are optimised together using a combined multi-variable objective function of maximising both profits from spot market wholesale (electricity or natural gas) and balancing power reserve products.

The optimisation results (cf. Figure 12) show that the maximum profits are obtained when most of the available plant capacity is used for balance power reserve. Electricity or natural gas sales on the arbitrage spot market primarily occur in those time steps where district heating demand specified in the agreed upon supply contracts has to be provided. In these
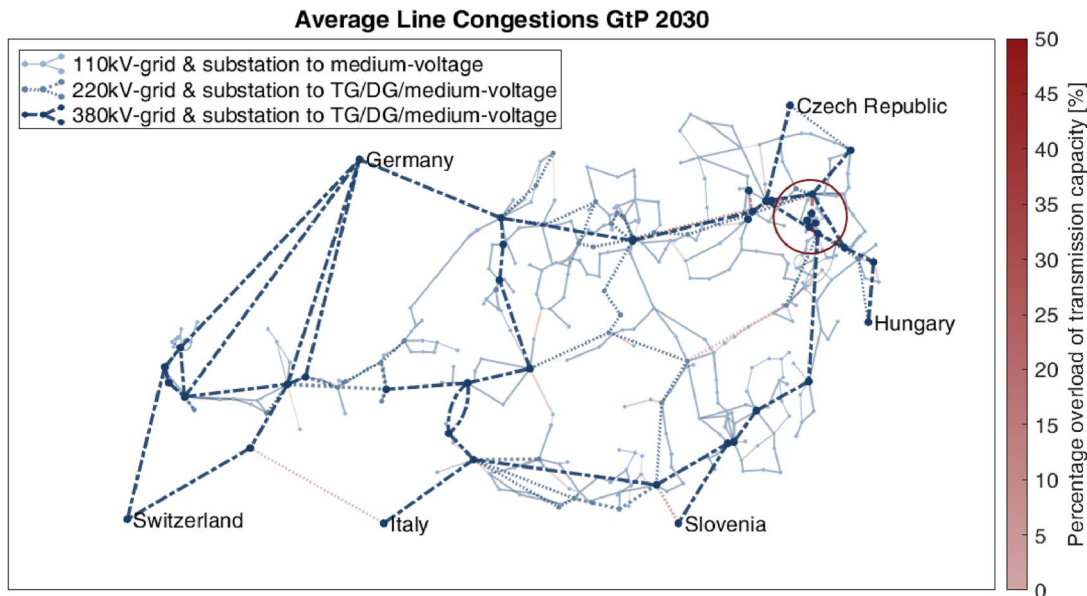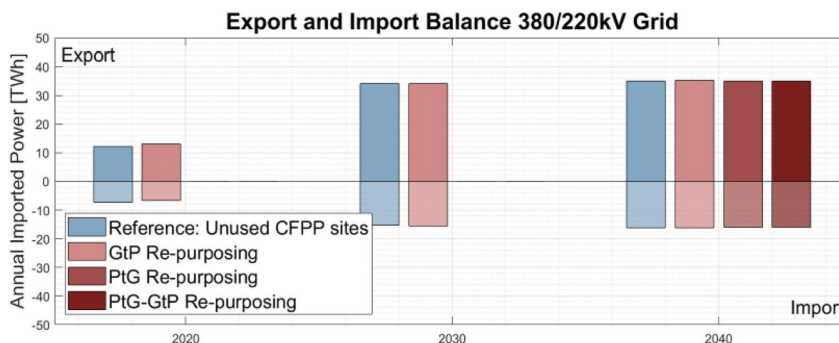
FIGURE 19 MES load flow simulation results from HyFlow: Location of average highest and most frequent line congestions for the 2030 Gas-to-Power (GtP) scenario for the Austrian transmission (TG) and distribution grids (DG)

FIGURE 20 MES load flow simulation results from HyFlow: Export and import balance

cases, two earning streams are available: electricity/natural gas and district heating. This result is obtained since the "pay-as-bid" market (balancing power reserve) tends to have higher prices for remuneration of balancing power than the "pay-as-cleared" electricity spot market. In the "pay-as-cleared" market, all power plants allocated for electricity generation to meet the demand are reimbursed at the same price. The remuneration for balancing power reserve is based on individual bids. Electricity spot market prices and gas spot market prices currently and in the assumed future price developments are close to each other. However, the revenues generated from gas sales are usually higher than those from electricity sales. The impact of these developments (cf. second research question) is that PtG units are preferred in the optimisation model, which mainly influences the combined PtG-GtP units. For these units, it is favourable in about 93% of the time steps to operate the PtG unit instead of the GtP unit, thus, obtaining larger profits from the gas spot market than electricity sales.

The economic benefit of the re-purposing technologies is discussed based on the obtained revenues and thus answers the third research question. The revenues from electricity sales vary between 11%–57%. At the same time, larger shares are obtained for GtP units at larger sites (e.g. Simmering), and smaller shares are obtained for the combined PtG-GtP units at smaller sites (e.g. Mellach). The high shares are found in the 2020 scenario as the spread between electricity and natural gas prices is most significant. Natural gas revenues have a high percentage of the total revenues due to the assumed price developments and lie between 53%–100%. Again, higher shares are present in the single PtG units, lower shares are found in the combined PtG-GtP units, while plant size has no influence. The revenues from the balancing power reserve of the re-purposing technologies are between 4%–27% of the total revenues. The higher shares are predominantly found for the GtP units in the 2030 scenario, as positive FR products are highly priced in the assumed future developments. The lower shares of balancing power reserve revenues are found in the combined PtG-GtP units due to the assumed future developments of negative FR products. In general, larger sites have a smaller share of balancing power reserve revenues as they produce larger amounts of energy for arbitrage activities on the energy spot markets resulting in higher electricity/

natural gas revenues. Considering the assumed developments for FR prices, specific trends can be deducted regarding which technologies are best suited to provide which FR products:

GtP units: The GtP units in the scenarios considered in this work provide mainly positive aFRR power (meaning, in case of activation, the units have to increase their power output). Nevertheless, all other FR products are also offered for positive and negative balancing power reserve. Frequency Containment Reserve is provided by the GtP unit primarily during the winter months. During these periods, regular operation is at a higher level due to increased heat demand and, thus, the requirement to fulfil the heat supply contract. This increases the frequency regulation band for FCR provision of the unit, which is bound to a symmetry condition; thus, a larger amount of FCR can be bid. Thus, balancing energy activation revenues are up to 50% for larger sites and up to 35% for smaller sites.

PtG units: In contrast, in optimised operation, PtG units provide primarily a combination of negative aFRR and negative mFRR power. The PtG units cannot provide FCR and positive FR products under the assumptions made for this work (cf. Table 2). Compared to the GtP units, it is more difficult for the PtG unit to provide positive FR power, as this would mean a reduction in electrical power procured from the grid. Since the PtG unit is also operated at a low power input representing a band profile (cf. Figure 12b), just enough to cover the heat demand, a power reduction is not possible due to the lower bounds' restriction in the optimisation model. Therefore, FCR cannot be bid as it is impossible to provide a symmetrical FCR frequency regulation band. Thus, balancing energy activation revenues are below 1% of total revenues for PtG units.

PtG-GtP units: Most of the time, the operation of the PtG unit is more profitable; similar FR products are provided for the single PtG unit. Since there are some time steps in which the GtP unit is operated, positive FR products are also bid, including symmetrical FCR. Therefore, balancing energy activation revenues are between 4%–7% for smaller sites and 1%–3% for larger sites. That lower shares of balancing energy activation revenues are found in larger sites is again due to higher revenue generation from arbitrage activities on the energy spot markets. Additionally, the share of the revenue from natural gas sales increases over time, resulting in even more future deployment times for the PtG units.

The low shares of balancing energy activation revenues in the single PtG units and the combined PtG-GtP units result from the activation profile used, representing the activation times that occurred in 2020. Therefore, depending on the time, amount, and FR activation product, single PtG and combined PtG-GtP units can activate more balancing energy and thus contribute to frequency stability within the grid, particularly in situations with excess energy generation. In 2030 and 2040, the activation times for balancing energy and corresponding FR products are highly likely to change. Therefore, the potential of these re-purposing technologies for balancing energy activation may also increase significantly. However, as activation time points and respective FR product activations are also highly uncertain, the 2020 activation was used to provide an example

under known circumstances. To account for this uncertainty, this work randomly varied the activation times and quantities of the real activation profile from 2020 and recalculated the corresponding revenues. This shows that the share of activation revenues in 2030 and 2040 for the PtG and PtG-GtP units is not significantly higher than the assumed 2020 profile. This is because the assumed price developments for balancing power reserve and balancing energy activation result in low prices for negative FR products, according to Spieker et al. [85]. If the price developments for negative FR products result in higher prices, the revenues also increase significantly. Thus, activation times and quantities have little impact on balancing energy activation revenues; a more substantial influence comes from corresponding price developments.

While the GtP units are fastest in reaching their payback period, the highest revenues can be achieved in total due to high balancing power reserve and balancing energy activation shares. In contrast, PtG units obtain higher revenue shares from natural gas sales but only minimal shares from balancing power reserve or balancing energy activation, leading to extended payback periods. What has not yet been considered within the ROI calculations is that certain unit components can be re-used at the sites in case of re-purposing. However, if such re-use is possible, these cost savings due to available components strongly depend on unit lifetime and maintenance and are site-specific. Nevertheless, these components do not have to be purchased again and reduce the investment costs and, thus, the duration of the payback period. As a result, re-purposing can prevent stranded assets and reduce the ROI of new plants and contribute to their profitability.

4.1 | Load flow investigations

As mentioned before, this work uses the Austrian maximum- and high-voltage grids as a case study to analyse the grid impact of re-purposing. However, the results obtained are valid within the ENTSO-E system and contribute to other regions. From the load flow simulations of the respective re-purposing scenarios and the comparison with the reference scenarios, it becomes clear that overloads occur due to the high RES expansion and increased EV and HP integration. Although these overloads cannot be entirely compensated by integrating certain re-purposing technologies at the former CFPP sites, the duration or the number of time steps with congestions can be reduced. Regarding the duration of these overloads, the PtG and PtG-GtP units can contribute to the reduction.

In contrast, the GtP units with energy spot markets and balancing power market optimised operation increase these congestions. In this context, the PtG and PtG-GtP units offer the potential for temporal flexibilisation, thus relieving the grid locally. However, since there are only three sites investigated and the re-purposing technologies are only operated at low power capacity due to the combined optimisation of the energy spot market and balancing power market (cf. Figure 12), their impact on the grids is only small for the scenarios considered in this paper (cf. research question four).

While greater congestions occur in high-demand regions, there are some additional lower congestions in some transmission lines in Austria. These overloads from Figure 19 in individual transmission lines of the 220 kV grid arise due to the RES expansion assumed in HyFlow. Local flexibility measures must be used to compensate for these overloads, which cannot be entirely compensated for with the re-purposing technologies at the fixed site locations of the CFPPs in Austria. The import and export balances show that only a minor influence of the re-purposing technologies is seen compared to the reference scenarios. This small influence is because, compared to the import and export volumes, the relatively small CFPPs only contribute small volumes. Decisive for the developments of these balances are mainly the expansion of RES and modern loads (EV and HP).

Additionally, as the MES load flow simulation framework HyFlow is still under development, it is impossible to consider loop flows. Such loop flows occur due to flows caused by electricity trading within one bidding zone that impact other bidding zones. Therefore, including loop flows in the model would lead to different results.

5 | CONCLUSIONS AND OUTLOOK

Re-purposing is essential to advance the coal phase-out and help to avoid the stranding of assets. Early identification of re-purposing potentials enables resource-efficient handling of existing assets and extensive re-use of the sites and their infrastructures.

However, re-purposing technologies must also be appropriately chosen to perform tasks of the previous CFPP sites or fulfil still-existing delivery contracts. From an economic point of view, the operation based on both the energy spot market and FR market-oriented operation allows for obtaining substantial revenues. Therefore, both markets were considered in the objective function of the operational optimisation performed in this work. As a result, optimising the operation of re-purposing profiles using a combined objective function allows higher profits than using two objective functions for energy spot and FR markets. However, the combined operational optimisation for both markets requires a large plant capacity to be allocated to balancing power reserve. Under regular operation, which covers heat demands and represents the activities on the spot markets, this additional capacity is unused. As a result, if all plants were operated this way, the total installed capacity in the energy system would need to be substantially increased.

Due to the assumed price developments of electricity and gas until 2040, sector coupling technologies generating natural gas profits (e.g. PtG or PtG-GtP) are preferred in operational optimisation. However, as GtP units allow for the provision of positive balancing products, which are more expensive than negative balancing reserve products (provided primarily by PtG units), higher revenues are achieved by the GtP units. Depending on the year in which the unit is purchased, pay-off periods are between two (2040) and five (2020) years for the GtP units, while PtG units only pay off after at least 7 years (2040). While the combined PtG-GtP units obtain the highest revenues, as the technology leading to the highest profits in each time step is chosen, their pay-off periods are the largest (over 10 years for purchase in 2040). This is due to the significantly higher CapEx as both PtG and GtP units have to be purchased. Therefore, based on the assumptions of this study, GtP units are preferable, in particular, since positive balancing power reserve prices are assumed to increase in the future. For profitable PtG units, further incentives or subsidies must be created, or efficiency enhancements must be achieved to make them more economical and attractive. Additionally, the steam turbine of the CCGT is a back-pressure thermal power unit since this work assumes a linear optimisation. Further work should also include the possibility of a steam extraction turbine, which considers a variable power coefficient via a non-linear optimisation, thereby increasing the unit's feasibility range.

In the context of re-purposing CFPP, there also needs to be more accurate assessments of what contribution in terms of investment cost savings the available assets at CFPP sites can provide. As some still functioning assets can be re-used, CapEx would be reduced since they do not have to be purchased again for the re-purposing technologies. As presented in the sensitivity analysis (cf. Figure 8), a reduction of CapEx would have the largest influence on increasing the ROI. However, such an assessment can only provide conclusive results for a specific site which demands knowledge of the remaining lifetime of each considered component. Therefore, this assessment is very time and data-intensive and cannot adequately provide a general estimate for other sites. However, concrete sites should be used to generate case studies that similar sites can adhere to. These assessments may also contribute to a more profitable operation of the PtG units, as it may lower investment costs by re-using the water treatment plant, the available area, the grid connections, and the personnel at the site, among others. Also, the GtP units may be able to re-use some components, such as the emission control system, personnel, and grid connections. However, the conversion from a coal CHP to a CCGT plant is relatively costly and complex compared to re-purposing using a PtG unit.

From a grid perspective, the market-oriented optimised operating profiles tend to show positive effects on mitigating overloads. However, GtP units slightly exacerbate the duration of the overloads, whereas the individual PtG and combined PtG-GtP units serve as temporal flexibility options to reduce grid strains. For this effect to be enhanced, the unit operation of the re-purposing technologies should not be optimised using a market-oriented approach. Still, it should adapt its operation to the volatile generation situation in the grid. This shows significant potential for reducing durations of congestion. In addition, to better support the grid, the CFPP sites should be equipped with sustainable technologies and other power plant sites. This could provide spatial flexibility and thus reduce the number of congested lines within the grid. As the Austrian CFPP sites tend to be located in the east of Austria and can therefore provide only local or regional compensation, the effect of reducing the number of congested lines cannot be

accomplished. Additionally, although the results from the Austrian case study of this work can be transferred to other ENTSO-E grids, detailed analysis for different connected zones as the ENTSO-E grid area might be necessary to evaluate sector coupling technologies for re-purposing CFPP adequately.

Since there are other re-purposing technologies, as mentioned in the introduction, these should also be considered as possible options for a comprehensive analysis of re-purposing. Increasingly, site-specific data, such as wind potentials in the respective region or main tasks of the original CFPP (e.g. grid stability support tasks), should also be considered so that specific re-purposing options can be identified in advance as reasonable. Then grid calculations should be conducted to determine the effect on the energy system. Based on the results of these analyses, the re-purposing strategy at the respective site should be selected.

CONFLICTS OF INTEREST

The authors declare that they have no known competing financial interests or personal relationships that could have appeared to influence the work reported in this paper.

DATA AVAILABILITY STATEMENT

Data derived from public domain The data to support the developed method and the findings of this study are publicly available, the corresponding links (URL/DOI) are listed in the references. Therefore, all the publicly available data is fully provided and cited in the reference list of this study.

NOMENCLATURE

aFRR	Automated Frequency Restoration Reserve
APG	Austrian Power Grid
CapEx	Capital Expenditures
CCGT	Combined Cycle Gas Turbine
CFPP	Coal-Fired Power Plant
CHP	Combined Heat and Power
DHPP	District Heating Power Plant
EXAA	Energy Exchange Austria
FCR	Frequency Containment Reserve
FRR	Frequency Restoration Reserve
GtP	Gas-to-Power
MES	Multi-Energy-Systems
mFRR	Manual Frequency Restoration Reserve
MILP	Mixed-Integer Linear Programming
OpEx	Operational Expenditures
PtG	Power-to-Gas
RES	Renewable Energy Sources
ROI	Return on Investment
SNG	Synthetic Natural Gas
TPP	Thermal Power Plant

ORCID

Anna Traupmann https://orcid.org/0000-0003-0580-4158

REFERENCES

1. World Coal Association: Coal & Electricity (2021). https://www.worldcoal.org/coal-facts/coal-electricity/
2. Reumerman, P., et al.: Bioenergy Retrofits for Europe´s Industry -The BIOFIT Project (2019)
3. Rauner, S., et al.: Coal-exit health and environmental damage reductions outweigh economic impacts. Nat. Clim. Change 10(4), 308–312 (2020). https://doi.org/10.1038/s41558-020-0728-x
4. Climate Analytics: Coal phase-out. https://climateanalytics.org/briefings/coal-phase-out/
5. United Nations (ed.) Paris Agreement. United Nations (2015)
6. Rocha, M., et al.: A Stress Test for Coal in Europe under the Paris Agreement: Scientific Goalposts for a Coordinated Phase-Out and Divestment (2017)
7. Europe Beyond Coal: Overview: National Coal Phase-Out Announcements in Europe: Status January 2021 (2021). https://beyond-coal.eu/wp-content/uploads/2021/01/Overview-of-national-coal-phase-out-announcements-Europe-Beyond-Coal-January-2021.pdf
8. Shrimali, G., Jindal, A.: Cost-benefit analysis of coal-plant Re-purposing: a case study for India. SSRN J. 30(2), 3118 (2020). https://doi.org/10.2139/ssrn.3646443
9. Qvist, S., et al.: Retrofit decarbonization of coal power plants—a case study for Poland. Energies 14(1), 120 (2021). https://doi.org/10.3390/en14010120
10. British Electricity International: Station Planning and Design: Incorporating Modern Power System Practice, 3rd ed (1991)
11. Climate Transparency: Managing the Phase-Out of Coal: A Comparison of Actions in G20 Countries
12. Breitenstein, M., et al.: Stranded Asset Risk and Political Uncertainty: The Impact of the Coal Phase-Out on the German Coal Industry (2020)
13. Öko-Institut Bundesnetzagentur: Kohlekraftwerke in Deutschland (2021). https://www.wwf.de/fileadmin/fm-wwf/Publikationen-PDF/WWF-Flyer-Kohlekraftwerke_in_Deutschland.pdf
14. International Energy Agency: Coal-Fired Power (2020)
15. Rives, K.: Clean Energy Storage May Give Coal-Fired Plants a Second Life (2022)
16. Huang, Z., et al.: ACT on RE+FLEX: accelerating coal transition through repurposing coal plants into renewable and flexibility centers. IEEE Access 9, 84811–27 (2021). https://doi.org/10.1109/ACCESS.2021.3087081
17. Minchener, A.: Flexible Operation of High Efficiency Coal Power Plants to Ensure Grid Stability when Intermittent Renewables Are Included, pp. 19–28 (2019). https://doi.org/10.1007/978-981-16-1657-0_2
18. World Bank Group: Coal Plant Repurposing for Ageing Coal Fleets in Developing Countries, 16th ed (2021)
19. United Nations General Assembly: Sustainable Development Goals (SDGs) - Goals (2022). https://www.globalgoals.org/goals/
20. Stoll, H.G., Smith, R.W., Tomlinson, L.O.: Performance and Economic Considerations of Repowering Steam Power Plants. SchenectadyNY (1996)
21. NACAA National Association of Clean Air Agencies: Implementing EPA´s Clean Power Plan: A Menu of Options (2015)
22. Song, F., et al.: Review of transition paths for coal-fired power plants. Global Energy Interconnection 4(4), 354–70 (2021). https://doi.org/10.1016/j.gloei.2021.09.007
23. Tzelepi, V., et al.: Biomass availability in Europe as an alternative fuel for full conversion of lignite power plants: a critical review. Energies 13(13), 3390 (2020). https://doi.org/10.3390/en13133390
24. European Union: BIOFIT - Bioenergy Retrofits for Europe´s Industry (2022). https://www.biofit-h2020.eu/
25. Rutz, D., et al.: Technical Options for Retrofitting Industries with Bioenergy: A Handbook, 1st ed (2020)
26. Emun, F., et al.: Integrated gasification combined cycle (IGCC) process simulation and optimization. Comput. Chem. Eng. 34(3), 331–8 (2010). https://doi.org/10.1016/j.compchemeng.2009.04.007
27. Randall, C.: Second Life for a Coal Power Plant in Germany (2022). https://www.electrive.com/2020/11/24/second-life-for-a-coal-power-plant-in-germany/
28. Renault Group: A second life for batteries: from energy usage to industrial storage. (2022) https://www.renaultgroup.com/en/news-on-

air/news/a-second-life-for-batteries-from-energy-usage-to-industrial-storage/

29. Mills, S.: Combining solar power with coal-fired power plants, or cofiring natural gas. Clean Energy 2(1), 1–9 (2018). https://doi.org/10.1093/ce/zky004

30. Geyer, M., Trieb, F., Giuliano, S.: Repurposing of Exisiting Coal-Fired Power Plants into Thermal Storage Plants for Renewable Power in Chile (2020)

31. University of Stuttgart: GreenDEALCO2: Green Deployment of E-Fuels and Liquids Based on CO2 for Closed and End-Of-Life Coal-Related Assets (2022). https://www.greendealco2.com/

32. Slavin, M.I., Brown, T.M.: Repurposing of Legacy Power Plants - Lessons for the Future (2011)

33. Energy Sector Management Assistance Program: Coal Plant Repurposing for Aging Coal Fleets in Developing CountriesWashington (2021)

34. VGB Powertech e.V.: Re-purposing Coal Power Plants during Energy Transition (RECPP) (2021). https://www.recpp.eu/

35. JT-Box: Just Transition Toolbox für Kohleregionen. (2021). https://wupperinst.org/p/wi/p/s/pd/1939

36. Climate Investment Funds: Climate Investment Funds (2022). https://www.climateinvestmentfunds.org/about-cif

37. Climate Investment Funds: Accelerating Coal Transition(ACT) Investment Program: Coal-To-Clean Transition (2022). https://www.climateinvestmentfunds.org/topics/accelerating-coal-transition

38. Powering Past Coal Alliance: Powering Past Coal Alliance (PPCA) (2022). https://www.poweringpastcoal.org/about/who-we-are

39. Jewell, J., et al.: Prospects for powering past coal. Nat. Clim. Change 9(8), 592–7 (2019). https://doi.org/10.1038/s41558-019-0509-6

40. Eveloy, V., Gebreegziabher, T.: A review of projected power-to-gas deployment scenarios. Energies 11(7), 1824 (2018). https://doi.org/10.3390/en11071824

41. Heinisch, V., Le Tuan, A.: Effects of Power-To-Gas on Power Systems: A Case Study of Denmark, pp. 1–6 (2015). https://doi.org/10.1109/PTC.2015.7232587

42. Buchholz, O.S., et al.: Power-to-Gas: storing surplus electrical energy. A design study. Energy Proc. 63, 7993–8009 (2014). https://doi.org/10.1016/j.egypro.2014.11.836

43. Khani, H., Farag, H.E.Z.: Optimal day-ahead scheduling of power-to-gas energy storage and gas load management in wholesale electricity and gas markets. IEEE Trans. Sustain. Energy 9(2), 940–51 (2018). https://doi.org/10.1109/TSTE.2017.2767064

44. Ma, Y., et al.: Modeling and optimization of combined heat and power with power-to-gas and carbon capture system in integrated energy system. Energy 236, 121392 (2021). https://doi.org/10.1016/j.energy.2021.121392

45. Yang, Y., et al.: Integrated operation optimization for CCHP micro-grid connected with power-to-gas facility considering risk management and cost allocation. Int. J. Electr. Power Energy Syst. 123, 106319 (2020). https://doi.org/10.1016/j.ijepes.2020.106319

46. Mazza, A., Bompard, E., Chicco, G.: Applications of power to gas technologies in emerging electrical systems. Renew. Sustain. Energy Rev. 92, 794–806 (2018). https://doi.org/10.1016/j.rser.2018.04.072

47. Walker, S.B., et al.: Benchmarking and selection of Power-to-Gas utilizing electrolytic hydrogen as an energy storage alternative. Int. J. Hydrogen Energy 41(19), 7717–31 (2016). https://doi.org/10.1016/j.ijhydene.2015.09.008

48. ITM achieves rapid response electrolysis in P2G energy storage. Fuel Cell. Bull. 2016(1):9 (2016). https://doi.org/10.1016/S1464-2859(16)30021-9

49. Witkowski, K., et al.: Role of thermal technologies for enhancing flexibility in multi-energy systems through sector coupling: technical suitability and expected developments. IET Energy Systems Integration 2(2), 69–79 (2020). https://doi.org/10.1049/iet-esi.2019.0061

50. Xing, X., et al.: Modeling and operation of the power-to-gas system for renewables integration: a review. CSEE JPES 4(2), 168–78 (2018). https://doi.org/10.17775/CSEEJPES.2018.00260

51. Verbund Thermal Power GmbH, Co, K.G.: District Heating Power Plant Mellach (2022). https://www.verbund.com/en-at/about-verbund/power-plants/our-power-plants/mellach-district-heating

52. Verbund Thermal Power GmbH & Co KG: Austria's Last Coal-Fired Power Plant Has Ceased Operation. Mellach (2020)

53. EVN AG: Thermische Erzeugung: Kraftwerk Dürnrohr (2022). https://www.evn.at/EVN-Group/Energie-Zukunft/Energie-aus-Niederosterreich/Gas-und-Kohle.aspx

54. ORF Österreichischer Rundfunk: Kohlekraftwerk Dürnrohr Abgeschaltet (2022). https://noe.orf.at/stories/3007102/

55. Energie GmbH, W.: Kraftwerk Simmering (2022). https://www.wienenergie.at/privat/erleben/standorte/kraftwerk-simmering/

56. QGIS.org: QGIS Geographic Information System. QGIS Association (2022)

57. Cooperation OGD Österreich: Open Data Österreich (2022). https://www.data.gv.at/

58. Flaticon: Icons made by freepik. https://www.flaticon.com/de/

59. Jin, T.: The effectiveness of combined heat and power (CHP) plant for carbon mitigation: evidence from 47 countries using CHP plants. Sustain. Energy Technol. Assessments 50(5), 101809 (2022). https://doi.org/10.1016/j.seta.2021.101809

60. Schnülle, C., Kenkel, P., Wassermann, T.: Multikriterielle Bewertung von Elektrolyse-und CO2-Capture Technologien für eine Power-to-Methanol Prozesskette (2020)

61. Milanzi, S., et al.: Technischer Stand und Flexibilität des Power-to-Gas-Verfahrend (2018)

62. Kreidelmeyer, S., et al.: Kosten und Transformationspfade für strombasierte Energieträger: Final Report for the project "Transformationspfade und regulatorischer Rahmen für synthetische Brennstoffe" (2020)

63. Estermann, T., et al.: Kurzstudie Power-to-X: Ermittlung des Potenzials von PtX-Anwendungen für die Netzplanung der deutschen ÜNB (2017)

64. Hermans, M., Bruninx, K., Delarue, E.: Impact of CCGT Start-Up Flexibility and Cycling Costs towards Renewables Integration (2022). https://core.ac.uk/download/pdf/153423129.pdf

65. Arakelyan, E., et al.: Increasing the Reliability and Manoeuvrability of the CCGT when Operating in the Variable Part of the Power Consumption Schedules by Switching the CCGT Steam Turbine to the Motor Mode. 1089 (2020)

66. Zohuri, B.: New approach to energy conversion technology. In: Molten Salt Reactors and Integrated Molten Salt Reactors, pp. 85–136

67. Seebregts, A.J., Simbolotti, G., Tosato, G.: Gas-fired Power (2022). https://iea-etsap.org/E-TechDS/PDF/E02-gas_fired_power-GS-AD-gct_FINAL.pdf

68. Ferat Toscano, C., et al.: Life cycle assessment of a combined-cycle gas turbine with a focus on the chemicals used in water conditioning. Sustainability 11(10), 2912 (2019). https://doi.org/10.3390/su11102912

69. statista: Projected Capital Expenditure of a Conventional Natural Gas Combustion Turbine Power Plant in the United States from 2021 to 2050 (2022). https://www.statista.com/statistics/243704/capital-costs-of-a-typical-us-gas-turbine-power-plant/

70. APG Austrian Power Grid AG: EXAA Spot Market Prices: Day Ahead Prices (2022). https://www.apg.at/en/markt/Markttransparenz/cross-border-exchange/EXAA-Spotmarkt

71. Energy Brainpool GmbH & Co. KG: Update: EU Energy Outlook 2050 - How Will Europe Evolve over the Next 30 Years? (2022). https://blog.energybrainpool.com/en/update-eu-energy-outlook-2050-how-will-europe-evolve-over-the-next-30-years/

72. Brainpool GmbH, E., Co, K.G.: Trends in the Development of Electricity Prices - EU Energy Outlook 2050 (2022). https://blog.energybrainpool.com/en/trends-in-the-development-of-electricity-prices-eu-energy-outlook-2050/

73. European Energy Exchange eex: Market Data - Natural Gas (2022). https://www.eex.com/de/marktdaten/erdgas

74. Sejkora, C., et al.: Interlinking the renewable electricity and gas sectors: a techno-economic case study for Austria. Energies 14(19), 6289 (2021). https://doi.org/10.3390/en14196289

75. Böhm, H., et al.: Projecting cost development for future large-scale power-to-gas implementations by scaling effects. Appl. Energy 264(11), 114780 (2020). https://doi.org/10.1016/j.apenergy.2020.114780

76. Environment Agency Austria: Scenarios WEM and WAM (2019) - Energy Economic Scenario with Regard to Energy and Climate Targets (2022). https://www.umweltbundesamt.at/energie/energieszenarien/energieszenarien2019

77. Cvetkovska, R., Nagovnak, P., Kienberger, T.: Pathways for ramping-up hydrogen into the natural gas system. In: Proceedings of the 17th Symposium Energieinnovation (EnInnov) (2022)

78. Dolna-Gruber, C., Knaus, K., Zwieb, L.: Stromgroßhandel - Preisentwicklung und wesentliche EinflussfaktorenVienna (2022)

79. Next Kraftwerke GmbH: Was Ist Regelenergie? (2022). https://www.next-kraftwerke.de/wissen/regelenergie

80. APG Austrian Power Grid AG: Procured Balancing Capacity (2022). https://www.apg.at/en/markt/Markttransparenz/Netzregelung/Zugeschlagene-Regelleistung

81. APG Austrian Power Grid AG: Balancing Energy Bids (2022). https://www.apg.at/en/markt/Markttransparenz/Netzregelung/Regelenergieangebote

82. APG Austrian Power Grid AG: Frequency Containment Reserve (FCR) (2022). https://www.apg.at/en/markt/Markttransparenz/Netzregelung/Primaerregelreserve

83. APG Austrian Power Grid AG: Automatic Frequency Restoration Reserve (AFRR) (2022). https://www.apg.at/en/markt/Markttransparenz/Netzregelung/Sekundaerregelreserve

84. APG Austrian Power Grid AG: Manual Frequency Restoration Reserve (MFRR) (2022). https://www.apg.at/en/markt/Markttransparenz/Netzregelung/Tertiaerregelung

85. Spieker, S., Kopiske, J., Tsatsaronis, G.: Flexibilität aus Wind-und Photovoltaikanlagen im Regelenergiemarkt 2035. 14 (2016)

86. Deutsche Energie-Agentur GmbH: dena-Studie Systemdienstleistungen 2030: Sicherheit und Zuverlässigkeit einer Stromversorgung mit hohem Anteil an erneuerbarer Energie (2014)

87. APG Austrian Power Grid AG: Power Plants - Generation Schedule (2022). https://www.apg.at/en/Energiezukunft/Glossar/Kraftwerksfahrplan

88. E-Control: Zusammensetzung des Gaspreises (2022). https://www.e-control.at/industrie/gas/gaspreis/preiszusammensetzung

89. RIS Rechtsinformationssystem des Bundes. In: Elektrizitätswirtschafts- und -organisationsgesetz (ElWOG 2010)

90. ZAMG Zentralanstalt für Meteorologie und Geodynamik: Jahrbuch (2022). https://www.zamg.ac.at/cms/de/klima/klimauebersichten/jahrbuch

91. bdew Bundesverband der Energie- und Wasserwirtschaft e.V: BDEW/VKU/GEODE-Leitfaden: Abwicklung von Standardlastprofilen Gas (2016). https://www.bdew.de/media/documents/Leitfaden_20160630_Abwicklung-Standardlastprofile-Gas.pdf 15 January 2022

92. Böckl, B., et al.: HyFlow—a hybrid load flow-modelling framework to evaluate the effects of energy storage and sector coupling on the electrical load flows. Energies 12(5), 956 (2019). https://doi.org/10.3390/en12050956

93. Greiml, M., et al.: Modelling, designing and operation of grid-based multi-energy systems. International Journal of Sustainable Energy Planning and Management 29(2020), 7–24 (2020). https://doi.org/10.5278/ijsepm.3598

94. Traupmann, A., Kienberger, T.: Novel network reduction method for cellular-based network models with enhanced modeling accuracy for multi-energy-system approaches. Int. J. Electr. Power Energy Syst. 137(4), 107827 (2022). https://doi.org/10.1016/j.ijepes.2021.107827

95. Greiml, M., Fritz, F., Kienberger, T.: Increasing installable photovoltaic power by implementing power-to-gas as electricity grid relief – a techno-economic assessment. Energy 235(5), 121307 (2021). https://doi.org/10.1016/j.energy.2021.121307

96. Kacprzyk, J., Gavrilova, M.L. (eds.) Generalized Voronoi Diagram: A Geometry-Based Approach to Computational Intelligence. Springer Berlin HeidelbergBerlin (2009)

97. Greiml, M., et al.: Modelling and simulation/optimization of Austria's national multi-energy system with a high degree of spatial and temporal resolution. Energies 15(10), 3581 (2022). https://doi.org/10.3390/en15103581

98. Technical University of Vienna, ethink Energy Research: Austrian Heat Map (2022). https://austrian-heatmap.gv.at/karte/

99. APG Austrian Power Grid AG: Power Grid (2022). https://www.apg.at/en/Stromnetz/APG-Netz

100. E-Control: The Gas Grid (2022). https://www.e-control.at/en/industrie/gas/gasnetz

101. Deutsch, M.: Wärmewende 2030: Schlüsseltechnologien zur Erreichung der mittel-und langfristigen Klimaschutzziele im Gebäudesektor (2017)

102. statista: Annual Amount of Heat Pumps in Operation in the European Union (EU) from 2013 to 2020 (2022). https://www.statista.com/statistics/739745/heat-pumps-in-operation-eu/

103. European Commission: EU Reference Scenario 2016: Energy, Transport and GHG Emissions Trends to 2050 (2016)

104. Pötscher, F., Winter, R., Lichtblau, G.: Elektromobilität in Österreich Szenario 2020 und 2050 (2010)

105. Sejkora, C., et al.: Exergy as criteria for efficient energy systems—a spatially resolved comparison of the current exergy consumption, the current useful exergy demand and renewable exergy potential. Energies 13(4), 843 (2020). https://doi.org/10.3390/en13040843

106. Lafarge: Werk Retznei (2022). https://www.lafarge.at/ueber-uns/werk-retznei

107. VDZ-online: Klimaschutz - Dekarbonisierung von Zement und Beton (2022). https://www.vdz-online.de/zementindustrie/klimaschutz

108. Stahl- und Walzwerk Marienhütte: Marienhütte Manifest (2022). https://www.marienhuette.at/fileadmin/user_upload/downloads/Manifest.pdf

109. Klima- und Energiefonds: NEOStahl – Neue Energieoptimierungsverfahren und –Modelle in der Prozessautomation zur CO2-Reduktion in der Stahlindustrie (2022). https://energieforschung.at/projekt/neostahl-neue-energieoptimierungsverfahren-und-modelle-in-der-prozessautomation-zur-co2-reduktion-in-der-stahlindustrie/

110. Donau Chemie Group: Sulphuric Acid Production (2022). https://www.donau-chemie.com/Products-Solutions/BU-Chemie/Schwefelsaure?lang=en-US

111. AGRANA: AGRANA – Official Opening of Bioethanol Plant in Pischelsdorf (2022). https://www.agrana.com/en/pr/all-press-releases/news-detail/agrana-official-opening-of-bioethanol-plant-in-pischelsdorf

112. OMV: Sustainability Report 2020 (2022). https://omv.online-report.eu/en/sustainability-report/2020/focus-areas/carbon-efficiency.html

113. Borealis Polyolefine GmbH: Sustainability Focus Areas (2022). https://www.borealisgroup.com/digital-annual-report-2020/non-financial-report/sustainability-focus-areas/energy-climate

114. Miehling, S., Fendt, S., Spliethoff, H.: Optimal integration of Power-to-X plants in a future European energy system and the resulting dynamic requirements. Energy Convers. Manag. 251(2), 115020 (2022). https://doi.org/10.1016/j.enconman.2021.115020